Computational petrology:

Subsolidus equilibria in the upper mantle

by

Silvano Sommacal

A thesis submitted for the degree of

Doctor of Philosophy

of The Australian National University

Canberra
July 2004

Declaration

This thesis contains the results of research undertaken at the Research School of Earth Sciences, The Australian National University. Except where acknowledged otherwise, the research and interpretation described in this thesis are my own. No part of this thesis has been submitted to any other university.

Silvano Sommacal

Acknowledgments

There are two people who, although in completely different ways, have played a crucial role in making this project possible. These two people are: my supervisor, Malcolm Sambridge, and my partner, Mariolina Pais Marden.

Malcolm agreed to supervise me in this challenging project and from the very beginning his involvement, dedication and commitment have been invaluable. Malcolm proved to be the perfect supervisor: brilliant, inspiring, innovative, organized, constructively critical when needed, and by the way, he is a pretty decent soccer player too. He showed and demonstrated to me how any problem can be solved with the right approach and the appropriate methodology. It is hard to imagine a more approachable supervisor than Malcolm. When I needed his help and advice he has always found time for me and our meetings would go on for hours. I really cannot see how this work could have had a positive outcome without all the high quality work and the large amount time Malcolm has dedicated to it. So, Malcolm, what I hope I have made clear is that, apart from being a wonderful supervisor, you are also a great person and I am perfectly aware of how much indebted I am to you and how lucky I have been in meeting you.

The role played by Mariolina behind this work, originates much earlier, long before I actually started my Ph.D. Several years ago, when by chance we met during a hike in my beautiful Dolomites, Mariolina had already planned to come to Australia, something that had never crossed my mind before. Why, after all, should I quit a safe job to go to a place where I cannot speak the language and the tallest mountain is as high as a hill in my backyard? Things then changed, the whole 'Australia idea' began growing on me, up to the point that we decided to come here together. That turned out to be one of the best decisions I have ever made and coming across Mariolina one of the most significant and fortunate moments in my life.

Special thanks to Jörg Hermann, my advisor and friend, for constant support and constructive discussions. Jörg is the colleague anyone would love having next door: smart, enthusiastic about science, always available for friendly and/or scientific conversations and never scared of sharing with others his already amazing knowledge.

My other supervisor Hugh O'Neill is also acknowledged.

This work makes use of a set of software routines known as FFSQP, written by J.L Zhou, A. L. Tits and C. T. Lawrence, and of the quadratic programming routine, QLD, of K. Schittkowski. I am thankful to all of these people for making their codes available to the wider community. Use has also been made of the automatic differentiation package TAF of R. Giering and T. Kaminski. I gratefully acknowledge these two authors for allowing me access to TAF.

This dissertation was carried out under a ANU scholarship.

Thanks to Andrew Berry (also my flatmate and who introduced me to the mystic world of cricket), Uli Faul, Bill Hibberson, Dagmar Kelly and all the other members (plus various visitors) of the Petrochemistry and Experimental Petrology Group for their contribution to making life at RSES so enjoyable. Quite often the time spent together during morning or afternoon tea breaks represented the highlight of my day as a 'scientist'.

With many other RSES people and a number of fellow 'cousins' from Geology, beg your pardon, Department of Earth and Marine Science, friendship started within the campus

but then extended far beyond its borders. Among the others, Alistair Hack (prior and after his ‘metamorphosis’), Dean Scott (who renamed as ‘woggish’ my spoken English), Eric Tenthorey, Sarah O’Callaghan, Julie Brown, Carl Spandler, Bridget Ayling, Chris Heath, Julian Ballard, Daniela Rubatto, Thomas Berly, Helen McGregor and, more recently, Nicole Keller, Katie Dowell and Heather Sparks.

A special mention goes to my other good friends who with their love and warmth played an important part towards my well being in Canberra. Names that come to my mind are those of Jacinta Cubis, Andrew ‘big fellow’ Brown, my other flatmate Laurence Vichie, Pete & Joe, Michael Westaway, Catherine ‘BM’ Pye, Dan Rayner, Dave Johnston, Dom Barbaro, Matthew Maurer; with the Wig & Pen and the Phoenix being our favorite venues.

Canberra might not be the most exciting place to live but it becomes much more pleasant if you are a sports person and like outdoor activities. I’ll take with me great memories of my indoor and outdoor soccer seasons (thanks to the ANU soccer club), lunch time running (thanks to Dave Osmond and to all the other guys of the ACT running club) and Touch Footy competitions.

Continuing a tradition I also have to acknowledge the ‘pink slippers’, which, in the past few months, have been hanging on my offices door to daily remind me that I was the ‘oldest’ student at RSES and it was time for me to finish.

Abstract

Processes that take place in the Earth's mantle are not accessible to direct observation. Natural samples of mantle material that have been transported to the surface as xenoliths provide useful information on phase relations and compositions of phases at the pressure and temperature conditions of each rock fragment. In the past, considerable effort has been devoted by petrologists to investigate upper mantle processes experimentally. Results of high temperatures, high pressure experiments have provided insight into lower crust-upper mantle phase relations as a function of temperature, pressure and composition. However, the attainment of equilibrium in these experiments, especially in complex systems, may be very difficult to test rigorously. Furthermore, experimental results may also require extrapolation to different pressures, temperatures or bulk compositions. More recently, thermodynamic modeling has proved to be a very powerful approach to this problem, allowing the deciphering the physicochemical conditions at which mantle processes occur. On the other hand, a comprehensive thermodynamic model to investigate lower crust-upper mantle phase assemblages in complex systems does not exist.

In this study, a new thermodynamic model to describe phase equilibria between silicate and/or oxide crystalline phases has been derived. For every solution phase the molar Gibbs free energy is given by the sum of contributions from the energy of the end-members, ideal mixing on sites, and excess site mixing terms. It is here argued that the end-member term of the Gibbs free energy for complex solid solution phases (e.g. pyroxene, spinel) has not previously been treated in the most appropriate manner. As an example, the correct expression of this term for a pyroxene solution in a general (Na-Ca-Mg-Fe^{2+}-Al-Cr-Fe^{3+}-Si-Ti) system is presented and the principle underlying its formulation for any complex solution phase is elucidated.

Based on the thermodynamic model an algorithm to compute lower crust-upper mantle phase equilibria for subsolidus mineral assemblages as a function of composition, temperature and pressure has been developed. Included in the algorithm is a new way to represent the total Gibbs free energy for any multi-phase complex system. At any given temperature and pressure a closed multi-phase system is at its equilibrium condition when the chemical composition of the phases present in the system and the number of moles of each are such that the Gibbs free energy of the system reaches its minimum value. From a

mathematical point of view, the determination of equilibrium phase assemblages can, in short, be defined as a constrained minimization problem. To solve the Gibbs free energy minimization problem a 'Feasible Iterate Sequential Quadratic Programming' method (*FSQP*) is employed. The system's Gibbs free energy is minimized under several different linear and non-linear constraints. The algorithm, coded as a highly flexible FORTRAN computer program (named '*Gib*'), has been set up, at the moment, to perform equilibrium calculations in NaO-CaO-MgO-FeO-Al_2O_3-Cr_2O_3-Fe_2O_3- SiO_2-TiO_2 systems. However, the program is designed in a way that any other oxide *component* could be easily added.

To accurately forward model phase equilibria compositions using '*Gib*', a precise estimation of the thermodynamic data for mineral end-members and of the solution parameters that will be adopted in the computation is needed. As a result, the value of these parameters had to be derived/refined for every solution phase in the investigated systems. A computer program (called '*GibInv*') has been set up, and its implementation is here described in detail, that allows the simultaneous refinement of any of the end-member and mixing parameters. Derivation of internally consistent thermodynamic data is obtained by making use of the Bayesian technique. The program, after being successfully tested in a synthetic case, is initially applied to pyroxene assemblages in the system CaO-MgO-FeO-Al_2O_3-SiO_2 (i.e. CMFAS) and in its constituent subsystems. Preliminary results are presented.

The new thermodynamic model is then applied to assemblages of Ca-Mg-Fe olivines and to assemblages of coexisting pyroxenes (orthopyroxene, low Ca- and high Ca clinopyroxene; two or three depending on *T-P*-bulk composition conditions), in CMFAS system and subsystems. Olivine and pyroxene solid solution and end-member parameters are refined, in part using '*GibInv*' and in part on a 'trial and error' basis, and, when necessary, new parameters are derived. Olivine/pyroxene phase relations within such systems and their subsystems are calculated over a wide range of temperatures and pressures and compare very favorably with experimental constraints.

Remarks on the structure of the thesis

The chapters of this thesis have been structured with the approximate form of a scientific paper with the exception of chapter 1 and chapter 7, the former being an introduction of the thesis, the latter a concluding section summarizing the most important results of this work. As a consequence, repetitions may occur, especially in the introductory sections and in the references sections.

-CONTENTS-

Computational petrology:

Subsolidus equilibria in the upper mantle

Chapter 1

Introduction

One goal of geological research is to understand the physical and chemical processes responsible for the origin and evolution of the earth (Chatterjee, 1991). In recent years, thermodynamic modeling has begun to play a crucial role towards the achievement of this goal. Several kinds of important information can be obtained by using this approach to study the chemical behavior of olivine, pyroxene and other rock forming minerals. In particular, thermodynamic modeling has been widely used in geology to compare experimental results with other studies and for extrapolating experimental results in temperature-pressure-compositional space. Moreover, if applied to natural rocks, assuming the observed mineral assemblage preserved in a rock records the state of chemical equilibrium, thermodynamics can help translate the compositional data of the coexisting minerals to temperature (T) and pressure (P) of their equilibration (Chatterjee, 1991).

A main aim of this project is the development of a model for lower crust-upper mantle subsolidus phase equilibria in complex multicomponent systems. Of crucial importance, therefore, is the derivation of a model that could correctly describe the thermodynamic behavior of any phase present in such systems. Many of the important rock-forming minerals (e.g. pyroxenes, olivines, garnets) observed in crust and/or mantle assemblages fall into the category of 'complex solid solutions', where mixing of cations can take place on two or more different sites (Ganguly and Saxena, 1987; Chatterjee, 1991). The modeling of the thermodynamic properties of such minerals is of great relevance for this study and, more generally, for the development of petrology as quantitative science. In chapter 2 of this thesis, the problem of modeling multisite, multicomponent ionic phases is comprehensively addressed and a formalism is proposed for the derivation of a general thermodynamic model that can be applied to any type of solution phase.

The successful employment of a model for petrologic investigation heavily depends on a correct estimation of its thermodynamic parameters. Thermodynamic data available today can basically be obtained in two different ways. The first one relies heavily on

calorimetric measurements and seeks to deal with each phase individually. Examples of this are the compilation of thermodynamic data of minerals and related substances by Robie et al. (1978) and by Robie and Hemingway (1995). Though calorimetry is and will remain a fundamental and indispensable source of thermodynamic data, thermodynamic datasets based exclusively on calorimetry seldom allow computation of phase diagrams sufficiently accurate for geochemical applications. There lies the need of a different type of database. This second type strives to relate the thermodynamic properties of the minerals to each other, to come up with what is known as an internally consistent set of thermodynamic data. Examples of such databases are those of Helgeson et al. (1978), Berman (1988), Holland and Powell (1990 and 1998), Gottschalk (1997) and Chatterjee et al. (1998). The development of these 'internally consistent databases for mineral end-members' has been a major advance in thermodynamic modeling. However, in order to model subsolidus equilibria that involve solid solutions phases, an accurate estimation of mixing parameters is also needed. Despite that most values for the mixing parameters can be found in the literature, an arbitrary combination of standard state thermodynamic properties with such values will not in general give results compatible with available experimental data (Berman and Aranovich, 1996). In chapter 6 of this thesis the procedure followed to write a program ('*GibInv*') that, based on the Bayesian technique (i.e. '*inverse*' approach), allows simultaneous refinement of end-member and solution parameters is described and its major features are illustrated in detail. The Bayesian method has been chosen because it combines the advantages of other techniques previously used with the same purpose, such as least square regression techniques (e.g. Gottschalk, 1997) and linear mathematical programming algorithms (e.g. Berman, 1988). Moreover, its employment in the derivation of internally consistent datasets has already proved to be successful (e.g. Olbricht et al., 1994).

Once an appropriate thermodynamic model is derived and assuming that end-member and mixing parameters data are available for any phase, it is possible, based on thermodynamic calculations, to determine the chemical composition of the phases present in a system and the number of moles of each such that, at any given *T-P* conditions, the Gibbs free energy of the system reaches its minimum value (i.e. system equilibrium condition). In the past, many different algorithms have been proposed to solve the Gibbs free energy minimization (i.e. GFEM) problem (e.g. van Zeggeren and Storey, 1970; Smith

and Missen, 1982; Ghiorso, 1985; Karpov et al., 1995; and references therein), all based on standard techniques of computational mathematics. In chapter 3 of the thesis the new algorithm developed in this study to forward model equilibrium phase assemblages is described in detail. To solve the GFEM problem a modern optimization method is employed. Its implementation and most significant features are also thoroughly illustrated.

In chapters 4 and 5 the first significant results that have been obtained using '*Gib*' for computing equilibrium phase assemblages as a function of *T-P* and bulk compositions are summarized. More specifically, chapter 4 deals with the thermodynamic modeling of Ca-Mg-Fe olivine. Phase assemblages are calculated along the binary Ca-Mg and Ca-Fe systems as well as within the quadrilateral and are subsequently compared to experimental data. Phase equilibria are initially computed using end-member and solution parameters values found in the literature. These parameters were then refined on a 'trial and error' basis, in order to better reproduce the existing experimental results. Similarly, in chapter 5, pyroxene phase equilibria are reproduced over a wide range of *T*, *P* and bulk composition conditions and compared to existing experimental data. In this case, values of end-member and solution parameters used in the computational process were initially derived using '*GibInv*' and subsequently modified on a 'trial and error' basis when required. Pyroxene phase compositions are calculated for the following systems: $CaO\text{-}MgO\text{-}SiO_2$ (i.e. CMS), $CaO\text{-}FeO\text{-}SiO_2$ (i.e. CFS), CMFS, $CaO\text{-}MgO\text{-}Al_2O_3\text{-}SiO_2$ (i.e. CMAS) and CMFAS. At the end of the chapters, the refined end-member and solution parameters for olivine (chapter 4), orthopyroxene and clinopyroxene (chapter 5), are reported.

References

Berman R. G. (1988) Internally-consistent thermodynamic data for minerals in the system $Na_2\text{-}K_2O\text{-}CaO\text{-}MgO\text{-}FeO\text{-}Fe_2O_3\text{-}Al_2O_3\text{-}SiO_2\text{-}TiO_2\text{-}H_2O\text{-}CO_2$. *Journal of Petrology* **29**, 445-552.

Berman R. G. and Aranovich L. Y. (1996) Optimized standard state and solution properties of minerals. I. Model calibration for olivine, orthopyroxene, cordierite, garnet, and ilmenite in the system $FeO\text{-}MgO\text{-}CaO\text{-}Al_2O_3\text{-}TiO_2\text{-}SiO_2$. *Contributions to Mineralogy and Petrology* **126**, 1-24.

Chatterjee N. D. (1991) Applied Mineralogical Thermodynamics. Selected topics. *Springer Verlag Berlin*.

Chatterjee N. D., Krüger R., Haller G., and Olbricht W. (1998) The Bayesian approach to an internally consistent thermodynamic database: theory, database, and generation of phase diagrams. *Contributions to Mineralogy and Petrology* **133**, 149-168.

Ganguly J. and Saxena S. K. (1987) Mixtures and Mineral Reactions. Springer-Verlag, New-York.

Ghiorso M. S. (1985) Chemical mass transfer in magmatic processes. I. Thermodynamic relations and numerical algorithms. *Contributions to Mineralogy and Petrology* **90**, 107-120.

Gottschalk M. (1997) Internally consistent thermodynamic data for rock forming minerals. *European Journal of Mineralogy* **9**, 175-223.

Helgeson, H.C., Delany, J.M., Nesbitt, H.W. and Bird, D.K., 1978. Summary and critique of the thermodynamic properties of rock-forming minerals. *American Journal of Science* **278A**, 1-229.

Holland T. J. B. and Powell R. (1990) An enlarged and updated internally consistent thermodynamic dataset with uncertainties and correlations: the system K_2O-Na_2O-CaO-MgO-MnO-FeO-Fe_2O_3-Al_2O_3-TiO_2-SiO_2-C-H-O_2. *Journal of Metamorphic Geology* **8**, 89-124.

Holland T. J. B. and Powell R. (1998) An internally consistent thermodynamic dataset for phases of petrological interest. *Journal of Metamorphic Geology* **16**, 309-403.

Karpov I. K., Chudnenko K. V., Bychinskii V. A., Kulik D. A., Pavlov A. L., Tret'yakov G. A., and Kashik S. A. (1995) Free energy minimization in calculation of heterogeneous equilibria. *Russian Geology and Geophysics* **36**(4), 1-16.

Olbricht W., Chatterjee N. D., and Miller K. (1994) Bayes estimation: a novel approach to derivation of internally consistent thermodynamic data for minerals, their uncertainties, and correlations. I. Theory. *Physics and Chemistry of Minerals* **21**, 36-49.

Robie, R.A., Hemingway, B.S. and Fisher, J.R., 1978. Thermodynamic properties of minerals and related substances at 298.15 K and 1 bar (10^5 Pascals) pressures and at higher temperatures. *United States Geological Survey Bulletin* **1452**, pp. 456.

Robie R. A. and Hemingway B. S. (1995) Thermodynamic properties of minerals and related substances at 298.15 K and 1 bar (10^5 Pascals) pressures and at higher temperatures. *United States Geological Survey Bulletin* **2131**, pp. 461.

Smith W. R. and Missen R. W. (1982) *Chemical Reaction Equilibrium Analysis*. Wiley.

van Zeggeren F. and Storey S. H. (1970) *The Computation of Chemical Equilibrium*. Cambridge University.

Chapter 2

Thermodynamic properties of multicomponent, multisite crystalline ionic solid solutions

2.1 Introduction

Many of the important rock-forming minerals such as pyroxenes, amphiboles, micas, etc., show complicated compositional variations, subject to rules of stoichiometry and charge balance dictated by their crystal structure. The development of petrology as a quantitative science depends on modeling the thermodynamic properties of such minerals. Yet most discussions of the thermodynamics of solid solutions treat only rather simple cases, leaving the impression that the thermodynamic description of the multicomponent, multisite solutions of interest to petrologists needs only a straightforward extension of the principles found in simple binary solid solutions. This is not the case. In this chapter the extra problems that the multisite, multicomponent crystalline ionic phases pose are pointed out and the formalism adopted in this work for their thermodynamic modeling is presented.

2.2 Compositional constraints on the formulation of the *G* function

In essence the task is to model the Gibbs free energy of a phase as a function of the chemical composition of the phase, i.e.:

$$G = f\left(n_i\right) \qquad \left(i = 1,...,t\right) \tag{2.1}$$

with:

n_i = number of moles of chemical element i

t = total number of chemical elements in the system

Heuristically, one possible approach might be to develop G as some enormous Taylor's series expansion in all elements present in the system, but this is impractical because the free energy function G is highly discontinuous in composition. For example, in

the three component system Ni-Mn-O, *G* for the rocksalt-structured phase varies smoothly between the compositions NiO and MnO, but a *G*-composition section taken across this join would show a very sharp minimum at the ratio $\frac{(\mathrm{Ni}+\mathrm{Mn})}{\mathrm{O}}=1$, as may be experimentally observed in the bounding binary joins Ni-O and Mn-O. For practical purposes, therefore, it is necessary to specify certain compositional constraints on the form of the *G* function.

The nature of these constraints depends on the fundamental chemical properties of the phase in question, and will therefore vary from one type of phase to another. For instance, the way gases are treated compared to condensed phases can be considered. For a gas, which is composed of individual molecules, *G* is formulated starting from the partial pressure of a pure gas for each of the constituent molecules. On the other hand, crystalline ionic solid solutions do not contain molecules and must be handled quite differently (the customary approach for simple examples will be briefly reviewed in section 2.5). Even the standard states commonly used are different: gases are traditionally referred to a standard state of the pure ideal gas at one bar and the temperature of interest, whereas for many kinds of condensed phases the standard state is commonly taken as the pure substance at the temperature and pressure of interest. At the same time, since there is no difficulty with using different thermodynamic formulations for different kinds of phases in the same problem, it is appropriate to use a model specifically designed for the chemical properties of the phase of interest.

The particular way chosen to formulate the Gibbs free energy of a condensed phase will depend on the nature of that phase. This is because different kinds of condensed phases follow fundamentally different constraint rules governing how their chemical compositions vary. The constraint rules governing complex silicate and oxide crystalline ionic solid solutions (i.e. CISS[1]) are:

[1] Throughout the rest of this chapter the abbreviation CISS is used to indicate 'complex silicate and oxide crystalline ionic solid solutions'.

Stoichiometry

The crystal structures of CISS phases define a number of sublattices, which fix the number of sites per formula unit[2] occupied by atoms of a certain kind.

Charge balance

Charge balance between cations and anions (in rock-forming minerals the latter are overwhelmingly O^{2-}, but also OH^-, F^-, CO_3^{2-}, etc.) appears to be strictly maintained in silicate and oxides of geological interest, assuming integral ionic charges corresponding to simple formal valence states (e.g. 4+ for Si, 3+ for Al, 2+ for Ca and Mg, etc.). Some elements exist in two or more oxidation states, but in formulating the thermodynamics of geological crystalline solutions these different states are treated as though they are different entities. For example, Fe is found in two oxidation states in silicates and oxides, Fe^{2+} and Fe^{3+}, and these cations are assumed to have separate identities like Mg^{2+} and Al^{3+} respectively, except, of course, that redox reactions can be written between components in which they occur. This fixity of formal valence as integers is despite excellent evidence from many sources that the electron distribution in such silicates and oxides is usually a long way from the ionic ideal (e.g. Brown, 1992).

It needs to be acknowledged here that the two types of constraint rules are not always rigorously followed in all known CISS. For example, one exception is the cation vacancies and interstitials in the mineral wüstite ($Fe_{1-x}O$), which need to be handled explicitly (O'Neill et al., 2003). Several common rock-forming minerals have cation vacancies, for example in the A site of amphiboles. To some extent these vacancies might be handled by considering them as a species in their own right; this means that a vacancy can be treated as if it were a 'cation' of zero charge. However, this further complication has not here been explored.

[2] The formula unit is a simplification of the unit cell. It is obtained by taking the number of atoms in the unit cell and dividing by an integer, so as to reduce, somewhat arbitrarily, these numbers to convenient smaller numbers, without losing the structural information needed to define the sublattices.

2.3 'Hierarchy of complexity' of crystalline ionic phases

The total Gibbs free energy of a crystalline phase (G) may be thought of as being made up of three types of contributions: 1) the free energies of its end-member 'constituents', $G^{e\text{-}m}$; 2) the free energy due to an idealized configurational entropy from mixing, $G^{id\text{-}mix}$ (given by the product: $T \cdot S^{id-mix}$); 3) the excess free energy of mixing, G^{ex}. This latter is a 'catch-all' term that in simple examples is primarily related to the difference in molar volumes of the end-member constituents ('size mismatch'), but may include corrections needed by simplified formulations of $G^{e\text{-}m}$ and $G^{id\text{-}mix}$, as well as other chemical bonding contributions apart from size mismatch.

These three types of contribution to the free energy are simply additive, so that:

$$G = G^{e\text{-}m} + G^{id\text{-}mix} + G^{ex} \tag{2.2}$$

This additivity enables each term to be considered independently for the purposes of erecting a solution model. This is not to say that the various physical contributions act independently; clearly they do not. It also means that the contributions to the chemical potential[3] of any component i, μ_i, can be similarly split up:

$$\mu_i = \mu_i^{e-m} + \mu_i^{id-mix} + \mu_i^{ex} \tag{2.3}$$

where:

$$\mu_i \equiv \left(\frac{\partial G}{\partial n_i} \right)_{T,P,n_{j \neq i}} \tag{2.4}$$

$$\mu_i^{e-m} \equiv \left(\frac{\partial G^{e-m}}{\partial n_i} \right)_{T,P,n_{j \neq i}} \tag{2.5}$$

$$\mu_i^{id-mix} \equiv \left(\frac{\partial G^{id-mix}}{\partial n_i} \right)_{T,P,n_{j \neq i}} \tag{2.6}$$

$$\mu_i^{ex} \equiv \left(\frac{\partial G^{ex}}{\partial n_i} \right)_{T,P,n_{j \neq i}} \tag{2.7}$$

[3] A comprehensive discussion on meaning and relevance of chemical potentials in the thermodynamic modeling of crystalline, ionic phases is given in section 3.2.

For the purposes of this discussion, it is useful to classify crystalline ionic phases according to a 'hierarchy of complexity' in four different levels.

Level-1: pure phases with invariant composition

A good example in nature is quartz, which closely approaches pure SiO_2 in composition. Of course, no phase is ever completely pure, but the significance of its departure from purity depends on the context. Small deviations from stoichiometry (e.g. in SiO_2, from the exact 2:1 ratio of O to Si) or small amounts of other elements (in quartz, Al or H, for example) may be basic to determining transport properties (e.g. diffusion, rheology, etc.), but generally have negligible effect on G^{total} as needed for calculating phase equilibria. Context is all-important in choosing the appropriateness of a solution model. The context considered here is that of phase equilibrium calculations only, hence this kind of complexity will not be discussed further. Note that for this type of phases: $G^{id-mix} = G^{ex} \equiv 0$, therefore: $G = G^{e-m}$.

Level-2: simple solutions

These solutions are composed of 'compositionally independent' end-members, the set of which can be defined uniquely and unambiguously. All true binary solid solutions are of this type, as are ternary and higher order solutions in which mixing takes place only on one crystallographic site. The aluminous garnet solid solution $(Ca,Mg,Fe^{2+},Mn)Al_2Si_3O_{12}$ is an example of geological interest. The thermodynamic modeling of this category of crystalline ionic solutions is a mature topic that has been comprehensively treated in many excellent textbooks and review articles (e.g. Guggenheim, 1952; Geiger, 1999).

Level-3: 'classical' reciprocal solid solutions

The next level of complexity occurs when it becomes possible to specify the composition of a solid solution using different sets of end-members. In 'classical' reciprocal solid solutions, different sets of atoms mix compositionally independently of other sets within the stoichiometry rules of the crystal structure. A full discussion of this type of solid solution was given by Wood and Nicholls (1978), who discussed the examples

of $(Mg,Fe^{2+})[Al,Cr,Fe^{3+}]_2O_4$ spinels and $\{Ca,Mg\}[Al,Cr]_2Si_3O_{12}$ garnets. The theory was developed in the field of molten salts (Flood et al., 1954; Blander, 1964; Grjotheim, 1981).

Level-4: reciprocal solutions with the inter-dependent substitutions

There are, however, reciprocal solid solutions in which the different sets of mixing atoms are not fully independent of each other because of charge-balance and stoichiometry constraints. Relatively simple examples involving four end-members (the minimum required to define a reciprocal system) are the solutions between Mg_2TiO_4 - $Fe_2^{2+}TiO_4$ - $MgAl_2O_4$ - $Fe^{2+}Al_2O_4$ spinels, $Mg_2Si_2O_6$ - $Fe_2^{2+}SiO_6$ - $MgAl_2SiO_6$ - $Fe^{2+}Al_2SiO_6$ orthopyroxenes, and $CaMgSi_2O_6$ - $CaFe^{2+}Si_2O_6$ - $Mg_2Si_2O_6$ - $Fe^{2+}Si_2O_6$ clinopyroxenes. Of course most natural ortho- or clino-pyroxenes comprehend both the latter two examples; in fact, the solid-solution behaviour of most pyroxenes, amphiboles, micas and other common rock-forming minerals involves mixing patterns of this type. The remaining part of this chapter will mainly focus on discussing this type of mixing behaviour, since it was not treated by Wood and Nicholls (1978), nor by other discussions of solid solution thermodynamics in the geological literature.

2.4 The experimental database for the mixing properties of CISS

The relative lack of discussion in the literature on the formulation of models for complex solid solutions is undoubtedly at least in part due to the lack of experimental data. Science in an idealized view works by induction, where observations and measurements lead to theories first. However, it is now widely recognized that deductive modes of reasoning may also play a significant role, as must be the case where the observations have not yet reached the point at which they can guide the formulation of a theory. In this section the experimental data on the thermodynamics of CISS are reviewed, with the aim of showing that the deductive reasoning employed in this work is justified.

The simplest examples of solution behaviour, namely those in binary systems are considered. The various methods that have been used to investigate the mixing properties of simple binary CISS can be grouped into six for the purposes of this discussion.

1) Displacement of univariant reactions in T-P space

For example, the reaction:

$$\underset{\text{Garnet}}{Ca_3Al_2Si_3O_{12}} + 2\ \underset{\text{Kyanite}}{Al_2SiO_5} + \underset{\text{Quartz}}{SiO_2} = 3\ \underset{\text{Plagioclase}}{CaAl_2Si_2O_8} \qquad (2.8)$$

has been used as the base reaction to study the binary garnet solid solutions $Ca_3Al_2Si_3O_{12}$ - $Mg_3Al_2Si_3O_{12}$ (Schmid et al., 1978; Wood, 1988), $Ca_3Al_2Si_3O_{12}$ - $Fe_3Al_2Si_3O_{12}$ (Cressey et al., 1978; Koziol, 1990) and $Ca_3Al_2Si_3O_{12}$ - $Mn_3Al_2Si_3O_{12}$ (Koziol, 1990 and 1996). Determining the displacement in pressure relative to the pressure of the univariant curve at which the four phases of the reaction coexist gives the activity of the $Ca_3Al_2Si_3O_{12}$ component in the garnet, i.e.:

$$RT\ ln\, a^{grt}_{Ca_3Al_2Si_3O_{12}} = \int_{P_{univ}}^{P} \Delta V^o(P,T)dP \qquad (2.10)$$

Note that this assumes that the other phases in the reaction do not change composition.

In principle, this approach can give very precise activities that are independent of any assumption regarding the form of the activity-composition relationships. In practice, however, the accuracy is often compromised by the need for a full equation of states for all phases to evaluate $\Delta V^o(T,P)$ as well as knowing the excess volume of mixing in the solid solution (e.g. Cressey et al., 1978). Secondly, the assumption of constant composition and stoichiometry of the other phases is often questionable (e.g. there will be a small amount of $MgAl_2Si_2O_8$ or $FeAl_2Si_2O_8$ components in plagioclase in the example considered), or deviations from the binary in the phase of interest (e.g. Fe^{3+} components in the garnet). Ignoring such minor details introduces systematic errors. Because of the way the data are often fitted, such systematic errors become incorporated into the derived activity-composition relations. As a result, a solution that in truth has a simple form of G^{ex} (i.e. would actually conform well to the simple regular solution model) is made to appear to have a more complex form of G^{ex}.

Moreover, measuring G^{ex} over a range of temperatures gives, in principle, its temperature dependence, hence excess entropies of mixing. (NB Commonly the simplifying

assumption is made that $G^{ex} = H^{ex} - T \cdot S^{ex}$). In practice this often results in wildly inaccurate estimates of excess entropies. There are usually good reasons why an experimental study covers only a certain temperature interval. For example, reaction kinetics may become too sluggish at low temperatures, while at high temperatures defect equilibria become increasingly important. Hence reported measurements at the temperature limits of a study are generally less accurate than can be achieved at an optimum temperature, thus distorting attempts to extract a temperature dependence of the quantity under investigation.

2) *Displacement of univariant redox reactions in μO_2-T space*

Either the chemical potential of oxygen (μO_2) is imposed, for example, by gas-mixing, and the resulting composition of the solid solution determined, or the composition of the solid solution is fixed and μO_2 is measured using an oxygen-specific solid electrolyte (e.g. O'Neill and Pownceby, 1993a and 1993b). Compared to the displacement of univariant reactions in *T-P* space this method has the advantage of not requiring equation-of-state data. A small number of simple solid solutions may be studied very accurately using this approach, for example, NiO-MnO (Pownceby and O'Neill, 1995) and CoO-MnO (Pownceby and O'Neill, 2000); but other seemingly almost as simple solid solutions have given discordant results (e.g. $FeTiO_3$-$MnTiO_3$, as discussed by O'Neill, 1998).

3) *Exchange reactions*

For example, the exchange of Fe^{2+} and Mg between many pairs of minerals has been determined, such as between $(Mg,Fe)_2SiO_4$ olivine and $(Mg,Fe)_2Si_2O_6$ orthopyroxene (von Seckendorff and O'Neill, 1993):

$$\underset{\text{olivine}}{1/2\ Mg_2SiO_4} + \underset{\text{orthopyroxene}}{1/2\ Fe_2Si_2O_6} = \underset{\text{olivine}}{1/2\ Fe_2SiO_4} + \underset{\text{orthopyroxene}}{1/2 Mg_2Si_2O_6} \qquad (2.11)$$

The equilibrium constant, *K*, for the reaction is therefore:

$$K = \left(\frac{a^{ol}_{Mg_2SiO_4} \cdot a^{opx}_{Fe_2Si_2O_6}}{a^{ol}_{Fe_2SiO_4} \cdot a^{opx}_{Mg_2Si_2O_6}} \right)^{\frac{1}{2}} = \left(\frac{X^{ol}_{Mg} \cdot X^{opx}_{Fe}}{X^{ol}_{Fe} \cdot X^{opx}_{Mg}} \right) \cdot \left(\frac{\gamma^{ol}_{Mg} \cdot \gamma^{opx}_{Fe}}{\gamma^{ol}_{Fe} \cdot \gamma^{opx}_{Mg}} \right) = K_D \cdot K_\gamma \qquad (2.12)$$

Note that the formulation of K_D already contains an important implicit assumption, which is that in both the olivine and orthopyroxene solutions the ideal configurational entropy corresponds to mixing on two sites per formula unit.

Since K is constant at constant temperature and pressure, studying the variation of K_D with composition gives information on the activity-composition relations (i.e. K_γ). As exchange reactions generally involve small amounts of free energy they are sensitive to the activity-composition relations. An advantage of the method is that K_D can be studied isothermally and isobarically, and this may be done at different temperatures and pressures, giving a test for internal consistency. However, it is the 'ratio' of the activities of both components of each solid solution that the method measures, that is, the ratios $\frac{a^{ol}_{Mg_2SiO_4}}{a^{ol}_{Fe_2SiO_4}}$ and $\frac{a^{opx}_{Mg_2Si_2O_6}}{a^{opx}_{Fe_2Si_2O_6}}$. This means that a form for the activity-composition relations needs to be assumed in order to carry out the data fitting, making the method less transparent for testing the merits of a particular model compared to the methods based on the displacement of univariant equilibria. Conversely, many of the possible deviations from true binary behaviour affect both components and will therefore tend to cancel out, so that errors from this source may be less.

A more severe limitation is that it turns out that the variation of K_D with composition is sensitive mainly to the difference in the mixing properties of the two solid solutions. Although this has been known for at least thirty years (Matsui and Nishikawa, 1974), just how severely this affects the reliability of the extraction of mixing properties continues to be underestimated (see von Seckendorff and O'Neill, 1993, for a detailed discussion the olivine-orthopyroxene example). For pairs of binary solid solutions, this means that the method can only ever give reliable results if the mixing properties of one solid solution are known a priori.

The complications caused by handling two phases at once might in principle be circumvented by making the two components of one of the phases dilute solutes in an inert solvent. A number of studies have been done using the exchange of cations between a solid

solution and aqueous chloride solution at high temperatures and pressures. For example, Orville (1972) used the exchange of Na and Ca between $NaAlSi_3O_8$-$CaAl_2Si_2O_8$ plagioclases and dilute chloride solution:

$$\underset{\text{plagioclase}}{2\ NaAlSi3O_8} + \underset{\text{aqueous}}{CaCl_2} = \underset{\text{plagioclase}}{CaAl_2Si_2O_8} + \underset{\text{aqueous}}{2\ NaCl} + \underset{\text{quartz}}{4\ SiO_2} \qquad (2.13)$$

The idea is that in dilute chlorite solution the activities of both NaCl and $CaCl_2$ obey Henry's law and are as first approximation not a function of concentration. Whether this is always true in chloride exchange experiments has been questioned (Bartholomew, 1989; Uchida et al., 1996). Moreover, Debye-Hückel theory shows that the mean activity coefficient even in very dilute solutions is a function of the ionic strength and therefore a function of the Na^+/Ca^{2+} ratio.

4) *Solvus and miscibility gap determinations*

Well-known examples include the alkali feldspar solvus on the join $NaAlSi_3O_8$-$KAlSi_3O_8$ and the miscibility gap between orthopyroxene and clinopyroxene in the join $Mg_2Si_2O_6$-$CaMgSi_2O_6$, both of which have been determined to very high accuracy in several studies (the latter also in this work, see chapter 5). Another example is the solvus in the spinel join $FeAl_2O_4$-Fe_3O_4, an experimental classic (Turnock and Eugster, 1962). Solvi can be considered a subset of exchange reactions, but with the exchange occurring between two compositions of the same phase, hence the problem of simultaneously determining activity-composition relations in two phases does not arise. However, since only two compositions along the *G-X* curve are present at any one *T-P* condition, a solution model must be assumed. On the other hand, the calculation of a miscibility gap such as between orthopyroxene and clinopyroxene in the join $Mg_2Si_2O_6$-$CaMgSi_2O_6$ requires two continuous activity-composition relationships, one for each structure, and additional information about the Gibbs fee energy differences of the end-members.

5) *Calorimetric data*

These data differ from the phase-equilibrium data in that they measure integral properties (ΔH^{mix} and ΔS^{vib}) rather than the partial differential property $\partial G/\partial n$. Heats of

solution data are available for a number of solutions, both from high-temperature oxide melt calorimetry and from near room-temperature hydrofluoric (HF) acid solution calorimetry (summarized in Geiger, 2001, his Table 3). Such data are typically an order of magnitude less precise than phase-equilibrium measurements, but are particularly valuable when used in conjunction with phase-equilibrium data for constraining 'short-range' order models for the configurational entropy of mixing (see also section 2.5.2). Low-temperature heat capacities, from which excess vibrational entropies of mixing may be determined, have been measured for just two CISS: $Mg_3Al_2Si_3O_{12}$-$Ca_3Al_2Si_3O_{12}$ garnets (Haselton and Westrum, 1980) and $NaAlSi_3O_8$-$KAlSi_3O_8$ alkali feldspars (Haselton et al., 1983).

6) *Investigation of natural paragenesis*

Many studies have attempted to extract thermodynamic mixing data from natural paragenesis (e.g. Ganguly and Kennedy, 1974, on garnets; Wood and Nicholls, 1978, on reciprocal effects in garnets and spinels; Sack, 1980, on olivines). The advantage of looking at natural samples is that a rock may have had millions of years to equilibrate, aided by high strain and/or fluids to promote recrystallization. Consequently, equilibrium may be established at temperatures well below those at which equilibrium could be achieved in the laboratory, enabling phenomena like unmixing across a solvus to be observed, which would not be accessible in the laboratory. The idea is that a metamorphic rock can be considered as natural phase equilibrium experiment, requiring only that the pressure and temperature of equilibration be deduced, perhaps from geothermobarometry applied to a subsystem of the rock. Where these attempts can be compared to experimental work, the results have often been disappointing. There are two obvious problems: firstly, most metamorphic rocks actually record a *T*-*P*-time path in their phase assemblages, rather than a unique *T*-*P* of equilibration; secondly, with rocks being natural systems, the thermodynamic model is often oversimplified, such that the effects of unaccounted components introduce systematic errors, which appear in the activity-composition relations as there is no other place for them, mathematically, in the model. As noted above in the discussion on experiments, the usual result is to make simple behaviour for G^{ex} look more complicated.

2.4.1 Strategies for the fitting of experimental data

The scarcity of unambiguous, precise experimental data on the thermodynamic properties of even binary CISS has allowed a range of world views to flourish on what their typical properties are, and consequently on what strategies are optimal for fitting the data. The two extreme world views are here summarized.

a) Mixing properties follow an essentially simple pattern, such that they can be adequately described using ideal entropies of mixing, unless order-disorder effects are important. Accordingly, G^{ex} is well described by a regular or subregular formalism (i.e. one or two 'W' parameters, adopting the Margules formalism, see section 2.5.1). The most important contribution to G^{ex} is size mismatch, and where this mismatch is modest the asymmetry in the mixing properties is negligible. Asymmetry (requiring the subregular model, see also Helffrich and Wood, 1989) occurs only when there is a large difference in ionic radius of the mixing cations, as in the mixing of Ca and Mg in the joins $CaMgSi_2O_6$-$Mg_2Si_2O_6$ clinopyroxenes or $Ca_3Al_2Si_3O_{12}$-$Mg_3Al_2Si_3O_{12}$ garnets, but nevertheless the extent of asymmetry is small. This view is concordant with that expressed in Onuma diagrams of trace-element partitioning relations (Blundy and Wood, 1994; Allan et al., 2001). Non-configurational entropies of mixing are also small, except where long-range ordering is incorporated into the G^{ex} term. The reasons for reports of large asymmetries or non-configurational entropies could be inadequate models or poor statistical fitting procedures, but also, importantly, failing to account for all the experimental imperfections as reviewed above, since the errors and misplaced assumptions in the entire thermodynamic model often get squeezed artificially into the last step of the model, the excess mixing properties.

b) Opposing this, is the view that fundamental thermodynamic theory imposes few constraints on mixing properties, beyond simple algebraic ones like the Gibbs-Duhem relation. Hence mixing properties may well exhibit complicated forms as a function of composition, with large asymmetries across a binary solid solution. Theoretical support comes from models in which there is a difference between the dilute compositional regions of a solid solution, where the strain fields around a substituting cation can relax completely,

and the middle regions of the solid solution where strain fields interact (e.g. Hayward and Salje, 1996). This might be modelled empirically using separate formulations for the different regions, which are not constrained to follow the Gibbs-Duhem relationship across the entire solid solution. This was argued by Darken (1967) for metal alloys and has been advocated for CISS by Powell (1987) (see also Powell and Holland, 1993).

2.5 Modeling of simple crystalline ionic solid solutions: the binary solution case

Since any complex solid solution can be considered to be bounded by a set of binary solid solutions, the formulation for the thermodynamics of the complex solid solution must reduce to that for a binary at the appropriate composition. A thorough understanding of binary solid solution thermodynamics is thus an essential prerequisite. In this section the most important features of binary solid solution thermodynamics for CISS are reviewed.

2.5.1 Derivation of G and μ in a simple case

A useful specific example among oxides is NiO-MnO (Pownceby and O'Neill, 1995). In this example, the contribution to G from the free energies of its end-member 'constituents' NiO and MnO, $G^{e\text{-}m}$, is given by a linear combination of their free energy of formation, $\Delta_{f,el}G°$(NiO) (i.e. G^{o-NiO})and $\Delta_{f,el}G°$(MnO) (i.e. G^{o-MnO}), thus:

$$G^{e-m} = X_{NiO}G^{o-NiO} + (1 - X_{NiO})G^{o-MnO} \qquad (2.14)$$

where, X_{NiO} is the mole fraction of NiO end-member.

The standard state is taken as the pure elements in their usual form at the temperature of interest and 1 bar pressure (i.e. Ni and Mn metals; O_2 gas).

The free energy from the ideal configurational entropy of mixing, $G^{id\text{-}mix}$, for simple solutions like this one, is in general given by (e.g. Chatterjee**,** 1991):

$$G^{id-mix} = T \cdot S^{id-mix} = -RT \cdot \sum_{i=1}^{t} X_i \, ln(X_i) \qquad (2.15)$$

where, t is the total number of end-members.

In this case it will be:

$$G^{id-mix} = -RT \cdot \left[X_{NiO}\, ln\, X_{NiO} + (1 - X_{NiO}) ln(1 - X_{NiO}) \right] \quad (2.16)$$

For a binary solid solution A-B, G^{ex} is generally formulated as a polynomial in powers of the mole fraction of one end-member, X_A. The constraint that G^{ex} must by definition go to 0 as X_A goes to both 0 and 1 requires that the polynomial has the general form:

$$G^{ex} = X_A (1 - X_A) \cdot \left[a_0 + a_1 X_A + a_2 X_A^2 + ... + a_n X_A^n \right] \quad (2.17)$$

Truncation at the first term gives rise to the simplest possible form, the 'regular solution'. Setting $a_0 \equiv W_{A-B} \equiv W_{B-A} \equiv W$, gives:

$$G^{ex} = X_A (1 - X_A) \cdot W \quad (2.18)$$

Including the next term is equivalent to a 'subregular solution'. This is generally written (Margules formalism, e.g. Grover, 1977):

$$G^{ex} = X_A (1 - X_A) \cdot (W_{A-B} X_B + W_{B-A} X_A) \quad (2.19)$$

where, W_{A-B} , W_{B-A} , are the so called Margules parameters.

Extension of this expression to multicomponent solutions is given in Helffrich and Wood (1989).

However, there are a number of different variations on how the polynomial is presented once it is expanded beyond the first term. A convenient way is the Redlich-Kister formalism (Redlich and Kister, 1948):

$$G^{ex} = X_A (1 - X_A) \cdot \left[A_0 + A_1 (2X_A - 1) + A_2 (2X_A - 1)^2 + ... + A_n (2X_A - 1)^n \right] \quad (2.20)$$

This is much used in the metallurgical literature (Hillert, 1998). Its advantages include a ready means (algebraically speaking) of extrapolating from binary solutions into multicomponent space (Hillert, 1998, p. 464). Truncation of the series at the first term

makes this formalism equivalent to the regular solution formalism with A_0 equivalent to $W_{A\text{-}B}$, and truncation at the second term is equivalent to the subregular formalism.

The effects of temperature on all formalisms for G^{ex} are easily accommodated by splitting up the parameters in the power series into temperature- and pressure- dependent terms, for example:

$$W_G = W_H + T \cdot W_S + P \cdot W_V \tag{2.21}$$

where:

$$W_S = \frac{\partial W}{\partial T} \tag{2.22}$$

$$W_V = \frac{\partial W}{\partial P} \tag{2.23}$$

For the NiO-MnO example, the experimental data are fit very well using a simple ideal configurational entropy of mixing and a two-term Redlich-Kister equation, with $A_0 = [11483 - (1.697) \cdot T]$ J/mol and $A_1 = -477$ J/mol (Pownceby and O'Neill, 1995). Such a result conforms with expectations in that the magnitude of G^{ex} is in excellent agreement with that expected from simple lattice strain theory (e.g. Urusov, 2001), while both the extent of asymmetry (the A_1 term) and the excess entropy (W_S) are small. This result is particularly important as of all binary CISS, NiO-MnO is experimentally the easiest for which to determine the mixing properties.

The calculation of chemical potentials for the NiO component gives[4]:

$$\mu_{NiO}^{e-m} \equiv (n_{NiO} + n_{MnO}) \cdot \left(\frac{\partial G^{e-m}}{\partial n_{NiO}} \right)_{T,P,n_{MnO}} = G^{o-NiO} \tag{2.24}$$

$$\mu_{NiO}^{id-mix} \equiv (n_{NiO} + n_{MnO}) \cdot \left(\frac{\partial G^{id-mix}}{\partial n_{NiO}} \right)_{T,P,n_{MnO}} = RT \ln X_{NiO} \tag{2.25}$$

[4] Only final derivations are here reported. A more detailed example of calculation of chemical potentials is presented in Appendix 3A.

$$\mu_{NiO}^{ex} \equiv \left(n_{NiO} + n_{MnO}\right) \cdot \left(\frac{\partial G^{ex}}{\partial n_{NiO}}\right)_{T,P,n_{MnO}} = \left(1 - X_{NiO}\right)^2 \cdot \left[A_0 + A_1\left(4X_{NiO} - 1\right)\right] \quad (2.26)$$

Hence:

$$\mu_{NiO} = G^{o-NiO} + RT\, ln\, X_{NiO} + \left(1 - X_{NiO}\right)^2 \cdot \left[A_0 + A_1\left(4X_{NiO} - 1\right)\right] \quad (2.27)$$

Relationships of this type are often expressed in the form:

$$\mu_i = G^{o-i} + RT\, ln\, X_i + RT\, ln\, \gamma_i \quad (2.28)$$

Hence,

$$\mu_i = G^{o-i} + RT\, ln\left(X_i \cdot \gamma_i\right) \equiv G^{o-i} + RT\, ln\left(a_i\right) \quad (2.29)$$

where γ_i is the activity coefficient, and the product $X_i \cdot \gamma_i$ is the activity, a_i.

If $G^{ex} = 0$, then for these simple binary solid solutions γ_i is obviously equal to 1 and $a_i = X_i$. The solution in such case is said to be 'ideal'.

Another important point here is that μ_i is independent of the free energy of formation of the other component j for these simple binary solutions (e.g. μ_{NiO} is independent of the value of G^{o-MnO}). This is so familiar from the treatment of solid solution properties given in textbooks that it may seem almost tautological. However, it is here argued that these simple solid solutions are special cases, and that, in general, the chemical potential of an end-member in a multicomponent, multisite solid solution is not independent of the free energies of formation of the other end-members (see section 2.6).

The above relations are easily extended to solutions in which mixing occurs over more than one site per formula unit (e.g. mixing of Ca and Mg on the dodecahedral site of garnet, $\{Ca,Mg\}_3Al_2Si_3O_{12}$). The entropy of mixing of the solid solution becomes:

$$S^{id-mix} = -R \cdot \sum_{i=1}^{t} X_i\, ln\left(X_i\right)^n \quad (2.30)$$

where n is the number of sites per formula unit over which the mixing takes place (e.g. $n = 3$ in the Ca-Mg garnet example).

Hence:

$$\sum_{i=1}^{p} n_i \cdot \left(\frac{\partial G^{id-mix}}{\partial n_i} \right)_{T,P,n_{j \neq i}} = nRT \ln X_i \qquad (2.31)$$

If $G^{ex} = 0$, then $a_i = \left(X_i\right)^n$.

2.5.2 Short range order

Although the evaluation of the configurational entropy (Eq. 2.30) from statistical thermodynamics now seems obvious for simple ionic crystals, there are alternative possibilities. Historically, the problem of how to model the configurational entropy of a solid solution first seems to have been treated explicitly in the geological literature by Bradley (1962) who considered mixing in $(Mg,Fe)_2SiO_4$ olivines (under the implicit assumption that the two different octahedral sites could be treated as though they were identical). The alternative possibility discussed by Bradley (1962), which had been earlier used by Bowen and Schairer (1935), was that mixing in $(Mg,Fe)_2SiO_4$ olivine involves 'molecular species' with the formulae Mg_2SiO_4 and Fe_2SiO_4, such that $a^{ol}_{Mg_2SiO_4} = X_{Mg}$, rather than $(X_{Mg})^2$.

Despite the fact that there is now unambiguous experimental evidence that solid solutions in which the mixing is one of cations with the same valence, like Mg and Fe^{2+} in olivine, or Ca and Mg in garnet, do mix as in the ionic model, there are many geologically important solid solutions involving coupled substitutions, in which the 'molecular species' approach turns out to be the more appropriate way to model the entropy of mixing. Kerrick and Darken (1975) discuss four different possibilities for the $CaAl_2Si_2O_8$ – $NaAlSi_3O_8$ plagioclase solid solution. There is much experimental evidence to show that in the orthopyroxene solid solution between $Mg_2Si_2O_6$-$MgAl_2SiO_6$ the entropy of mixing is better approximated by mixing on one site (Wood and Banno, 1973; Klemme and O'Neill, 2000).

This can be rationalized as a very high degree of short-range order due to a requirement for local charge balance in the crystal structure.

Unfortunately, whereas long range order can be studied by standard diffraction methods, short range order is amenable only by techniques that investigate nearest neighbour effects. Furthermore, results are not sufficiently accurate for quantitative thermodynamic purposes, although they may be very useful in guiding thermodynamic modeling. At present, however, short-range order is accounted for empirically in the G^{ex} term from the difference between the measured total free energy G of a solid solution and that calculated from G^{id-mix}.

2.5.3 Long range order

Using Eq. (2.30) to calculate the contribution of the configurational entropy to the free energy of mixing is possible only for quite simple crystal structures in which the substituting atoms mix only on one crystallographic site (like garnet). Most of the common rock-forming minerals have crystallographically distinct sites over which cations of similar size are distributed non-randomly. A simple example is the much studied $(Mg,Fe)_2Si_2O_6$ orthopyroxene binary (e.g. Mueller, 1962; Thompson, 1969, 1970; Ganguly, 1986; Shi et al., 1992; Strimpfl et al., 1999). The orthopyroxene crystal structure contains two geometrically distorted octahedral sites, conventionally labelled M1 and M2, over which Mg and Fe are distributed non-randomly, with Fe preferring the larger and more distorted M2 site. The degree of long-range ordering can be described using an order parameter, *s*, which must be defined relative to a standard state. In the $(Mg,Fe)_2Si_2O_6$ orthopyroxene solution the two end-members are completely ordered (i.e. $Mg_2Si_2O_6$ and $Fe_2Si_2O_6$). For this type of solutions, the standard state is taken as complete disorder, that is, random mixing of the cations. It is then possible to define for the purposes of a reference an ideal entropy of mixing $S^{id\text{-}mix}$ as that due to random mixing on the total number of sites per formula unit.

The free energy of the solid solution can then be formulated as a function of both *s* and composition, x_{Mg} (where, $x_{Mg} = \dfrac{n_{Mg_2Si_2O_6}}{n_{Mg_2Si_2O_6} + n_{Fe_2Si_2O_6}}$ and $n_{Mg_2Si_2O_6}$ and $n_{Fe_2Si_2O_6}$ are the number of moles of $Mg_2Si_2O_6$ and $Fe_2Si_2O_6$ in solution), by writing the configurational

entropy as in Eq. (2.34), with site occupancies defined as a function of s and x_{Mg}, and the total non-configurational free energy of the solid solution as a power series in s and x_{Mg} (cf. Thompson, 1969):

$$G^{mix} = -T \cdot S^{config} + G^{o-d} + G^{ex} \tag{2.32}$$

where:

$$G^{o-d} = s \cdot \left(a_0 + a_{1,0}s + a_{1,1}s \cdot x_{Mg} + a_{2,0}s^2 \cdot x_{Mg} + ...\right) \tag{2.33}$$

For non-convergent ordering there is no restriction on the terms in s (e.g. Thompson, 1969; Carpenter, 1994).

The configurational entropy S^{config} is given in the usual way (e.g. Ganguly and Saxena, 1987):

$$S^{config} = -R\left(\sum_{\zeta}\sum_{i} n_{\zeta} X_i^{\zeta} \ln X_i^{\zeta}\right) \tag{2.34}$$

where, the summation is over all species i ('ions') on each crystallographically distinct site, ζ; X_i^{ζ} is the fraction of i in site ζ and n_{ζ} the total number of sites ζ per formula unit. (Note that for crystals with only one type of site or for random mixing, S^{config} is of course identical to $S^{id\text{-}mix}$).

The excess free energy of mixing G^{ex} then accounts for those contributions to lattice strain effects, etc., that are independent of s, and may also be given in the usual ways; for example, by applying the Margules formalism as in Helffrich and Wood (1989).

At internal equilibrium G is at a minimum with respect to the state of order-disorder (i.e. $dG/ds = 0$). If the parameters in the power series for $G^{o\text{-}d}$ are known, the value of s can be calculated at a given value of x_{Mg}. This value of s can then be substituted back into Eq. (2.33) to calculate the contribution to the free energy of mixing from the non-configurational entropy, $G^{o\text{-}d}$ (a mathematically more elegant but conceptually perhaps less

transparent way of doing this in one step has been given by Ghiorso, 1991, and Holland and Powell, 1996, their Appendix 1). The terms in $G^{o\text{-}d}$ can be constrained, in principle, by studying the order-disorder as a function of temperature and composition. However, it is important to note that there may be terms in G that do not contain s, which are written here as G^{ex}; these terms obviously disappear in the differential dG/ds, hence the condition $dG/ds = 0$ contains no information on these terms. Thus knowledge of the cation distribution as a function of temperature and composition cannot alone constrain the activity-composition relations of the solid solution.

Where the terms without s are large compared to the terms in s, the contribution from order-disorder may have only a minor effect on the thermodynamic mixing properties at high temperatures. This seems to be the case in many spinel solid solutions. The thermodynamic properties of several binary spinel solid solutions involving the mixing of 3^+ cations (or charge-balanced $2^+ + 4^+$ cations such as in the Fe_2TiO_4-Fe_3O_4 binary) have been measured, including those both with and without significant cation order-disorder, which allows an assessment of the relative importance of this factor compared to lattice strain energies. These data show that the size mismatch between the substituting cations is by far the most important factor contributing to the net deviations from an ideal mixing model, and this factor can be modelled independently of the cation order-disorder effect using a regular solution parameter (O'Neill and Navrotsky, 1984; see particularly their Fig. 14 in which the regular solution parameter $W_{A\text{-}B}$ is plotted against a volume mismatch term for 3^+ and (2^++4^+) cations).

Historically, the view that the order-independent mixing terms may exist has not been universally accepted, and several early studies have in fact sought to constrain macroscopic thermodynamic mixing properties from cation order-disorder measurements, particularly in $(Mg,Fe)_2Si_2O_6$ orthopyroxenes (Mueller, 1962; Saxena, 1973). This may be because it is difficult to justify the order-independent terms if one views the excess mixing in solid solutions as due to A-B type 'interactions' of the type described in section 2.5.4. But this is not a problem if the excess energy of mixing is viewed instead mainly due to lattice strain, as it is here argued to be more appropriate for ionic crystals.

As emphasised by Thompson (1969, 1970) and Sack (1980), the contribution to the free energy of mixing from order-disorder comes in two parts, that is, from both the

$T \cdot S^{config}$ and $G^{o\text{-}d}$ terms. An important general point is that the two quantities $T \cdot \left(S^{config} - S^{id-mix}\right)$ and $G^{o\text{-}d}$ are opposite in sign and thus tend to cancel each other out, increasingly so with increasing temperature. For solid solutions in which the order-disorder does not occur in the end-members, as in $(Mg,Fe)_2Si_2O_6$ orthopyroxene, $S^{config} < S^{id\text{-}mix}$, hence the contribution of this term to G^{ss} (where, here, $G^{ss} = G^{mix} - G^{ex}$) is such as to produce positive deviations from ideality, while the ordering energy $G^{o\text{-}d}$ produces negative deviations. If $G^{o\text{-}d}$ has a simple form in the order parameter, s, (i.e. only the a_0 term in Eq. 2.33 is important), then $G^{o-d} > -T \cdot \left(S^{config} - S^{id-mix}\right)$ and the net result is that the solution has negative deviations from ideality (NB In the absence of a contribution from G^{ex}). For solutions in which the end-members also show order-disorder phenomena (like spinels, see O'Neill and Navrotsky, 1984), this simple relationship does not hold, but nevertheless the tendency for $G^{o\text{-}d}$ to compensate for the difference between $T \cdot S^{config}$ and $T \cdot S^{id-mix}$ remains a general conclusion. Hence a better approximation, at least at high temperatures, is achieved by simply ignoring long-range ordering between sites, than by taking the $T \cdot S^{config}$ alone, without the compensating $G^{o\text{-}d}$ term.

Secondly, the appearance of rigour conferred by explicitly considering long-range order wears thin when the problems of extrapolating such models into multicomponent solid solutions have to be confronted. In the case of $(Mg,Fe)_2Si_2O_6$ orthopyroxenes, for example, nothing is known about the effects of other components, such as Al_2O_3, on ordering. Neutron diffraction measurements on $Mg_2Si_2O_6$-$MgAl_2SiO_6$ orthopyroxenes show that Al is actually considerably disordered between the two octahedral sites M1 and M2 and not confined to the smaller M1 site (S.A.T. Redfern and H.St.C. O'Neill, personal communication), but unlike Mg-Fe^{2+} order-disorder, this has never been taken into account in thermodynamic modeling. Indeed, what is modelled in solid solution formalisms that include effects of order-disorder is always incomplete and is usually quite arbitrary.

In summary, the explicit modeling of order-disorder in multicomponent solid solutions greatly increases the complexity level, for little gain in accuracy to which the mixing properties can be represented. Moreover, only a few of the important bounding binary joins in the common-rock-forming solid solutions have been studied for order-disorder. For example, in orthopyroxenes the join $Mg_2Si_2O_6$-$Fe_2Si_2O_6$ has been studied to

exhaustion (e.g. Strimpfl et al., 1999), but the exact relationship between order-disorder and the macroscopic free energy of mixing still remains contested (Aranovich, 2004).
Therefore, in this work it is proposed to model solid solutions with long-range order in one of two ways:

1) where disordering is extensive, as in $(Mg,Fe)_2Si_2O_6$ orthopyroxenes or in the various spinel solid solutions reviewed in O'Neill and Navrotsky (1984), it is essentially ignored, modeling an ideal entropy of mixing using the appropriate number of sites per formula unit. The difference is then accounted for entirely empirically in the G^{ex} term.

2) where ordering is almost complete, as in $(Ca,Mg)_2Si_2O_6$ pyroxenes, $(Ca,Mg)_2SiO_4$ olivines, or low-temperature $(Ca,Mg)CO_3$ carbonates, end-members are defined at the perfectly ordered composition, in these examples at $CaMgSi_2O_6$, $CaMgSiO_4$ and $CaMg(CO_3)_2$ respectively.

Accordingly, when deriving G expressions for complex solutions, the simplified assumption that $S^{config} \equiv S^{id}$ (i.e. $G^{o\text{-}d} = 0$) has been made and to express $G^{id\text{-}mix}$ Eq. (2.70) has been used. This implies that cations of a like charge and size (e.g. Mg and Fe^{2+}, or Al, Cr and Fe^{3+}) are assumed to partition randomly between the sites they occupy. Thus, the site occupancies X_{ik}'s that appear in Eq. (2.70) (and also in Eq. 2.71) should more properly be called 'virtual' site occupancies, since they are defined without taking into account order-disorder phenomena. Similarly sites they occupy should be called 'virtual' sites (see also section 2.8 and section 3.4).

Results presented in chapter 4 and chapter 5 of this thesis attest the validity of this approach.

2.5.4 Contributions to the excess free energy of mixing (G^{ex})

At one level, Eq. (2.18) can be viewed as a purely empirical way of representing experimental data, with no phenomenological implications. However, Eq. (2.18) can also be given a physical basis. One way to do this is to consider interaction energies between A and B in the solid solution (e.g. Putnis, 1992, pp. 277-278). The energy of interaction between nearest-neighbour A-A, B-B and A-B pairs is w_{A-A}, w_{B-B} and w_{A-B} respectively. Now, the probability of an A-A nearest neighbour pair occurring in the crystal structure is

X_A^2, of a B-B pair is X_B^2 (NB $X_B = 1 - X_A$), and of a A-B pair is $2X_B X_A$. Hence the total energy, *I*, due to the sum of interactions per mole is:

$$I = \frac{1}{2} z\mathrm{N} \cdot \left(\mathrm{w}_{\mathrm{A\text{-}A}} X_A^2 + \mathrm{w}_{\mathrm{B\text{-}B}} X_B^2 + 2\mathrm{w}_{\mathrm{A\text{-}B}} X_A X_B \right) \tag{2.35}$$

where, *z* is the number of nearest neighbours and N is Avogadro's number.

The energy of pure A and B are $\frac{1}{2} z\mathrm{N} \cdot \left(\mathrm{w}_{\mathrm{A\text{-}A}} \right)$ and $\frac{1}{2} z\mathrm{N} \cdot \left(\mathrm{w}_{\mathrm{B\text{-}B}} \right)$ respectively, hence the excess energy of the solid solution relative to a 'mechanical mixture' of the end-members is:

$$G^{ex} = \frac{1}{2} z\mathrm{N} \cdot \left(2\mathrm{w}_{\mathrm{A\text{-}B}} - \mathrm{w}_{\mathrm{A\text{-}A}} - \mathrm{w}_{\mathrm{B\text{-}B}} \right) X_A X_B \tag{2.36}$$

Comparison with Eq. (2.18) shows that:

$$W_{A-B} = \frac{1}{2} z\mathrm{N} \cdot \left(2\mathrm{w}_{\mathrm{A\text{-}B}} - \mathrm{w}_{\mathrm{A\text{-}A}} - \mathrm{w}_{\mathrm{B\text{-}B}} \right) \tag{2.37}$$

Although this phenomenology reproduces the algebra of the regular solution formalism, it seems doubtful if such 'interactions' have any physical basis in ionic solid solutions, where the nearest neighbours of a cation are anions, not the other kind of substituting cation. However, the regular solution formalism can also be derived quite differently, from the simple idea that cations of different size substituting onto the same site in an ionic crystal lattice will cause strain in that lattice. The theory, the basic version of which was originally due to Wasastjerna (1949) (see also Hovi, 1950), has recently been reviewed by Urusov (2000, 2001) and Geiger (2001). It assumes that the energy from compressing (or expanding) a cation of a different size (i.e. ionic radius) substituting into a crystal lattice is at least partially compensated for by the lattice relaxing around that cation. In a simple form of the theory, the excess enthalpy of mixing of a binary solid solution is approximately (Urusov, 2001):

$$H^{ex} = cX_A(1 - X_A)V(\Delta R/R)^2 \quad (2.38)$$

with:

c = constant that depends on crystal structure (e.g. 2.25 for the rocksalt structure)
V = molar volume
ΔR = difference in interatomic distance (i.e. $r_A - r_B$, where r is the ionic radius)
R = interatomic distance.

Davies and Navrotsky (1983) showed empirically that excess enthalpies of mixing are proportional to the difference in the molar volumes, and suggested the relationship:

$$W_{i-j} = k\left|V_i - V_j\right|/\left(V_i + V_j\right) \quad (2.39)$$

The constant k varies for cations or anions of different charges, and for different structures. Urusov (2000, 2001) has pointed out from theoretical considerations that $W_{A\text{-}B}$ should be more nearly proportional to the square of the volume difference, which is supported by more recent measurements (Geiger, 2001). This general approach has received a considerable boost over the last decade from studies of trace-element partitioning between crystals and silicate melt (Blundy and Wood, 1994 and 2003). These studies have looked at the systematics of different cations with the same charge mixing within a given crystal structure (e.g. as in the Onuma diagrams of mineral/melt trace-element partitioning). This leads to the working hypothesis that the excess free energies of mixing due to strain should be quite small among sets of like cations (e.g. the divalent cation set Mg, Fe^{2+}, Mn, Ni; or the trivalent set Al, Cr, Fe^{3+}) in complex ionic solid solutions compared to the simple oxides.

In principle, effects other than strain may contribute to G^{ex}. These include differences in the degree of covalency of the bonding between the end-members. Not much appears to be known about this in the context of oxides and silicates, though covalency effects may be important in explaining the anomalous mixing properties of solid solutions involving second- and third-row transition–metal cations with incompletely-filled d-shells

(e.g. the Platinum Group Elements), which occur in the low-spin configuration. For example, there is only limited solid solution between the rutile-structured oxides TiO_2 and RuO_2 (Hrovat et al., 1996), despite the end-members having almost identical molar volumes.

For transition-element cations another potential contribution is from crystal field effects. The crystal-field stabilization energy (CFSE) is expected to vary as the inverse fifth power of the cation-anion distance (e.g. Burns, 1993; Langer, 2001), hence could potentially change greatly across a solid solution unless compensated by full relaxation. The empirical evidence shows that nearly full relaxation must in fact occur, as crystal-field effects do not contribute significantly to G^{ex} in well-studied cases; for example, in the binaries NiO-MnO (Pownceby and O'Neill, 1995) and Cr_2O_3-Al_2O_3 (Chatterjee et al., 1982), in which crystal-field effects would be among the largest achievable for first-row transition-metal cations, G^{ex} is close to that predicted from lattice strain alone.

2.5.5 Excess non-configurational entropies of mixing

One way of looking at non-configurational (or vibrational) entropies of mixing is to consider the total non-configurational entropy of a solid. In the simplest approximation, the Einstein model, this is given by (e.g. Gopal, 1969):

$$S_E = 3nR\left[\frac{T_E/T}{\exp\{T_E/T\}} - \ln\left(1-\exp\{T_E/T\}\right)\right] \qquad (2.40)$$

This reduces to approximately $3nR$ at $T_E/T = 1$, which for ionic solids is in the temperature regime of interest to the thermodynamics of rock-forming minerals. The Einstein approximation is based on the assumption that heat capacity, hence entropy, derives very simply from lattice vibrations in three dimensions. Considered thus, it would seem unlikely that excess vibrational entropies, which are a result of deviations in the vibrational behaviour of the solid solution compared to its end-members, and are therefore very much second-order effects, should ever amount to more than a modest fraction of R, or a few J/K mol.

Another perspective comes from the theoretical view that excess vibrational entropies should be correlated with excess volumes, for example according to the relation (e.g. Pownceby and O'Neill, 1994):

$$S^{ex} \approx \frac{3nR\gamma V^{ex}}{V} \tag{2.41}$$

where γ is the Gruneisen parameter, which is often about 1 to 2 for crystalline solids.

Molar volumes of CISS can be measured much more easily to high accuracy than other thermodynamic properties (Geiger, 2000), hence quite a lot is known about volume deviations from ideality (i.e. deviations from Vegard's law). Measured values of V^{ex}/V are rarely more than 1%, as in, for example, $NaAlSi_3O_8$-$KAlSi_3O_8$ alkali feldspars (Hovis, 1988) and $Mg_3Al_2Si_3O_{12}$-$Ca_3Al_2Si_3O_{12}$ garnets (Ganguly et al., 1993), leading to the expectation that values of S^{ex} should be not much more than ~ 1 J/K mol.

In conclusion, in this work, to express G^{ex} for any crystalline solution the general equation developed by Helffrich and Wood (1989) is used (see Eq. 2.71). This general equation expands to multicomponent subregualr solid solutions, but also reduces to binary symmetrical solutions.

2.6 Classical reciprocal solutions

A phase is considered in which two crystallographically distinct cation sites, s1 and s2, are occupied by the two different groups of cations (A,B) and [P,Q], respectively (see also Wood and Nicholls, 1978). The general formula of a phase of this type is:

$$^{s1}(A,B)_{n1}{}^{s2}[P,Q]_{n2}X_m \qquad (2.42)$$

where, n1 and n2 represent the number of sites s1 and s2 per formula unit.

Geologically important examples are $^{dod}\{Ca,Mg\}_3{}^{oct}(Al,Cr)_2Si_3O_{12}$ garnets or $^{tet}[Mg,Fe^{2+}]^{oct}(Al,Cr)_2O_4$ spinels (omitting consideration of Mg-Al and Fe^{2+}-Al order-disorder in the latter for the moment).

The compositions of such solutions can be represented by a square in two-dimensional space as in Fig (2.1).

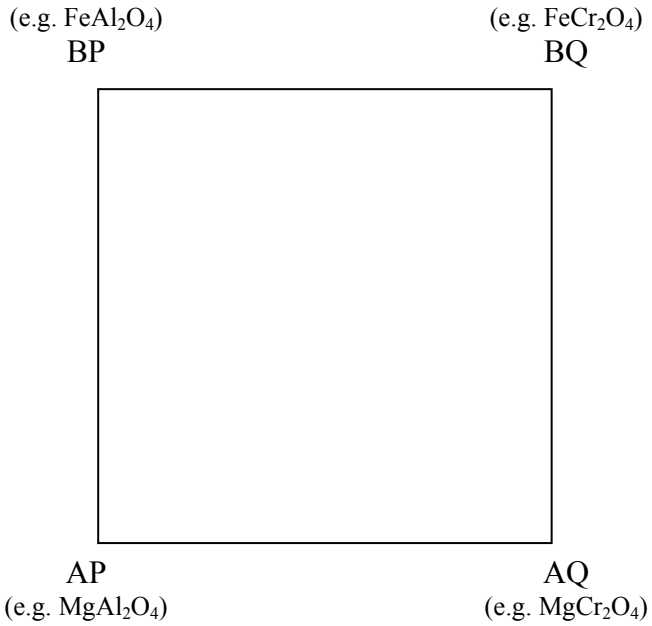

Fig. 2.1 Two-dimension compositional space for a (AP, AQ, BP, BQ) reciprocal solution.

In a three dimensional space, instead, the free energy surface $G^{e\text{-}m}$ is fixed at the corner compositions (i.e. the compositions of the four end-members, which will be referred

to here as AP, AQ, BP and BQ) by the free energies of formation of these end-members, G^{o-AP}, G^{o-AQ}, G^{o-BP} and G^{o-BQ}. Since four points do not generally lie in a plane, the surface must be curved, while coplanarity could occur, but only by coincidence (see Ganguly, 2001, his Fig. 1). This important property means that the tangent from the free energy surface to any of the four end-member compositions, e.g. $\left(\frac{\partial G^{e-m}}{\partial n_{AP}}\right)_{T,P,n_{AQ},n_{BP},n_{BQ}}$, will not in general coincide with G^{o-AP} (as it would be in a simple binary solution). Moreover, $\left(\frac{\partial G^{e-m}}{\partial n_{AP}}\right)_{T,P,n_{AQ},n_{BP},n_{BQ}}$ must obviously depend on the relative positions of G^{o-AQ}, G^{o-BP} and G^{o-BQ}, since these define the curvature of the surface. Multisite reciprocal solutions, therefore, differ in a fundamental way from the simple solutions considered in the previous section, in that the chemical potential of an end-member is not in general independent of the free energies of formation of the other end-members.

An equation describing the $G^{e\text{-}m}$ surface may be constructed as follows. In the context of their respective subsystems, the four binary solid solutions (A,B)P, (A,B)Q, A[P,Q], and B[P,Q] are straightforward examples of the binary solid solutions discussed in the previous section. In each of these binary systems, therefore, $G^{e\text{-}m}$ must be a linear combination of the free energies of formation of the relevant end-members. For example, for (A,B)P:

$$G^{e-m} = X_A^{s1} G^{o-AP} + X_B^{s1} G^{o-BP} \tag{2.43}$$

An equation that reduces to these conditions along the binaries is:

$$G^{e-m} = X_A^{s1} X_P^{s2} G^{o-AP} + X_B^{s1} X_P^{s2} G^{o-BP} + X_A^{s1} X_Q^{s2} G^{o-AQ} + X_B^{s1} X_Q^{s2} G^{o-BQ} \tag{2.44}$$

Here it is proposed that the factors $X_A^{s1} X_P^{s2}$, $X_B^{s1} X_P^{s2}$, etc. be identified as the 'probabilities' associated with the occurrence of a particular end-member in the solid solution (see also Wood and Nicholls, 1978).

The general form for $G^{e\text{-}m}$ for any complex solid solution is then given by:

$$G^{e-m} = \sum_{i}^{m} \Psi^{i} G^{o-i} \tag{2.45}$$

with:

Ψ^{i} = probability of occurrence of end-member *i*

m = total number of possible stoichiometric, charge-balanced end-members that define the compositional limits of the solid solution.

Note that this latter restriction means that in this formulation those end-members defined by order-disorder phenomena are excluded.

Note also that as probabilities the condition is required:

$$\sum_{i}^{m} \Psi^{i} = 1 \tag{2.46}$$

Given Eq. (2.45), the contribution to the chemical potential of an end-member (e.g. AP) is readily obtained (NB Only final derivations are reported):

$$\begin{aligned} \mu_{AP}^{e-m} &\equiv \left(n_{AP} + n_{AQ} + n_{BP} + n_{BQ}\right) \cdot \left(\frac{\partial G^{e-m}}{\partial n_{AP}}\right)_{T,P,n_{AQ},n_{BP},n_{BQ}} \\ &= G^{e-m} + \left(1 - X_{A}^{s1}\right) \cdot \left(\frac{\partial G^{e-m}}{\partial X_{A}^{s1}}\right)_{T,P,X_{P}^{s2}} + \left(1 - X_{P}^{s2}\right) \cdot \left(\frac{\partial G^{e-m}}{\partial X_{P}^{s2}}\right)_{T,P,X_{A}^{s1}} \\ &= G^{o-AP} + \left(1 - X_{A}^{s1}\right)\left(1 - X_{P}^{s2}\right) \cdot \left[G^{o-BP} + G^{o-AQ} - G^{o-BQ} - G^{o-AP}\right] \end{aligned} \tag{2.47}$$

The term inside the square brackets is commonly given as ΔG_{REC}^{o}, since it refers to the free energy of the hypothetical reciprocal reaction:

AP + BQ = AQ + BP (2.48)

The free energy from the ideal entropy of mixing is given, as usual, from Eq. (2.15) and taking into account the multisite nature of the mixing, as:

$$G^{id-mix} = RT \cdot \left[n_1 \left(X_A^{s1} \, ln \, X_A^{s1} + X_B^{s1} \, ln \, X_B^{s1} \right) + n_2 \left(X_P^{s2} \, ln \, X_P^{s2} + X_Q^{s2} \, ln \, X_Q^{s21} \right) \right] \tag{2.49}$$

Hence:

$$\mu_{AP}^{id} = \left(\frac{\partial G^{id-mix}}{\partial n_{AP}} \right)_{T,P,n_{AQ},n_{BP},n_{BQ}} = RT \, ln \left[\left(X_A^{s1} \right)^{n1} \left(X_P^{s2} \right)^{n2} \right] \tag{2.50}$$

As a result, even if G^{ex} is zero, it will be:

$$\mu_{AP} = G^{o-AP} + \left(1 - X_A^{s1} \right) \left(1 - X_P^{s2} \right)) \Delta G_{REC}^{o} + RT \, ln \left[\left(X_A^{s1} \right)^{n1} \left(X_P^{s2} \right)^{n2} \right] \tag{2.51}$$

This shows that the solution cannot be ideal unless the free energy change of the reciprocal reaction given by Eq. (2.48) is equal to zero (i.e. $\Delta G_{REC}^{o} = 0$) (Wood and Nicholls, 1978).

2.7 Generalization of the reciprocal solution model

A phase is now considered in which two crystallographically distinct cation sites, s1 and s2, are occupied by the two different groups of cations (A,B,C,D,….) and [P,Q,R,S,….], respectively. The general formula of a phase of this type is:

$$^{s1}(A,B,C,D,\ldots.)_{n1}{}^{s2}[P,Q,R,S,\ldots.]_{n2}X_m \qquad (2.52)$$

The equivalent expression of Eq. (2.44) for this case is:

$$G^{e-m} = \sum_a \sum_p X_a^{s1} X_p^{s2} G^{o-ap} \qquad (2.53)$$

with:

a = A, B, C, D, etc.
p = P, Q, R, S, etc.

A geologically important example is the $^{dod}\{Ca,Mg,Fe^{2+},Mn\}_3{}^{oct}(Al,Cr,Fe^{3+})_2Si_3O_{12}$ garnet solid solution.

The contribution to the chemical potential of an end-member (e.g. AP) is then (cf. Eq. 2.47):

$$\begin{aligned}\mu_{AP}^{e-m} &\equiv \left(n_{AP} + n_{AQ} + n_{AR} + n_{BP} + n_{BQ} + n_{BR} + \ldots.\right)\cdot\left(\frac{\partial G^{e-m}}{\partial n_{AP}}\right)_{T,P,n_{AQ},n_{BP},n_{BQ},n_{AR},\ldots} \\ &= G^{o-AP} + \sum_b \sum_q X_b^{s1} X_q^{s2}\left[G^{o-Aq} + G^{o-bP} - G^{o-bq} - G^{o-AP}\right]\end{aligned} \qquad (2.54)$$

with:

b = B, C, D, etc.
q = Q, R, S, etc.

Note that the last term in Eq. (2.54) is equivalent algebraically to Eq. (33) of Wood and Nicholls (1978) but it is here expressed in a simpler form.

Using the probability approach, the extension to a solution with mixing taking place on three independent sublattices, i.e.:

$$^{s1}(A,B,C,D,\ldots.)_{n1}{}^{s2}[P,Q,R,S,\ldots.]_{n2}{}^{s3}\{U,V,W\ \ldots.\}_{n3}X_m \qquad (2.55)$$

is straightforward. Since the probability of an end-member APU is simply:

$$\Psi^{APU} = X_A^{s1} X_P^{s2} X_U^{s3} \qquad (2.56)$$

Hence:

$$G^{e-m} = \sum_a \sum_p \sum_u X_a^{s1} X_p^{s2} X_u^{s3} G^{o-apu} \qquad (2.57)$$

with:

a = A, B, C, etc.
p = P, Q, R, etc.
u = U, V, W, etc.

It is difficult to find a simple but realistic example that is of genuine geological importance (i.e. one in which the sets of substituting ions are independent – most are more complicated, see section 2.8), but the substitution of Ge for Si on the tetrahedral site in garnet would give the solution $^{dod}\{Ca,Mg,Fe^{2+},Mn\}_3{}^{oct}(Al,Cr,Fe^{3+})_2{}^{tet}[Si,Ge]_3O_{12}$. Similarly one could imagine mixing of Na with K, of Mg with Fe^{2+} and of OH^- with F^- in phlogopitic biotites of formula $(K,Na)(Mg,Fe)_3AlSi_3O_{10}(OH,F)_2$.

For a solution {A,B,C}(P,Q)[U,V] with ternary mixing on one site and binary mixing on two other sites, the contribution to the chemical potential of an end-member APU from G^{e-m} is then:

$$
\begin{aligned}
\mu_{APU}^{e-m} \equiv & \left(n_{APU} + n_{AQU} + n_{APV} + n_{BPU} + n_{BQU} + n_{BPV} + ...\right)\left(\frac{\partial G^{e-m}}{\partial n_{APU}}\right)_{T,P,n_{BQV},..} \\
& = G^{o-APU} \\
& + X_B^{s1} X_Q^{s2}\left[G^{o-BPU} + G^{o-AQU} - G^{o-BQU} - G^{o-APU}\right] \\
& + X_Q^{s2} X_V^{s3}\left[G^{o-AQU} + G^{o-APV} - G^{o-AQV} - G^{o-APU}\right] \\
& + X_B^{s1} X_V^{s3}\left[G^{o-BPU} + G^{o-APV} - G^{o-BPV} - G^{o-APU}\right] \\
& + 2X_B^{s1} X_Q^{s2} X_V^{s3}\begin{bmatrix} G^{o-APU} + G^{o-BQU} + G^{o-BPV} + G^{o-AQV} \\ G^{o-BPU} - G^{o-AQU} - G^{o-APV} - G^{o-BQV} \end{bmatrix} \\
& + X_C^{s1} X_Q^{s2}\left[G^{o-CPU} + G^{o-AQU} - G^{o-CQU} - G^{o-APU}\right] \\
& + X_C^{s1} X_V^{s3}\left[G^{o-CPU} + G^{o-APV} - G^{o-CPV} - G^{o-APU}\right] \\
& + 2X_C^{s1} X_Q^{s2} X_V^{s3}\begin{bmatrix} G^{o-APU} + G^{o-CQU} + G^{o-CPV} + G^{o-AQV} \\ - G^{o-CPU} - G^{o-AQU} - G^{o-APV} - G^{o-CQV} \end{bmatrix}
\end{aligned}
\qquad (2.58)
$$

The important point is that the expression for μ^{e-m} for a 3-site reciprocal solution contains both binary and ternary terms.

Conceptually, the extension of the model to even more sublattices is trivial in terms of writing G^{e-m}, but the derivation of the chemical potential of an end-member obviously becomes increasingly tedious as the number of sublattices increases. This is particularly evident in more complicated cases where the sublattices are not compositionally independent, as in most rock-forming minerals with more than two sublattices (pyroxenes, amphiboles, micas, etc., see also section 2.8).

2.7.1 The importance of charge-balance in defining end-members

The example of $NaAlSi_2O_6$-$CaMgSi_2O_6$ clinopyroxenes

In the examples of the garnet and spinel solid solutions considered so far, the mixing on each sublattice involves sets of cations with the same valence. It is possible, in principle, to conceptualise a reciprocal solid solution involving the coupled substitution of

cations with different valences on two sublattices: for example the substitution Na+Al = Ca+Mg in clinopyroxenes on the join $NaAlSi_2O_6$-$CaMgSi_2O_6$.

The chemical potential of $NaAlSi_2O_6$, $\mu^{cpx}_{NaAlSi_2O_6}$, in clinopyroxene solid solutions can be measured by displacement in *T-P* space of the univariant reaction:

$$\underset{\text{clinopyroxene}}{NaAlSi_2O_6} + \underset{\text{quartz}}{SiO_2} = \underset{\text{plagioclase}}{NaAlSi_3O_8} \qquad (2.59)$$

Holland (1990) has carefully reviewed the experimental results in the binary join $NaAlSi_2O_6$-$CaMgSi_2O_6$, and shown that they fit the relationship:

$$\mu^{cpx}_{NaAlSi_2O_6} = G^{o-NaAlSi_2O_6} + 2RT\,ln\,X^{cpx-NaAlSi_2O_6} + A\left(1 - X^{cpx-NaAlSi_2O_6}\right)^2 \qquad (2.60)$$

with:

$A = 26\pm2$ kJ mol^{-1}.

Where, the factor of two in the term for the ideal partial molar entropy of mixing term indicates random mixing of Al with Mg on the M1 site, and, independently, of Na with Ca on the M2 site; i.e. with no local charge balance, as it would be required by short range order of Na with Al and Ca with Mg.

The main point of interest here is that the physical basis for the *A* parameter can be interpreted in two quite different ways (Holland, 1990). On one hand it could be regarded as the regular solution parameter expected from the strain effects accompanying mixing of Na and Ca on M2 plus Mg and Al on M1:

$$A\left(1 - X^{cpx}_{NaAlSi_2O_6}\right)^2 = W^{M2}_{Ca-Na}\left(1 - X^{M2}_{Na}\right)^2 + W^{M1}_{Mg-Al}\left(1 - X^{M1}_{Al}\right)^2 \qquad (2.61)$$

Maintaining overall charge neutrality in the binary requires:

$$X^{M2}_{Na} = X^{M1}_{Al} = X^{cpx}_{NaAlSi_2O_6} \qquad (2.62)$$

Therefore:

$$A = W^{M2}_{Ca-Na} + W^{M1}_{Mg-Al} \qquad (2.63)$$

Alternatively, both Wood and Nicholls (1978) and Holland (1990) have pointed out that the same algebraic expression would result if the $NaAlSi_2O_6$-$CaMgSi_2O_6$ binary were regarded as a diagonal join in the reciprocal system: $NaAlSi_2O_6$-$NaMgSi_2O_6^{1-}$-$CaAlSi_2O_6^{1+}$-$CaMgSi_2O_6$. Then, from Eq. (2.47):

$$A = \Delta G^o_{REC} = G^{o-(NaAlSi_2O_6)} + G^{o-(CaMglSi_2O_6)} - G^{o-(NaMgSi_2O_6)^{-1}} - G^{o-(CaAlSi_2O_6)^{+1}} \qquad (2.64)$$

The point that this raises is whether hypothetical charged end-members such as $NaMgSi_2O_6^{1-}$ and $CaAlSi_2O_6^{1+}$ need to be considered in formulating the Gibbs free energy reference surface of complex solid solutions.

Now, from simple ionic theory, the electrostatic energy needed to separate a crystal AB into $A^{z_{cat}}$ and $B^{z_{an}}$ ions is given by:

$$U_E = \frac{N_A z_{cat}.z_{an} e^2 M}{4\pi\varepsilon_o r} = 1389 \frac{z_{cat}.z_{an} M}{r} \text{ kJ Å}^{-1} \text{ mol}^{-1} \qquad (2.65)$$

with:

M = Madelung constant
N_A = Avogadro's number
e = charge on an electron
r = appropriate interionic distance in the crystal (in Å)
ε_o = permittivity in a vacuum.

An order-of-magnitude estimate of the lattice energy change accompanying the reaction:

$$NaAlSi_2O_6 + CaMgSi_2O_6 = NaMgSi_2O_6^{1-} + CaAlSi_2O_6^{1+} \qquad (2.66)$$

is then about 10^3 kJ/mol for typical next-nearest neighbour interatomic distances. Clearly this is much larger than observed.

Although Wood and Nicholls (1978) in this example did not consider any physical constraints on the magnitude of ΔG^{o}_{REC}, they did argue that large values of ΔG^{o}_{REC} would be accompanied by short-range order, which would operate to produce local charge balance. As a practical consideration, unless electroneutrality in reciprocal solutions is specified as a 'constraint rule', then a free-energy minimization calculation is likely to result in phase compositions that are not charge-balanced. To avoid this, it is necessary anyway to include an electroneutrality constraint, and this is most simply and logically done in the definition of $G^{e\text{-}m}$ by assigning zero probability to hypothetical charged end-members.

2.8 Reciprocal solid solutions with linked substitutions.

In the 'classical' reciprocal solid solutions considered in the previous section, mixing on each sublattice occurs independently of the other sublattices. However, there are many geologically important solid solutions in which the mixing is not independent, because the same cations are involved on more than one sublattice: simple examples involving mixing of four end-members are $Mg_2Si_2O_6$-$Fe_2Si_2O_6$-$CaMgSi_2O_6$-$CaFeSi_2O_6$ and $Mg_2Si_2O_6$-$Fe_2Si_2O_6$-$MgAl_2Si_2O_6$-$FeAl_2Si_2O_6$ pyroxenes (both ortho- and clinopyroxene), and Mg_2TiO_4-Fe_2TiO_4-$MgAl_2O_4$-$FeAl_2O_4$ spinels. The olivine solid solution Mg_2SiO_4-Fe_2SiO_4-$CaMgSiO_4$-$CaFeSiO_4$ is another example that is almost the same as the first pyroxene example. The compositional space defined by the first example is logically represented by a trapezoid (see Fig. 2.2), created by truncating the compositional triangle $Mg_2Si_2O_6$-Fe_2Si_2O6-$Ca_2Si_2O_6$ at the $CaMgSi_2O_6$-$CaFeSi_2O_6$ join, in accord with the idea that the high degree of ordering on the binaries between $Ca_2Si_2O_6$ and $Mg_2Si_2O_6$ and between $Ca_2Si_2O_6$ and $Fe_2Si_2O_6$ is best handled by making the ordered compositions into end-members. Likewise, the $Mg_2Si_2O_6$-$Fe_2Si_2O_6$-$MgAl_2SiO_6$-$FeAl_2SiO_6$ solution could be considered to form a compositional trapezoid truncating the compositional triangle $Mg_2Si_2O_6$-$Fe_2Si_2O_6$-Al_4O_6. In this way, $MgAl_2SiO_6$ is treated as the ordered intermediate compound between $Mg_2Si_2O_6$ and a hypothetical Al_4O_6 pyroxene end-member.

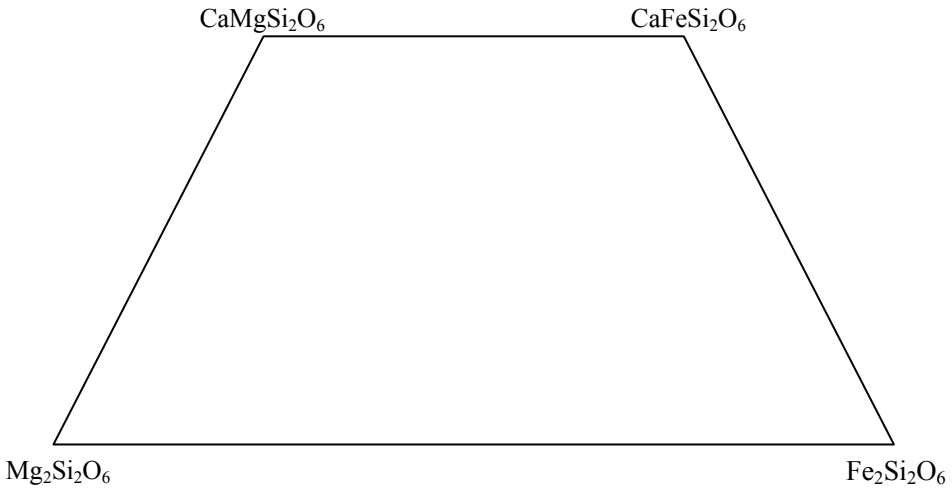

Fig. 2.2 Two-dimension compositional space for a Mg_2Si_2O6-$Fe_2Si_2O_6$-$CaMgSi_2O_6$-$CaFeSi_2O_6$ pyroxene solution.

The approach followed in this work is to formulate the free energy of such solid solutions using the same principle as for 'classical' reciprocal solid solutions, with $G^{e\text{-}m}$ weighted according to the probability Ψ of each end-member. The $G^{id\text{-}mix}$ and G^{ex} terms are treated as before (i.e. using Eq. 2.70 and Eq. 2.71). Note that the ordering of Mg and Fe^{2+} between the M1 and M2 sites is ignored. For the first pyroxene example, the complete formulation of $G^{e\text{-}m}$, $G^{id\text{-}mix}$, G^{ex} in terms of the number of atoms of Ca, Mg and Fe^{2+} per formula unit[5] (N_{Ca}, N_{Mg} and N_{Fe}) and adopting the 'virtual' site occupancies of Table (2.1) (where, in this case, $N_{Na} = N_{Al} = 0$) , is:

$$G^{e-m} = \left[\begin{array}{l} \dfrac{N_{Mg}}{N_{Mg} + N_{Fe^{2+}}} N_{Ca} G^{o-CaMgSi_2O_6} + \dfrac{N_{Mg}}{N_{Mg} + N_{Fe^{2+}}} (1 - N_{Ca}) G^{o-Mg_2Si_2O_6} \\ + \dfrac{N_{Fe^{2+}}}{N_{Mg} + N_{Fe^{2+}}} N_{Ca} G^{o-CaFeSi_2O_6} + \dfrac{N_{Fe^{2+}}}{N_{Mg} + N_{Fe^{2+}}} (1 - N_{Ca}) G^{o-Fe_2Si_2O_6} \end{array} \right] \tag{2.67}$$

$$G^{id-mix} = -RT \cdot \left[\begin{array}{l} N_{Ca}\, ln\, N_{Ca} + (1 - N_{Ca}) \dfrac{N_{Mg}}{N_{Mg} + N_{Fe}} ln\left((1 - N_{Ca}) \dfrac{N_{Mg}}{N_{Mg} + N_{Fe}} \right) \\ + (1 - N_{Ca}) \dfrac{N_{Fe}}{N_{Mg} + N_{Fe}} ln\left((1 - N_{Ca}) \dfrac{N_{Fe}}{N_{Mg} + N_{Fe}} \right) \\ + \dfrac{N_{Mg}}{N_{Mg} + N_{Fe}} ln\left(\dfrac{N_{Mg}}{N_{Mg} + N_{Fe}} \right) \\ + \dfrac{N_{Fe}}{N_{Mg} + N_{Fe}} ln\left(\dfrac{N_{Fe}}{N_{Mg} + N_{Fe}} \right) \end{array} \right] \tag{2.68}$$

[5] Note that the number of atoms (cations) per formula unit are directly related to the 'virtual' site occupancies by means of 'mass balance' constraints, as explained in detail in section 3.4.

$$G_{ex} = \left[\begin{array}{l} N_{Ca} \cdot (1-N_{Ca}) \dfrac{N_{Mg}}{N_{Mg}+N_{Fe}} \cdot \left(N_{Ca} + \dfrac{1}{2}(1-N_{Ca}) \dfrac{N_{Fe}}{N_{Mg}+N_{Fe}} \right) \cdot W_{MgCa}^{M2} \\ + N_{Ca} \cdot (1-N_{Ca}) \dfrac{N_{Mg}}{N_{Mg}+N_{Fe}} \cdot \left(N_{Ca} + \dfrac{1}{2}(1-N_{Ca}) \dfrac{N_{Fe}}{N_{Mg}+N_{Fe}} \right) \cdot W_{CaMg}^{M2} \\ + N_{Ca} \cdot (1-N_{Ca}) \dfrac{N_{Fe}}{N_{Mg}+N_{Fe}} \cdot \left(N_{Ca} + \dfrac{1}{2}(1-N_{Ca}) \dfrac{N_{Mg}}{N_{Mg}+N_{Fe}} \right) \cdot W_{FeCa}^{M2} \\ + N_{Ca} \cdot (1-N_{Ca}) \dfrac{N_{Fe}}{N_{Mg}+N_{Fe}} \cdot \left((1-N_{Ca}) \dfrac{N_{Fe}}{N_{Mg}+N_{Fe}} + \dfrac{1}{2}(1-N_{Ca}) \dfrac{N_{Mg}}{N_{Mg}+N_{Fe}} \right) \cdot W_{CaFe}^{M2} \\ + (1-N_{Ca}) \dfrac{N_{Mg}}{N_{Mg}+N_{Fe}} \cdot (1-N_{Ca}) \dfrac{N_{Fe}}{N_{Mg}+N_{Fe}} W_{MgFe}^{M2} \\ + \dfrac{N_{Mg}}{N_{Mg}+N_{Fe}} \cdot \dfrac{N_{Fe}}{N_{Mg}+N_{Fe}} W_{MgFe}^{M1} \end{array} \right] \quad (2.69)$$

The formulation of G^{ex} is that of a subregular ternary model (between Ca, Mg and Fe^{2+}) in the M2 site with no ternary interaction parameter (see, e.g. Cheng and Ganguly, 1994, their Eq. 2.1; see also Helffrich and Wood, 1989, for the formulation of a general subregular model) that in this work is employed for the modeling of clinopyroxene solid solutions. Asymmetric mixing is assumed between Ca and Mg (i.e. $W_{CaMg}^{M2} \neq W_{MgCa}^{M2}$) and between Ca and Fe^{2+} (i.e. $W_{CaFe}^{M2} \neq W_{FeCa}^{M2}$), as demanded by the experimental data from the binary joins $CaMgSi_2O_6$-$Mg_2Si_2O_6$ and $CaFeSi_2O_6$ and $Fe_2Si_2O_6$ respectively, but with symmetric mixing between Mg and Fe^{2+} on this site (i.e. $W_{MgFe}^{M2} = W_{FeMg}^{M2}$), and on the M1 site (i.e. $W_{MgFe}^{M1} = W_{FeMg}^{M1}$). It would be also proposed that $W_{MgFe}^{M2} = W_{MgFe}^{M1}$. The model used for the orthopyroxene solid solution is the same except that symmetric mixing is assumed also between Ca-Mg and Ca-Fe on the M2 site. In principle, this model could be calibrated with data only from the binaries, if the free energies of formation of the end-members are known. The model employed in this work to model Ca-Mg-Fe olivines is identical to the clinopyroxene one. Results from application of the model to olivine and pyroxene assemblages are presented in chapter 4 and chapter 5, respectively.

2.8.1 Some examples of formulating the solution thermodynamics of multicomponent, multisite rock-forming minerals

Pyroxenes

Natural rock-forming pyroxenes commonly contain as major constituent the cations Na, Ca, Mg, Fe^{2+}, Al, Cr, Fe^{3+}, Si and Ti. The pyroxene formula unit is defined as containing six oxygens, with four cations that, in the approach followed in this work, are arranged on three 'virtual' sublattices, which correspond approximately to the crystallographic M1 and M2 octahedral sites and the two tetrahedral sites T per formula unit. Here it is briefly summarized the way a model for a somewhat simplified system with the cations Na, Ca, Mg, Fe^{2+}, Al and Si has been set up.

The first task is to group the cations according to their formal valances and ordering characteristics, defining the 'virtual' sublattice occupancies. It is here important to point out that these site occupancies, given in Table (2.1), are equivalent to those of Table (3.1) and Table (6.1), although apparently formulated in a different way. In chapter 3 the issue of number and type of constraints that, depending on phase and system considered, have to be imposed on the site occupancies, is thoroughly addressed. Site occupancies of Table (2.1), then, simply correspond to those of Table (3.1), once it is imposed they satisfy all the required constraints and using the number of cations per formula unit to express them.

Table 2.1 Virtual site occupancies for a pyroxene phase in a Na-Ca-Mg-Fe^{2+}-Al-Si system.

Cation	**[(a)]Virtual M2**	**[(a)]Virtual M1**	**Virtual T**
Na	N_{Na}	-	-
Ca	N_{Ca}	-	-
Mg	$(1-N_{Na}-N_{Ca})N_{Mg}/N_{M^{2+}}$	$(1-N_{Al}/2)N_{Mg}/N_{M^{2+}}$	-
Fe^{2+}	$(1-N_{Na}-N_{Ca})N_{Fe^{2+}}/N_{M^{2+}}$	$(1-N_{Al}/2)N_{Fe^{2+}}/N_{M^{2+}}$	-
Al	-	$N_{Al}/2$	$N_{Al}/2$
Si	-	-	$2-(N_{Al}/2)$

Notes: [(a)] $N_{M^{2+}} = N_{Mg} + N_{Fe^{2+}}$.

Next all possible stoichiometric end-members not related by order-disorder are identified. For each end-member the probability 'weight' Ψ is evaluated (Table 2.2).

Table 2.2 List of stoichiometric, charge balanced end-members and corresponding probability of occurrence for a pyroxene phase in a Na-Ca-Mg-Fe^{2+}-Al-Si system.

End-member	[(a)] Ψ
$NaAlSi_2O_6$	N_{Na}
$Mg_2Si_2O_6$	$(1-N_{Ca})(1-N_{Na}/2-N_{Al}/2)N_{Mg}/N_{M^{2+}}$
$Fe_2Si_2O_6$	$(1-N_{Ca})(1-N_{Na}/2-N_{Al}/2)N_{Fe^{2+}}/N_{M^{2+}}$
$CaMgSi_2O_6$	$N_{Ca}(1-N_{Na}/2-N_{Al}/2)N_{Mg}/N_{M^{2+}}$
$CaFeSi_2O_6$	$N_{Ca}(1-N_{Na}/2-N_{Al}/2)N_{Fe^{2+}}/N_{M^{2+}}$
$CaAl_2SiO_6$	$N_{Ca}(N_{Al}/2-N_{Na}/2)$
$MgAl_2SiO_6$	$(1-N_{Ca})(N_{Al}/2-N_{Na}/2)N_{Mg}/N_{M^{2+}}$
$FeAl_2SiO_6$	$(1-N_{Ca})(N_{Al}/2-N_{Na}/2)N_{Fe^{2+}}/N_{M^{2+}}$

Notes: [(a)] $N_{M^{2+}} = N_{Mg} + N_{Fe^{2+}}$.

There are in total eight end-members and it may be easily checked that $\sum_{i=1}^{8} \Psi^i = 1$.

Incorporating Cr in the model would produce four additional end-members, each corresponding to one in the Table containing Al (i.e. $MgCr_2SiO_6$, $FeCr_2SiO_6$, $CaCr_2SiO_6$, $NaCrSi_2O_6$). Note that Cr is assumed to replace Al, as shown experimentally for the ternary $Mg_2Si_2O_6$-$MgAl_2SiO_6$- $MgCr_2SiO_6$ by Klemme and O'Neill (2000), that is, ordered end-members like $MgCrAlSiO_6$ are empirically observed not to be appropriate. Fe^{3+} would be treated similarly, hence four more end-members. Clearly trying to incorporate order-disorder effects to account for all possible Al-Cr-Fe^{3+} combinations would in any case be prohibitive in terms of their numbers. For Ti, replacement of Ti for Si produces eight possible end-members in the 7-component system (i.e. Na, Ca, Mg, Fe^{2+}, Al, Si and Ti), logically eight more if Cr and Fe^{3+} were included, but the values of Ψ attached to such hypothetical end-members ($MgCr_2TiO_6$ etc.) are clearly extremely small for real systems and one could safely decide to neglect them. In Table (2A.1) (see Appendix 2A) the complete list of end-members identified for a Na, Ca, Mg, Fe^{2+}, Al, Cr, Fe^{3+}, Si and Ti pyroxene phase and the probability of occurrence of each end-member are reported.

As said in the previous section, the way to treat the G^{id} and G^{ex} terms remains unchanged. The general expressions used in this work to calculate G^{id} and G^{ex} for any multicomponent, multisite crystalline phase are given by, respectively:

$$G^{ideal} = -TS^{ideal} = RT \sum_{k=1}^{n} \sum_{i=1}^{c} q_{ik} X'_{ik} \, ln \, X'_{ik} \tag{2.70}$$

$$G^{ex} = \sum_{k=1}^{n} Q_k \sum_{i=1}^{c} \sum_{y>i}^{c} X'_{ik} X'_{yk} \left\{ \begin{array}{l} W_{ik-yk} \cdot \left[X'_{yk} + \frac{1}{2} \sum_{\substack{j \neq i \\ j \neq y}}^{c} X'_{jk} \right] + \\ W_{yk-ik} \cdot \left[X'_{ik} + \frac{1}{2} \sum_{\substack{j \neq i \\ j \neq y}}^{c} X'_{jk} \right] \end{array} \right\} \tag{2.71}$$

$$+ \sum_{i=1}^{c} \sum_{y>i}^{c} \sum_{j>y}^{c} X'_{ik} X'_{yk} X'_{jk} W_{ik-yk-jk}$$

with:

$$X'_{ik} = \frac{X_{ik}}{Q_k} \tag{2.72}$$

Where, where Q_k denotes the total number of sites in the sublattice k, q_{ik} the number of sites of sublattice k where mixing is assumed taking place, n the total number of sublattices k, X_{ik} the site occupancy of the cation i on the *k-th* sublattice, and c the total number of cations i.

These expressions are very similar to those for G^{id} and G^{ex} found in the literature (e.g. Chatterjee, 1991; Helffrich and Wood, 1989; respectively). The only difference is the introduction in Eq. (2.70) of the factor q_{ik}. This factor has been added to ensure that the adoption of 'virtual' site occupancies will not lead to an incorrect estimation of G^{id}. An example may help to clarify this point. In a pyroxene phase, as explained above, Cr is assumed to replace Al. As a result, it appears to occupy also a 'virtual' site T (see also Table 3.1), while the presence of Cr in a 'real' site T is unlikely on crystal-chemical

grounds. This means that in the calculation of G^{id} associated to the 'virtual' site T only the contribution from a Cr-Al mixing should be considered, while the contribution from a hypothetical Si-Cr mixing should be left out. This can be readily obtained by setting in Eq. (2.70), for k = T and i = Cr, $q_{ik} = X_{53} + X_{63}$, instead of $q_{ik} = Q_k = 2$, where X_{53} = Al in 'virtual' T and X_{63} = Cr in 'virtual' T. In this way Cr-Al entropy of mixing in site T is calculated only for that portion of the 'virtual' site where mixing between Al and Cr does occur.

Mg-Fe^{2+}-Ti-Al spinels

The way that the reciprocal solid solution approach can be used to formulate the thermodynamic properties of spinel solid solutions with the general composition $(Mg,Fe^{2+})[Al,Cr,Fe^{3+}]_2O_4$ is well known (Wood and Nicholls, 1978, O'Neill and Wall, 1987). These spinels form a 'classical' reciprocal system because the mixing of Mg and Fe^{2+} occurs, compositionally speaking, independently of the mixing of Al, Cr and Fe^{3+}. However, adding Ti to the system (which involves the end-members Mg_2TiO_4 and Fe_2TiO_4) introduces an extra degree of complexity, since the maintenance of charge balance requires that the substitution of Ti is linked to the substitution of an equal number of Mg plus Fe^{2+} cations (i.e. $Ti+M^{2+} = 2R^{3+}$, where M^{2+} refers to Mg and Fe^{2+} and R^{3+} to Al, Cr and Fe^{3+}). The essential features of the thermodynamics can be explained using the subsystem Mg_2TiO_4-Fe_2TiO_4-$MgAl_2O_4$-$FeAl_2O_4$. First the virtual site occupancies are defined (see Table 2.3).

Table 2.3 Virtual site occupancies for a spinel phase in a Mg-Fe^{2+}-Al-Ti system.

Cation	Virtual A site	Virtual B site
Mg	$N_{Mg}/\left(N_{Mg}+N_{Fe^{2+}}\right)$	$\left[N_{Mg}/\left(N_{Mg}+N_{Fe^{2+}}\right)\right]\cdot\left(2-N_{Al}-N_{Ti}\right)$
Fe^{2+}	$N_{Fe^{2+}}/\left(N_{Mg}+N_{Fe^{2+}}\right)$	$\left[N_{Fe^{2+}}/\left(N_{Mg}+N_{Fe^{2+}}\right)\right]\cdot\left(2-N_{Al}-N_{Ti}\right)$
Al	-	N_{Al}
Ti	-	N_{Ti}

Then, for the four end-members (Mg_2TiO_4-Fe_2TiO_4-$MgAl_2O_4$-$FeAl_2O_4$), the probability weightings are calculated (Table 2.4):

Table 2.4 List of end-members and corresponding probability of occurrence for a spinel phase in a Mg-Fe^{2+}-Al-Ti system.

End-member	Ψ
Mg_2TiO_4	$\left[N_{Mg}/\left(N_{Mg}+N_{Fe^{2+}}\right)\right]\cdot N_{Ti}$
Fe_2TiO_4	$\left[N_{Fe^{2+}}/\left(N_{Mg}+N_{Fe^{2+}}\right)\right]\cdot N_{Ti}$
$MgAl_2O_4$	$\left[N_{Mg}/\left(N_{Mg}+N_{Fe^{2+}}\right)\right]\cdot\left(1-N_{Ti}\right)$
$FeAl_2O_4$	$\left[N_{Mg}/\left(N_{Mg}+N_{Fe^{2+}}\right)\right]\cdot\left(1-N_{Ti}\right)$

As a result, the expression of $G^{e\text{-}m}$ is:

$$G^{e-m} = \frac{N_{Mg}}{N_{Mg}+N_{Fe^{2+}}} N_{Ti} G^{o-Mg_2TiO_4} + \frac{N_{Fe^{2+}}}{N_{Mg}+N_{Fe^{2+}}} N_{Ti} G^{o-Fe_2TiO_4} + \frac{N_{Mg}}{N_{Mg}+N_{Fe^{2+}}}\left(1-N_{Ti}\right) G^{o-MgAl_2O_4} + \frac{N_{Fe^{2+}}}{N_{Mg}+N_{Fe^{2+}}}\left(1-N_{Ti}\right) G^{o-FeAl_2O_4} \quad (2.73)$$

Extension to Mg-Fe^{2+}-Ti-Al-Fe^{3+}-Cr spinels

Although straightforward, the extension to a more general system is instructive, as it shows the logic of the approach for a case of practical interest. Expression of $G^{id\text{-}mix}$ and G^{ex} can be obtained, as usually, from Eq. (2.70) and Eq. (2.71), respectively, so only the derivation of $G^{e\text{-}m}$ is discussed here. The 'virtual' site occupancies are given in Table (2.5).

Table 2.5 Virtual site occupancies for a spinel phase in a Mg-Fe^{2+}-Al-Cr-Fe^{3+}-Ti system.

Cation	**Virtual A site**	[(a)]**Virtual B site**
Mg	$N_{Mg}/\left(N_{Mg}+N_{Fe^{2+}}\right)$	$\left[N_{Mg}/\left(N_{Mg}+N_{Fe^{2+}}\right)\right]\cdot\left(2-N_R-N_{Ti}\right)$
Fe^{2+}	$N_{Fe^{2+}}/\left(N_{Mg}+N_{Fe^{2+}}\right)$	$\left[N_{Fe^{2+}}/\left(N_{Mg}+N_{Fe^{2+}}\right)\right]\cdot\left(2-N_R-N_{Ti}\right)$
Al	-	N_{Al}
Cr	-	N_{Cr}
Fe^{3+}	-	$N_{Fe^{3+}}$
Ti	-	N_{Ti}

Notes: [(a)] $N_R = N_{Al} + N_{Cr} + N_{Fe^{3+}}$.

Next all possible stoichiometric end-members not related by order-disorder are identified. For each end-member the probability weighting Ψ is evaluated (Table 2.6).

Table 2.6 List of end-members and corresponding probability of occurrence for a spinel phase in a Mg-Fe^{2+}-Al-Cr-Fe^{3+}-Ti system.

End-member	[(a)] Ψ
Mg_2TiO_4	$\left[N_{Mg}/\left(N_{M^{2+}}\right)\right]\cdot N_{Ti}$
Fe_2TiO_4	$\left[N_{Fe^{2+}}/\left(N_{M^{2+}}\right)\right]\cdot N_{Ti}$
$MgAl_2O_4$	$\left[N_{Mg}/\left(N_{M^{2+}}\right)\cdot\left(N_{Al}/N_R\right)\right]\cdot\left(1-N_{Ti}\right)$
$FeAl_2O_4$	$\left[N_{Fe^{2+}}/\left(N_{M^{2+}}\right)\cdot\left(N_{Al}/N_R\right)\right]\cdot\left(1-N_{Ti}\right)$
$MgCr_2O_4$	$\left[N_{Mg}/\left(N_{M^{2+}}\right)\cdot\left(N_{Cr}/N_R\right)\right]\cdot\left(1-N_{Ti}\right)$
$FeCr_2O_4$	$\left[N_{Fe^{2+}}/\left(N_{M^{2+}}\right)\cdot\left(N_{Cr}/N_R\right)\right]\cdot\left(1-N_{Ti}\right)$
$MgFe_2O_4$	$\left[N_{Mg}/\left(N_{M^{2+}}\right)\cdot\left(N_{Fe^{3+}}/N_R\right)\right]\cdot\left(1-N_{Ti}\right)$
$FeFe_2O_4$	$\left[N_{Fe^{2+}}/\left(N_{M^{2+}}\right)\cdot\left(N_{Fe^{3+}}/N_R\right)\right]\cdot\left(1-N_{Ti}\right)$

Notes: [(a)] $N_{M^{2+}} = N_{Mg} + N_{Fe^{2+}}$;
$N_R = N_{Al} + N_{Cr} + N_{Fe^{3+}}$.

As a result, the expression of $G^{e\text{-}m}$ in this case is:

$$G_{e-m} = \left[\begin{array}{l} \left(\frac{N_{Mg}}{N_{M^{2+}}}\right)N_{Ti}\cdot G^{o-Mg_2TiO_4} + \left(\frac{N_{Fe^{2+}}}{N_{M^{2+}}}\right)N_{Ti}\cdot G^{o-Fe_2TiO_4} \\ + \left(\frac{N_{Mg}}{N_{M^{2+}}}\right)\left(\frac{N_{Al}}{N_R}\right)\left(1-N_{Ti}\right)\cdot G^{o-MgAl_2O_4} + \left(\frac{N_{Fe^{2+}}}{N_{M^{2+}}}\right)\left(\frac{N_{Al}}{N_R}\right)\left(1-N_{Ti}\right)\cdot G^{o-FeAl_2O_4} \\ + \left(\frac{N_{Mg}}{N_{M^{2+}}}\right)\left(\frac{N_{Cr}}{N_R}\right)\left(1-N_{Ti}\right)\cdot G^{o-MgCr_2O_4} + \left(\frac{N_{Fe^{2+}}}{N_{M^{2+}}}\right)\left(\frac{N_{Cr}}{N_R}\right)\left(1-N_{Ti}\right)\cdot G^{o-FeCr_2O_4} \\ + \left(\frac{N_{Mg}}{N_{M^{2+}}}\right)\left(\frac{N_{Fe^{3+}}}{N_R}\right)\left(1-N_{Ti}\right)\cdot G^{o-MgFe_2O_4} + \left(\frac{N_{Fe^{2+}}}{N_{M^{2+}}}\right)\left(\frac{N_{Fe^{3+}}}{N_R}\right)\left(1-N_{Ti}\right)\cdot G^{o-FeFe_2O_4} \end{array}\right] \quad (2.74)$$

The contribution to the chemical potential of representative end-members (e.g. Mg_2TiO_4 and $MgAl_2O_4$) is therefore (NB Only final derivations are reported):

$$\mu^{e-m}_{Mg_2TiO_4} = \begin{bmatrix} G^{o-Mg_2TiO_4} + \left(\frac{N_{Fe^{2+}}}{N_{M^{2+}}}\right)\left(\frac{N_{Al}}{N_R}\right)(1-N_{Ti})\cdot\Delta G^o_{REC(1)} \\ + \left(\frac{N_{Fe^{2+}}}{N_{M^{2+}}}\right)\left(\frac{N_{Cr}}{N_R}\right)(1-N_{Ti})\cdot\left[\Delta G^o_{REC(1)} - 2\Delta G^o_{REC(2)}\right] \\ + \left(\frac{N_{Fe^{2+}}}{N_M{}^2}\right)\left(\frac{N_{Fe^{3+}}}{N_R}\right)(1-N_{Ti})\cdot\left[\Delta G^o_{REC(1)} - 2\Delta G^o_{REC(3)}\right] \end{bmatrix} \quad (2.75)$$

$$\mu^{e-m}_{MgAl_2O_4} = \begin{bmatrix} G^{o-MgAl_2O_4} - \left(\frac{N_{Fe^{2+}}}{N_{M^{2+}}}\right)\left(\frac{N_{Al}}{N_R}\right)N_{Ti}\cdot\Delta G^o_{REC(1)} \\ - \left(\frac{N_{Fe^{2+}}}{N_{M^{2+}}}\right)\left(\frac{N_{Cr}}{N_R}\right)N_{Ti}\cdot\left[\Delta G^o_{REC(1)} - 2\Delta G^o_{REC(2)}\right] \\ - \left(\frac{N_{Fe^{2+}}}{N_{M^{2+}}}\right)\left(\frac{N_{Fe^{3+}}}{N_R}\right)N_{Ti}\cdot\left[\Delta G^o_{REC(1)} - 2\Delta G^o_{REC(3)}\right] \\ - \left(\frac{N_{Fe}}{N_{M^{2+}}}\right)\left(\frac{N_{Cr}}{N_R}\right)\cdot\Delta G^o{}_{REC(2)} - \left(\frac{N_{Fe}}{N_{M^{2+}}}\right)\left(\frac{N_{Fe^{3+}}}{N_R}\right)\cdot\Delta G^o_{REC(3)} \end{bmatrix} \quad (2.76)$$

where:

$$\Delta G^o_{REC(1)} = G^{o-Fe_2TiO_4} + 2G^{o-MgAl_2O_4} - 2G^{o-FeAl_2O_4} - G^{o-Mg_2TiO_4} \quad (2.77)$$

$$\Delta G^o_{REC(2)} = G^{o-FeCr_2O_4} + G^{o-MgAl_2O_4} - G^{o-FeAl_2O_4} - G^{o-MgCr_2O_4} \quad (2.78)$$

$$\Delta G^o_{REC(3)} = G^{o-FeFe_2O_4} + G^{o-MgAl_2O_4} - G^{o-FeAl_2O_4} - G^{o-MgFe_2O_4} \quad (2.79)$$

In the expression for $\mu^{e-m}_{MgAl_2O_4}$ it may be checked that setting N_{Ti} = 0 eliminates all but the last two terms, which are those of a 'classical' reciprocal solid solution. This example shows that although it remains a simple matter to write down the formulation of $G^{e\text{-}m}$ for correlated reciprocal solid solutions in quite complex systems, calculating the resulting values of μ_i^{e-m} can become tedious. This is a general principle.

2.9 Summary

The formalism presented here provides a straightforward means of writing down the free energy G of any compositionally complex crystalline ionic solid solution (CISS). The chemical potential of any end-member constituent i in the phase may then be calculated from the defining relationship:

$$\mu_i \equiv \left(\frac{\partial G}{\partial n_i} \right)_{T,P,n_{j \neq i}}$$

However, the algebraic form of μ_i can become quite complicated for multicomponent phases. To avoid this problem, any differentiation could be carried out numerically, or using computer algebra.

Another feature of the suggested formalism is that no assumption needs to be made concerning the identity of possible thermodynamic components in the phase. The definition of a thermodynamic component includes the stipulation that the set chosen should be the minimum number to describe the compositional variation in the phase. Clearly, the number of end-members in reciprocal solid solution phases exceeds the number needed to describe the composition of the phase, hence not all the possible end-members in such systems can be chosen as components. This causes problems with existing free-energy minimization schemes, which have all been developed to minimise the free energy of a system ($\mathbf{G}^{\mathbf{system}}$) starting from relationships such as (see also section 3.2 on this point):

$$\mathbf{G}^{\mathbf{system}} = \sum_{\phi=1}^{p} \sum_{i=1}^{c} n_i^{\phi} \mu_i^{\phi}$$

or:

$$\mathbf{G}^{\mathbf{system}} = \sum_{\phi=1}^{p} n^{\phi} \sum_{i=1}^{c} x_i^{\phi} \mu_i^{\phi}$$

Where, *c* is the total number of *components* in the system, *p* the total number of phases in the system, n^{ϕ} the number of moles of phase ϕ in the system, n_i^{ϕ} the number of moles of *component i* in phases ϕ, μ_i^{ϕ} is the chemical potential of component *i* in phase ϕ and x_i^{ϕ}

$\left(x_i^{\phi} = n_i^{\phi} \Big/ \sum_{i=1}^{c} n_i^{\phi} \right)$ is the molar fraction of *component i* in phase ϕ.

Clearly, there would be considerable advantage in developing an algorithm to directly minimize $\mathbf{G}^{\mathbf{system}}$ without either having to compute chemical potentials or defining phase components.

2.10 References

Allan N. L., Blundy J. D., Purton J. A., Lavrentiev M. Y., and Wood B. J. (2001) Trace element incorporation in minerals and melts. In *Solid solutions in silicate and oxide systems / EMU Notes in Mineralogy*, Vol. 3 (ed. G. C. A.), pp. 251-302. Eötvös Univ. Press.

Aranovich L. Y. (2004) Model independent phase equilibrium constraints on the ferrosilite activity in the binary Fe-Mg orthopyroxene solid solution. *American Mineralogist* **89**, 432-437.

Bartholomew P. R. (1989) Interpretation of the solution properties of Fe-Mg olivines and aqueous Fe-Mg chlorides from ion-exchange experiments. *American Mineralogist* **74**, 37-49.

Blander M. (1964) Thermodynamic properties of molten salt solutions. In *Molten salt chemistry* (ed. M. Blander), pp. 127-237. Wiley.

Blundy J. D. and Wood B. J. (1994) Prediction of crystal-melt partition coefficients from elastic moduli. *Nature* **372**, 452-454.

Blundy J. D. and Wood B. J. (2003) Mineral-melt partitioning of uranium, thorium and their daughters. *Reviews in mineralogy and geochemistry* **52**, 59-123.

Bowen N. L. and Schairer J. F. (1935) The system, MgO-FeO-SiO_2. *American Journal of Science* **29**, 151-217.

Bradley R. S. (1962) Thermodynamic calculations on phase equilibria involving fused salts, Part II. Solid solutions and application to the olivines. *American Journal of Science* **260**, 550-554.

Brown I. D. (1992) Chemical and steric constraints in inorganic solids. *Acta Crystallographica* **B48**, 553-572.

Burns R. G. (1993) *Remote Geochemical Analysis: Elemental and Mineralogical Composition*. Cambridge Univ. Press.

Carpenter M. A., Powell R., and Salje E. K. H. (1994) Thermodynamics of nonconvergent cation ordering in minerals .1. An alternative approach. *American Mineralogist* **79**, 1053-1067.

Chatterjee N. D. (1991) *Applied Mineralogical Thermodynamics. Selected topics.* Springer Verlag Berlin.

Chatterjee N. D., Leistner H., Terhart L., Abraham K., and Klaska R. (1982) Thermodynamic mixing properties of corundum eskolaite, α-$(Al,Cr^{+3})_2O_3$, crystalline solutions at high-temperatures and pressures. *American Mineralogist* **67**, 725-735.

Cheng W. J. and Ganguly J. (1994) Some aspects of multicomponent excess free-energy models with subregolar binaries. *Geochimica and cosmochimica acta* **58**, 3763-3767.

Cressey G., Schmid R., and Wood B. J. (1978) Thermodynamic properties of almandine-grossular garnet solid-solutions. *Contributions to Mineralogy and Petrology* **67**, 397-404.

Darken L. S. (1967) Thermodynamics of binary metallic solutions. *Met. Soc. AIME Trans.* **239**, 80-89.

Davies P. K. and Navrotsky A. (1983) Quantitative correlations of deviations from ideality in binary and pseudobinary solid solutions. *Journal of Solid State Chemistry* **46**, 1-22.

Flood H., Forland T., and Gzotheim K. (1954) Über den Zusammenhang zwischen Konzentration und Aktivitäten in geschmolzenen Salzmischungen. *Zeitschrift für Anorganische Allgemeine Chemie* **276**, 290-315.

Ganguly J. (1986) Disordering energy versus disorder in minerals - A phenomenological relation and application to ortho-pyroxene. *Journal of Physics and Chemistry of solidus* **47**, 417-420.

Ganguly J. (2001) Thermodynamic modelling of solid solutions. In *Solid solutions in silicate and oxide systems / EMU Notes in Mineralogy*, Vol. 3 (ed. C. A. Geiger), pp. 37-69. Eötvös Univ. Press.

Ganguly J., Cheng W., and O'Neill H. S. C. (1993) Syntheses, volume, and structural changes of garnets in the pyrope-grossular join: implications for stability and mixing properties. *American Mineralogist* **78**, 583-593.

Ganguly J. and Kennedy G. C. (1974) The energetics of natural garnet solid solution 1. mixing of the alumino silicate end-members. *Contributions to Mineralogy and Petrology* **48**, 137-148.

Ganguly J. and Saxena S. K. (1987) *Mixtures and Mineral Reactions*. Springer Verlag Berlin.

Geiger C. A. (1999) Thermodynamics of $(Fe^{2+},Mn^{2+},Mg,Ca)_3Al_2Si_3O_{12}$ garnet: an analysis and review. *Mineralogy and Petrology* **66**, 271-299.

Geiger C. A. (2000) Volumes of mixing in aluminosilicate garnets: solid solution and strain behaviour. *American Mineralogist* **85**, 893-897.

Geiger C. A. (2001) Thermodynamic mixing properties of binary oxide and silicate solid solutions determined by direct measurements: The role of strain. In *Solid solutions in silicate and oxide systems / EMU Notes in mineralogy*, Vol. 3 (ed. C. A. Geiger), pp. 71-100. Eötvös Univ. Press.

Ghiorso M. S. (1991) Thermodynamics of minerals and melts. *Reviews of geophysics* **29**, 446-456.

Gopal E. S. R. (1966) *Specific heats at low temperatures*. Heywood Books.

Grjotheim K. (1981) Characteristics and thermodynamics of fused-salts. *Physics and Chemistry of the Earth* **13-4**, 231-247.

Grover J. (1977) Chemical mixing in multicomponent solutions: an introduction to the use of margules and other thermodynamic excess functions to represent non-ideal behaviour. In *Thermodynamics in Geology* (ed. D. G. Fraser), pp. 67-97. D. Reidel Publishing Company.

Guggenheim E. A. (1952) *Mixtures*. Clarendon Press.

Haselton Jr H. T., Hovis G. L., Hemingway B. S., and Robie R. A. (1983) Calorimetric investigation of the excess entropy of mixing in analbite-sanidine solid solutions: lack of evidence fo Na,K short-range order and implications for two feldspar thermometry. *American Mineralogist* **86**, 398-413.

Haselton Jr H. T. and Westrum Jr E. F. (1980) Low-temperature heat capacities of synthetic pyrope, grossular, and $pyrope_{60}grossular_{40}$. *Geochimica et Cosmochimica Acta* **44**, 701-709.

Hayward S. A. and Salje E. K. H. (1996) Displacive phase transition in anorthoclase: The "plateau effect" and the effect of Ti-T2 ordering on the transition temperature. *American Mineralogist* **81**, 1332-1336.

Helffrich G. and Wood B. J. (1989) Subregular model for multicomponent solutions. *American Mineralogist* **74**, 1016-1022.

Hillert M. (1998) *Phase equilibria, phase diagrams and phase transformations: their thermodynamic basis*. Cambridge Univ. Press.

Holland T. J. B. (1990) Activities of components in omphacitic solid solutions. *Contributions to Mineralogy and Petrology* **105**, 446-453.

Holland T. J. B. and Powell R. (1996) Thermodynamics of order-disorder in minerals .II. Symmetric formalism applied to solid solutions. *American mineralogist* **81**, 1425-1437.

Hovi V. (1950) On Wasastjerna theory of the heat of formation of solid solutions. *Soc. Sci. Fenn. Comment. Phys.-Math.* **15(5)**, 1-15.

Hovis G. L. (1988) Enthalpies and volumes related to K-Na mixing and Al-Si order/disorder in alkali feldspars. *Journal of Petrology* **29**, 731-763.

Hrovat M., Holc J., Samardzija Z., and Drazic G. (1996) The extent of solid solubility in the RuO_2-TiO_2 system. *Journal of Materials Research* **11**, 727-732.

Kerrick D. M. and Darken L. S. (1975) Statistical thermodynamic models for ideal oxide and silicate solutions, with application to plagioclase, pp. 1431-1442.

Klemme S. and O'Neill H. S. C. (2000) The effect of Cr on the solubility of Al in orthopyroxene: experiments and thermodynamic modelling. *Contributions of Mineralogy and Petrology* **140**, 84-98.

Koziol A. M. (1990) Activity-composition relationships of binary Ca-Fe and Ca-Mn garnets determined by reversed, displaced equilibrium experiments. *American Mineralogist* **75**, 319-327.

Koziol A. M. (1996) Quaternary (Ca-Fe-Mg-Mn) garnet: Displaced equilibrium experiments and implications for current garnet mixing models. *European Journal of Mineralogy* **8**, 453-460.

Langer K. (2001) A note on mean distances, $R_{[MOb]}$, in substituted polyhedra, $[(M_{1-x}M_x')O_6]$, in the crystal structures of oxygen based solid solutions: local *versus* crystal averaging methods. *Zeitschrift fur Kristallographie* **216**, 87-91.

Matsui Y. and Nishizawa O. (1974) Iron (II)-magnesium exchange equilibrium between olivine and calcium-free pyroxene over a temperature range 800°C to 1300°C. *Bulletin de la Societe Francaise Mineralogie et de cristallographie* **97**, 122-130.

Mueller R. F. (1962) Energetics of certain silicate solutions. *Geochimica et Cosmochimica Acta* **26,** 581-598.

O'Neill H. S. C. (1998) Partitioning of Fe and Mn between ilmenite and olivine at 1100 ^{o}C: constraints on the thermodynamic mixing properties of $(Fe,Mn)TiO_3$ ilmenite solid solutions. *Contributions to Mineralogy and Petrology* **133**, 284-296.

O'Neill H. S. C. and Navrotsky A. (1984) Cation distributions and thermodynamic properties of binary spinel solid solutions. *American Mineralogist* **69**, 733-753.

O'Neill H. S. C. and Pownceby M. I. (1993a) Thermodynamic data from redox reactions at high temperatures. I. An experimental and theoretical assessment of the electrochemical method using stabilized zirconia electrolytes, with revised values for the Fe — "FeO", Co — CoO, Ni — NiO and Cu— Cu_2O oxygen buffers, and new data for the W — WO_2 buffer. *Contributions to Mineralogy and Petrology* **114**, 296-314.

O'Neill H. S. C. and Pownceby M. I. (1993b) Thermodynamic data from redox reactions at high temperatures. II. The MnO-Mn_3O_4 oxygen buffer, and implications for the thermodynamic properties of MnO and Mn_3O_4. *Contributions to Mineralogy and Petrology* **114,** 315-320.

O'Neill H. S. C., Pownceby M. I., and McCammon C. A. (2003) The magnesiowüstite: iron equilibrium and its implications for the activity-composition relations of $(Mg,Fe)_2SiO_4$ olivine solid solutions. *Contributions to Mineralogy and Petrology* **146**, 308-325.

O'Neill H. S. C. and Wall V. J. (1987) The olivine-orthopyroxene-spinel oxygen geobarometer, the nickel precipitation curve and the oxygen fugacity of the Earth's upper mantle. *Journal of Petrology* **28**, 1169-1191.

Orville P. M. (1972) Plagioclase cation exchange equilibria with aqueous chloride solution at 700° C and 2000 bars in the presence of quartz. *American Journal of Science* **272**, 234-272.

Powell R. (1987) Darken quadratic formalism and the thermodynamics of minerals. *American Mineralogist* **72**, 1-11.

Powell R. and Holland T. J. B. (1993) The applicability of least-squares in the extraction of thermodynamic data from experimentally bracketed mineral equilibria. *American Mineralogist* **78**, 107-112.

Pownceby M. I. and O'Neill H. S. C. (1994) Thermodynamic data from redox reactions at high-temperatures .III. Activity-composition relations in Nil-Pd alloys from EMF-measurements at 850-1250-K, and calibration of the NiO+Ni-Pd assemblage as a redox sensor. *Contributions to Mineralogy and Petrology* **116**, 327-339.

Pownceby M. I. and O'Neill H. S. C. (1995) Thermodynamic data from redox reactions at high temperatures. V. Thermodynamic properties of NiO-MnO solid solutions by a solid electrolyte (EMF) cell technique. *Contributions to Mineralogy and Petrology* **119**, 409-421.

Pownceby M. I. and O'Neill H. S. C. (2000) Thermodynamic data from redox reactions at high temperatures. VI. Thermodynamic properties of CoO-MnO solid solutions from emf measurements. *Contributions to Mineralogy and Petrology* **140,** 28-39.

Putnis A. (1992) *Introduction to mineral sciences*. Cambridge: Univer. Press.

Redlich O. and Kister A. T. (1948) Algebraic representation of thermodynamic properties and the classification of solutions. *Industrial and engineering chemistry* **40(2)**, 345-348.

Sack R. O. (1980) Some constraints on the thermodynamic mixing properties of Fe-Mg orthopyroxenes and olivines. *Contribution to Mineralogy and Petrology* **71**, 257-269.

Saxena S. K. (1973) *Thermodynamics of Rock-Forming Crystalline Solutions*. Springer-Verlag.

Schmid R., Cressey G., and Wood B. J. (1978) Experimental-determination of univariant equilibria using divariant solid-solution assemblages. *American Mineralogist* **63**, 511-515.

Shi P. F., Saxena S. K., and Sundman B. (1992) Sublattice solid-solution model and its application to ortho-pyroxene $(Mg,Fe)_2Si_2O_6$. *Physics and Chemistry of minerals* **18**, 393-405.

Strimpfl M., Ganguly J., and Molin G. (1999) Fe^{2+}-Mg order-disorder in orthopyroxene: equilibrium fractionation between the octahedral sites and thermodynamic analysis. *Contributions to Mineralogy and Petrology* **136**, 297-309.

Thompson J. B. (1969) Chemical reactions in crystals. *American Mineralogist* **54**, 341-375.

Thompson J. B. (1970) Chemical reactions in crystals: corrections and clarification. *American Mineralogist* **55**, 528-532.

Turnock A. C. and Eugster H. P. (1962) Fe-Al oxides: phase relationships below 1000 ^oC. *Journal of Petrology* **3**, 533-565.

Uchida E., Gima M., and Imai N. (1996) Experimental study on ion exchange of Ca^{2+}, Fe^{2+} and Mn^{2+} between garnet solid solution and 2N aqueous chloride solution at 600 ^oC and 1 kb. *Journal of Mineralogy, Petrology and Economic Geology* **91**, 305-318.

Urusov V. S. (2000) Comparison of semi-empirical and *ab initio* calculations of the mixing properties of MO-M'O solid solutions. *Journal of Solid State Chemistry* **153**, 357-364.

Urusov V. S. (2001) The phenomenological theory of solid solutions. In *Solid solutions in silicate and oxide systems / EMU Notes in Mineralogy*, Vol. 3 (ed. C. A. Geiger), pp. 121-153. Eötvös Univ. Press.

von Seckendorff V. and O'Neill H. S. C. (1993) Experimental determination of the partitioning of Mg and Fe^{2+} between olivine and orthopyroxene at 900, 1000 and 1150°C and 1.6 GPa: constraints on activity-composition relations in binary Mg-Fe olivine and orthopyroxene solid solutions. *Contributions to Mineralogy and Petrology* **113,** 196-207.

Wasastjerna J. A. (1949) On the theory of the heat of formation of solid solutions. *Soc. Sci. Fenn. Comment. Phys.-Math.* **15(3)**, 1-13.

Wood B. J. (1988) Activity measurements and excess entropy–volume relationships for pyrope–grossular garnets. *Journal of Geology* **96**, 721-729.

Wood B. J. and Banno S. (1973) Garnet-orthopyroxene and orthopyroxene-clinopyroxene relationships in simple and complex systems. *Contributions to Mineralogy and Petrology* **42**, 109-124.

Wood B. J. and Nicholls J. (1978) The thermodynamic properties of reciprocal solid solutions. *Contributions to Mineralogy and Petrology* **66**, 389-400.

Appendix 2A

End-members and probability weightings for a pyroxene phase in the Na-Ca-Mg-Fe^{2+}-Al-Cr-Fe^{3+}-Si-Ti system

Table 2A.1 In the left column all possible stoichiometric, charge-balanced, Si-bearing end-members not related by order-disorder for a pyroxene (either ortho- or clinopyroxene) phase in a general (Na-Ca-Mg-Fe^{2+}-Al-Cr-Fe^{3+}-Si-Ti) system are listed. For each end-member the probability 'weight' Ψ is presented in the right column. The Ti-bearing end-members and corresponding probabilities of occurrence, that are not here reported, are immediately obtained by simply substituting Si with Ti. This gives sixteen more end-members.

End-member	[(a)] Ψ
$NaAlSi_2O_6$	$N_{Na}\left(N_{Al}/N_R\right)\left(N_{Si}/N_T\right)$
$NaCrSi_2O_6$	$N_{Na}\left(N_{Cr}/N_R\right)\left(N_{Si}/N_T\right)$
$NaFeSi_2O_6$	$N_{Na}\left(N_{Fe^{3+}}/N_R\right)\left(N_{Si}/N_T\right)$
$Mg_2Si_2O_6$	$\left(1-N_{Ca}\right)\left(1-N_{Na}/2-N_R/2\right)\left(N_{Mg}/N_{M^{2+}}\right)\left(N_{Si}/N_T\right)$
$Fe_2Si_2O_6$	$\left(1-N_{Ca}\right)\left(1-N_{Na}/2-N_R/2\right)\left(N_{Fe^{2+}}/N_{M^{2+}}\right)\left(N_{Si}/N_T\right)$
$CaMgSi_2O_6$	$N_{Ca}\left(1-N_{Na}/2-N_R/2\right)\left(N_{Mg}/N_{M^{2+}}\right)\left(N_{Si}/N_T\right)$
$CaFeSi_2O_6$	$N_{Ca}\left(1-N_{Na}/2-N_R/2\right)\left(N_{Fe_{2+}}/N_{M^{2+}}\right)\left(N_{Si}/N_T\right)$
$CaAl_2SiO_6$	$N_{Ca}\left(N_R/2-N_{Na}/2\right)\left(N_{Al}/N_R\right)\left(N_{Si}/N_T\right)$
$MgAl_2SiO_6$	$\left(1-N_{Ca}\right)\left(N_R/2-N_{Na}/2\right)\left(N_{Al}/N_R\right)\left(N_{Mg}/N_{M^{2+}}\right)\left(N_{Si}/N_T\right)$
$FeAl_2SiO_6$	$\left(1-N_{Ca}\right)\left(N_R/2-N_{Na}/2\right)\left(N_{Al}/N_R\right)\left(N_{Fe^{2+}}/N_{M^{2+}}\right)\left(N_{Si}/N_T\right)$
$CaCr_2SiO_6$	$N_{Ca}\left(N_R/2-N_{Na}/2\right)\left(N_{Cr}/N_R\right)\left(N_{Si}/N_T\right)$
$MgCr_2SiO_6$	$\left(1-N_{Ca}\right)\left(N_R/2-N_{Na}/2\right)\left(N_{Cr}/N_R\right)\left(N_{Mg}/N_{M^{2+}}\right)\left(N_{Si}/N_T\right)$
$FeCr_2SiO_6$	$\left(1-N_{Ca}\right)\left(N_R/2-N_{Na}/2\right)\left(N_{Cr}/N_R\right)\left(N_{Fe^{2+}}/N_{M^{2+}}\right)\left(N_{Si}/N_T\right)$
$CaFe_2SiO_6$	$N_{Ca}\left(N_R/2-N_{Na}/2\right)\left(N_{Fe^{3+}}/N_R\right)\left(N_{Si}/N_T\right)$
$MgFe_2SiO_6$	$\left(1-N_{Ca}\right)\left(N_R/2-N_{Na}/2\right)\left(N_{Fe^{3+}}/N_R\right)\left(N_{Mg}/N_{M^{2+}}\right)\left(N_{Si}/N_T\right)$
$FeFe_2SiO_6$	$\left(1-N_{Ca}\right)\left(N_R/2-N_{Na}/2\right)\left(N_{Fe^{3+}}/N_R\right)\left(N_{Fe^{2+}}/N_{M^{2+}}\right)\left(N_{Si}/N_T\right)$

Notes: [(a)] $N_{M^{2+}} = N_{Mg} + N_{Fe^{2+}}$;

$N_R = N_{Al} + N_{Cr} + N_{Fe^{3+}}$;

$N_T = N_{Si} + N_{Ti}$.

Chapter 3

Gibbs free energy minimization: a new approach to the forward modeling of equilibrium phase assemblages

3.1 Introduction

The determination of equilibrium phase assemblages as a function of pressure, temperature and composition is an important part of igneous and metamorphic petrology. In most cases, however, these assemblages are not accessible to direct observation. Moreover, the extremely sluggish kinetics of the majority of the phase equilibria reactions makes them very difficult to be reproduced in the laboratory. Further complications arise from the difficulty of extrapolating simple system data into complex systems, of establishing true reversal of reactions involving solid solution phases and of interpreting non-equilibrium phase assemblages and the history of the rock.

In recent years thermodynamic modeling has proved to be a powerful method to solve these problems. Thermodynamics has found widespread application in geology as it provides a very effective tool to compare experimental results with other studies and to extrapolate experimental data in pressure-temperature-compositional space. One of the most important and useful properties of thermodynamic modeling is the possibility of predicting stable phase relationships. Once an appropriate model is derived (see also chapter 2) and reliable end-member and solution parameters data are available (see also chapter 6), it is possible, based on thermodynamic calculations, to infer the stability of phase assemblages even at conditions beyond the range of current experimental techniques.

In this chapter the new thermodynamically based algorithm derived for this study, which has been adopted (see chapters 4 and 5) to compute equilibrium phase assemblages as a function of composition, temperature and pressure, is described. The algorithm has been coded as a highly flexible FORTRAN computer program (named '*Gib*'), and it has been set up, at the moment, to perform equilibrium calculations in NaO-CaO-MgO-FeO-Al_2O_3-Cr_2O_3-Fe_2O_3-TiO_2-SiO_2 systems. However, the program is designed in a way that any other oxide *component* could be easily added. Similarly, so far, a total of eleven phases

(i.e. [6]orthopyroxene, clinopyroxene, [7]pigeonite, garnet, olivine, spinel, plagioclase, quartz, kyanite, sillimanite, corundum; see also section 3.4) are included in the program. Additional phases could be added to the program and included in the minimization process at any time and in a straightforward manner.

3.2 Determining system equilibrium conditions: review of previous methods and the new approach adopted in this work

In general when searching for the equilibrium condition of a multiphase system two different although equally valid methodologies can be followed.

In one case determination of equilibrium is achieved by direct application of the Gibbs Free Energy Minimum Principle which states that the equilibrium value of any unconstrained internal parameter in a system at constant temperature, T, and pressure, P, minimizes the system's Gibbs free energy. It follows that, at equilibrium conditions:

$$\mathbf{G}^{\mathbf{system}} = minimum \quad \Rightarrow \quad dG = 0, \quad d^2G > 0 \tag{3.1}$$

The alternative way to investigate the equilibrium conditions of a system comes from the observation that a system is in stable equilibrium when no thermodynamic processes are possible within it. There are three thermodynamic processes that can take place in a closed multiphase system, each one characterized by a different potential: heat transfer (=T), mechanical work (=P) and mass transfer (= chemical potential $\Rightarrow \mu$). More specifically, T represents the intensive measure of the contribution to the system's free energy of any heat transfer within the system. In the same way P represents the intensive measure of the contribution to the system's free energy of any mechanical work done within the system. Similarly the chemical potential, μ, is the intensive measure of the contribution to the system's free energy of any mass transfer within the system. If these

[6] Throughout the rest of this chapter the abbreviations *opx* = orthopyroxene, *cpx* = clinopyroxene, *pig* = pigeonite, *grt* = garnet, *ol* = olivine, *sp* = spinel, *pl* = plagioclase, *qtz* = quartz, *ky* = kyanite, *sil* = sillimanite, *cor* = corundum will in most cases be used.
[7] The program has been set up in a way that the low-Ca clinopyroxene (i.e. pigeonite) can also be treated as a distinct 'phase'.

potentials are uniform in any part of the system then no thermal, mechanical or chemical process can occur.

Usually one would assume to deal with a system at constant T and P, that is, temperature and pressure have the same value in any part of the system. In such cases, the system's equilibrium conditions are reached when the chemical potential for every *component i* also has the same value throughout the system, i.e.:

$$\mu_i^1 = \mu_i^2 = \ldots = \mu_i^p \qquad (i = 1,\ldots,c) \tag{3.2}$$

with:

c = total number of *components* in the system

p = total number of phases in the system

In the past decades, many different algorithms have been proposed to find the equilibrium phase composition for heterogeneous systems at constant T and P. Van Zeggeren and Storey (1970), Smith and Missen (1982), Ghiorso (1985) and more recently Karpov et al. (1995) have reviewed available methods. These methods can basically be grouped into two types:

1. A numerical solution of a set of equilibrium equations as in Eq. (3.2) for every *component* in the system (e.g. Helgeson et al., 1970; Wolery, 1979; Reed, 1982; Bina and Wood, 1987; Powell and Holland, 1988);
2. A direct minimization of $\mathbf{G}^{\mathbf{system}}$ as in Eq. (3.1) (e.g. Van Zeggeren and Storey, 1970; Shvarov, 1978; Dorofeyeva and Khodakovskiy, 1981; Saxena and Eriksson, 1983; Ghiorso, 1985; De Capitani and Brown, 1987; Harvie et al., 1987; Ghiorso and Sack, 1995; Saxena, 1996; Takeno, 2001; Davies et al., 2002).

In recent years the direct minimization of the $\mathbf{G}^{\mathbf{system}}$ (i.e. method 2) using non-linear optimization techniques has become the far more popular approach for dealing with composite systems that involve a large number of chemical end-members.

For any heterogeneous system of fixed composition consisting of a number p of phases the expression of general equilibrium conditions is given by Eq. (3.1), where:

$$\mathbf{G}^{\mathbf{system}} = \sum_{\phi=1}^{p} \boldsymbol{G}^{\phi} = n^1 G^1 + n^2 G^2 + \ldots + n^p G^p = \sum_{\phi=1}^{p} n^{\phi} G^{\phi} \qquad (3.3)$$

with:

$\boldsymbol{G^{\phi}} = n^{\phi} G^{\phi}$ = total Gibbs free energy of phase ϕ

n^{ϕ} = number of moles of phase ϕ in the system

G^{ϕ} = molar Gibbs free energy for phase ϕ

For every phase ϕ in the system the molar Gibbs free energy, $G^{\phi} = G\left(T, P, X_{ik}^{\phi}\right)$, is a function of T, P and composition, as expressed by (X_{ik}^{ϕ}), the site occupancy[8] of cation *'i'* in sublattice *'k'*. The usual general expression of G^{ϕ} is then given by (e.g. Chatterjee, 1991):

$$^{9}G^{\phi} = G^{end\text{-}members} + G^{ideal} + G^{excess} \qquad (3.4)$$

In chapter 2 it was explained how the expressions for $G^{e\text{-}m}$, G^{id} and G^{ex} would vary depending on the phase considered, and how in past studies different expressions have been adopted for these terms. In the same chapter, the way expressions of $G^{e\text{-}m}$, G^{id} and G^{ex} have been formulated in this study for the phases included in '*Gib*' was also shown.

In a general case one wants to be able to solve the Gibbs free energy minimization (i.e. GFEM) problem given by Eq. (3.1) for systems that contain any type of phase including complex multi-site solid solution phases (e.g. pyroxene, spinel, etc.; see also section 2.8), where mixing takes place on different sublattices. If Eq. (3.4) is then adopted

[8] In this work the assumption of an idealized case where cations of a like charge and size (e.g. Mg and Fe^{2+}, or Al, Cr and Fe^{3+}) partition randomly between the sites they occupy has been made. Accordingly, the site occupancies X_{ik}^{ϕ}'s have been identified not only on 'crystal-chemical' basis, but also following 'thermodynamic modeling' considerations (see also section 3.4 on this point). As mentioned in section (2.5.3), it would then be more appropriate to call them 'virtual site occupancies'. For simplicity, however, in the rest of this chapter the term 'site occupancy' has been used.

[9] Throughout the rest of this chapter the abbreviations $G^{e\text{-}m}$ for $G^{end\text{-}member}$, G^{id} for G^{ideal}, G^{ex} for G^{excess} are used.

to represent the molar Gibbs free energy for any phase ϕ in the system, a minimization of $\mathbf{G}^{\mathbf{system}}$ as given by Eq. (3.3), independently from the actual expressions chosen to represent $G^{e\text{-}m}$, G^{id} and G^{ex}, should necessarily be carried out under several different constraints. More specifically, charge balance and stoichiometry constraints on each sublattice should be included for every phase ϕ in the system, as well as mass balance constraints for every cation in the system and non-negativity constraints on number of moles per phase and on site occupancies throughout the whole system. Furthermore if order-disorder phenomena need to be taken into account, additional ratio constraints have to be included. In section 3.3 a detailed description of form and meaning of all these constraints is presented.

The problems caused by this situation have usually been avoided in the past by expressing G^{ϕ} and $\boldsymbol{G}^{\boldsymbol{\phi}}$ in a different way. A commonly adopted expression of $\boldsymbol{G}^{\boldsymbol{\phi}}$ is (e.g. Ganguly and Saxena, 1987):

$$\boldsymbol{G}^{\boldsymbol{\phi}} = \sum_{i=1}^{c} n_i^{\phi} \mu_i^{\phi} \tag{3.5}$$

with:

n_i^{ϕ} = number of moles of *component i* in phases ϕ

μ_i^{ϕ} = chemical potential of *component i* in phases ϕ

c = total number of *components* in phase ϕ

Accordingly, the expression of G^{ϕ} is derived dividing $\boldsymbol{G}^{\boldsymbol{\phi}}$ by $\sum_{i=1}^{c} n_i^{\phi}$, that is, the sum of the number of moles of all phase *components*:

$$G^{\phi} = \frac{\boldsymbol{G}^{\phi}}{\sum_{i=1}^{c} n_i^{\phi}} = \sum_{i=1}^{c} x_i^{\phi} \mu_i^{\phi} \tag{3.6}$$

Where, $x_i^{\phi} = \dfrac{n_i^{\phi}}{\sum_{i=1}^{c} n_i^{\phi}}$ = molar fraction of *component i* in phase ϕ

As a result, adopting Eq (3.5) to express $\boldsymbol{G^{\phi}}$, the expression of $\mathbf{G^{system}}$ for a system consisting of a number *p of* phases, becomes:

$$\boldsymbol{G^{system}} = \sum_{\phi=1}^{p} \sum_{i=1}^{c} n_i^{\phi} \mu_i^{\phi} \tag{3.7}$$

Or in the molar form:

$$G^{molar-system} = \sum_{\phi=1}^{p} \sum_{i=1}^{c} x_i^{\phi} \mu_j^{\phi} \tag{3.8}$$

This obviously does not change the nature of the problem, which is still the minimization of $\mathbf{G^{system}}$. However, either the adopted expression of $\mathbf{G^{system}}$ is given by Eq (3.7) or Eq. (3.8) (e.g. Van Zeggeren and Storey, 1970; Smith and Missen, 1982; Ghiorso 1985; Harvie et al., 1987; Ghiorso and Sack, 1995; Saxena, 1996; Takeno, 2001; Davies et al., 2002), or it is still given by Eq. (3.3), but Eq. (3.6) instead of Eq. (3.4) is used to express G^{ϕ} (e.g. Brown and Skinner, 1974; Connolly and Kerrick, 1986; De Capitani and Brown, 1987; Cheynet, 2002).

The main advantage of the adoption of chemical potentials ($\mu_i^{\phi}{}'s$) in the computation is that the minimization can be carried out under a reduced number of constraints (usually simply mass balance and non-negativity constraints), since the other constraints are implicitly satisfied within the chemical potential expression. As a consequence relatively simple numerical techniques can be employed.

On the other hand, the use of chemical potentials in the derivation and minimization of $\mathbf{G^{system}}$ may carry an intrinsic contradiction. By definition, the chemical potential of a

component i, μ_i, tells how $\mathbf{G}^{\mathbf{system}}$ changes when an infinitesimal amount of that *component*, dn_i, is added to or removed from the system, holding T, P and the other compositional variables (i.e. n_j with $j \neq i$) constant. Accordingly, the expression of μ_i for any *component i* in the system is obtain by differentiating $\mathbf{G}^{\mathbf{system}}$ with respect to the number of moles of that *component* in the system (e.g. Anderson and Crerar, 1993):

$$\mu_i = \left(\frac{\partial \mathbf{G}^{\mathbf{system}}}{\partial n_i} \right)_{T,P,n_{j \neq i}} \tag{3.9}$$

Which, in the equivalent 'molar' form, becomes (e.g. Reusser, 1994; for binary systems):

$$\mu_i = G^{molar-system} + (1 - x_i) \cdot \left(\frac{\partial \mathrm{G}^{\text{molar-system}}}{\partial x_i} \right)_{T,P,x_{j \neq i}} \tag{3.10}$$

A relation analogous to Eq. (3.10) also holds for a multicomponent solution if the derivative of $G^{molar-system}$ with respect to the x_i is taken at constant T, P and constant relative amounts of all components other than i, *i.e.* at constant $x_j : x_k : x_l : \ldots$ (Darken, 1950). This multicomponent expression is often referred to as the *Darken equation*, and has been applied by Sack and Loucks (1985) and Ghiorso (1990) to the problems of multicomponent mineral solid solutions (Ganguly, 2001). Thus, it appears clear that in order to derive the expression of μ_i an appropriate expression of $\mathbf{G}^{\mathbf{system}}$ and/or $G^{molar\text{-}system}$ has first to be obtained.

The commonly adopted general expression of μ_i has the form (e.g. Chatterjee, 1991):

$$\mu_i = G_i^o + RT \ln a_i \tag{3.11}$$

Where, $a_i = x_i \cdot \gamma_i$ represents the activity of *component i* in the solution and γ_i is the activity coefficient.

Such expression of μ_i has been derived (e.g. Anderson and Crerar, 1993) by first using Eq. (3.4) and Eq. (3.3) to obtain G^{ϕ} and $\mathbf{G}^{\mathbf{system}}$ respectively, then applying either Eq. (3.9) or Eq. (3.10). In Appendix 3A an example of derivation of μ_i using Eq. (3.9) is presented.

The approach followed in former studies when mathematically formulating the GFEM problem has always been to use an equation like Eq. (3.11) for deriving the expressions of phase/system *components*, then to substitute such expressions into Eq. (3.5) and/or Eq. (3.6). Accordingly, the expression of $\mathbf{G}^{\mathbf{system}}$ used in the minimization process is then obtained. The clear contradiction in this approach is that the quantities μ_i used to derive the expression of $\mathbf{G}^{\mathbf{system}}$ that is minimized would implicitly assume that $\mathbf{G}^{\mathbf{system}}$ had previously already been defined by first using an equation like Eq. (3.4) to express G^{ϕ} and then substituting G^{ϕ} into Eq. (3.3). It would certainly be a more direct and, perhaps, a more 'coherent' a minimization algorithm that made use of the 'original' $\mathbf{G}^{\mathbf{system}}$ expression, that is, the expression that explicitly or implicitly was initially used to derive the μ_i's expressions (see also Appendix 3A).

The main advantage of employing chemical potentials in the minimization process comes from a computational point of view, as relatively simple numerical methods can be used (see also section 3.5.1 for a general review of this matter). None of the methods previously embraced would be suitable to solve the GFEM problem if formulated using the 'original' $\mathbf{G}^{\mathbf{system}}$ expression. In recent years, however, sophisticated constrained algorithms have become widely available through public domain software packages. The employment of such methods could allow the GFEM problem to be solved even if formulated using the 'original' $\mathbf{G}^{\mathbf{system}}$ expression, and this is the approach followed in this study (N.B. A detailed description of how the forward problem has been outlined and of the numerical technique used to solve it is given in sections 3.3 and 3.5).

Here lies the most significant innovation presented in this chapter on the way to solve the GFEM problem: minimizing directly the 'original' $\mathbf{G}^{\mathbf{system}}$, without going through

the derivation of the chemical potential's expression for every system *component*. In Fig. 3.1 the difference between past and present approaches is summarized.

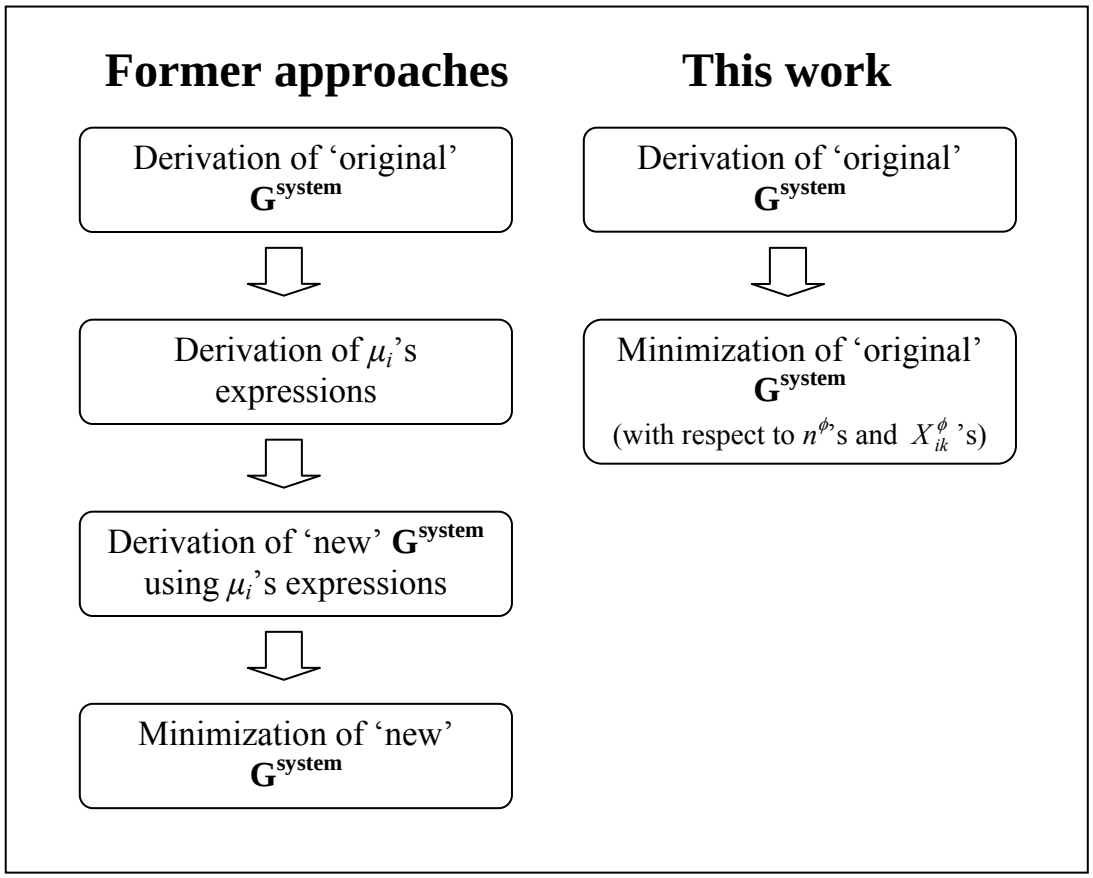

Fig.3.1 Schematic representation of the 'path' followed in previous works to solve the GFEM problem compared to the approach adopted in this study.

A solid argument in favor of this innovative approach is obviously that the conceptual contradiction that affects former approaches is clearly avoided. At the same time the possibility of doing a 'direct' minimization of $\mathbf{G}^{\mathbf{system}}$ prevents from other problems and limits related to the adoption of chemical potentials.

The actual differentiation of $\mathbf{G}^{\mathbf{system}}$ or $G^{molar\text{-}system}$, as in Eq. (3.9) or Eq. (3.10) respectively, that leads to the derivation of the μ_i's expressions can, in fact, be very difficult especially when dealing with complex solid solutions. General ways to obtain such expressions have been proposed for solutions with variable degrees of order-disorder (e.g. Ghiorso, 1990), in which case the use of computer software becomes advisable to perform

the needed algebraic calculations. The derived μ_i's expressions can be very complex and somehow confusing even for systems that are relatively simple from a compositional point of view such as quadrilateral pyroxenes (e.g. Sack and Ghiorso, 1994b) or quadrilateral amphiboles (Ghiorso and Evans, 2002). Dealing with systems characterized by larger number of oxide *components* the μ_i's expressions become more and more complicated (e.g. Sack and Ghiorso, 1994c). The number of parameters contained in such expressions can be so large that checking their validity could become unfeasible. Furthermore, in general, the chemical potential expressions have to be manually coded into the minimization algorithm and considering their complexity coding errors can be introduced.

Derivation of chemical potential expressions can be controversial also for another reason. By definition in order to get the chemical potential's expression for a *component i* the differentiation of $\mathbf{G}^{\mathbf{system}}$ or $G^{molar\text{-}system}$ has to be performed with respect to the number of moles or the molar fraction of that *component* provided that it is an 'independent' *component* (e.g. Anderson and Crerar, 1993). As long as one is dealing with simple solutions the choice of 'independent' *components* is usually straightforward as all the *components* needed to describe the composition of the phases in the system can be considered to be 'independent'. By contrast, when a system contains complex solid solutions not all the *components* that can be defined within the system are 'independent' (Chatterjee, 1991). These *components* can in fact be intimately related to each other, sometimes through reciprocal reactions (see Wood and Nicholls, 1978). In these cases the choice of which are the 'independent' *components* whose expression has to be derived and included in the minimization process is not straightforward. In some cases a compromise must be made, for instance dividing all the system's possible *components* into 'real' *components* (i.e. 'independent') and 'end-member' *components*, that is, *components* whose expressions can be obtained from a combination of those of the 'real' ones (e.g. Sack and Ghiorso, 1994c). However, the division between 'real' and end-member' *components* still appears to be quite arbitrary and, even more important, the choice itself of 'general' (i.e. without distinguishing between 'independent' and not) system *components* is not without shortcomings. By definition, the *components* of a system are identified by the smallest set of chemical formulae required to describe the composition of all the phases in a system. Despite the simplicity of this definition, solids and solid solutions present a terminology

problem. Although the number of *components* possessed by a system in a given state is fixed, the identity of these *components* is not (Anderson and Crerar, 1993). For example, systems can be considered as having a different number of *components* in different stable equilibrium states. Pure albite ($NaAlSi_3O_8$) is a one-*component* system at ambient pressure, but at high pressures and temperatures it breaks down to jadeite ($NaAlSi_2O_6$) and quartz (SiO_2), and two *components* are required to describe the same bulk composition simply because the number of possible phases has changed. Many other similar examples could be used to show ambiguities and doubts connected to the choice of system's *components*.

In this study, by directly minimizing the 'original' $\mathbf{G}^{\mathbf{system}}$, any possible contentious issue related to the derivation of chemical potential expressions and/or to the choice of system's *components* is clearly avoided. This new approach is valid irrespective of the actual expressions of $G^{e\text{-}m}$, G^{id} and G^{ex} used to obtain the $\mathbf{G}^{\mathbf{system}}$ expression. This means that the thermodynamic model described in chapter 2 could be at any time modified or one could even decide to use a completely different model. Moreover, any particular phase could be treated using the '$n \cdot \mu$' approach where this is convenient, as, for example, in treating oxygen fugacity or any component in an open system whose chemical potential is fixed externally. In any case the GFEM problem would still be outlined and solved in the same way and, thanks to the high flexibility of the computer program written to perform the computation (see also section 3.5), only minor adjustments to the codes would be needed.

3.3 Mathematical formulation of the GFEM problem

The goal of the forward problem is to find the chemical composition of the phases present in the system and the number of moles of each phase that minimize the Gibbs free energy of the system at a given temperature and pressure condition. In section 3.2 it was shown that the expression of $\mathbf{G}^{\mathbf{system}}$ to minimize is given by Eq. (3.3). To express G^{ϕ}, Eq. (3.4) is then used, while the formalism adopted to derive expressions of $G^{e\text{-}m}$, G^{id} and G^{ex} for any phase included in the program '*Gib*' was presented in chapter 2. In the previous section it was also said that for any silicate or oxide crystalline phase ϕ in the system the chemical composition is expressed through the site occupancies, X_{ik}^{ϕ}'s. Therefore, the

number of moles, n^{ϕ}'s, and site occupancies, X_{ik}^{ϕ}'s, are the *unknowns* whose values are sought such that $\mathbf{G}^{\mathbf{system}}$ is minimized. Given these *unknowns* the minimization process in a general case has to be carried out under several constraints. All the possible constraints that may have to be imposed on the solution are listed below. In sections 3.3.1 and 3.3.2 a detailed description is presented of the form these constraints take for any phase included in the program.

For every cation *i* in the system mass balance (*non-linear equality*) constraints:

$$\mathbf{M_i} = \sum_{\phi=1}^{p} n^{\phi} \sum_{k=1}^{n} X_{ik}^{\phi} \tag{3.12}$$

with:

p = total number of phases in the system
n = total number of sublattices in phase ϕ
$\mathbf{M_i}$ = total number of moles of cation i in the system.

For each phase ϕ stoichiometry (*linear equality*) constraints on every sublattice *k*:

$$S_k^{\phi} = \sum_{i=1}^{c} X_{ik}^{\phi} \tag{3.13}$$

with:

c = total number of cations in one mole of phase ϕ

where, the value of S_k^ϕ depends on the type of phase and sublattice considered (e.g., if ϕ = *grt* and *k* = dodecahedral X site, then $S_k^\phi = 3$; or if ϕ = *ol* and *k* = octahedral M2 site, then $S_k^\phi = 1$)

For each phase ϕ charge balance (*linear equality*) constraints:

$$C^\phi = \sum_{i=1}^{c} \beta_i \sum_{k=1}^{n} X_{ik}^\phi \qquad (3.14)$$

with:

β_i = individual charge of cation *i*

where, the value of C^ϕ depends on the type of phase considered (e.g., if ϕ = spinel, then $C^\phi = 8$; or if ϕ = pyroxene, then $C^\phi = 12$)

For each phase ϕ and each site occupancy X_{ik}^ϕ non-negativity *(linear inequality)* constraints:

$$n^\phi \geq 0 \qquad X_{ik}^\phi \geq 0 \qquad (3.15)$$

Furthermore, for the complex solutions phases (i.e. pyroxene, olivine and spinel) included in the program in some cases additional ratio (*non-linear equality*) constraints are imposed on the solution. Ratio constraints can be applied to handle order/disorder phenomena, that is, random and/or non-random distributions of same cations among different sublattices (e.g. Mg and Fe^{2+} among sublattices M2 and M1 in pyroxene and in olivine solid solution). In section 3.4 an example is presented to show how, by imposing the appropriate ratio constraints, order/disorder phenomena are handled in the minimization process for a pyroxene solution. In an analogous way, the same phenomena are handled for the other complex solution phases. The general form of ratio constraints is:

$$C_\omega\left(X_{ik}^\phi\right) = 0 \qquad (\omega = 1,\ldots,s) \qquad (3.16)$$

with:

s = total number of 'independent' ratio constraints per phase

In Appendix 3B the procedure followed to derive Eq. (3.16) in the pyroxene solution case is shown.

Not every solid solution needs all these constraints imposed on it simultaneously. For some phases (e.g. garnet), the charge balance constraints are unnecessary for the range of compositions treated in this study because they are automatically satisfied by stoichiometry constraints (NB It would not be true if garnets were considered with 3+ cations in the dodecahedral sites, like REE garnets, or 4+ cations like Zr in the octahedral sites). In other cases (e.g. pyroxene) the need to impose charge balance constraints or not depends on the system's bulk composition. Moreover, for phases that can be found merely as pure end-member (e.g. quartz) the only constraints that have to be imposed are mass balance and non-negativity. Therefore, in general, the number and type of constraints that will be active during the minimization process will depend on the nature of the system (i.e. bulk composition, number and type of phases) whose Gibbs free energy is minimized. The examples presented in sections 3.4 and 3.3.2 will help to clarify this point.

3.4 Example of general problem solved: the pyroxene case

The pyroxene phase provides an ideal case to show the general type of problem that the program can solve where all the possible constraints may have to be imposed. At the same time this example is also useful to illustrate how, depending on the system's bulk composition, despite dealing with the same solution phase, only a restricted number of constraints will be needed. Notice that, as explained in chapter 2, the same thermodynamic model applies to the three different types of pyroxene included in the program '*Gib*'. As a consequence, the argument of this section is indistinguishably valid for any pyroxene phase.

All possible constraints imposed on pyroxene solutions are listed and described as follows.

non negativity constraints

Non-negativity constraints (i.e. $n^{\phi-px}$, $X_{ik}^{\phi-px} \geq 0$) are imposed to avoid that during the computation the value of number of moles for a phase and of its site occupancies could take a negative value.

These constraints are always needed.

mass balance constraints

Mass balance constraints (i.e. Eq. 3.12) are imposed to ensure that the compositions and amounts of all the phases at equilibrium add up to the system's initial bulk composition. For a pyroxene phase, consider the cation distribution as given by Table 3.1; the total amount of every cation *i*, N_i, is given, on a molar scale, by the horizontal sum across sites. For example, the total amount of Na (i.e. N_{Na}) in one mole of *px* is:

$$N_{Na}^{px} = X_{11}^{px} + X_{12}^{px} + X_{13}^{px} \tag{3.17}$$

Accordingly to Table 3.1, $X_{12}^{px} = X_{13}^{px} \equiv 0$. Eq. (3.17) can then be written:

$$N_{Na}^{px} = X_{11}^{px} \tag{3.18}$$

Similarly, the total amount of Ca (i.e. N_{Ca}) in one mole of *px* is:

$$N_{Ca}^{px} = X_{21}^{px} \tag{3.19}$$

While, the total amount of Mg, (i.e. N_{Mg}) in one mole of *px* is:

$$N_{Mg}^{px} = X_{31}^{px} + X_{32}^{px}; \tag{3.20}$$

And so on for all the other cations *i*.

The molar amounts of each cation have then to be multiplied by the number of moles of the pyroxene phase (i.e. $n^{\phi-px}$). The same will be done with any other phase to obtain the total amounts of every cation in the system (see Eq. 3.12).

Mass balance constraints are always needed.

The stoichiometry, charge balance and ratio constraints are directly related to the mineral's crystal-chemical formula. In the pyroxene structure, cations can be found on three energetically different types of sites: highly distorted octahedral sites, named M2 (one per formula unit, i.e. *pfu*), more regular octahedral sites, named M1 (one *pfu*), tetrahedral sites, named T (two *pfu*). This leads to the pyroxene general formula:

$$^{10}(M2)_1(M1)_1(T)_2O_6 \qquad (3.21)$$

In a general NaO-CaO-MgO-FeO-Al_2O_3-Cr_2O_3-Fe_2O_3-TiO_2-SiO_2 system, the site occupancies for a pyroxene phase can be represented as in Table 3.1:

Table 3.1. Cation distribution in pyroxene phase

cation	charge	site: M2	site: M1	site: T
Na	1+	X_{11}	#	#
Ca	2+	X_{21}	#	#
Mg	2+	X_{31}	X_{32}	#
Fe^{2+}	2+	X_{41}	X_{42}	#
Al	3+	#	X_{52}	X_{53}
Cr	3+	#	X_{62}	X_{63}
Fe^{3+}	3+	#	X_{72}	X_{73}
Si	4+	#	#	X_{83}
Ti	4+	#	#	X_{93}

Given this cation distribution Eq. (3.21) can be re-written:

[10] The two tetrahedral sites *pfu* in *cpx* (C2/c) are equivalent, while there are two distinct tetrahedral sites in the *opx* structure. In this work, however, the distinction between the two T sites in the *opx* structure has net been considered crucial for the purpose of thermodynamic modeling. Accordingly, Eq. (3.21) has been considered adequate to describe both *opx* and *cpx* crystal-chemical formulae.

$$\left(X_{11}^{px}, X_{21}^{px}, X_{31}^{px}, X_{41}^{px}\right)_1^{M2}\left(X_{32}^{px}, X_{42}^{px}, X_{52}^{px}, X_{62}^{px}, X_{72}^{px}\right)_1^{M1}\left(X_{53}^{px}, X_{63}^{px}, X_{73}^{px}, X_{83}^{px}, X_{93}^{px}\right)_2^{T} O_6 \qquad (3.22)$$

Some of the choices made, which are summarized in Table 3.1, may be controversial. The presence of Cr in site T, for instance, has never been proved and is unlikely on crystal-chemical grounds (and similarly for Fe^{3+} and its site occupancy X_{73}). At the same time it is well known that Ti can be found in site M1. As a result, a site occupancy X_{92} should be contemplated in the table while it is not.

It is important to emphasize that crystal-chemical considerations, although being an important criteria in determining phase site occupancies, have not been the only one. In chapter 2 the procedure followed to formulate a general model for pyroxene solid solutions has been discussed. It has also been explained how the choice of the end-members needed to describe pyroxene solutions thermodynamically was made according to that model. The site occupancies of Table 3.1 reflect choices and assumptions made when deriving the thermodynamic model and selecting model's end-members. More precisely, similarly to Al, also Cr and Fe^{3+} were assumed able to generate Tschermak end-members, and therefore they have been considered as substituting for Al. This explains the presence of site occupancies X_{63} and X_{73} in Table 3.1. In an analogous way Ti is assumed to substitute for Si in the generation of possible end-members. For this reason only the site occupancy X_{93} appears in the table while X_{92} has been left out.

At the same time the program has been set up in a way that allows the highest flexibility in the allocation of the site occupancies. This means that at any time it could be decided to include a X_{92} site occupancy or exclude X_{63} and X_{73}. The program could also handle any other possible site occupancy of Table 3.1, including unrealistic situations such as assuming Na to be present in site T, or Si in site M1, etc. On the other hand, any assumption made regarding cations distribution must be consistent with the thermodynamic model adopted.

An example will help to clarify this point. It can, for example, be assumed that the model discussed in chapter 2 proved to be inadequate and, for instance, one decided that Fe^{3+}-Tschermark is not a meaningful thermodynamic end-member for a pyroxene phase. From the 'cation distribution' point of view, this would simply mean that in Table 3.1 the site occupancy X_{73} has to be left out and only X_{72} will appear. However, from the

'thermodynamic model' point of view, rearranging the site occupancy table is not enough. The presence of the site occupancy X_{73} was necessitated by the assumption that a Fe^{3+}-Tschermark end-member could be used in order to model the Fe^{3+} present in the pyroxene solution. Deciding that the Fe^{3+}-Tschermark end-member is not appropriate implies that another end-member has to be chosen to account for the presence of Fe^{3+}. As a consequence, the thermodynamic model would need to be modified to include the new Fe^{3+}-containing end-member and a new expression of $G^{e\text{-}m}$ would have to be derived. Once this is done, table 3.1 could be accordingly updated. Only in this way consistency between model and site occupancy will be maintained.

Adopting a similar procedure, site occupancy tables have been derived for any other phase included in the program (see section 3.4.3). To proceed consistently with the way these tables are organized, the cations in the program have been assigned the following indexes:

1 = Na
2 = Ca
3 = Mg
4 = Fe^{2+}
5 = Al
6 = Cr
7 = Fe^{3+}
8 = Si
9 = Ti

These indexes are then usually used to specify the type of system one is dealing with. For instance, to refer to a CaO-MgO-SiO_2 (i.e. CMS) system, a 2,3,8 (i.e. Ca, Mg, Si) notation can be used; to refer to a NaO-CaO-MgO-Al_2O_3-SiO_2 (i.e. Na-CMAS) system, a 1,2,3,5,8 (i.e. Na, Ca, Mg, Al, Si), etc.

The remaining part of the exposition in this section assumes that the site occupancy distribution for a pyroxene phase is as given by Table 3.1.

stoichiometry constraints

The stoichiometry of the pyroxene crystal structure requires three constraints, one for each different sublattice (Eq. 3.21 or Eq. 3.22). These constraints are given by the vertical sums of site occupancies in Table 3.1. Considering only non-empty site occupancies[11], one obtains:

$$X_{11}^{px} + X_{21}^{px} + X_{31}^{px} + X_{41}^{px} \qquad = S_{M2}^{px} = 1 \tag{3.23}$$

$$X_{32}^{px} + X_{42}^{px} + X_{52}^{px} + X_{62}^{px} + X_{72}^{px} = S_{M1}^{px} = 1 \tag{3.24}$$

$$X_{53}^{px} + X_{63}^{px} + X_{73}^{px} + X_{83}^{px} + X_{93}^{px} = S_{T}^{px} = 2 \tag{3.25}$$

Stoichiometry constraints are always needed.

ratio constraints

In the pyroxene structure some cations can be found in more than one sublattice. In the present study, given the thermodynamic model derived in chapter 2 and the subsequent site occupancies of Table 3.1, cations that are assumed to partition among energetically different sites are: Mg and Fe^{2+} (between M2 and M1); Al, Cr and Fe^{3+} (between M1 and T). The way cation partitioning takes place is, in general, a function of several different parameters: *T*, *P*, bulk compositions. As a result, order-disorder phenomena can be used as indicator of crystallization conditions (e.g. Ganguly, 1982; Akamatsu et al., 1993; Ganguly et al. 1997; see also Pasqual et al., 2000; and references therein). Therefore, it appears useful during the minimization process to be given the option of modeling such phenomena. In order to do that, some additional constraints have been introduced in the program '*Gib*', which have been given the name of 'ratio constraints'.

For instance, to model the distribution of Mg and Fe^{2+} between M2 and M1 assuming complete disorder between the two sites, the ratio constraints are:

$$\frac{X_{31}^{px}}{X_{31}^{px} + X_{41}^{px}} = \frac{X_{32}^{px}}{X_{32}^{px} + X_{42}^{px}}; \qquad \frac{X_{41}^{px}}{X_{31}^{px} + X_{41}^{px}} = \frac{X_{42}^{px}}{X_{32}^{px} + X_{42}^{px}} \tag{3.26}$$

[11] Cations site vacancies are well known in pyroxenes. A significant example is represented by the end-member $(Ca_{0.5}Vac_{0.5})AlSi_2O_6$. This end-member, which is important for clinopyroxenes found in some SiO_2-rich eclogite xenoliths from kimberlites, has not been considered in the model for two reasons: 1) simplicity; 2) it is not a significant end-member in assemblages with olivine.

Note that by imposing one of the two constraints the other will automatically be satisfied (i.e. only one is an independent constraint).

And similarly, ratio constraints may be imposed to model the assumption that Al, Cr and Fe^{3+} are equally distributed between M1 and T sites (cf. Klemme and O'Neill, 2000):

$$\frac{X_{52}^{px}}{X_{52}^{px}+X_{62}^{px}+X_{72}^{px}}=\frac{X_{53}^{px}}{X_{53}^{px}+X_{63}^{px}+X_{73}^{px}} \tag{3.27}$$

$$\frac{X_{62}^{px}}{X_{52}^{px}+X_{62}^{px}+X_{72}^{px}}=\frac{X_{63}^{px}}{X_{53}^{px}+X_{63}^{px}+X_{73}^{px}} \tag{3.28}$$

$$\frac{X_{72}^{px}}{X_{52}^{px}+X_{62}^{px}+X_{72}^{px}}=\frac{X_{73}^{px}}{X_{53}^{px}+X_{63}^{px}+X_{73}^{px}} \tag{3.29}$$

Here, by imposing two of the three constraints the third will automatically be satisfied.

It is worthwhile to emphasize here that ratio constraints are not strictly needed as the minimization could be carried out without them. These constraints have been introduced to enable the possibility of modeling order-disorder phenomena and for this reason they have been coded in a way that they can easily be included or removed. During the minimization the choice of imposing them or not is left to the operator. To do that, in the program '*Gib*' (see Appendix 3C) an option is allowed for them to be switched 'on' or 'off'.

In some cases, ratio constraints cannot be applied at all. For example, when dealing with pyroxenes in the simple system CaO-MgO-SiO_2 where the only cation that can occupy two different sites is Mg, the existence of stoichiometry constraints on every sublattice automatically determines how Mg has to distribute between M2 and M1. A slightly different case is presented by the system CaO-MgO-Al_2O_3-SiO_2 where there are two cations (Mg and Al) that can be found on two different sites, but these cations can only partly substitute for each other. Mg can be found on M2 and M1 sites, while Al occurs on M1 and T. In this case the combined existence of stoichiometry and charge balance

constraints dictates the way Mg and Al are partitioned among M2, M1 and T. As a result, no ratio constraints need to be imposed. Similarly, for any other system it can easily be inferred when ratio constraints can be applied[12]. Depending on a system's bulk composition the program automatically handles any case where ratio constraints cannot be activated.

charge balance constraints

There is one more essential requirement that solution phase compositions have to meet. The values of the X_{ik}^{ϕ}'s, must be such that the net ionic charge summed over the mineral formula will be neutral. In the pyroxene chemical formula (e.g. Eq. 3.21) there are six oxygens per formula unit, which means 12 negative charges. As a consequence, using again the site occupancies of Table 3.1, the constraint of charge balance gives:

$$\begin{aligned}&\left[1^{+}\cdot\left(X_{11}^{px}\right)\right]+\\&\left[2^{+}\cdot\left(X_{21}^{px}\right)\right]+\left[2^{+}\cdot\left(X_{31}^{px}+X_{32}^{px}\right)\right]+\left[2^{+}\cdot\left(X_{41}^{px}+X_{42}^{px}\right)\right]+\\&\left[3^{+}\cdot\left(X_{52}^{px}+X_{53}^{px}\right)\right]+\left[3^{+}\cdot\left(X_{62}^{px}+X_{63}^{px}\right)\right]+\left[3^{+}\cdot\left(X_{72}^{px}+X_{73}^{px}\right)\right]+\\&\left[4^{+}\cdot\left(X_{83}^{px}\right)\right]+\left[4^{+}\cdot\left(X_{93}^{px}\right)\right]\\&=12\end{aligned} \tag{3.30}$$

Despite charge-balance neutrality of chemical formulas being a necessary requirement, these constraints do not always have to be imposed, as sometimes they are automatically ensured by the stoichiometry constraints. For a pyroxene phase charge balance constraints will not be needed in the system 2, 3&4, 8&9 and its subsystems, while they will have to be imposed in any other case.

All the information referring to pyroxene phases can then be displayed using an 'information box', as presented in Fig. 3.2.

[12] To summarize, for a pyroxene phase in the system (1&2, 3or4, 5or6or7, 8&9) and its related subsystems, ratio constraints cannot be applied, while they can in any other system. Notice that in the system (1&2, 3or4, 5or6or7, 8&9) cations 1 and 2 and cations 8 and 9 are, respectively, considered interchangeable, while if cation 3 is present cation 4 is not and, similarly, the presence of one among 5, 6 and 7 will exclude the presence of the other 2. As a result, subsystems 2,3,8; 2,3,9; 1and 2,3,5,8, etc., will be included, while subsystems 2, 3 and 4, 8; or 1 and 2, 3, 5 and 6, 8; etc., will not be included in the (1&2, 3or4, 5or6or7, 8&9) system. In an analogous way subsystems included in any other system (see later in this section and section 3.4.3) can be easily identified.

Pyroxene solid solution

Crystal chemical formula: $(M2)_1(M1)_1(T)_2O_6$

Table 3.1 Cation distribution in pyroxene phase

cation	charge	site: M2	site: M1	site: T
Na	1+	X_{11}	#	#
Ca	2+	X_{21}	#	#
Mg	2+	X_{31}	X_{32}	#
Fe^{2+}	2+	X_{41}	X_{42}	#
Al	3+	#	X_{52}	X_{53}
Cr	3+	#	X_{62}	X_{63}
Fe^{3+}	3+	#	X_{72}	X_{73}
Si	4+	#	#	X_{83}
Ti	4+	#	#	X_{93}

Mass balance constraints:

$$\mathbf{M_i^{px}} = n^{px} \cdot \sum_{k=1}^{3} X_{ik}^{px} \qquad (i = \text{Na, Ca, Mg, } Fe^{2+}\text{, Al, Cr, } Fe^{3+}\text{, Si, Ti})$$

Stoichiometry constraints:

$$X_{11}^{px} + X_{21}^{px} + X_{31}^{px} + X_{41}^{px} = S_{M2}^{px} = 1$$
$$X_{32}^{px} + X_{42}^{px} + X_{52}^{px} + X_{62}^{px} + X_{72}^{px} = S_{M1}^{px} = 1$$
$$X_{53}^{px} + X_{63}^{px} + X_{73}^{px} + X_{83}^{px} + X_{93}^{px} = S_{T}^{px} = 2$$

Ratio constraints:

$$\frac{X_{31}^{px}}{X_{31}^{px} + X_{41}^{px}} = \frac{X_{32}^{px}}{X_{32}^{px} + X_{42}^{px}}; \frac{X_{41}^{px}}{X_{31}^{px} + X_{41}^{px}} = \frac{X_{42}^{px}}{X_{32}^{px} + X_{42}^{px}}; \frac{X_{52}^{px}}{X_{52}^{px} + X_{62}^{px} + X_{72}^{px}} = \frac{X_{53}^{px}}{X_{53}^{px} + X_{63}^{px} + X_{73}^{px}}$$
$$\frac{X_{62}^{px}}{X_{52}^{px} + X_{62}^{px} + X_{72}^{px}} = \frac{X_{63}^{px}}{X_{53}^{px} + X_{63}^{px} + X_{73}^{px}}; \qquad \frac{X_{72}^{px}}{X_{52}^{px} + X_{62}^{px} + X_{72}^{px}} = \frac{X_{73}^{px}}{X_{53}^{px} + X_{63}^{px} + X_{73}^{px}}$$

Charge balance constraint:

$$\left[1^+ \cdot \left(X_{11}^{px}\right)\right] + \left[2^+ \cdot \left(X_{21}^{px}\right)\right] + \left[2^+ \cdot \left(X_{31}^{px} + X_{32}^{px}\right)\right] + \left[2^+ \cdot \left(X_{41}^{px} + X_{42}^{px}\right)\right] + \left[3^+ \cdot \left(X_{52}^{px} + X_{53}^{px}\right)\right] +$$
$$\left[3^+ \cdot \left(X_{62}^{px} + X_{63}^{px}\right)\right] + \left[3^+ \cdot \left(X_{72}^{px} + X_{73}^{px}\right)\right] + \left[4^+ \cdot \left(X_{83}^{px}\right)\right] + \left[4^+ \cdot \left(X_{93}^{px}\right)\right]$$
$$= 12$$

mass balance, stoichiometry constraints ⇒ always needed
charge balance constraint ⇒ not needed in system 2, 3&4, 8&9 and related subsystems
ratio constraints ⇒ not needed in system (1&2, 3or4, 5or6or7, 8&9) and related subsystems

Fig. 3.2 'Information box' for pyroxene phase

3.4.1 Unknowns versus constraints: proving that the forward problem can have a solution

Given the number of constraints that have to be imposed during the minimization process a concern might arise that the GFEM problem could be *over-constrained*, and, as a consequence, it could have no solution at all. To clarify this point and show that within the system, despite the number of constraints imposed, there will in general be some degrees of freedom, two examples are presented. In the first one (i.e. *sample-case I*) it will be assumed to deal with a 2,3,8, two-pyroxene (*opx* + *cpx*) system. In the second one (i.e. *sample-case II*) it will be again a two-pyroxene (*opx* + *cpx*) assemblage, but this time in the very general 1,2,3,4,5,6,7,8,9 system.

Sample-case I

2,3,8 system

2 phases: *opx* + *cpx*

Since the only cations present in the system are Ca, Mg and Si, the general Table 3.1 reduces to Table 3.2:

Table 3.2 Cation distribution for *opx* and *cpx* in *sample-case I*

cation	charge	site: M2	site: M1	site: T
Ca	2+	X_{21}	#	#
Mg	2+	X_{31}	X_{32}	#
Si	4+	#	#	X_{83}

The total number of variables for this *sample-case I* is equal to 10:

$$n^{opx}, n^{cpx}, X_{21}^{opx}, X_{31}^{opx}, X_{32}^{opx}, X_{83}^{opx}, X_{21}^{cpx}, X_{31}^{cpx}, X_{32}^{cpx}, X_{83}^{cpx}$$

These variables are related to one another by a number of constraints:

3 mass balance constraints (one for each cation in the system)

3 stoichiometry constraints for phase *opx*

3 stoichiometry constraints for phase *cpx*

charge balance constraints $\Rightarrow$ not needed

ratio constraints $\Rightarrow$ not needed

This gives a total of 9 *independent* constraints and 10 variables, which leaves one degree of freedom to the system. Therefore, the problem is not *over-constrained* and it can have a solution. At the same time there will be just one *free variable* to minimize $\mathbf{G}^{\mathbf{system}}$ with.

Sample-case II

1,2,3,4,5,6,7,8,9 system

2 phases: *opx* + *cpx*

The site occupancy distribution in this case is given by Table 3.1.

The total number of variables for *sample-case II* is equal to 30:

$$n^{opx}, n^{cpx},$$
$$X_{11}^{opx}, X_{21}^{opx}, X_{31}^{opx}, X_{41}^{opx}, X_{32}^{opx}, X_{42}^{opx}, X_{52}^{opx}, X_{62}^{opx}, X_{72}^{opx}, X_{53}^{opx}, X_{63}^{opx}, X_{73}^{opx}, X_{83}^{opx}, X_{93}^{opx},$$
$$X_{11}^{cpx}, X_{21}^{cpx}, X_{31}^{cpx}, X_{41}^{cpx}, X_{32}^{cpx}, X_{42}^{cpx}, X_{52}^{cpx}, X_{62}^{cpx}, X_{72}^{cpx}, X_{53}^{cpx}, X_{63}^{cpx}, X_{73}^{cpx}, X_{83}^{cpx}, X_{93}^{cpx}$$

These variables are related to one another by a number of constraints:

9 mass balance constraints (one for each cation in the system)

3 stoichiometry constraints for phase *opx*

3 stoichiometry constraints for phase *cpx*

1 charge balance constraint for phase *opx*

1 charge balance constraint for phase *opx*

3 *independent* ratio constraints for phase *opx*

3 *independent* ratio constraints for phase *cpx*

This gives a total of 23 *independent* constraints and 30 variables, which leaves seven degrees of freedom to the system. As a result, also in this case the problem is not *over-constrained* and there will be seven *free variables* to minimize $\mathbf{G}^{\mathbf{system}}$ with.

3.4.2 Remarks on the 'book-keeping' notation used

These two examples can also be used to clarify a doubt that could be raised about the relationship between variables and the 'book-keeping' notation adopted in the mathematical formulation of the GFEM problem.

As explained early in this chapter, the site occupancies, X_{ik}^{ϕ}, together with number of moles, n^{ϕ}'s, are the *unknowns* of the forward problem. For pyroxene phases, Table 3.1 has been used to represent site occupancy distributions, and analogous tables have been employed to represent the cation distributions for other phases (see section 3.4.3). Regardless of the system's bulk composition and the type of phase they refer to, these tables have been set up in exactly the same way. As a result, every site occupancy table consists of the same number of columns (i.e. same number of sublattices) and the same number of rows (i.e. same number of cations). The main advantage of this arrangement is that the notation adopted to specify a site occupancy will be the same for any phase in the system. In this way, cations occupying the same or analogous sublattices among different phases are identified with the same site occupancy, the only difference being the superscript used to specify which phases they belong to. Hence, the site occupancies $X_{52}^{opx}, X_{52}^{cpx}, X_{52}^{pig}, X_{52}^{grt}, X_{52}^{sp}$, all refer to Al. More specifically they indicate Al in site M1 for *opx*, *cpx* and *pig*, Al in site Y for *grt* and Al in site B for *spinel* (see also Table 3.1, Table 3.3 and Table 3.5).

The other important advantage of this procedure is that, as already explained describing Table 3.1, it allows flexibility in the distribution of cations between different phases and sites. This means that every cation present in the system could, in theory, be assigned to any phase and, within it, be distributed among any of its sublattices.

On the other hand, the adopted notation could perhaps cause confusion and even generate an error when the program has to select which among all possible phase site occupancies are the real *unknowns* to use for the minimization process. Setting up site

occupancy tables in the same way for any phase ϕ, independently of the type of phase and of the number and type of cations present in the system, could give the impression that the *unknowns* selected for the minimization will invariably be the same. This would be incorrect. For example, a general 1,2,3,4,5,6,7,8,9 system with two phases, *grt* and *opx,* is considered. If, then, ϕ = *opx*, *k* = M2 and *i* = 1, the site occupancy X_{11}^{opx} is identified, which in this case (see Table 3.1) is a 'real' variable. On the other hand, if ϕ = *grt*, *k* = X and *i* = 1, the site occupancy X_{11}^{grt} is identified, which will never be a 'real' variable (see Table 3.3). Another example: two pyroxenes (*opx* + *cpx*) in a 2,3,4,8 system. In this case for either pyroxenes (i.e. ϕ = *opx* or ϕ = *cpx*) if *k* = M2 and *i* = 1 site occupancies X_{11}^{opx} and X_{11}^{cpx} will never represent real *unknowns*. Many other similar examples could be brought up.

In the program this potential cause of inconsistency is handled in a very simple way. At the time of setting up site occupancy tables, the number and type of site occupancies for each phase that, depending on the system' bulk composition, will be treated as *unknowns* have been specified. This means that, the program 'knows' that, for instance, X_{11}^{grt} will never be an *unknown*, while X_{11}^{opx} may or may not be an *unknown* depending on the bulk composition. In this way, only the 'active' site occupancies are, during the computation, used to satisfy the constraints imposed and to calculate equilibrium phase compositions. At any time, the user can decide to change the status of any site occupancy from 'inactive' to 'active'.

3.4.3 'Information boxes' for other phases included in the program

Following an analogous procedure to the one described for pyroxene phases, the number and type of constraints to be imposed on the solid solution have been summarized in 'information boxes'. In the remaining part of this section all these 'information boxes' are presented. In some cases (see below) some additional notes are added to clarify choices and assumptions made on the derivation of site occupancy tables.

Figure 3.3: Garnet solid solution

Figure 3.4: Olivine solid solution.

For simplicity, Ti, which is only a trace component in olivine, has been left out of olivine phase. Similarly other very minor substitutions (in olivine as well as in any other phase included in the program) have not been considered (e.g. Cr^{3+} in olivine, Mg, Fe^{2+} and Fe^{3+} in plagioclase, Ca and Si in spinel, etc.).

Figure 3.5: Spinel solid solution

Figure 3.6: Plagioclase solid solution

Figure 3.7: 'Corundum' solid solution + pure phases

Considering the similarity of their chemical formulas and the possibility of forming solid solutions, corundum (i.e.Al_2O_3), eskolaite (i.e. Cr_2O_3) and hematite (i.e. Fe_2O_3) can be treated as end-members of a 'corundum' solid solution phase. A reduced version of the general site occupancy table has been used to represent the cations' distribution of the 'corundum' phase (see Table 3.7). However, during the minimization process, any of these end-members can also be assumed to be present in the system only as a pure phase.

Garnet solid solution

Crystal chemical formula: $(X)_3(Y)_2(Z)_3O_{12}$

Table 3.3 Cation distribution in garnet phase

cation	charge	site: X	site: Y	site: Z
Na	1+	#	#	#
Ca	2+	X_{21}	#	#
Mg	2+	X_{31}	#	#
Fe^{2+}	2+	X_{41}	#	#
Al	3+	#	X_{52}	#
Cr	3+	#	X_{62}	#
Fe^{3+}	3+	#	X_{72}	#
Si	4+	#	#	X_{83}
Ti	4+	#	#	X_{93}

Mass balance constraints:

$$\mathbf{M_i^{grt}} = n^{grt} \cdot \sum_{k=1}^{3} X_{ik}^{grt} \qquad (i = \text{Ca, Mg, } Fe^{2+}\text{, Al, Cr, } Fe^{3+}\text{, Si, Ti})$$

Stoichiometry constraints:

$$X_{21}^{grt} + X_{31}^{grt} + X_{41}^{grt} = S_X^{grt} = 3$$
$$X_{52}^{grt} + X_{62}^{grt} + X_{72}^{grt} = S_Y^{grt} = 2$$
$$X_{83}^{grt} + X_{93}^{grt} = S_Z^{grt} = 3$$

mass balance, stoichiometry constraints ⇒ always needed

charge balance constraint ⇒ not needed (i.e. always automatically satisfied by stoichiometry constraints)

ratio constraints ⇒ not needed

Fig. 3.3 'Information box' for garnet phase

Olivine solid solution

Crystal chemical formula: $(M2)_1(M1)_1(T)_1O_4$

Table 3.4 Cation distribution in olivine phase

cation	charge	site: M2	site: M1	site: T
Na	1+	#	#	#
Ca	2+	X_{21}	#	#
Mg	2+	X_{31}	X_{32}	#
Fe^{2+}	2+	X_{41}	X_{42}	#
Al	3+	#	#	#
Cr	3+	#	#	#
Fe^{3+}	3+	#	#	#
Si	4+	#	#	X_{83}
Ti	4+	#	#	#

Mass balance constraints:

$$\mathbf{M_i^{ol}} = n^{ol} \cdot \sum_{k=1}^{3} X_{ik}^{ol} \qquad (i = \text{Ca, Mg, } Fe^{2+}\text{, Si})$$

Stoichiometry constraints:

$$X_{21}^{ol} + X_{31}^{ol} + X_{41}^{ol} = S_{M2}^{ol} = 1$$
$$X_{32}^{ol} + X_{42}^{ol} = S_{M1}^{ol} = 1$$
$$X_{83}^{ol} = S_T^{ol} = 1$$

Ratio constraint:

$$\frac{X_{31}^{ol}}{X_{31}^{ol} + X_{41}^{ol}} = \frac{X_{32}^{ol}}{X_{32}^{ol} + X_{42}^{ol}}$$

mass balance, stoichiometry constraints ⇒ always needed

charge balance constraint ⇒ not needed (i.e. always automatically satisfied by stoichiometry constraints)

ratio constraint ⇒ not needed in system 2, 3or4, 8 and related subsystems

Fig. 3.4 'Information box' for olivine phase

Spinel solid solution

Crystal chemical formula: $(A)_1(B)_2O_4$

Table 3.5 Cation distribution in spinel phase

cation	charge	site: A	site: B	site: T
Na	1+	#	#	#
Ca	2+	#	#	#
Mg	2+	X_{31}	X_{32}	#
Fe^{2+}	2+	X_{41}	X_{42}	#
Al	3+	#	X_{52}	#
Cr	3+	#	X_{62}	#
Fe^{3+}	3+	#	X_{72}	#
Si	4+	#	#	#
Ti	4+	#	X_{92}	#

Mass balance constraints:

$$\mathbf{M_i^{sp}} = n^{sp} \cdot \sum_{k=1}^{3} X_{ik}^{sp} \qquad (i = \text{Mg, } Fe^{2+}\text{, Al, Cr, } Fe^{3+}\text{, Ti})$$

Stoichiometry constraints:

$$X_{31}^{sp} + X_{41}^{sp} = S_A^{sp} = 1$$
$$X_{32}^{sp} + X_{42}^{sp} + X_{52}^{sp} + X_{62}^{sp} + X_{72}^{sp} = S_B^{sp} = 2$$

Ratio constraint:

$$\frac{X_{31}^{sp}}{X_{31}^{sp} + X_{41}^{sp}} = \frac{X_{32}^{sp}}{X_{32}^{sp} + X_{42}^{sp}}$$

Charge balance constraint:

$$\left[2^+ \cdot \left(X_{31}^{sp} + X_{32}^{sp}\right)\right] + \left[2^+ \cdot \left(X_{41}^{sp} + X_{42}^{sp}\right)\right] + \left[3^+ \cdot \left(X_{52}^{sp}\right)\right] + \left[3^+ \cdot \left(X_{62}^{sp} +\right)\right] + \left[3^+ \cdot \left(X_{72}^{sp}\right)\right] + \left[4^+ \cdot \left(X_{92}^{sp}\right)\right] = 8$$

mass balance, stoichiometry constraints ⇒ always needed

charge balance constraint ⇒ not needed in system 2&3, 5&6 and related subsystems

ratio constraint ⇒ not needed in system 2&3, 5&6 and related subsystems

Fig. 3.5 'Information box' for spinel phase

Plagioclase solid solution

Crystal chemical formula: $(W)_1(Z)_4O_8$

Table 3.6 Cation distribution in plagioclase phase

cation	charge	site: X	site: Y	site: Z
Na	1+	X_{11}	#	#
Ca	2+	X_{21}	#	#
Mg	2+	#	#	#
Fe^{2+}	2+	#	#	#
Al	3+	#	#	X_{53}
Cr	3+	#	#	#
Fe^{3+}	3+	#	#	#
Si	4+	#	#	X_{83}
Ti	4+	#	#	#

Mass balance constraints:

$$\mathbf{M_i^{pl}} = n^{pl} \cdot \sum_{k=1}^{3} X_{ik}^{pl} \qquad (i = \text{Na, Cg, Al, Si})$$

Stoichiometry constraints:

$$X_{11}^{pl} + X_{21}^{pl} = S_W^{pl} = 1$$
$$X_{53}^{pl} + X_{83}^{pl} = S_Z^{pl} = 4$$

Charge balance constraint:

$$\left[1^+ \cdot \left(X_{11}^{pl}\right)\right] + \left[2^+ \cdot \left(X_{21}^{pl}\right)\right] + \left[3^+ \cdot \left(X_{53}^{pl}\right)\right] + \left[4^+ \cdot \left(X_{83}^{pl} +\right)\right] = 16$$

mass balance, stoichiometry constraints ⇒ always needed

charge balance constraint ⇒ always needed

ratio constraints ⇒ not needed

Fig. 3.6 'Information box' for plagioclase phase

‘Corundum’ solid solution

Crystal chemical formula: $(B)_2 O_3$

Table 3.7 Cation distribution in ‘corundum’ phase

cation	charge	site: B
Al	3+	X_{52}
Cr	3+	X_{62}
Fe^{3+}	3+	X_{72}

Mass balance constraints:

$$\mathbf{M_i^{cor}} = n^{cor} \cdot \sum_{k=1}^{3} X_{ik}^{cor} \qquad (i = \text{Al, Cr, } Fe^{3+})$$

Stoichiometry constraints:

$$X_{52}^{cor} + X_{62}^{cor} + X_{72}^{cor} = S_B^{cor} = 2$$

mass balance, stoichiometry constraints ⇒ always needed
charge balance constraint ⇒ not needed
ratio constraints ⇒ not needed

Quartz

Chemical formula: SiO_2

Kyanite

Chemical formula: Al_2SiO_5

Sillimanite

Chemical formula: Al_2SiO_5

mass balance constraints ⇒ always needed
stoichiometry constraints ⇒ not needed
charge balance constraint ⇒ not needed
ratio constraints ⇒ not needed

Fig. 3.7 ‘Information box’ for corundum, quartz, kyanite, sillimanite phases

3.5 Solving the GFEM problem

3.5.1 Review of previous methods and advantages of employing modern minimization techniques

Following the 'chemical potential' approach many numerical methods have been proposed in the past to solve the Gibbs free energy minimization problem. All are based on standard methods of computational mathematics. For example, those by Storey and van Zeggeren (1964), Eriksson (1975), Saxena (1982), Wood and Holloway (1984) and Bina and Wood (1987) make use of the steepest descent type of algorithm, while those by Sundman et al. (1985), Ghiorso (1985), De Capitani and Brown (1987), Harvie et al. (1987) and Ghiorso and Sack (1995) make use of quadratic approximation methods (e.g. conjugate gradients).

Many of these GFEM algorithms have been developed with particular applications in mind, and have shown to perform well in those cases. However, in some cases the existing algorithms are not quite suited to the particular problems to be solved. For example, even though most make use of Lagrange multiplier techniques to impose linear equality constraints, they often resort to quite 'ad hoc' methods for imposing non-negativity constraints, usually by introducing non-linear (exponential) transformations of variables (e.g. Storey and Van Zeggeren, 1964; Wood and Holloway, 1984). This can create numerical problems when solution values approach zero (for a discussion see Greenberg, Weare and Harvie, 1985). Other algorithms like that of De Capitani and Brown (1987) transform their particular GFEM problem into a coupled set of linear and non-linear programming steps.

Numerical techniques for constrained optimization comprise an active field of research, in which major advances have occurred in the past twenty years. The numerical methods adopted in former studies show that the development of Gibbs free energy algorithms has, to a large extent, taken place independently of the advances in constrained optimization. Hence, it appears that Earth scientists have not been able to take advantage of modern optimization methods developed in the computational sciences. Modern methods can, in fact, tackle the general minimization problem and avoid any transformation of variables. They can also find initial guess solutions that satisfy the constraints (a problem

which has itself been the subject of independent study by Earth Scientists, Asimov and Ghiorso, 1998). Modern methods also converge rapidly, are usually quite robust to numerical instabilities, and can handle more complex non-linear equality and inequality constraints, which may be useful if one had reason to impose such constraints on a solution.

3.5.2 Solution by a Feasible Iterate Sequential Quadratic programming (FSQP) algorithm

The GFEM problem falls within the more general class of constrained optimization problem usually called non-linear programming (see Gill et al. 1981, for a discussion). The problem is non-linear because in general for every phase ϕ the molar Gibbs free energy G^{ϕ} depends non-linearly on the site occupancies X_{ik}^{ϕ}'s. In addition, as shown in sections 3.3 and 3.4, in a general case, the minimization of $\mathbf{G}^{\mathbf{system}}$ has to be performed under several different, linear and non-linear, types of constraints.

Given the complexity of the general problem, the minimization program '*Gib*', written for this study, has been built using the Feasible Iterate Sequential Quadratic programming (*FSQP*) algorithm of Panier and Tits (1993), Zhou, Tits and Lawrence (1998). The *FSQP* method is a modern optimization technique that can handle minimization/optimization problems in general form, which means including all forms of constraints (i.e. general *linear* and *non-linear inequalities*, as well as *non-linear equality* constraints). It can also deal with zero, one or multiple objective functions simultaneously. In the case where no objective function is supplied (i.e. the Gibbs function given by Eq. 3.3 is absent) the task becomes one of finding a single 'feasible' solution, which is one of many that merely satisfy the constraints (i.e. Eq. 3.12-3.16, in a general case). The Gibbs free energy problem is then to find a feasible solution that is also a (global) minimum of the non-linear Gibbs function in Eq. (3.3).

The complete *FSQP* algorithm makes use of a series of techniques described and analyzed in Panier and Tits (1993), Bonnans et al. (1992), Zhou and Tits (1993), and Schittkowski, (1986). To solve the minimization problem, it needs to be provided by the user with an initial guess solution for the site occupancies and number of moles per phase. If these values do no satisfy all the constraints, then they are used as the starting point for a 'step 1' optimization problem where the objective is simply to satisfy the constraints. This

is accomplished by solving a series of sub-minimization problems, where at each stage the objective function is built from the constraint which is most violated. The solution from step 1 is then a feasible solution used as the starting point for the constrained minimization problem.

A highly flexible (FORTRAN) computer program is available from the authors of *FSQP* which implements the general algorithm (Zhou, Tits and Laurence, 1998). In the implementation for this work this code has been used as the basis of a Gibbs free energy minimization solver. The algorithm has 'super-linear' convergence, which makes it practical for routine use. The *FSQP* code used in this work is part of a library of similar software which can be obtained through the Optimization Technology Centre (OTC) of the Argonne National Laboratory[13].

3.5.3 Automatic differentiation

Another very important feature of the GFEM algorithm adopted in this study is the use of automatic differentiation tools. All the previous GFEM methods cited in this chapter (with the exception of Bina, 1998) require derivatives of $\mathbf{G}^{\mathbf{system}}$ to be evaluated and chemical potential expressions to be explicitly written down. This means that analytical expressions for derivatives must be determined beforehand and coded into the minimization algorithm. If these expressions are changed then the process must be repeated. On the other hand, in this work, thanks to the technique known as automatic differentiation, there is no need to determine analytical derivatives of $\mathbf{G}^{\mathbf{system}}$.

The mathematical background and the theory of automatic differentiation is described in detail in Griewank (1989), Griewank and Corlis (1991), and Berz et al., (1996). The automatic differentiation package used in this work is: TAF (i.e. Transformations of Algorithms in Fortran), which is a source-to-source automatic differentiation tool for Fortran-77 and Fortran-95 programs (e.g. Giering and Kaminski, 2003). The main idea behind automatic differentiation is that any mathematical function that can be evaluated using a computer code (in this case the Gibbs function in Eq. 3.1 and the expressions for constraints given by Eq. 3.12-3.16) can be broken down into a combination of simpler elementary function, like x^2, exp, log, etc. This is self-evident since

[13] This is a facility accessible via the world wide web. Full details can be found at www-fp.mcs.anl.gov/oct.

there are only a finite number of possible commands in a programming language, e.g. FORTRAN or C. The derivatives of each of these elementary functions are known and so the derivatives of any combination of them can be found using the chain rule of differentiation (see Stephenson 1973). These are the steps that one would normally take in writing down analytical expressions for derivatives of complicated functions. Automatic differentiation performs the same task by analyzing the computer code used to evaluate the function and in effect 'writing a similar code in the same language' for the derivatives.

From the mathematical point of view, a first advantage of automatic differentiation is that it combines the complete flexibility of purely numerical derivatives, e.g. finite differences (Press et al., 1992), with the accuracy of analytical derivative expressions.

From the point of view of thermodynamic modeling, an important aspect of automatic differentiations tools is that they allow considerable flexibility in the form of $\mathbf{G}^{\mathbf{system}}$, and hence in the range of problems that can be addressed. It could, for instance, be assumed that the model presented in chapter 2 is incorrect, or it could be decided to add other phases in the system. In either case, in the GFEM algorithm, one would only have to modify the $\mathbf{G}^{\mathbf{system}}$ expression, with no need to determine its analytical derivatives. This could be done at any time as it would require just few minor changes to the computer code.

Finally, another significant advantage of automatic differentiation is that it removes the possibility of 'coding errors' which often occur when translating complex expressions into a computer language.

3.6 Determination of G^{system} global minimum using '*Gib*'

One of the most useful features of '*Gib*', the program written to compute equilibrium phase compositions, is that it is extremely easy to use. Program setup and use are discussed in Appendix 3C, while results of applications of the program are reported in chapters 4 and 5.

3.6.1 Multiple minima in the free energy function

As pointed out by Bina (1998) the presence of multiple minima in the Gibbs free energy function may occur in a variety of cases and especially for systems that contain complex solid solutions and/or phases subject to abrupt phase transitions. Most constrained

optimization algorithms like *FSQP* do not deal with this case directly. A requirement for their use is that the objective function (or functions) is smoothly varying, and in practice this usually means that they will locate a minimum of $\mathbf{G}^{\mathbf{system}}$ 'in the neighborhood' of the starting guess. The *FSQP* algorithm adopted here cannot guarantee global minimal solutions, only local ones under the constraints imposed. In fact, no (practical) numerical method can guarantee a global minimum. Bina (1998) describes a simulated annealing algorithm for addressing the multiple minima problem. With *FSQP* this problem has been faced in the simplistic but, nevertheless, very effective way of setting up a routine to restart the algorithm from several different initial guesses. Solutions obtained are then compared. The attainment of identical solutions (i.e. same compositions and number of moles of phases at equilibrium) from different initial guesses makes it reasonable to assume that no local minima have been encountered and that the solution found represents the global minimum of $\mathbf{G}^{\mathbf{system}}$. The only negative aspect of this procedure is that using a 'routine' of initial guesses can be quite time consuming from a computational point of view. For this reason '*Gib*' has been left the option for the operator to use only one initial guess per time. In that case, before running the program, a file named 'g*ib.initial*' has to be opened and values of site occupancies and number of moles for phases included in the computation have to be written. The file is then saved and it will be automatically called by '*Gib*'.

It is worth emphasizing here that in all applications of the program the 'multiple minima problem' has never appeared to be a real issue. The *FSQP* algorithm performs so effectively that regardless if the initial guess is a 'good one' (i.e. all the constraints satisfied and values of site occupancies and number of moles close to those of probable solution) or a very 'bad one' (i.e. with all the constraints violated and both site occupancies and number of moles set equal to zero), it generally converges to the correct global minimum routinely.

3.7 References

Akamatsu T., Kumazawa M., Aikawa N., and Takei H. (1993) Pressure effect on the divalent cation distribution in nonideal solid solution of forsterite and fayalite. *Physics and Chemistry of Minerals* **19**, 431-444.

Anderson G. M. and Crerar D. A. (1993) Thermodynamics in Geochemistry. The Equilibrium Model. *Oxford University Press*.

Asimov P. D. and Ghiorso M. S. (1998) Algorithmic modifications extending MELTS to calculate subsolidus phase relations. *American Mineralogist* **83**, 1127-1132.

Berz M., Bishof C., Corliss G. F., and Griewank A. (1996) Computational differentiation: Techniques, Applications, and Tools. *Proc. in Appl. Math. 89 SIAM*.

Bina C. R.. and Wood B. J. (1987) The olivine-spinel transition: experimental and thermodynamic constraints and implications for the nature of the 400 km seismic discontinuity. *Journal of Geophysical Research* **92**, 4853-4866.

Bina C. R. (1998) Free energy minimization by simulated annealing with applications to lithosperic slabs and mantle plumes. *Pure and Applied Geophysics* **151**, 605-618.

Bonnans J. F., Panier E. R., Tits A. L., and Zhou J. L. (1992) Avoiding the Maratos effect by means of a nonmonotone line search. II. Inequality constrained problems — feasible iterates, SIAM. *Journal of Numeric Analysis* **29**, 1187-1202.

Brown T. H. and Skinner B. J. (1974) Theoretical prediction of equilibrium phase assemblages in multicomponent systems. *American Journal of Science* **274**, 961-986.

Chatterjee N. D. (1991) Applied mineralogical thermodynamics. In *Selected topics*. Springer Verlag.

Cheynet B., Chevalier P. Y., and Fisher E. (2002) Thermosuite. *Calphad* **26**, 167-174.

Connolly J. A. D. and Kerrick D. M. (1986) An algorithm and computer program for calculating composition phase diagrams. *Calphad* **11**, 1-55.

Darken L. S. (1950) Application of the Gibbs-Duhem equation to ternary and multicomponent systems. *Journal of the American Chemical Society* **72**, 2909-2914

Davies R. H., Dinsdale A. T., Gisby J. A., Robinson J. A. J., and Martin S. M. (2002) MTDATA-Thermodynamic and phase equilibrium software from the National Physical Laboratory. *Calphad* **26**, 229-271.

De Capitani C. and Brown T. H. (1987) The computation of chemical equilibrium in complex systems containing non-ideal solutions. *Geochimica et Cosmochimica Acta* **51**, 2639-2652.

Dorofeyeva V. A. and Khodakovskiy I. L. (1981) Calculation of the equilibrium composition of multicomponent systems by "minimization" method from the equilibrium constants. *Geochem Internat* **18**(1), 80-85.

Eriksson G. (1975) Thermodynamic studies of high temperature equilibria. XII. SOLGASMIX, A computer program for calculation of equilibrium compositions in multiphase systems. *Chemica Scripta* **8**, 100-103.

Ganguly J (1982) Mg-Fe order-disorder in ferromagnesian silicates: II. Thermodynamics, kinetics and geological applications. In *Advances in Physical Geochemistry* (ed. S. K. Saxena), **Vol. 2**, 55-99. Springer-Verlag, New-York.

Ganguly J. (2001) Thermodynamic modelling of solid solutions. In *Solid solutions in silicate and oxide systems / EMU Notes in Mineralogy*, Vol. 3 (ed. C. A. Geiger), pp. 37-69. Eötvös Univ. Press.

Ganguly J. and Saxena S. K. (1987) Mixtures and Mineral Reactions. Springer-Verlag, New-York.

Ganguly J., Strimpfl M., and Molin G. (1997) Orthopyroxene chronometry of meteorites: II. Towards a general relation between cooling rate and closure temperature of cation ordering and application to the Steinbach meteorite. Experimental determination of thermodynamic and kinetic parameters. In *Lunar and Planetary Science* **XXVIII**, 391-392. Lunar and planetary Institute, Houston, Texas.

Ghiorso M. S. (1985) Chemical mass transfer in magmatic processes. I. Thermodynamic relations and numerical algorithms. *Contributions to Mineralogy and Petrology* **90**, 107-120.

Ghiorso M. S. (1990) Application of the Darken equation to mineral solid solutions with variable degrees of order-disorder. *American Mineralogist* **75**, 539-543.

Ghiorso M. S. and Sack R. O. (1995) Chemical mass transfer in magmatic processes IV. A revised and internally consistent thermodynamic model for the interpolation and extrapolation of liquid-equilibria in magmatic systems at elevated temperatures and pressures. *Contributions to Mineralogy and Petrology* **119**, 197-212.

Ghiorso M. S. and Evans B. W. (2002) Thermodynamics of the amphiboles: Ca-Mg-Fe^{2+} quadrilateral. *American Mineralogist* **87**, 79-98.

Giering R. and Kaminski T. (2003) Applying TAF to generate efficient derivative code of Fortran 77-95 programs. *PAMM* **2**(1), 54-57.

Gill P. E., Murray W., and Wright M. H. (1981) *Practical optimization*. Academic.

Greenberg J. P., Weare J. H., and Harvie C. E. (1985) An equilibrium computation algorithm for complex highly non ideal systems, application to silicate phase equilibria. *High Temperature Science* **20**, 141-162.

Griewank A. (1989) On automatic differentiation. In *Mathematical programming: Recent Developments and Applications* (ed. M. Iri and K. Tanabe), pp. 83-108. Kluwer.

Griewank A. and Corliss G. F. (1991) Automatic differentiation of algorithms: Theory, Implementation and Application. *Proceedings in Applied Mathematics 53, SIAM*.

Harvie C. E., Greenberg J. P., and Weare J. H. (1987) A chemical equilibrium algorithm for highly non-ideal multiphase systems: free energy minimization. *Geochimica et Cosmochimica Acta* **51**, 1045-1057.

Helgeson H. C., Brown T. H., Nigrini A., and Jones T. A. (1970) Calculation of mass transfer in geochemical processes involving aqueous solutions. *Geochimica et Cosmochimica Acta* **34**, 569-592.

Karpov I. K., Chudnenko K. V., Bychinskii V. A., Kulik D. A., Pavlov A. L., Tret'yakov G. A., and Kashik S. A. (1995) Free energy minimization in calculation of heterogeneous equilibria. *Russian Geology and Geophysics* **36**(4), 1-16.

Klemme S. and O'Neill H. St. C. (2000) The effect of Cr on the solubility of Al in orthopyroxene: experiments and thermodynamic modelling. *Contributions to Mineralogy and Petrology* **140**, 84-98.

Panier E. R. and Tits A. L. (1993) On combining feasibility, descent and superlinear convergence in inequality constrained optimization. *Mathematical Programming* **59**, 261-276.

Pasqual D., Molin G., and Tribaudino M. (2000). Single-crystal thermometric calibration of Fe-Mg order-disorder in pigeonites. *American Mineralogist* **85**, 953-962.

Powell R. and Holland T. J. B. (1988) An internally consistent thermodynamic dataset with uncertainties and correlations: 3. Applications to geobarometry, worked examples and a computer program. *Journal of Metamorphic Geology* **6**, 173-204.

Press W. H., Flannery B. P., and Vetterling W. T. (1992) *Numerical Recipes, 2nd edition*. Cambridge University Press.

Reed M. H. (1982) Calculation of multicomponent chemical equilibria and reaction processes in systems involving minerals, gases and an aqueous phase. *Geochimica et Cosmochimica Acta* **46**, 513-528.

Reusser E. (1994) Free energy minimization in systems of fixed compositions. *Proceedings of the V Summer School Quantitative Phase Diagram Applications in Earth Material Sciences*.

Sack R. O. and Ghiorso M. S. (1994b) Thermodynamics of multicomponent pyroxenes: II. Phase relations in the quadrilateral. *Contributions to Mineralogy and Petrology* **116**, 287-300.

Sack R. O. and Ghiorso M. S. (1994c) Thermodynamics of multicomponent pyroxenes: III. Calibration of $Fe^{2+}(Mg)_{-1}$, $TiAl_2(MgSi_2)_{-1}$, $TiFeX(MgSi_2)_{-1}$, $AlFe^{3+}(MgSi)_{-1}$, $NaAl(CaMg)_{-1}$, $Al_2(MgSi)_{-1}$ and $Ca(Mg)_{-1}$ exchange reactions between pyroxenes and silicate melts. *Contributions to Mineralogy and Petrology* **118**, 271-296.

Sack R. O. and Loucks R. R. (1985) Thermodynamic properties of tethraedrite-tennantites: Constraints on the independence of the Ag↔Ca, Fe↔Zn, Cu↔Fe, Ag↔Sb exchange reactions. *American Mineralogist* **71**, 257-269.

Saxena S. K. (1982) Computation of multicomponent phase equilibria. In *Advances in Physical Geochemistry* (ed. S. K. Saxena), pp. 225-242. Springer-Verlag, New-York.

Saxena S. K. (1996) Earth mineralogical model: Gibbs free energy minimization computation in the system MgO-FeO-SiO_2. *Geochimica et Cosmochimica Acta* **60**, 2379-2395.

Saxena S. K. and Eriksson G. (1983) Theroetical computation of mineral assemblages in pyrolite and lherzolite. *Journal of Petrology* **24**, 538-555.

Schittkowski K. (1986) QLD: A FORTRAN Code for quadratic Programming, User's Guide. Mathematisches Institut, Universität Bayreuth.

Shvarov Y. U. (1978) Minimization of the thermodynamic potential of an open chemical system. *Geochem. Internat.* **15**(6), 200-203.

Smith W. R. and Missen R. W. (1982) *Chemical Reaction Equilibrium Analysis*. Wiley.

Stephenson G. (1973) *Mathematical methods for science students, 2nd ed.* Longman.

Storey S. H. and van Zeggeren F. (1964) Computation of chemical equilibrium compositions. *Can. J. Chem. Eng.* **42**, 54-55.

Sundman B., Jansson B., and Anderson J. O. (1985) The thermo-calc databank system. *Calphad* **9**, 153-190.

Takeno N. (2001) FLASK-SK: A program to compute chemical equilibria in metamorphic petrology. *Computers and Geosciences* **27**, 1179-1188.

van Zeggeren F. and Storey S. H. (1970) *The Computation of Chemical Equilibrium*. Cambridge University.

Wolery T. J. (1979) Calculation of Chemical Equilibrium Between Aqueous Solutions and Minerals: The EQ3/6 Software Package. Lawrence Livermore Laboratory Document UCRL-52658, p. 41.

Wood B. J. and Holloway J. R. (1984) A thermodynamic model for subsolidus equilibria in the system CaO-MgO-Al_2O_3-SiO_2. *Geochimica et Cosmochimica Acta* **48**, 159-176.

Wood B. J. and Nicholls J. (1978) The thermodynamic properties of reciprocal solid solutions. *Contributions to Mineralogy and Petrology* **66**, 389-400.

Zhou J. L. and Tits A. L. (1993) Nonmonotone line search for minimax problems. *Journal of Optimization Theory and Applications* **76**, 455-476.

Zhou J. L., Tits A. L., and Lawrence C. T. (1998) User's guide for FFSQP: a FORTRAN code for solving constrained nonlinear (Minimax) optimization problems, generating iterates satisfying all inequality and linear constraints. Electrical Engineering Department. University of Maryland.

Appendix 3A

Example of derivation of chemical potential expression applying Eq. 3.9

The garnet solid solution is considered:

$$\left(Ca, Mg, Fe^{2+}\right)_3^X \left(Al\right)_2^Y Si_3^T O_{12} \qquad (3A.1)$$

In this solution phase three *components* can be identified: $Ca_3Al_2Si_3O_{12}$ (grossular, i.e. *gr*), $Mg_3Al_2Si_3O_{12}$ (pyrope, i.e. *py*), $Fe_3^{2+}Al_2Si_3O_{12}$ (almandine, i.e. *alm*). Note that in this argument the term '*component*' instead of 'end-member' is adopted for the entity used to describe the chemical composition of garnet phase. This is done to be consistent with terminology adopted in GFEM algorithms that have been developed following the 'chemical potential' approach.

The equation normally used to derive the chemical potential expression for any of the above *component* was given in section 3.2 (i.e. Eq. 3.11):

$$\mu_i = G_i^o + RT\, ln\, a_i$$

Where, $a_i = x_i \cdot \gamma_i$ represents the activity of *component i* in the solution, and γ_i is the activity coefficient.

For simplicity, it can be now assumed that the garnet solution is ideal. As a result, activity coefficients will be equal to zero (i.e. γ_i's = 0), and for every *component* '*i*' in solution activities will be given by molar fractions x_i's (i.e. $a_i \equiv x_i$). In this case, Eq. (3.11) reduces to:

$$\mu_i = G_i^o + RT \ln x_i \qquad (3A.2)$$

Using now Eq. (3A.2) to derive the chemical potential expression for the pyrope *component* one obtains (e.g. Chatterjee, 1991):

$$\mu_{py} = G^{o}_{py} + RT \ln X^{3}_{Mg} \qquad (3A.3)$$

Where, X_{Mg}:

$$X_{Mg} = \frac{n_{Mg}}{n_{Ca} + n_{Mg} + n_{Fe^{2+}}} \qquad (3A.4)$$

represent the molar fraction of cations Mg, in sites X (see also Table 3.3) and $n_{Ca}, n_{Mg}, n_{Fe^{2+}}$ are the total number of moles of cations Ca, Mg and Fe^{2+} in the system.

Similar expressions can be derived for any of the other solution *components*:

$$\mu_{gr} = G^{o}_{gr} + RT \ln X^{3}_{Ca} \qquad (3A.5)$$

$$\mu_{alm} = G^{o}_{alm} + RT \ln X^{3}_{Fe^{2+}} \qquad (3A.6)$$

These are the type of expressions that would be used to minimize $\mathbf{G}^{\mathbf{system}}$ when adopting any of the GFEM algorithms cited in chapter 3.

In the remaining part of this Appendix 3A it will be proved that Eq. (3A.3) (and analogously Eq. 3A.5 and Eq. 3A.6) can be obtained by directly applying Eq. (3.9):

$$\mu_i = \left(\frac{\partial \mathbf{G}^{\mathbf{system}}}{\partial n_i} \right)_{T,P,n_{j \neq i}}$$

Where, $\mathbf{G}^{\mathbf{system}}$ is given by Eq. (3.3) and G^{ϕ} by Eq. (3.4).

For simplicity, the garnet phase can be assumed to be the only phase present in the system. As a consequence, since it was also assumed the garnet solution to be ideal, Eq. (3.3) and Eq. (3.4) reduce to:

$$\mathbf{G}^{\mathbf{system}} = \boldsymbol{G}^{\boldsymbol{\phi}\text{-}\boldsymbol{grt}} = n^{grt} \cdot G^{\phi - grt} \tag{3A.7}$$

$$G^{\phi\text{-}grt} = G^{e\text{-}m} + G^{id} \tag{3A.8}$$

Expressions for $G^{e\text{-}m}$ and G^{id} can be obtained from Chatterjee (1991). Accordingly:

$$G^{e\text{-}m} = x_{gr} G^{o}_{gr} + x_{py} G^{o}_{py} + x_{alm} G^{o}_{alm} \tag{3A.9}$$

Where, x_{gr}, x_{py} and x_{alm}:

$$x_{gr} = \frac{n_{gr}}{n_{gr} + n_{py} + n_{alm}}; \quad x_{py} = \frac{n_{py}}{n_{gr} + n_{py} + n_{alm}}; \quad x_{alm} = \frac{n_{alm}}{n_{gr} + n_{py} + n_{alm}} \tag{3A.10}$$

represent the molar fraction in solution of *components gr*, *py* and *alm* respectively, while n_{gr}, n_{py} and n_{alm} represent the total number of moles of these *components* in the system.

$$G^{id} = 3RT\left(X_{Ca} \ln X_{Ca} + X_{Mg} \ln X_{Mg} + X_{Fe^{2+}} \ln X_{Fe^{2+}}\right) \tag{3A.11}$$

Where, X_{Ca} and $X_{Fe^{2+}}$ (analogously to X_{Mg}, see also Eq. 3A.4):

$$X_{Ca} = \frac{n_{Ca}}{n_{Ca} + n_{Mg} + n_{Fe^{2+}}}; \; X_{Fe^{2+}} = \frac{n_{Fe^{2+}}}{n_{Ca} + n_{Mg} + n_{Fe^{2+}}} \tag{3A.12}$$

represent the molar fraction of cations Ca and Fe^{2+}, in sites X.

Since $G^{\phi\text{-}grt}$ can be split into the two distinct terms $G^{e\text{-}m}$ and G^{id}, Eq. (3A.7) can then be written:

$$\mathbf{G}^{\mathbf{system}} = \mathbf{G}^{\boldsymbol{\phi}\textbf{-}\mathbf{grt}} = n^{grt} \cdot G^{\phi - grt} = n^{grt} \cdot \left(G^{e-m} + G^{id}\right) \tag{3A.13}$$

Therefore, the chemical potential of each *component i* can be represented as the sum of two different terms:

$$\mu_i = \left(\frac{\partial \mathbf{G}^{\mathbf{system}}}{\partial n_i}\right)_{T,P,n_{j\neq i}} = \left[\frac{\partial\left(n^{grt} \cdot G^{e-m}\right)}{\partial n_i}\right]_{T,P,n_{j\neq i}} + \left[\frac{\partial\left(n^{grt} \cdot G^{id}\right)}{\partial n_i}\right]_{T,P,n_{j\neq i}} \tag{3A.14}$$

The additive nature of the terms which make up $\mathbf{G}^{\mathbf{sytem}}$, and thus μ_i, allows each to be dealt with individually before combining to give the complete μ_i expression. Hence, for the pyrope *component*:

$$\mu_{py} = \mu_{py}^{e-m} + \mu_{py}^{id} \tag{3A.15}$$

First the expression of μ_{py}^{e-m} is derived.

$$\begin{aligned} \mu_{py}^{e-m} &= \left[\frac{\partial\left(n^{grt} \cdot G^{e-m}\right)}{\partial n_{py}}\right]_{T,P,n_{j\neq py}} \\ &= \left[\frac{\partial\left(n^{grt} \cdot \left(x_{gr} G_{gr}^{o} + x_{py} G_{py}^{o} + x_{alm} G_{alm}^{o}\right)\right)}{\partial n_{py}}\right]_{T,P,n_{j\neq py}} \end{aligned} \tag{3A.16}$$

With:

$$n^{grt} = n_{gr} + n_{py} + n_{alm} \tag{3A.17}$$

Substituting Eq. (3A.10) and Eq. (3A.17) into Eq. (3A.16), yields:

$$\mu_{py}^{e-m} = \left[\frac{\partial\left(n_{gr} G_{gr}^{o} + n_{py} G_{py}^{o} + n_{alm} G_{alm}^{o}\right)}{\partial n_{py}}\right]_{T,P,n_{j\neq py}} = G_{py}^{o} \tag{3A.18}$$

The expression of μ_{py}^{id} is now derived.

In the garnet solution considered in this exposition the G^{id} term (see also Eq. 3A.11) is given only by the mixing taking place on the sublattice X, being the other sublattice Y entirely occupied by Al. As a consequence, the expression of $\left(n^{grt} \cdot G^{id}\right)$ in Eq. (3A.14) is given by:

$$n^{grt} \cdot G^{id} = \left[\frac{1}{3}\left(n_{Ca} + n_{Mg} + n_{Fe^{2+}}\right) \cdot 3RT\left(X_{Ca} \ln X_{Ca} + X_{Mg} \ln X_{Mg} + X_{Fe^{2+}} \ln X_{Fe^{2+}}\right)\right] \quad (3A.19)$$

For the pyrope (i.e. $Mg_3Al_2Si_3O_{12}$) *component*, the ideal part of the chemical potential expression will then reduce to:

$$\mu_{py}^{id} = \frac{1}{3}\mu_{Mg}^{id} \quad (3A.20)$$

With:

$$\mu_{py}^{id} = \left[\frac{\partial\left[\left(n_{Ca} + n_{Mg} + n_{Fe^{2+}}\right) \cdot 3RT\begin{pmatrix} X_{Ca}\, ln\, X_{Ca} + \\ X_{Mg}\, ln\, X_{Mg} + \\ X_{Fe^{2+}}\, ln\, X_{Fe^{2+}} \end{pmatrix}\right]}{\partial n_{Mg}}\right]_{T,P,n_{j \neq Mg}} \quad (3A.21)$$

Substituting the appropriate terms from Eq. (3A.4) and Eq. (3A.12) into Eq. (3A.21), yields:

$$\mu_{Py}^{id} = 3RT \cdot \frac{\partial}{\partial n_{Mg}} \left[\left(n_{Ca} + n_{Mg} + n_{Fe^{2+}} \right) \cdot \left(\begin{array}{l} \dfrac{n_{Ca}}{n_{Ca} + n_{Mg} + n_{Fe^{2+}}} \ln \dfrac{n_{Ca}}{n_{Ca} + n_{Mg} + n_{Fe^{2+}}} + \\ \dfrac{n_{Mg}}{n_{Ca} + n_{Mg} + n_{Fe^{2+}}} \ln \dfrac{n_{Mg}}{n_{Ca} + n_{Mg} + n_{Fe^{2+}}} + \\ \dfrac{n_{Fe^{2+}}}{n_{Ca} + n_{Mg} + n_{Fe^{2+}}} \ln \dfrac{n_{Fe^{2+}}}{n_{Ca} + n_{Mg} + n_{Fe^{2+}}} \end{array} \right) \right]_{T,P,n_{j \neq Mg}} \qquad (3A.22)$$

$$\mu_{Py}^{id} = 3RT \cdot \left[\ln n_{Mg} - \ln\left(n_{Ca} + n_{Mg} + n_{Fe^{2+}} \right) + 1 - \left(\frac{n_{Ca} + n_{Mg} + n_{Fe^{2+}}}{n_{Ca} + n_{Mg} + n_{Fe^{2+}}} \right) \right] \qquad (3.A.23)$$

$$\mu_{Py}^{id} = 3RT \cdot \ln \frac{n_{Mg}}{n_{Ca} + n_{Mg} + n_{Fe^{2+}}} = 3RT \cdot \ln X_{Mg} = RT \cdot \ln X_{Mg}^{3} \qquad (3A.24)$$

$$\mu_{Py}^{id} = RT \cdot \ln X_{Mg}^{3} \qquad (3A.25)$$

Finally, substituting Eq. (3A.25) and Eq. (3A.18) into Eq. (3A.15), the complete expression of the chemical potential of pyrope *component* is obtained:

$$\mu_{py} = G_{py}^{o} + RT \ln X_{Mg}^{3} \qquad (3A.26)$$

Eq. (3A.26) and Eq. (3A.3) are clearly identical.

Appendix 3B

Derivation of general expression for ratio constraints

A pyroxene phase in a general 1,2,3,4,5,6,7,8,9 system is considered, where partitioning of similar cations (same formal ionic charge and similar cationic radius) among different sublattices is assumed to be random. Three out of the five constraints given by Eq. (3.26-3.29) are independent and have to be imposed. It can be chosen that the first of Eq. (3.26) and Eq. (3.27-3.28) are the three 'independent' constraints to impose, i.e.:

$$\frac{X_{31}^{px}}{X_{31}^{px}+X_{41}^{px}}=\frac{X_{32}^{px}}{X_{32}^{px}+X_{42}^{px}} \tag{3B.1}$$

$$\frac{X_{52}^{px}}{X_{52}^{px}+X_{62}^{px}+X_{72}^{px}}=\frac{X_{53}^{px}}{X_{53}^{px}+X_{63}^{px}+X_{73}^{px}} \tag{3B.2}$$

$$\frac{X_{62}^{px}}{X_{52}^{px}+X_{62}^{px}+X_{72}^{px}}=\frac{X_{63}^{px}}{X_{53}^{px}+X_{63}^{px}+X_{73}^{px}} \tag{3B.3}$$

Eq. (3B.1), Eq. (3B.2), Eq. (3B.3) can be rewritten:

$$X_{31}^{px}\left(X_{32}^{px}+X_{42}^{px}\right)=X_{32}^{px}\left(X_{31}^{px}+X_{41}^{px}\right)\ \Rightarrow X_{31}^{px}X_{42}^{px}=X_{32}^{px}X_{41}^{px} \tag{3B.4}$$

$$\begin{aligned}&X_{52}^{px}\left(X_{53}^{px}+X_{63}^{px}+X_{73}^{px}\right)=X_{53}^{px}\left(X_{52}^{px}+X_{62}^{px}+X_{72}^{px}\right)\\&\Rightarrow X_{52}^{px}\left(X_{63}^{px}+X_{73}^{px}\right)=X_{53}^{px}\left(X_{62}^{px}+X_{72}^{px}\right)\end{aligned} \tag{3B.5}$$

$$\begin{aligned}&X_{62}^{px}\left(X_{53}^{px}+X_{63}^{px}+X_{73}^{px}\right)=X_{63}^{px}\left(X_{52}^{px}+X_{62}^{px}+X_{72}^{px}\right)\\&\Rightarrow X_{62}^{px}\left(X_{63}^{px}+X_{73}^{px}\right)=X_{63}^{px}\left(X_{62}^{px}+X_{72}^{px}\right)\end{aligned} \tag{3B.6}$$

This means that each of the above ratio constraints can be represented with a simplified expression of the type:

$$C_1\left(X_{31}^{px}\right)=X_{31}^{px}X_{42}^{px}-X_{32}^{px}X_{41}^{px}=0 \tag{3B.7}$$

$$C_2\left(X_{52}^{px}\right)=X_{52}^{px}\left(X_{63}^{px}+X_{73}^{px}\right)-X_{53}^{px}\left(X_{62}^{px}+X_{72}^{px}\right)=0 \tag{3B.8}$$

$$C_3\left(X_{62}^{px}\right)=X_{62}^{px}\left(X_{63}^{px}+X_{73}^{px}\right)-X_{63}^{px}\left(X_{62}^{px}+X_{72}^{px}\right)=0 \tag{3B.9}$$

In this way, for any phase ϕ in the system, the ratio constraints become *non-linear equality* constraints of the form:

$$C_{\omega}\left(X_{ik}^{\phi}\right)=0 \qquad (\omega=1,\ldots,s), \quad (\phi=1,\ldots,p) \tag{3B.10}$$

with:

s = total number of independent ratio constraints per phase
p = total number of phases in the system

These *non-linear equality* constraints may be imposed on the GFEM problem along with the other mass balance (*non-linear equality*), stoichiometry (*linear equality*), charge balance (*linear equality*) and positivity *(linear inequality)* constraints. All constraint types are routinely handled by the *FSQP* algorithm.

Appendix 3C

Using '*Gib*': example of '*gib.in*' file and of the program's output

Before every computation the user has to open a file, named '*gib.in'*, where all the information about *T, P* and system's bulk composition, needed during the computation, has to be entered and saved, while end-member and solution parameters that will be used during the computation are stored in a separate file ('*gib.dat*') and they can be at any time modified by the operator. The program, once it is run, automatically calls the 'g*ib.in*' file. At the end of the computation, accordingly to the information provided, the output of the program will appear on the screen displaying the solution found.

Information to pass to '*Gib*' is:

- Number of phases present in the system
- Type of phases (every phase is identified by a different index; 1 ⇒ *opx*, 2 ⇒ *cpx*, 3 ⇒ *pig*, 4 ⇒ *grt*, 5 ⇒ *ol*, 6 ⇒ *sp*, 7 ⇒ *pl*, 8 ⇒ *qtz*, 9 ⇒ *ky*, 10 ⇒ *sil*, 11 ⇒ *cor*)
- Total number of cations present in the system
- Type of system (identified by number and type of cations; 1 ⇒ Na, 2 ⇒ Ca, 3 ⇒ Mg, 4 ⇒ Fe^{2+}, 5 ⇒ Al, 6 ⇒ Cr, 7 ⇒ Fe^{3+}, 8 ⇒ Si, 9 ⇒ Ti. In this way, for instance, 2,3,4,8 specifies CaO-MgO-FeO-SiO_2 system, etc.)
- The system's bulk composition, expressed in term of number of moles of every cation
- The option to include non-linear ratio constraints for each phase. Where, y ⇒ yes (ratio constraints included), n ⇒ no.
- Pressure (in bar) and temperature (in Kelvin degrees) conditions
- Internal control parameters ('*precision value'* and '*scale factor'*) of optimization solver convergence rate and influence of rounding errors. The program rather than having these parameters fixed will cycle through a range and merely chooses a single solution, which is the best in the sense that it is the most stable minimum misfit.

In Fig. 3.8 and Fig 3.9 examples of a 'gib.in' file used in a real case and of its related output are presented. The case considered is a possible 5 phases (*opx*, *cpx*, *pig*, *ol* and *qtz*) assemblage in a CaO-MgO-FeO-SiO_2 system, at pressure of 7 kbar (i.e. P = 7000 bar) and temperature of 830^{o}C (i.e. T = 1103 K). (NB Other results from applications of the program on CMFS systems are presented and discussed in chapters 4 and 5). Considering the type of phases for *opx*, *cpx*, *pig* and *ol* ratio constraints are imposed, while for quartz no need of ratio constraints.

```
#-----------------------------------------------------
#         Input file for program Gib
#-----------------------------------------------------
#
5                           :Number of phases (np)
1,2,3,5,8                   :Phase types (i=1,np)
0,0,0,0,0                   :Phase options (i=1,np)
4                           :Number of cations (nc)
2,3,4,8                     :Cation types (i=1,nc)
#
#             system's bulk composition
#
0.0                 :Number of moles of cation 1 (=Na)
0.5                 :Number of moles of cation 2 (=Ca)
0.045               :Number of moles of cation 3 (=Mg)
1.455               :Number of moles of cation 4 (=Fe2+)
0.0                 :Number of moles of cation 5 (=Al)
0.0                 :Number of moles of cation 6 (=Cr)
0.0                 :Number of moles of cation 7 (=Fe3+)
2.0                 :Number of moles of cation 8 (=Si)
0.0                 :Number of moles of cation 9 (=Ti)
#
#
y,y,y,y,n           :Include non-linear ratio constraints for each phase ? (y or n)
#
#
7000                : P (Pressure, bar)
1103                : T (Temperature, K)
#
#
# Solver options
#
-5,-5               :precision value used in convergence test by solver (eps)
-3,+5               :scale factor used to multiply objective function (ffsqp3)
```

Fig. 3.8 Example of '*gib.in*' file used to compute equilibrium phase compositions in CaO-MgO-FeO-SiO_2 system.

Note that the output of the program (see Fig 3.9) indicates that for the system considered, at these specific *P*, *T* and bulk composition conditions, although 5 phases are initially included in the computation, the minimum is reached by an assemblage of three phases (*cpx* + *ol* +*qtz*).

Phase	Cation	Site	Site occup.
OPX	Ca	X_{21}	0.000
OPX	Mg	X_{31}	0.000
OPX	Mg	X_{32}	0.000
OPX	Fe2+	X_{41}	0.000
OPX	Fe2+	X_{42}	0.000
OPX	Si	X_{83}	0.000
	number of moles: 0		
CPX	Ca	X_{21}	0.714
CPX	Mg	X_{31}	0.011
CPX	Mg	X_{32}	0.038
CPX	Fe2+	X_{41}	0.275
CPX	Fe2+	X_{42}	0.962
CPX	Si	X_{83}	2.000
	number of moles: 0.698		
PIG	Ca	X_{21}	0.000
PIG	Mg	X_{31}	0.000
PIG	Mg	X_{32}	0.000
PIG	Fe2+	X_{41}	0.000
PIG	Fe2+	X_{42}	0.000
PIG	Si	X_{83}	0.000
	number of moles: 0		
OL	Ca	X_{21}	0.006
OL	Mg	X_{31}	0.019
OL	Mg	X_{32}	0.019
OL	Fe2+	X_{41}	0.975
OL	Fe2+	X_{42}	0.981
OL	Si	X_{83}	1.000
	number of moles: 0.302		
QTZ	Si	X_{83}	1.000
	number of moles: 0.302		

Fig 3.9 Output of '*Gib*' obtained using the '*gib.in*' file given in Fig 3.8 as input file.

Chapter 4

Thermodynamic modeling of Ca-Mg-Fe^{2+} olivine

4.1 Introduction

The important rock forming mineral olivine is an essential phase in many mafic and most ultramafic rocks. Together with pyroxenes and an aluminous phase (plagioclase, spinel or garnet, depending on pressure), it constitutes the peridotite of the earth's upper mantle. Nearly monomineralic olivine rocks called dunites are thought to be formed either as olivine cumulates from primitive basalts, or, in certain cases, by the passage of primitive basaltic melts by porous flow within the upper mantle, which dissolves orthopyroxene while precipitating olivine (Kelemen et al., 1995). This occurs because the primary phase volume of olivine expands greatly with decreasing pressure during basalt crystallization (e.g. Kushiro, 2001). This same effect ensures that olivine is the first major phase to crystallize during ascent of any basalt that is produced in equilibrium with olivine; thus olivine fractionation is almost a ubiquitous process during the evolution of basalts, and indeed olivine phenocrysts are common in primitive basalts.

To a first approximation the olivine in ultramafic or mafic rocks is a simple binary solid solution between the end-members forsterite (Fo, Mg_2SiO_4) and fayalite (Fa, Fe_2SiO_4). However, these naturally occurring ferromagnesian olivines also contain minor amounts of other divalent cations, in particular Ca, Mn, Ni and Co, which substitute for Mg and Fe in the olivine structure. Despite the fact that the abundance of these elements rarely exceed more than 1-2% (i.e. Ca < 1%, Mn < 1%, Ni < 4000 ppm, Co < 150 ppm; Simkin and Smith, 1970; Stormer, 1973; Stosch, 1981; Deer et al., 1992), their presence and partitioning between coexisting phases can be of great relevance for a better interpretation of magmatic processes.

Simkin and Smith (1970) showed how the amount of Ca in Mg-Fe olivines could be used as an indicator of the crystallization environment of the host rock. Their study, based on the analysis of minor elements in olivines from different types of magmatic rocks, revealed that plutonic olivines contained less Ca than olivines from hypabyssal and

extrusive environments. This correlation suggested that the Ca content of natural olivines could represent a valid geobarometer. The solubility of Ca in ferromagnesian olivines coexisting with other phases, in particular clinopyroxene, orthopyroxene and garnets has also been widely studied for its petrologic relevance. In the experimental studies of Finnerty (1977) and Finnerty and Boyd (1978) the abundance of Ca in forsterite in equilibrium with coexisting peridotite phases (orthopyroxene, clinopyroxene, garnet) was found to correlate negatively with increasing pressure (i.e. P) and positively with increasing temperature (i.e. T). The Ca-Mg exchange reaction between olivine and clinopyroxene is accompanied by a significant change in molar volume (ΔV of reaction), such that it can be employed as quantitative geobarometer in many systems of petrologic interest including spinel peridotites and garnet lherzolites (Adams and Bishop, 1982 and 1986). Köhler and Brey (1990) experimentally determined the content of Ca of forsteritic olivines in equilibrium with clinopyroxene. Their experiments were performed over a wide T-P range (2-60 kb and 900-1400 ^{o}C, which covers most of the equilibration conditions for upper mantle peridotites recovered as xenoliths at the Earth's surface). While this work showed that the solubility of Ca in olivine could be used as geobarometer in spinel peridotites, for which no other pressure-sensitive reactions exist, it also confirmed that the solubility is sensitive to temperature, which means that in practice its utility as a barometer is limited by the need for accurate temperature measurements. The partitioning of Ca between olivine and liquid has also been proposed as a geothermometer (Jurewicz and Watson, 1988; Libourel, 1999). However, the amount of Ca in igneous olivine is also known to be sensitive to Mg/Fe ratios. Kawasaki and Ito (1994) showed that the solubility of Ca in olivine increases with increasing of Fe/(Fe+Mg) in the system, while Kawasaki (1995, 1998a and 1999) found that the amount of Ca in olivine coexisting with clinopyroxene is highly sensitive to compositional variation as well as dependent on temperature and pressure. Further, Davidson and Lindsley (1994) found that the Ca content of coexisting augite and olivine heavily affects the distribution of Mg and Fe between these phases. This effect of olivine composition indicates the need for a thorough understanding of the thermodynamic properties of Ca-Mg-Fe olivine solid solutions. In this chapter a thermodynamic model for solid solutions minerals, whose derivation has been described in Chapter 2 of the theses, is applied to olivine assemblages in the Ca-Mg-Fe-Si system. This

will represent a first significant test to verify the validity of the new approach in modeling complex solid solutions outlined in the previous chapters of the theses.

4.2 Crystal-chemical considerations on modeling Ca-Mg-Fe olivine

Although Ca_2SiO_4 with the olivine structure is known (e.g. Remy et al., 1997; Reynard et al., 1997), in Ca-poor olivines (i.e. with Ca/(Ca+Mg+Fe)<0.5) all Ca is ordered into the M2 site, thus suggesting that, like Ca-Mg-Fe pyroxenes or Ca-Mg-Fe carbonates, the olivine solid solution is appropriately treated as a complex solid solution between the non-independent end-members Mg_2SiO_4, Fe_2SiO_4, $CaMgSiO_4$ and $CaFeSiO_4$. This view is strongly supported by the existence of asymmetrical solvi between Mg_2SiO_4 and $CaMgSiO_4$ and between Fe_2SiO_4 and $CaFeSiO_4$ in the respective binary joins, as will be discussed further below. In this respect the solution model for Ca-Mg-Fe olivines should then be similar to that for Ca-Mg-Fe orthopyroxene or clinopyroxene. However, unlike for either pyroxene solid solution, in the case of the olivine solution all of the four bounding end-members are stable at accessible *T, P* conditions, hence their free energies could in principle be determined calorimetrically. This would provide an independent constraint on the solution modelling, however the necessary data are not all available.

The olivine structure contains two distinct types of octahedral site, commonly named M1 and M2, where the divalent cations Ca, Mg and Fe can be found. The M1 site is smaller and more symmetric, while M2 is less symmetric and larger. Due presumably mainly to their different ionic radii related, Ca, Mg and Fe partition differently between the M1 and M2 sites. Mg and Fe, characterized by a similar ionic radius, can be found in both sites, while Ca, whose ionic radius is considerably bigger, should be confined to the larger M2 site. A number of single-crystal X-ray diffraction studies (e.g. Motoyama and Matsumoto, 1989; Ottonello el al., 1990; see Akamatsu et al., 1993 and Kawasaki, 1998b for a comprehensive review) have shown that Fe has a slight preference for the M1 site. Some of these studies have also indicated that the extent of this preference, usually expressed through the distribution coefficient K_D, where $K_D = (Fe+Mg)^{M1} / (Fe+Mg)^{M2}$, may be a function of temperature, pressure and possibly compositional and kinetic effects (Akamatsu et al., 1993). At the same time, most of the

analysis on olivine at upper mantle/lower crust conditions indicate K_D values very close to unity, usually varying within the small range 0.9~1.2. This suggests that under those *T-P* conditions the distribution of Mg and Fe between the two sites can be considered almost completely disordered. For the larger atoms of Ca, on the other hand, crystallographic studies show a completely different behavior with a very strong preference for the bigger M2 site (Brown, 1980; Lumpkin et al., 1983). Mukhopadhyay and Lindsley (1983) have discussed the possibility of a certain degree of disorder, maintaining that a small amount of Ca could enter the M1 site. Accurate investigation of cations disordering for Fe-free olivines has been carried out by Adams and Bishop (1985). Their analysis of unit-cell parameters on synthesized olivines raised the possibility of a small degree of Ca-Mg disordering between the M1 and M2 sites. The degree of disorder appeared to be compositionally dependent, being higher in the forsterite limb, and probably temperature related, starting at temperatures of about 1200 ^{o}C. However, the same authors after careful examination of their experiments concluded that the apparent disorder was always very limited and nearly within the stated errors limits of Ca being completely ordered. It should be noted that Adams and Bishop worked exclusively on quenched specimens, and it is possible that at the very high temperatures of their study a small amount of Ca-Mg order-disorder would reorder completely on quenching (cf. order-disorder in the spinel Mg_2TiO_4, discussed by O'Neill et al., 2003).

On the evidence of at most small amounts of disordering of Ca into the M1 site, a solution model has been chosen that allows a random mixing of Mg and Fe between the two octahedral sites (i.e. K_D=1)[14] , and a complete partitioning of Ca on the M2 site. Such a model implies that any possible energy contributions due to disordering of Ca onto the M1 site will be ignored.

An appropriate crystal-chemical formula for olivine in the CMFS (Ca-Mg-Fe-Si) system would then be $(Ca, Mg, Fe)^{M2}(Mg, Fe)^{M1}SiO_4$, where the composition of any olivine in the system can be fully expressed in terms of the four end-members: forsterite, fayalite, monticellite (Mo, $CaMgSiO_4$) and kirschsteinite (Kst, $CaFeSiO_4$).

[14] As shown in Chapter 3 a completely disordered distribution of Mg and Fe among M2 and M1 sites is obtained by imposing the ratio constraint $\left(\frac{Mg}{Mg + Fe}\right)^{M2} = \left(\frac{Mg}{Mg + Fe}\right)^{M1}$ on the solution.

The principle underlying the formulation of the general model for complex solid solutions was given in Chapter 2. Accordingly to the model, the formulation of the 'end-member' part[15] of the molar Gibbs free energy (i.e. G^{e-m}), for Ca-Mg-Fe olivines is exactly that for Ca-Mg-Fe pyroxenes (see Chapter 5), i.e.:

$$
\begin{aligned}
G^{e\text{-}m} = & \left[\left(1 - N_{Ca}\right) \cdot \frac{N_{Mg}}{N_{Mg} + N_{Fe^{2+}}} \right] \cdot G^{o-Fo} + \\
& \left[\left(1 - N_{Ca}\right) \cdot \frac{N_{Fe^{2+}}}{N_{Mg} + N_{Fe^{2+}}} \right] \cdot G^{o-Fa} + \\
& \left[N_{Ca} \cdot \frac{N_{Mg}}{N_{Mg} + N_{Fe^{2+}}} \right] \cdot G^{o-Mo} + \\
& \left[N_{Ca} \cdot \frac{N_{Fe^{2+}}}{N_{Mg} + N_{Fe^{2+}}} \right] \cdot G^{o-Kst} +
\end{aligned}
$$

While, for the 'ideal' and the 'excess' parts of the molar Gibbs energy (i.e. G^{id} and G^{ex}), Eq. (2.70) and Eq. (2.71) have, respectively, been used.

A similar approach has previously been followed by Davidson and Lindsley (1989) and Hirschmann (1991).

4.3 Model calibration

In Chapter 6 it will be shown how one can obtain consistent thermodynamic data from the model once a proper thermodynamic model has been derived. It will also be shown that the numerical technique used, although it has provided some very encouraging preliminary results, still needs some refinements. For this reason, the program *'GibInv'* described in Chapter 6 has not yet been extended to phases other than pyroxenes; therefore, for the olivine solid solutions of interest here an alternative way of calibration has been adopted.

[15] Remembering that for any solution phase ϕ, the molar Gibbs free energy can be considered as given by the sum of the contributions due to the end-member ($G^{e\text{-}m}$), ideal (G^{id}) and excess (G^{ex}) parts.

Existing thermodynamic databases and previous studies on the mixing properties of quadrilateral olivine and on cation partitioning between olivine and coexisting phases provide a starting point. These data were used as initial estimates at the beginning of the calibration procedure, then, when necessary, refined on a 'trial and error' basis in order to reproduce the available experimental results satisfactorily. In general during the calibration process, the solid solutions parameters (i.e. Margules parameters) were considered free to be adjusted, in view of the large variety of values that such parameters have been reported in former studies (see Table 4.1). On the other hand, if thermodynamic data for the four end-members needed refinement (see Table 4.2), it was chosen to adjust only the value of the enthalpy of formation, while the entropy, heat capacity functions, volumes and coefficients of thermal expansion and compressibility were left unchanged, since these are either well determined by measurement, or best kept well restrained within theoretical limits.

The 'trial and error' procedure adopted is certainly not as elegant as that based on the Bayesian approach described in Chapter 6. Nevertheless, the quality of the results obtained attests its validity.

4.4 Experimental constraints on model calibration and selection of initial estimates

In the past, a number of studies have been conducted on the four subsystems (Mo-Kst, Fo-Fa, Fo-Mo, Fa-Kst) that bound the quadrilateral Ca-Mg-Fe olivine system as well as on phase equilibria between olivines and coexisting phases. These studies will be reviewed in order to choose appropriate initial guesses for solution parameters and end-member thermodynamic data.

4.4.1 Mo-Kst join

Within this series while structure and crystal chemistry of the monticellite end-member have been investigated by Sharp et al., (1987), not many experiments have been done to examine the solution properties along the monticellite-kirschsteinite join, nor to study the structure of the kirschsteinite end-member. This lack of data is in part due to the scarcity of such olivine in natural rocks and in part to the difficulty of synthesizing pure kirschsteinite in the laboratory. However, despite the poverty of experimental evidence it

has been proposed that a continuous solid solution exists between the two end-members (e.g. Schairer and Osborn, 1950; Papike and Cameron, 1976; Brown, 1980). The above studies do not provide any additional insight on the Mg-Fe partitioning between members of the monticellite and kirschsteinite solid solutions.

4.4.2. Fo-Fa join

Among the four subsystems present in the quadrilateral olivine, the forsterite-fayalite solid solution has certainly been the most widely investigated. As already pointed out in section 4.1, the olivine found in natural rocks approximates a Mg-Fe binary solution, generally containing less than 2% of other elements. Good knowledge of the thermodynamic properties of magnesian-ferrian olivine is important in order to calculate temperature and pressure of formation of olivine-bearing rocks and to estimate the transition boundaries of olivine at high pressure and temperature. As a consequence, the solution properties of forsterite-fayalite olivine have been the object of many studies in petrology, mineralogy and mineral physics.

Previous studies on solution properties can basically be grouped into two types: those based on analysis of Fe-Mg exchange equilibria (e.g. Kawasaki and Matsui, 1977; O'Neill and Wood 1979; O'Neill and Wall, 1987; Wiser and Wood, 1991; Koch-Müller et al., 1992; Kawasaki and Ito, 1992 and 1994; von Seckendorff and O'Neill, 1993) and those from calorimetric measurements (e.g. Thierry et al., 1981; Wood and Kleppa, 1981; Kojitani and Akaogi, 1994). Despite the fact that Mg-Fe mixing takes place on two energetically different sites (M2 and M1), all the above works agree in assuming that the difference between Mg-Fe mixing parameters of M1 and M2 sites is very small. As a consequence the Margules parameters needed to describe the solution on the M2 and M1 sites (one or two depending on the adoption of either the symmetric or the asymmetric model) have usually been given the same value (i.e. either [16] $W^{M2}_{Mg-Fe} = W^{M1}_{Mg-Fe} = W^{M2}_{Fe-Mg} = W^{M1}_{Fe-Mg}$ symmetric model, or $W^{M2}_{Mg-Fe} = W^{M1}_{Mg-Fe} \neq W^{M2}_{Fe-Mg} = W^{M1}_{Fe-Mg}$ asymmetric model).

[16] The interaction (Margules) parameter of the free energy of mixing W_G is decomposed as follows: $W_G = W_H + T \cdot W_S + P \cdot W_V$, where W_H, W_S and W_V represent the contributions of enthalpy, entropy and volume terms to the free energy of mixing, respectively.

Thierry et al. (1981) concluded that no excess enthalpy of solution could be discerned at 1180K and 1atm for the forsterite-fayalite solution. Similarly, Davidson and Mukhopadhyay (1984) and Davidson and Lindsley (1989) in their models opted to neglect the Mg-Fe interactions. All other investigations have concluded that Mg-Fe olivines have small positive deviations from ideal mixing.

Wood and Kleppa (1981) concluded that the forsterite-fayalite solution should be regarded as asymmetric with respect to composition, in apparent contrast with previous studies (e.g. Kawasaki and Matsui, 1977; O'Neill and Wood, 1979; see Table 4.1 for a summary of some of the *W's* values adopted in previous work). However, subsequent investigations have not confirmed this proposition. For example, Wiser and Wood (1991) measured the activity–compositions relations at 1400K and 1atm pressure and showed that within experimental uncertainty the solution can be treated as symmetric and analogous conclusion has been reached in several other studies (e.g. von Seckendorff and O'Neill, 1993; Kojitani and Akaogi, 1994). In the present work, accordingly with most of the reviewed studies, a symmetric regular solution model has been adopted.

Looking at the values of Mg-Fe interaction parameters for symmetric models listed in Table 4.1, it is evident that they appear to consistently fall within the range of 5.0 ± ~2.0. The only values that are in clear disagreement are those of Kawasaki and Matsui (1977) and Sack and Ghiorso (1989). These authors assessed a much higher non-ideality to the solution ($W^{G}_{Mg-Fe} \geq 10kJ$), however such a large value appeared to be incompatible with the majority of both calorimetric and exchange equilibria studies (e.g. Wiser and Wood, 1991; von Seckendorff and O'Neill, 1993).

In this work on the base of the study conducted by O'Neill et al., (2003) a value of $W^{H}_{Mg-Fe} = 2.6kJ$ has been used an initial guess. Moreover, accordingly with most of the reported studies it has been chosen to neglect the non-ideal parameters for entropy and volume (i.e. $W^{S}_{Mg-Fe} = W^{V}_{Mg-Fe} = 0; \Rightarrow W^{G}_{Mg-Fe} \equiv W^{H}_{Mg-Fe}$). In view of the symmetric nature of the solution and the fact that interactions on M2 and M1 sites can be considered to be practically equivalent to each other, it will then be:

$$W^{M2}_{Mg-Fe} = W^{M2}_{Fe-Mg} = W^{M1}_{Mg-Fe} = W^{M1}_{Fe-Mg} = 2.6kJ \text{ . (NB One cation site basis).}$$

4.4.3. Fo-Mo join

All the available experimental data in the forsterite-monticellite series (Biggar and O'Hara, 1969; Yang, 1973; Warner and Luth, 1973; Adams and Bishop, 1985; Kawasaki, 2001; this work) exhibit only a limited miscibility between the end-members at various temperature and pressure conditions.

Studies by Biggar and O'Hara (1969) and Yang (1973) on the miscibility gap at one atmosphere agreed in showing the solution as asymmetric (i.e. $W_{Ca-Mg} \neq W_{Mg-Ca}$) although they dissented on the extent of the asymmetry. Warner and Luth (1973) investigated the miscibility gap in the temperature range within 800 and 1300 ^{o}C, and at pressures of 2, 5, 10 kbar. They concluded that the solution gap was nearly symmetric (i.e. $W_{Ca-Mg} \approx W_{Mg-Ca}$). Mukhopadhyay and Lindsley (1983) showed that a symmetric solution model could adequately described the Warner and Luth's data at 2 kbar and Davidson and Mukhopadhyay (1984) again adopted the regular solution model (see Table 4.1 for a list of proposed Margules parameters' values). Adams and Bishop (1985) investigated the Fo-Mo series in the temperature range of 1100 to 1490 ^{o}C at 5 and 10 kbar. Their reversal experiments unveiled that the miscibility gap is asymmetric, with the monticellite limb presenting a greater degree of solution than the forsterite limb. The two authors concluded also that pressure has no measurable effect on either solvus limb at 5 and 10 kbar, although, based on results on their single-phase experiments, they would predict an increase of miscibility with increasing pressure. Furthermore, in their asymmetric model they assumed a quite strong positive non-ideality in the entropy of mixing (i.e. $W_S > 0$, see Table 4.1) caused presumably by disorder phenomena.

The study of Kawasaki (2001) and the new experimental data presented in this work (Shi and O'Neill, in preparation; see Fig. 4.1), both at 1 atmosphere pressure and at several different temperatures, confirm a quite pronounced asymmetry in the solvus, with forsterite-reach olivines displaying a higher departure form ideality than monticellite-reach olivines. Kawasaki's work also shows agreement with Adams and Bishop's conclusion that the pressure effect is small and the solvus would narrow when increasing the pressure due to the negative excess volume of Ca-Mg olivine.

For the solution parameters in this study the values from Adams and Bishop's work have been chosen as initial guess.

4.4.4. Fa-Kst join

Examination of the early work by Bowen et al. (1933) indicates that a solvus should be present in the subsolidus region of the system, as the difference in ionic size between Ca and Fe^{2+} would also suggest. However, there is complete solid solution at temperatures just below the solidus. This enabled Johnson and Muan (1967) to study the join between fayalite and kirschsteinite at 1080 ^{o}C by equilibrating these solutions with $CaSiO_3$-$FeSiO_3$ pyroxene and pyroxenoid solutions (high SiO_2 activity) and CaO-"FeO" calcium-wüstite (low SiO_2 activity), both in equilibrium with metallic iron.

Mukhopadhyay and Lindsley (1983) performed reversed experiments at 1 kbar and vacuum pressure showing the presence of a miscibility gap below temperatures of approximately 1041 ^{o}C. They also showed that a simple symmetric model (i.e. $W_{Ca-Fe} = W_{Fe-Ca}$, see Table 4.1) could be used to represent the Fa-Kst solid solution. Consistently with Mukhopadhyay and Lindsley's work, Davidson and Mukhopadhyay (1984), Davidson and Lindsley (1989), Hirschmann (1991) and Kawasaki (1998b), all judged that a symmetric model was adequate to describe the solution.

Sokol and al. (2002) studied individual grains of calcian fayalite and ferroan kirschsteinite, as well as fayalite-kirschsteinite intergrowths found in the groundmass of basic crystallized melts from the Chelyabinsk basin. Analysis of their data seems to attest a certain asymmetry in the solvus, with the fayalite limb showing a slightly larger solubility respect to the kirschsteinite limb. The new experimental data at 1 atmosphere pressure condition presented in this work (Shi and O'Neill, in preparation; see Fig. 4.5) appear to confirm the asymmetry of the solvus. As a consequence an asymmetric solution model (i.e. $W_{Ca-Fe} \neq W_{Fe-Ca}$) was adopted here, although perforce the symmetric Margules values of Mukhopadhyay and Lindsley (1983) have been chosen as the initial guess.

4.4.5. End-member data

Thermodynamic data for forsterite, fayalite and monticellite end-members can be found in various databases (e.g. Berman 1988; Holland and Powell, 1990 and 1998;

Gottschalk 1997 and Chatterjee et al. 1998), while information on the kirschsteinite end-member can be obtained from previous works on quadrilateral olivine (Davidson and Mukhopadhyay, 1984; Davidson and Lindsley, 1989; Hirschmann, 1991).

In this study, data for forsterite, fayalite and monticellite from Holland and Powell (1990, 1998) were used as starting point in the calibration procedure. For the kirschsteinite end-member the initial guess' value of enthalpy of formation ($\Delta_f H$) has been derived from Davidson and Mukhopadhyay (1984). The entropy, heat capacity functions, volumes and coefficients of thermal expansion and compressibility were obtained following the procedure discussed in Berman and Brown (1985).

The list of the adopted values for the end-members is reported in Table 4.2.

4.5 Model results

4.5.1 Fo-Mo join

Compositions of coexisting low and high-calcium olivines are plotted on isobaric phase diagrams at 1 atm, 5 kbar and 10 kbar in figures 4.1, 4.2 and 4.3, respectively.

Experimental data from Kawasaki (2001) and this work at 1 atmosphere pressure show a very good agreement over a wide range of temperatures. Plotted in Fig. 4.1 are also the results of the early study by Biggar and O'Hara (1969), which appear to be remarkably consistent with the more recent data, despite the use of metastable starting materials in their experiments, which have previously raised doubts about the achievement of equilibrium (see Adams and Bishop, 1985 for a detailed discussion on Biggar and O'Hara's work). In Figs. 4.2 and 4.3 experimental data of Adams and Bishop (1985) at 5 and 10 kbar are plotted.

All the above mentioned experiments have been selected in order to test the validity of the model. On the other hand, works of Warner and Luth (1973) and Yang (1973), that appear to be in clear disagreement with the other studies (see Adams and Bishop, 1985 for a critical review of the above cited works) have here not been used as a comparison.

Solution and end-member parameters adopted in this work for the phase equilibrium calculation are given in Tables 4.1 and 4.2. Since forsterite and monticellite are isostructural, end-member data values are not needed for the calculation of the Fo-Mo solvus. As a consequence, data of Holland and Powell (1990) and (1998) were not altered during the calibration process. On the other hand, solution parameters of Adams and Bishop (1985) had to be refined. In agreement with the large majority of former studies it was chosen not to give any pressure dependence to the solution parameters, while, accordingly with the selected initial guess, a temperature dependence has been assigned to these parameters.

The resulting miscibility gaps calculated with the model are plotted as a solid curve in Figs. 4.1, 4.2, and 4.3.

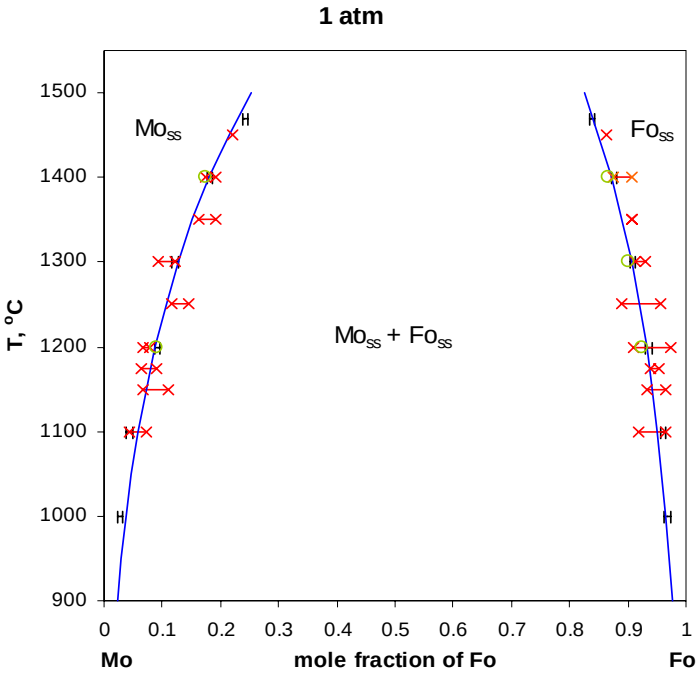

Fig. 4.1. The Mo-Fo miscibility gap at 1 atm. Data from this work are plotted as error bars, data from Kawasaki (2001) as red crosses, data from Biggar and O'Hara (1969) as green open circles. Solid curve is the calculated miscibility gap.

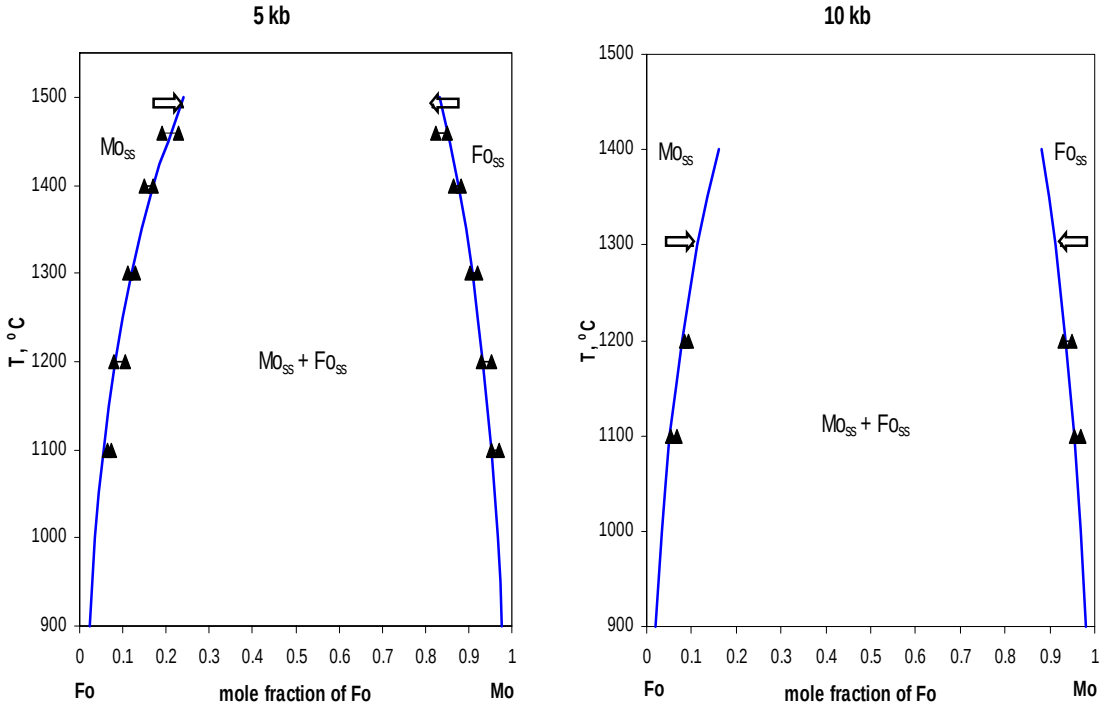

Fig. 4.2 (left) and **Fig. 4.3** (right). The Fo-Mo miscibility gap at 5 kbar and 10 kbar. Plotted as filled triangles are data from Adams and Bishop (1985). Arrows at 1490 °C (Fig. 4.2) and at 1300 °C (Fig. 4.3) indicate the direction of compositional changes. Solid curve is the calculated miscibility gap.

The model appears to fit in a very satisfactory way the available experimental data at all pressure-temperature conditions. In particular it very well reproduces the asymmetry in the solvus and its apparent temperature dependence. The model seems also to confirm that no pressure dependence for the solution parameters is needed, based at least on the available data at 5 and 10 kbar. It would probably be more appropriate to have some additional experimental data at high pressure before coming to a definitive conclusion on this issue.

4.5.2 Fa-Kst join

The only available experimental data that could be used to test the model are those of Mukhopadhyay and Lindsley (1983) and the new data presented in this work. Experimental results of Mukhopadhyay and Lindsley's work at 1 kbar and vacuum pressure are plotted in Fig. 4.4, while the new data presented in this work are plotted on the isobaric phase diagram of Fig. 4.5.

In their study, Mukhopadhyay and Lindsley determined the compositions of coexisting low and high-calcium olivines by microprobe analysis and from X-ray determinative curve. Both experimental results are plotted in Fig. 4.4. As the two authors already commented, the two methods lead to compositions that are in agreement with each other for temperatures up to 900 ^{o}C, while above that temperature X-ray and microprobe data are not compatible any more. Bearing in mind the uncertainty associated to their high temperature results, they inferred a solvus to exist below approximately 1041 ^{o}C.

For the new high temperature data (i.e. $T \geq 900$ ^{o}C) of this work, compositions of coexisting olivines have been determined by microprobe analysis. Ignoring the slightly different pressure conditions, present data show a good agreement when compared to the microprobe analysis at analogous temperature values of the former study. However, a graphical analysis of the results plotted in Fig. 4.5 seems to suggest a lower maximum temperature for the solvus.

As already said in section 4.4.4 while Mukhopadhyay and Lindsley data, given the quite large uncertainty of their results, could be fitted with a simple symmetric model, analysis of most recent works seems to prove that the asymmetric model here adopted is

more appropriate. Moreover, similarly to the approach followed to model the Fo-Mo join, it was decided to assign to the solution parameters a positive non-ideal value of entropy of mixing (i.e. $W_S > 0$) and to neglect a possible pressure effect (i.e. $W_V = 0$). Lack of experimental data at high pressure for the Fa-Kst solid solution, in fact, does not help constraining the W_V parameter.

Solution parameters adopted in the computation are given in Table 4.1. Solution and end-member parameters adopted in this work for the phase equilibrium calculation are given in Tables 4.1 and 4.2. Fayalite and kirschsteinite are isostructural, as a consequence, similarly to the Fo-Mo solid solutions, initial end-member values were not altered during the calibration process.

In Figs. 4.4 and 4.5, plotted as a solid curve, are the miscibility gaps calculated when using the model. The computed phase compositions show an excellent agreement with the new data presented in this work (Fig. 4.5). At the same time the model appears to fit in a satisfactory way also Mukhopadhyay and Lindsley's data (Fig. 4.4). Furthermore, applying the model, the maximum temperature for the solvus at 1atm pressure conditions is calculated to be around 1015 ^{o}C, which means some 25 ^{o}C less than what Mukhopadhyay and Lindsley concluded from their experiments.

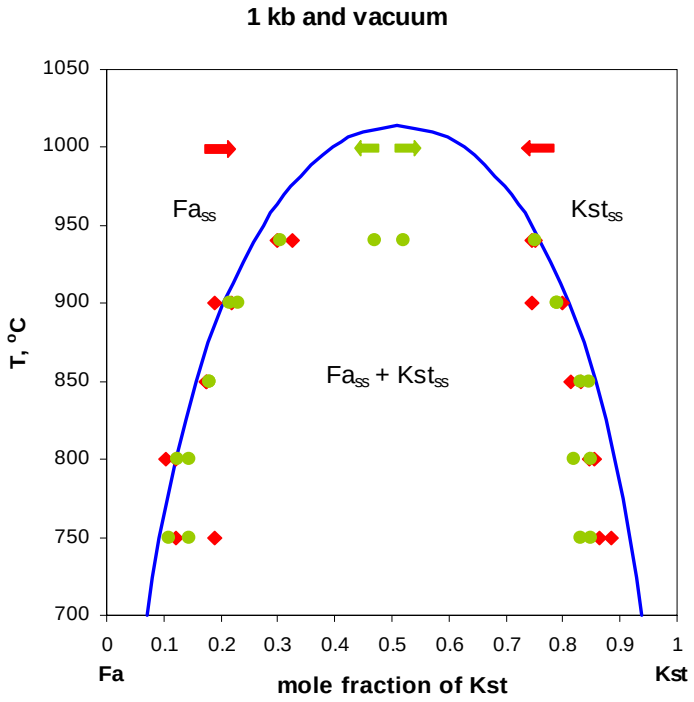

Fig. 4.4. Fa-Kst miscibility gap at 1 kbar ($T \leq 900$ °C) and vacuum ($T \geq 940$ °C) conditions. Experimental data from Mukhopadhyay and Lindsley (1983). X-ray compositions represented by red diamonds, microprobe analysis by green circles. Arrows at 1000 °C give the direction of compositional changes. Solid curve is the calculated miscibility gap (at 1 kbar).

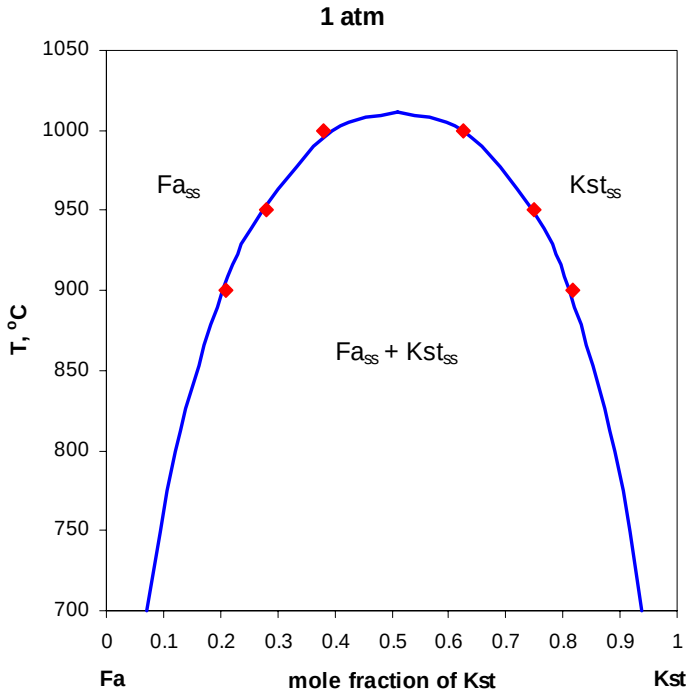

Fig. 4.5. Fa-Kst miscibility gap at 1 atm. Experimental data from this work are plotted as red diamonds. Solid curve is the calculated miscibility gap.

4.5.3 Ca-Mg-Fe olivines

Apart from the new data presented in this work (Shi and O'Neill, in preparation), previously only Davidson and Mukhopadhyay (1984) have performed reversed experiments on quadrilateral olivines. In their study, equilibrium phase compositions of four pairs of coexisting high-Ca/low-Ca olivines have been determined. Experiments were conducted a low pressure (1 kbar and vacuum conditions) and temperatures within 800 and 1100 ^{o}C. The same two authors have then used the four tielines obtained in their experiments in order to model the solution properties of the quadrilateral olivines and afterwards also Hirschmann (1991) based the calibration of his model mainly on these miscibility constraints. Results of the Davidson and Mukhopadhyay's work are plotted in Figs. 4.6a and 4.6b.

A new series of phase equilibrium data for Ca-Mg-Fe olivines is here presented. These new data, plotted in Figs. 4.6a, 4.6b and 4.6c represent the results of reversed experiments conducted at 1 bar pressure and at temperatures of 1000, 1100 and 1200 ^{o}C, and they cover a wide range of different bulk compositions from Mg-rich to Fe-rich olivines. These experiments, providing a large number of tielines, give a very valuable contribution in order to ascertain the gap in miscibility between high and low-Ca olivines at the above mentioned *T-P* conditions. Furthermore, examination of Figs. 4.6a and 4.6b shows that there is a good consistency between the new data and those of the early study by Davidson and Mukhopadhyay. All these data have then been used to test the model.

Former applications of the model to the Fo-Mo and Fa-Kst joins consented to verify and, when necessary, refine the standard state properties of the four end-members and the Ca-Mg, Ca-Fe mixing parameters. These values, therefore, have now to be considered as fixed. The only other solution parameter needed to fully depict the quadrilateral solution is the Margules parameter that accounts for the non-ideality of Mg-Fe mixing on M1 and M2 sites. As said in section 4.4.2 it was assumed W_{Mg-Fe} to have the value of 2.6 kJ after the work of O'Neill et al., (2003).

Plotted in Figs. 4.6a, 4.6b and 4.6c are the phase equilibrium compositions as calculated applying the model. The bulk composition of the computed phase data is the same as of the experimental data, so that a direct comparison between the two is meaningful.

Examination of the three figures shows that the model very well reproduces the experimental data at almost all conditions. The calculated tielines are in excellent accord with the experimentally determined ones. The agreement is very satisfactory with both the new data and the data of Davidson and Mukhopadhyay (1984), the only exception being the Davidson and Mukhopadhyay's experimental data at 1 kbar and 800 ^{o}C (see Fig. 4.6a). In this case, the calculated and experimental determined compositions look to be substantially dissimilar, causing the two respective tielines to clearly differ. Giving the excellent agreement between any other experimental and calculated data point and the fact that the slightly higher pressure conditions cannot account for such discrepancy, an inaccuracy in the experimental data seems to be the most likely explanation for this disagreement.

Fig. 4.6. Depicted are calculated and experimental determined compositions of coexisting Ca-Mg-Fe olivines at 1 bar and 1000 **(a)**, 1100 **(b)** and 1200 **(c)** ^{o}C. Results of computation are plotted as blue boxes, experimental data from this work and from Davidson and Mukhopadhyay (1984) are plotted as red and pink boxes, respectively. Shown are also calculated (blue stars) and Davidson and Mukhopadhyay (pink stars) data at 800 ^{o}C and 1 kbar pressure. Few representative tielines between calculated (in blue) and experimentally determined (in red/pink) olivines are also plotted.

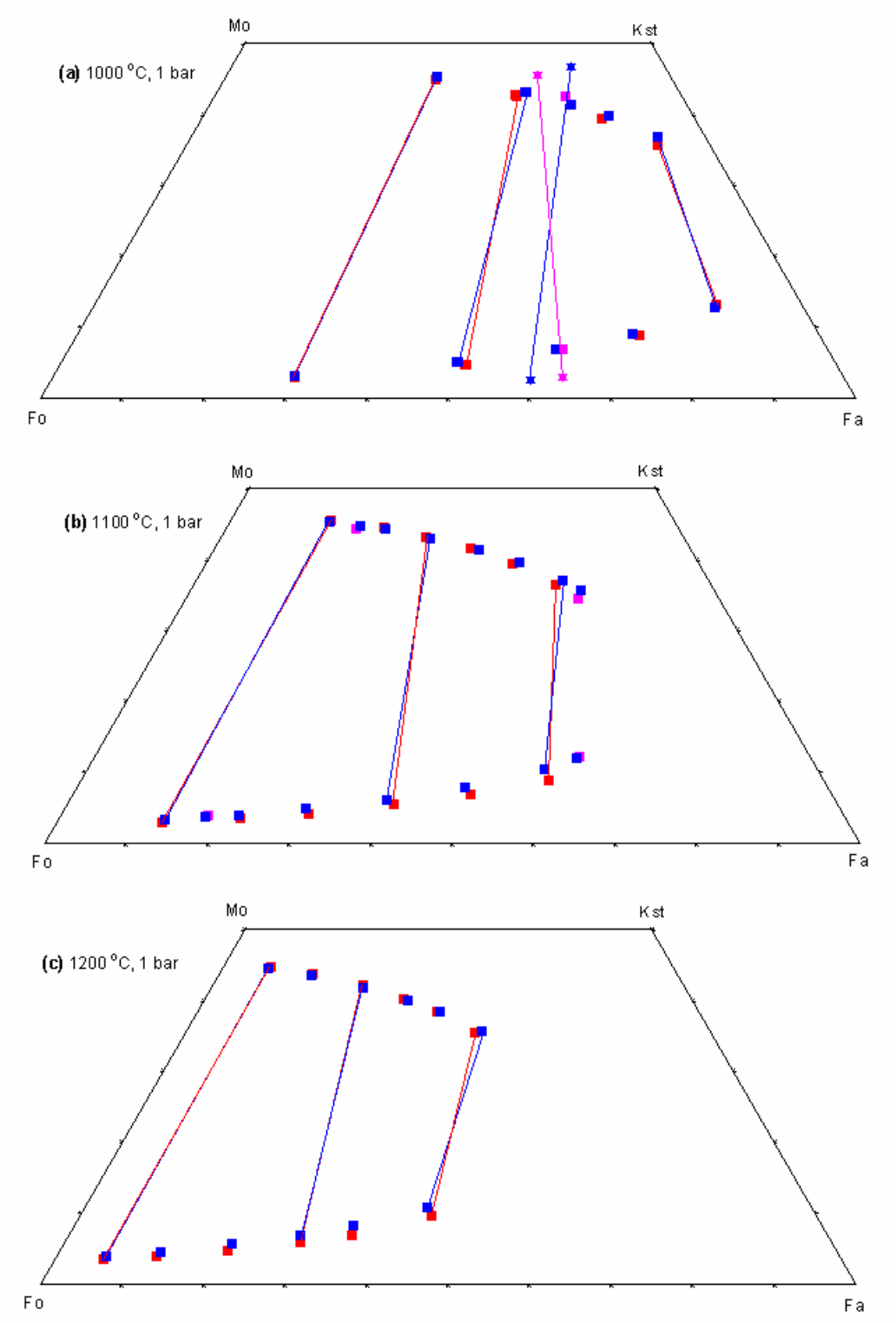
Mo
Kst
(a) 1000 °C, 1 bar
Fo
Fa
Mo
Kst
(b) 1100 °C, 1 bar
Fo
Fa
Mo
Kst
(c) 1200 °C, 1 bar
Fo
Fa

4.6 Model application

In the final section of this chapter it will be shown how the thermodynamic model for quadrilateral olivine here derived can be successfully employed as a tool for petrogenetic investigation. In particular the model will be applied to estimate the equilibrium temperature for coexisting iron rich high/low-Ca olivines studied by Sokol et al., (2002).

Sokol et al. analyzed the composition of assemblages of iron rich olivines from intergrowths found in the groundmass of *parabasalts* of the Chelyabinsk brown-coal basin. They assumed that an originally homogeneous (Ca, Mg, $Fe)_2SiO_4$ olivine during the cooling process entered a two phase field. As a consequence, lamellae of high-Ca olivine were formed in a matrix of low-Ca olivine. The exsolution phenomenon in Ca-rich olivine was then used as a tool to investigate the cooling history of the melts.

Sokol et al., after plotting the compositions of the coexisting olivine pairs on the phase diagram of Davidson and Mukhopadhyay (1984), concluded that the interval at the time of exsolution should be $980 \leq T \leq 800$ ^{o}C. The olivine's pairs were shown to fit reasonably well the miscibility gap surface even though Davidson and Mukhopadhyay's model treated the solid solution as symmetric while more recent data appeared to confute their assumption.

In this work, using the improved model, the equilibrium composition temperature for some of the olivines from Sokol et al.'s study has been calculated. Based on the Ca-content and on the Mg/Fe ratio the olivines were selected that have presumably crystallized at respectively the higher and lower temperatures. Then the temperature of crystallization was calculated also for few other olivines that crystallized at some intermediate temperature conditions during the cooling process. The olivines from Sokol et al.'s work contained some manganese as well as negligible amount of sodium and phosphorus. The model cannot account for the presence of manganese; so, prior to proceed in the computation, a recalculation of the original olivine compositions has been made necessary. Since manganese in the olivine structure can be treated as a substitute for Mg and Fe its original amount has been proportionally redistributed between these two elements.

The recalculated compositions of coexisting olivines from Sokol et al. are plotted in the diagram of Fig. 4.7. Plotted in the same diagram are also the compositions of the computed equilibrium phases at the indicated temperatures. The accord between experimental and calculated compositions is very satisfactory.

Interpretation of the results from the model disagrees in part with the conclusions previously drawn by Sokol et al., (2002). On one hand, the inferred equilibrium temperatures appear to confirm that olivine should have undergone exsolution at temperature lower than 1030 ^{o}C as expected for olivine of that composition (Sokol et al., 2002). More precisely the highest exsolution temperature recorded would be ≈977 ^{o}C, very close to the value previously indicated (≈980 ^{o}C). On the other hand, based on the model, the exsolution process should have stopped at temperature just below 900 ^{o}C (≈897 ^{o}C), which is considerably higher than ≈800 ^{o}C as obtained when applying Davidson and Mukhopadhyay (1984)'s model. This would imply an interval of exsolution of 977≤T≤896, which is substantially smaller than previously thought.

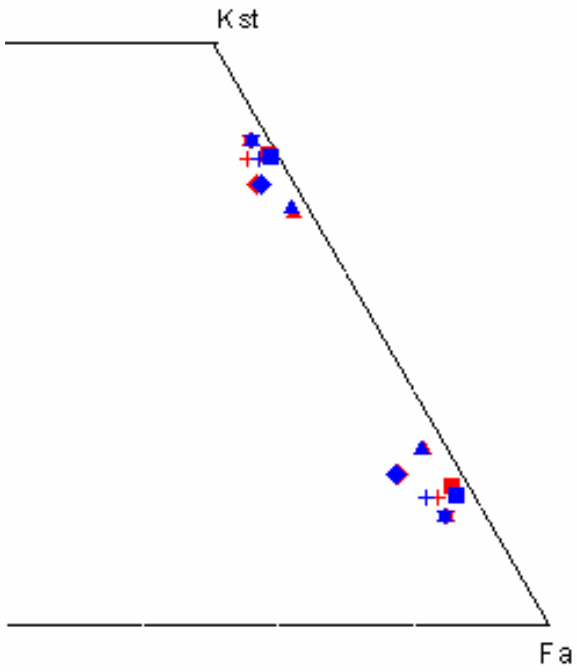

Fig. 4.7. Plotted are compositions of coexisting olivines from Sokol et al., (2002) (red symbols), and as calculated with the model (blue symbols). Each blue symbol indicates a different equilibrium temperature: *star* = 896 ^{o}C; *plus* = 920 ^{o}C; *box* = 930 ^{o}C; *diamond* = 967 ^{o}C; *triangle* = 977 ^{o}C.

Table 4.1. List of mixing parameters for $(Ca, Mg, Fe)_2SiO_4$ olivines (unit in kJ).

Parmeter	Value	Reference
$W_{Ca-Mg} = W_{Mg-Ca}$	33.922 ± 0.116	Mukhopadhyay and Lindsley (1983)
$W_{Ca-Mg} = W_{Mg-Ca}$	32.9	Davidson and Mukhopadhyay (1984)
W_{Ca-Mg}	43.1 - T*6.01*E-3	Adams and Bishop (1985)
W_{Mg-Ca}	61.2 - T*15.2*E-3	Adams and Bishop (1985)
W_{Ca-Mg}	30.9 + P*0.49*E-3	Davidson and Lindsley (1989)
W_{Mg-Ca}	34.25 + P*0.43*E-3	Davidson and Lindsley (1989)
$W_{Ca-Mg} = W_{Mg-Ca}$	34.5 ± 5.0 + P*0.35*E-3	Hirshmann (1991)
$W_{Ca-Mg} = W_{Mg-Ca}$	32.12	Kawasaki (1998)
W_{Ca-Mg}	36.32 ± 0.34	Kawasaki (2001)
W_{Mg-Ca}	32.72 ± 0.32	Kawasaki (2001)
W_{Ca-Mg}	43.470 - T*4.25*E-3	this work
W_{Mg-Ca}	52.580 - T*12.32E-3	this work
$W_{Ca-Fe} = W_{Fe-Ca}$	21.866 ± 0143	Mukhopadhyay and Lindsley (1983)
$W_{Ca-Fe} = W_{Fe-Ca}$	21.4	Davidson and Mukhopadhyay (1984)
$W_{Ca-Fe} = W_{Fe-Ca}$	21.56	Davidson and Lindsley (1989)
$W_{Ca-Fe} = W_{Fe-Ca}$	21.9 ± 0.1	Hirshmann (1991)
$W_{Ca-Fe} = W_{Fe-Ca}$	26.76 ± 0.9	Kawasaki (1998)
W_{Ca-Fe}	33.966 - T*10.0*E-3	this work
W_{Fe-Ca}	35.866 - T*11.0*E-3	this work
[a), (b)] W_{Mg-Fe}	11.6	Kawasaki and Matsui (1977)
W_{Mg-Fe}	4.415	O'Neill and Wood (1979)
W_{Mg-Fe}	4.1868	Wood and Kleppa (1981)
W_{Fe-Mg}	8.3736	Wood and Kleppa (1981)
W_{Mg-Fe}	0	Davidson and Mukhopadhyay (1984)
W_{Mg-Fe}	5	O'Neill and Wall (1987)
W_{Mg-Fe}	0	Davidson and Lindsley (1989)
W_{Mg-Fe}	10.17 ± 0.25	Sack and Ghiorso (1989)
W_{Mg-Fe}	3.7 ± 0.8	Wiser and Wood (1991)
W_{Mg-Fe}	7.12 ± 1.8	Koch-Müller et al. (1992)
W_{Mg-Fe}	5.45 ± 0.574	von Seckendorff and O'Neill (1993)
W_{Mg-Fe}	6.44 + P*0.09	Kawasaki and Ito (1994)
W_{Mg-Fe}	2.6	this work

Notes: [a] Interaction Mg-Fe parameters are given in one cation site basis

[b] It is also implied that $W^{M2}_{Mg-Fe} = W^{M1}_{Mg-Fe} = W^{M2}_{Fe-Mg} = W^{M1}_{Fe-Mg}$, unless otherwise specified.

Table 4.2. Thermodynamic properties of olivine end-members adopted in the computation. $\Delta_f H$ is the molar enthalpy of formation; S^o is the molar entropy of formation; *A, B, C* and *D* are molar heat capacity polynomial coefficients, where the heat capacity is: $Cp = A + BT + CT^{-2} + dT^{-1/2}$; *V* is the molar volume, αV and βV are the coefficient of thermal expansion and compressibility, respectively, multiplied by molar volume. Units: kJ, K and kbar. Sources: for forsterite, fayalite and monticellite, $\Delta_f H$ and S^o are from Holland and Powell (1998), any other parameter from Holland and Powell (1990); for kirschsteinite: this work.

end-member	$\Delta_f H$	S^o	A	B	C	D	V	αV	βV
forsterite	-2171.85	0.0951	0.2349	1.07E-06	-542.9	-1.9064	4.37	1.60E-04	3.20E-03
fayalite	-1478.22	0.151	0.0599	7.06E-05	-5743.7	2.0121	4.63	1.41E-04	4.00E-03
monticellite	-2252.9	0.1081	0.2507	-1.04E-05	-797.2	-1.9961	5.15	1.90E-04	4.40E-03
kirschsteinite [(a)]	-1912.515	0.13655	0.1632	2.43E-05	-3397.6	-0.03685	5.28	1.81E-04	4.80E-03

Notes: [(a)] Davidson and Mukhopadhyay (1984) estimated the value of $F^o \equiv 2 \cdot \left(G^o_{Mo} - G^o_{Kst}\right) + G^o_{Fa} - G^o_{Fo} = 12.66kJ$, which applied to the above G^o_{Mo}, G^o_{Fa} and G^o_{Fo}'s data lead to the value of $G^o_{Kst} = 1912.414kJ$, adopted as initial guess.

4.7 References

Adams G. E. and Bishop F. C. (1982) Experimental investigation of Ca-Mg exchange between olivine, orthopyroxene and clinopyroxene: potential for geobarometry. *Earth and Planetary Science Letters* **57**, 241-250.

Adams G. E. and Bishop F. C. (1985) An experimental investigation of thermodynamic mixing properties and unit-cell parameters of forsterite-monticellite solid solutions. *American Mineralogist* **70**, 714-722.

Adams G. E. and Bishop F. C. (1986) The olivine-clinopyroxene geobarometer: experimental results in the CaO-FeO-MgO-SiO_2 system. *Contributions to Mineralogy and Petrology* **94**, 230-237.

Akamatsu T., Kumazawa M., Aikawa N., and Takei H. (1993) Pressure effect on the divalent cation distribution in nonideal solid solution of forsterite and fayalite. *Physics and Chemistry of Minerals* **19**, 431-444.

Berman R. G. (1988) Internally-consistent thermodynamic data for minerals in the system Na_2-K_2O-CaO-MgO-FeO-Fe_2O_3-Al_2O_3-SiO_2-TiO_2-H_2O-CO_2. *Journal of Petrology* **29**, 445-552.

Berman R. G. and Brown T. H. (1985) Heat capacity of mineral in the system Na_2O-K_2O-CaO-MgO-FeO-Fe_2O_3-Al_2O_3-SiO_2-TiO_2-H_2O-CO_2: Representation, estimation, and high temperature extrapolation. *Contributions to Mineralogy and Petrology* **89**, 168-183.

Biggar G. M. and O'Hara M. J. (1969) Monticellite and kirschsteinite crystalline solutions. *Journal of American Ceramic Society* **52**, 249-252.

Bowen N. L., Schairer J. F., and Posnjak E. (1933) The system Ca_2SiO_4-Fe_2SiO_4. *American Journal of Science* **26**, 273-297.

Brown G. E. (1980) Olivines and silicate spinels, In Orthosilicate, (P.H. Ribbie, ed.), Mineral Soc., Washington, DC. *Reviews in Mineralogy* **5**, 275-381.

Chatterjee N. D., Krüger R., Haller G., and Olbricht W. (1998) The Bayesian approach to an internally consistent thermodynamic database: theory, database, and generation of phase diagrams. *Contributions to Mineralogy and Petrology* **133**, 149-168.

Davidson P. M. and Lindsley D. H. (1989) Thermodynamic analysis of pyroxene-olivine-quartz equilibria in the system CaO-MgO-FeO-SiO_2. *American Mineralogist* **74**, 18-30.

Davidson P. M. and Lindsley D. H. (1994) Effect of Ca content and SiO_2 activity on augite + olivine equilibria. *American Mineralogist* **79**, 1123-1124.

Davidson P. M. and Mukhopadhyay D. K. (1984) Ca–Fe–Mg olivines: phase relations and a solution model. *Contributions to Mineralogy and Petrology* **86**, 256-263.

Deer W. A., Howie R. A., and Zussman J. (1992) Rock-forming minerals. - Orthosilicates. Longman, London and New York. **Vol. 1A**, 3-15.

Finnerty A. A. (1977) Exchange of Mn, Ca, Mg and Al between synthetic garnet, orthopyroxene, clinopyroxene and olivine. *Carnegie Institution of Washington, Yearbook* **76**, 572-579.

Finnerty A. A. and Boyd F. R. (1978) Pressure-dependent solubility of calcium in forsterite coexisting with diopside and enstatite. *Carnegie Institution of Washington, Yearbook* **77**, 713-717.

Gottschalk M. (1997) Internally consistent thermodynamic data for rock forming minerals. *European Journal of Mineralogy* **9**, 175-223.

Hirschmann M. (1991) Thermodynamics of multicomponent olivines and the solution properties of $(Ni,Mg,Fe)_2SiO_4$ and $(Ca,Mg,Fe)_2SiO_4$ olivines. *American Mineralogist* **76**, 1232-1248.

Holland T. J. B. and Powell R. (1990) An enlarged and updated internally consistent thermodynamic dataset with uncertainties and correlations: the system K_2O-Na_2O-CaO-MgO-MnO-FeO-Fe_2O_3-Al_2O_3-TiO_2-SiO_2-C-H-O_2. *Journal of Metamorphic Geology* **8**, 89-124.

Holland T. J. B. and Powell R. (1998) An internally consistent thermodynamic dataset for phases of petrological interest. *Journal of Metamorphic Geology* **16**, 309-403.

Johnson R. E. and Muan A. (1967) Activity-composition relations in solid solutions of the system CaO-"FeO"-SiO_2 in contact with metallic iron at 1080 ^oC. *Transactions of the Metallurgical society of Aime* **Vol. 239**, 1931-1939.

Jurewicz A. J. G. and Watson E. B. (1988) Cations in olivines. 1. Calcium partitioning and calcium-magnesium distribution between olivines and coexisting melts, with petrologic applications. *Contributions to Mineralogy and Petrology* **99**, 176-185.

Kawasaki T. (1995) Empirical formulation for the distribution of Ca^{2+} between olivine and Ca-rich clinopyroxene at 7.5 GPa pressure. The Earth's Central Part: Its Structure and Dynamics (Yukutake, T., ed.). *Terra Sci. Pub. Co., Tokyo*, 45-55.

Kawasaki T. (1998a) Effects of pressure and Ca^{2+} on the Fe-Mg partitioning between olivine and clinopyroxene. *Reviews of High Pressure Science and Technology* **7**, 95-97.

Kawasaki T. (1998b) Thermodynamic formulations of $(Ca,Fe,Mg)_2SiO_4$ olivine. *Mineralogical Magazine* **20**, 135-149.

Kawasaki T. (1999) Thermodynamic analysis of partitioning of Ca, Fe and Mg between olivine and clinopyroxene. *Geochemical Journal* **33**, 1-25.

Kawasaki T. (2001) Experimental constraints on mixing properties of forsterite–monticellite olivine under atmospheric pressure. *Journal of Mineralogical and Petrological Sciences* **96**, 54-66.

Kawasaki T. and Ito E. (1992) Exchange of Fe^{2+} and Mg^{2+} between olivine and clinopyroxene at 7.5 GPa and 1300 ^oC, In High-Pressure Research: Application to Earth and Planetary Sciences, (Y. Syono and M.H. Manghnani, ed.). *Geophys. Monogr.,* **67**(Mineral. Phys., 3, Terra Sci. Pub. Co., Tokyo.), 305-313.

Kawasaki T. and Ito E. (1994) An experimental determination of exchange reaction of Fe^{2+} and Mg^{2+} between olivine and Ca-rich clinopyroxene. *American Mineralogist* **79**, 461-477.

Kawasaki T. and Matsui Y. (1977) Partitioning of Fe^{2+} and Mg^{2+} between olivine and garnet. *Earth and Planetary Science Letters* **37**, 159-166.

Kelemen P. B., Shimizu N. and Salters V. J. M. (1995) Extraction of mid-ocean-ridge basalt from the upwelling mantle by focused flow of melt in dunite channels. *Nature* **375**, 747-753.

Koch-Müller M., Cemic L., and Langer K. (1992) Experimental and thermodynamic study of Fe-Mg exchange between olivine and orthopyroxene in the system MgO-FeO-SiO_2. *European Journal of Mineralogy* **4**, 115-135.

Köhler T. P. and Brey G. P. (1990) Calcium exchange between olivine and clinopyroxene calibrated as a geothermobarometer for natural peridotites from 2 to 60 kb with applications. *Geochimica et Cosmochimica Acta* **54**, 2375-2388.

Kojitani H. and Akaogi M. (1994) Calorimetric study of olivine solid solutions in the system Mg_2SiO_4 – Fe_2SiO_4. *Physics and Chemistry of Minerals* **20**, 536-540.

Kushiro I. (2001) Partial melting experiments on peridotite and origin of mid-ocean ridge basalt. *Annual review of Earth and Planetary Sciences* **29**, 71-107.

Libourel G. (1999) Systematics of calcium partitioning between olivine and silicate melt: implications for melt structure and calcium content of magmatic olivines. *Contributions to Mineralogy and Petrology* **136**, 63-80.

Lumpkin G. R., Ribbe P. H., and Lumpkin N. E. (1983) Composition, order-disorder and lattice parameters of olivines: Determinative methods for Mg-Mn and Mg-Ca silicate olivines. *American Mineralogist* **68**, 1174-1182.

Motoyama T. and Matsumoto T. (1989) The crystal structures and the cation distributions of Mg and Fe of natural olivines. *Mineralogical Journal* **14**, 338-350.

Mukhopadhyay D. K. and Lindsley D. H. (1983) Phase relations in the join kirschsteinite ($CaFeSiO_4$) – fayalite (Fe_2SiO_4). *American Mineralogist* **68**, 1089-1094.

O'Neill H. S. C. and Wall V. J. (1987) The olivine-orthopyroxene-spinel oxygen geobarometer, the nickel precipitation curve and the oxygen fugacity of the Earth's upper mantle. *Journal of Petrology* **28**, 1169-1191.

O'Neill H. S. C. and Wood B. J. (1979) An experimental study of Fe-Mg partitioning between garnet and olivine and its calibration as a geothermometer. *Contributions to Mineralogy and Petrology* **70**, 59-70.

O'Neill H. S. T., Pownceby M. I., and McCammon C. A. (2003) The magnesiowustite: iron equilibrium and its implications for the activity-composition relations of $(Mg,Fe)_2SiO_4$ olivine solid solutions. *Contributions to Mineralogy and Petrology* **146**, 308-325.

Ottonello G., Princivalle F., and Della Giusta A. (1990) Temperature, composition, and f_{o2} effects on intersite distribution of Mg and F^{2+} in olivines. Experimental evidence and theoretical interpretation. *Physics and Chemistry of Minerals* **17**, 301-312.

Papike J. J. and Cameron M. (1976) Crystal chemistry of silicate minerals of geophysical interest. *Reviews of Geophysical Space Physics* **14**, 37-80.

Remy C., Andrault D., and Madon M (1997) High-temperature, high-pressure X-ray investigation of dicalcium silicate. *Journal of American Ceramic Society* **80**, 851-860.

Reynard B., Remy C., and Takir F. (1997) High-pressure Raman spectroscopic study of Mn_2GeO_4, Ca_2GeO_4, Ca_2SiO_4 and $CaMgGeO_4$ olivines. *Physics and Chemistry of Minerals* **24**, 77-84.

Sack R. O. and Ghiorso M. S. (1989) Importance of considerations of mixing properties in establishing an internally consistent thermodynamic database: thermochemistry of minerals in the system $Mg_2SiO_4 – Fe_2SiO_4 – SiO_2$. *Contributions to Mineralogy and Petrology* **102**, 41-68.

Schairer J. F. and Osborn E. F. (1950) The system CaO-MgO-FeO-SiO_2: I. Preliminary data on the join $CaSiO_3$-MgO-FeO. *Journal of American Ceramic Society* **33**, 160-167.

Sharp Z. D., Hazen R. M., and Finger L. W. (1987) High-pressure crystal chemistry of monticellite, $CaMgSiO_4$. *American Mineralogist* **72**, 748-755.

Simkin T. and Smith J. V. (1970) Minor element distribution in olivine. *Journal of Geology* **78**, 304-325.

Sokol E., Sharygin V., Kalugin V., Volkova N., and Nigmatulina E. (2002) Fayalite and kirschsteinite solid solutions in melts from burned spoil-heaps, South Urals, Russia. *European Journal of Mineralogy* **14**, 795-807.

Stormer J. C. (1973) Calcium zoning in olivine and its relationship to silica activity and pressure. *Geochimica et Cosmochimica Acta* **37**, 1815-1821.

Stosch H. G. (1981) Sc, Cr, Co and Ni partitioning between minerals from spinel peridotite xenoliths. *Contributions to Mineralogy and Petrology* **78**, 166-174.

Thierry P., Colinet C. C., Mathieu J. C., Regnard J. R., and Amosse J. (1981) Thermodynamic properties of the forsterite-fayalite (Mg_2SiO_4-Fe_2SiO_4) solid solution. Determination of heat of formation. *Physics and Chemistry of Minerals* **7**, 43-46.

von Seckendorff V. and O'Neill H. (1993) An experimental study of Fe-Mg partitioning between olivine and orthopyroxene at 1173, 1273 and 1473 K and 1.6 Gpa. *Contributions to Mineralogy and Petrology* **113**, 196-207.

Warner R. D. and Luth W. C. (1973) Two-phase data for the join monticellite ($CaMgSiO_4$)-forsterite (Mg_2SiO_4): experimental results. *American Mineralogist* **56**, 998-1008.

Wiser N. M. and Wood B. J. (1991) Experimental determination of activities in Fe—Mg olivine at 1400 K. *Contributions to Mineralogy and Petrology* **108**, 146-153.

Wood B. J. and Kleppa O. J. (1981) Thermochemistry of forsterite-fayalite olivine solutions. *Geochimica et Cosmochimica Acta* **45**, 569-581.

Yang H. Y. (1973) New data on forsterite and monticellite solid solutions. *American Mineralogist* **58**, 343-345.

Chapter 5

Pyroxene thermodynamics:

phase relations in the system CaO-MgO-FeO-Al_2O_3-SiO_2 and its subsystems

5.1 Introduction

Pyroxenes occupy a position that is chemically central to the composition of mafic and ultramafic rocks. They represent the most important group of rock-forming ferromagnesian silicates and they occur as stable phases in nearly all igneous rocks. Pyroxenes are also found in many metamorphic rocks of widely different compositions either as primary or minor constituent. Thus, there are relatively few rock bulk compositions in which pyroxenes cannot be formed under most set of *T*, *P* and volatile conditions that could be found within the crust or the mantle of the earth (Robinson, 1980).

Due to their importance in earth sciences, pyroxenes have been the object of various petrologic and thermodynamic investigations. Of particular interest for petrologists are natural mineral assemblages containing coexisting [17]orthopyroxene and clinopyroxene. Petrologists have long recognized the possibility of gaining thermometric and barometric information for a variety of rocks based on the composition of coexisting pyroxenes (e.g. Davis and Boyd, 1966; Wood and Banno, 1973; Ross and Huebner, 1975; Saxena and Nehru, 1975; Lindsley and Dixon, 1976; Perkins and Newton, 1980; Kretz, 1982; Lindsley, 1983; Gasparik, 1984; Nickel and Brey, 1984; Nickel et al., 1985; Davidson and Lindsley, 1985 and 1989; Tribaudino and Bruno, 1993; Latypov et al., 2001; Bulatov et al., 2002), and both orthopyroxene and clinopyroxene have been analyzed with thermodynamic solution models for use in geothermometry and geobarometry (e.g. Wood and Banno, 1973; Wells, 1977; Davidson and Lindsley, 1985 and 1989).

A great deal of experimental effort has in the past focused on the calibration of two-pyroxene thermobarometers. However, as more experimental data become available and as

[17] Throughout the rest of this chapter the abbreviations *px* = pyroxene(s), *opx* = orthopyroxene, *cpx* = clinopyroxene, *pig* = pigeonite, *ol* = olivine, *qtz* = quartz will in most cases be used.

applications of these thermobarometers become more ambitious, the need for more accurate internally consistent thermodynamic models becomes apparent. Furthermore, a straightforward application of these models for geothermometry/geobarometry purposes necessarily requires a precise estimation of end-member and solution parameters for both *opx* and *cpx* solid solutions.

In this chapter, a general thermodynamic model for solid solutions minerals, whose derivation has been described in chapter 2 of this thesis, is applied to pyroxene assemblages in CaO-MgO-FeO-Al_2O_3-SiO_2 (i.e. CMFAS) system and its subsystems[18]. Employing the Gibbs free energy minimization algorithm described in chapter 3, pyroxenes phase equilibria in these systems are reproduced over a wide range of *T*, *P* and bulk composition conditions and compared to existing experimental data. This represents a very significant test to verify the validity of the new approach to model complex solid solutions outlined in the previous chapters and the ability of the program '*Gib'* (see also chapter 3) to efficiently solve minimization problems in complex systems, where a large number of constraints need to be imposed on solutions (see also section 3.4).

A final purpose of this chapter is to present an internally consistent set of end-member and mixing parameters for the *opx* and *cpx* solid solutions (see Table 5.1 and Table 5.2). These parameters can then be used as starting point in the construction of more precise two-pyroxene thermobarometers.

5.2 Remarks on the solution model adopted and on the procedure followed in the model's calibration

The principle underlying the formulation of a general thermodynamic model for complex solid solutions, here applied to depict both orthopyroxene and clinopyroxene solid solutions (i.e. opx_{ss} and cpx_{ss}, respectively), is given in chapter 2. Accordingly to the model, any solid solution involving Ca-Mg-Fe^{2+}-Al pyroxenes can be fully described in terms of seven end-members: enstatite (En, $Mg_2Si_2O_6$), ferrosilite (Fs, $Fe_2Si_2O_6$), diopside (Di, $CaMgSi_2O_6$), hedenbergite (Di, $CaFeSi_2O_6$), Ca-Tschermak (CaTs, $CaAl_2SiO_6$), Mg-Tschermak (MgTs, $MgAl_2SiO_6$) and Fe^{2+}-Tschermak (Fe^{2+}Ts, $Fe^{2+}Al_2SiO_6$). It follows that,

[18] Application of the model in CaO-MgO-FeO-SiO_2 (i.e. CMFS) system will be also to *px-ol-qtz* assemblages, depending on bulk composition and *T*, *P* conditions (see section 5.5.1).

for a pyroxene solution in the general Ca-Mg-Fe^{2+}-Al case, the expression of the 'end-member' part[19] of the molar Gibbs free energy (i.e. G^{e-m}), is given by (NB Same expression for both opx_{ss} and cpx_{ss}):

$$
\begin{aligned}
G^{e\text{-}m} = & \left[\left(1 - N_{Ca}\right) \cdot \left(1 - \frac{N_{Al}}{2} \right) \cdot \frac{N_{Mg}}{N_{Mg} + N_{Fe^{2+}}} \right] \cdot G^{o-En} + \\
& \left[\left(1 - N_{Ca}\right) \cdot \left(1 - \frac{N_{Al}}{2} \right) \cdot \frac{N_{Fe^{2+}}}{N_{Mg} + N_{Fe^{2+}}} \right] \cdot G^{o-Fs} + \\
& \left[N_{Ca} \cdot \left(1 - \frac{N_{Al}}{2} \right) \cdot \frac{N_{Mg}}{N_{Mg} + N_{Fe^{2+}}} \right] \cdot G^{o-Di} + \\
& \left[N_{Ca} \cdot \left(1 - \frac{N_{Al}}{2} \right) \cdot \frac{N_{Fe^{2+}}}{N_{Mg} + N_{Fe^{2+}}} \right] \cdot G^{o-Hd} + \\
& \left[N_{Ca} \cdot \left(\frac{N_{Al}}{2} \right) \right] \cdot G^{o-CaTs} + \left[\left(1 - N_{Ca}\right) \cdot \left(\frac{N_{Al}}{2} \right) \cdot \frac{N_{Mg}}{N_{Mg} + N_{Fe^{2+}}} \right] \cdot G^{o-MgTs} + \\
& \left[\left(1 - N_{Ca}\right) \cdot \left(\frac{N_{Al}}{2} \right) \cdot \frac{N_{Fe^{2+}}}{N_{Mg} + N_{Fe^{2+}}} \right] \cdot G^{o-Fe^{2+}Ts}
\end{aligned}
\tag{5.1}
$$

Expressions of G^{e-m} for pyroxene solutions in any other case investigated in this chapter are obtained in a straightforward manner from Eq. (5.1). For example, considering a CMFS system (i.e. no Al present), where the four end-members En, Fs, Di and Hd are required to bound any possible solid solution, the expression of G^{e-m} (after eliminating Al from Eq. 5.1) becomes[20]:

[19] Remembering that for any solution phase ϕ, the molar Gibbs free energy can be considered as given by the sum of the contributions due to the end-member (i.e. $G^{e\text{-}m}$), ideal (i.e. G^{id}) and excess (i.e. G^{ex}) parts.

[20] The program '*Gib*' automatically performs this operation. This means that, depending on the system's bulk composition, the program automatically selects which end-members have to be 'activated' and, consequently, what is the correct expression of $G^{e\text{-}m}$ to use during the computation.

$$G^{e\text{-}m} = \begin{aligned} &\left[\left(1-N_{Ca}\right)\cdot\frac{N_{Mg}}{N_{Mg}+N_{Fe^{2+}}}\right]\cdot G^{o-En} + \\ &\left[\left(1-N_{Ca}\right)\cdot\frac{N_{Fe^{2+}}}{N_{Mg}+N_{Fe^{2+}}}\right]\cdot G^{o-Fs} + \\ &\left[N_{Ca}\cdot\frac{N_{Mg}}{N_{Mg}+N_{Fe^{2+}}}\right]\cdot G^{o-Di} + \\ &\left[N_{Ca}\cdot\frac{N_{Fe^{2+}}}{N_{Mg}+N_{Fe^{2+}}}\right]\cdot G^{o-Hd} + \end{aligned} \qquad (5.2)$$

In a similar way, G^{e-m} expressions for pyroxene solutions in any of the other CMFAS subsystems are obtained.

For the 'ideal' and the 'excess' parts of the molar Gibbs energy, Eq. (2.70) and Eq. (2.71) have, respectively, been used in both orthopyroxene and clinopyroxene solid solutions. Furthermore, in applying Eq. (2.71), the symmetric regular Margules formulation has been adopted for the opx_{ss} in every system investigated. On the other hand, for the cpx_{ss}, the asymmetric Margules formulation has been used to describe non-ideal Ca-Mg and Ca-Fe mixing. To model Mg-Fe (see also section 5.5 on this point), Mg-Al and Fe-Al excess mixing on site, the symmetric formulation has been adopted.

5.2.1 Calibration of the model

The computer program '*GibInv*' developed during the course of this study (see also chapter 6) that allows the simultaneous refinement of end-member (*E*) and mixing (*W*) parameters has been employed for the calibration of the thermodynamic model. The procedure followed in the calibration process, which is described in detail in chapter 6 (section 6.10), will be here briefly summarized.

The program '*GibInv*' is set up in a way to allow the refinement of any of the *E* and *W* parameters (see section 6.9). However, during the fitting process it was opted to adjust only $\Delta_f H$ (i.e. enthalpy of formation), S^o (entropy) and *W* parameters, while heat capacity functions (i.e. *A, B, C, D, E* parameters) molar volumes (*V*) and coefficients of thermal expansion (α) and compressibility (β) were left unchanged.

Thermodynamic data for some of the system's end-members can be found in previous works (e.g. Berman 1988; Davidson and Lindsley, 1989; Holland and Powell, 1990 and 1998; Sack and Ghiorso, 1994b; Robie and Hemingway 1995; Gottschalk 1997; Klemme 1998; Chatterjee et al. 1998). In the fitting process, data from Holland and Powell (1990 and 1998), Sack and Ghiorso (1994b) and Klemme (1998) were used as initial guesses for the *E* parameters to be refined. For these end-members, values of heat capacity functions, molar volumes, thermal expansion and compressibility coefficients have been adopted from Holland and Powell (1990) and Klemme (1998). On the other hand, for those end-members where no thermodynamic data were available, values of $\Delta_f H$ and S^o have been derived from scratch, while heat capacity functions, volumes and coefficients of thermal expansion and compressibility were obtained following the procedure discussed in Berman and Brown (1985).

For both orthopyroxene and clinopyroxene solid solutions, values of mixing (*W*) parameters have been derived from scratch. Any interaction parameter representing the free energy of mixing W_G may in principle be split up into terms dependent on temperature and pressure:

$$W_G = W_H + T \cdot W_S + P \cdot W_V \qquad (5.1)$$

where W_H, W_S and W_V represent the contributions of, respectively, enthalpy, entropy and volume terms. Initially, as explained in section 6.10, W_S and W_V were also treated as unknowns and included in the fitting process. However, this did not seem to improve the quality of the fitting. In addition, the standard deviations of their output values were very high. It was then decided to set $W_S = W_V \equiv 0$ and keep W_H as the only parameter to refine.

The fitting has been carried out in different steps. Initially it has been performed on the simple CaO-MgO-SiO_2 (i.e. CMS) system. Once the *E* and *W* parameters in this system (W^{M2}_{Ca-Mg}, W^{M2}_{Mg-Ca}, $\Delta_f H^{En}$, $\Delta_f H^{Di}$, S^{o-En} and S^{o-Di} for both opx_{ss} and cpx_{ss}) were refined, their values were considered known and, consequently, they were not fitted again. A similar

approach was taken to the fitting in the CaO-FeO-SiO_2 (i.e. CFS) system for the parameters W_{Ca-Fe}^{M2}, W_{Fe-Ca}^{M2}, $\Delta_f H^{Fs}$, $\Delta_f H^{Hd}$, S^{o-Fs} and S^{o-Hd}. Therefore, when performing the fitting of the CMFS system, the only parameters whose value needed to be derived were the Margules parameters that account for the non ideal Mg-Fe^{2+} mixing on M1 and M2 sites, i.e.: W_{Mg-Fe}^{M2}, W_{Fe-Mg}^{M2}, W_{Mg-Fe}^{M1} *and* W_{Fe-Mg}^{M1}, for both opx_{ss} and cpx_{ss}. Proceeding in this way, the value of all the other *E* and *W* parameters needed to compute pyroxene phase equilibria in the investigated systems has been either refined or derived. A very important benefit of this procedure is that the internal consistency of the model is ensured.

At the end, to better reproduce existing experimental data, the value of the *E* and *W* parameters, as obtained using *'GibInv'*, needed to be slightly adjusted. This additional 'refinement' has been done on a 'trial and error' basis. Comparison between the actual values of the *E* and *W* parameters used in the phase equilibria computation (see Tables 5.1 and 5.2) and those obtained in the fitting process (see Tables 6.9 and 6.10) can give an indication of the extent of the adjustment required. Note that for each parameter the correction made has always been well within the output standard deviation's value (given in Tables 6.9 and 6.10).

In the next sections, pyroxene phase equilibria, results of the computational process, are shown and compared to experimental data. Computed results are presented following the same order adopted in the fitting process, i.e.: CMS, CFS, CMFS, CMAS, CMFAS.

5.3 CMS system

The miscibility gap between enstatite and diopside is probably the most important geothermometer of upper mantle rocks and its correct determination is of great importance for the estimation of pressure-temperature distributions in the earth's crust and mantle. Although studies in simple systems cannot be extrapolated directly to natural rocks, the understanding of the ideal case of pure Ca, Mg-pyroxenes provides the foundation for all thermometers, regardless whether they are strictly thermodynamic, semi- or purely empirical (Nickel and Brey, 1984).

Atlas (1952) probably first recognized the potential of the En-Di miscibility gap as geothermometer and, after Davis and Boyd (1966) showed its temperature dependence at 30 kbar, the binary system $Mg_2Si_2O_6$-$CaMgSi_2O_6$ has been in the past three decades the subject of intensive experimental and theoretical studies. Experimental investigations at a range of pressures and temperatures (e.g. Nehru and Wyllie, 1974; Warner and Luth, 1974; Mori and Green, 1975 and 1976; Lindsley and Dixon, 1976; Finnerty, 1977; Perkins and Newton, 1980; Lindsley, 1981; Schweitzer, 1982; Brey and Huth, 1984; Nickel and Brey, 1984; Gasparik, 1996) have widely contributed to a better understanding of the phase equilibria relationship among the En-Di join. At the same time, a large number of thermochemical studies have been conducted and several different models have been proposed to describe thermodynamically both enstatite and diopside solid solutions (e.g. Holland et al., 1979; Lindsley and al., 1981; Nickel and Brey, 1984; Fei et al., 1986; Carlson and Lindsley, 1988; Davidson and al., 1988; Gasparik, 1990; Shi et al., 1993).

In this work, phase equilibria relationships along the En-Di join have been reproduced over a wide range of temperatures and pressures, and the calculated compositions of coexisting pyroxenes are plotted on isobaric phase diagrams in Fig. 5.1. Plotted in Fig. 5.1 are also results of experimental studies, where, in selecting the data that have been used as a comparison, bracketed results were preferred to unreversed experiments.

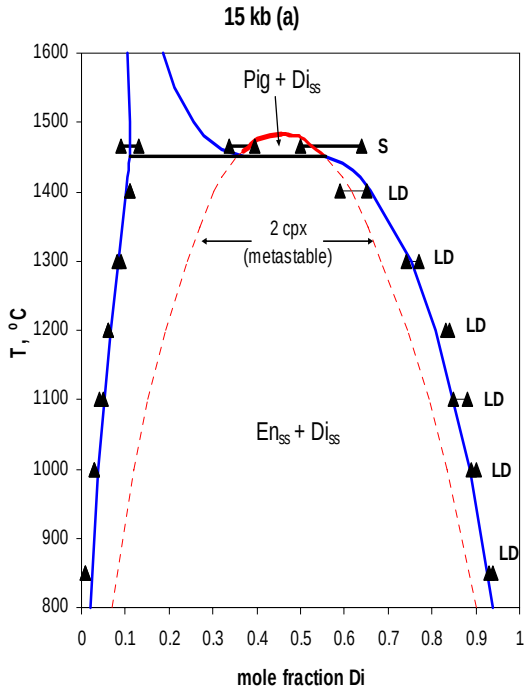
15 kb (a)
Pig + Di$_{ss}$
S
LD
2 cpx
(metastable)
LD
LD
LD
LD
LD
En$_{ss}$ + Di$_{ss}$
T, °C
mole fraction Di

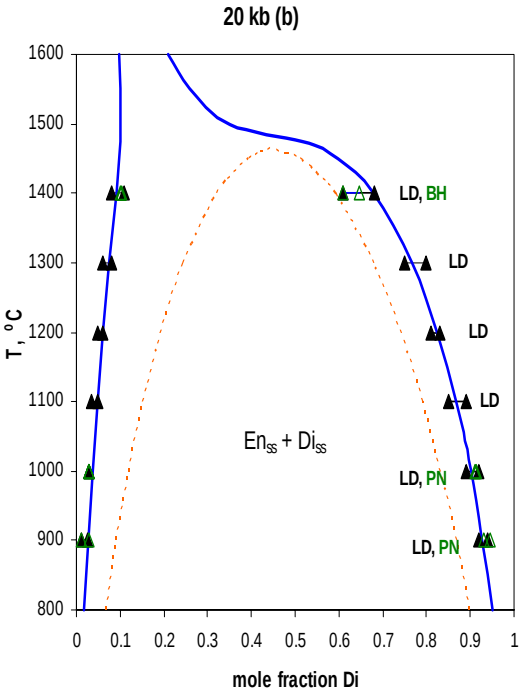
20 kb (b)
LD, BH
LD
LD
LD
LD, PN
LD, PN
En$_{ss}$ + Di$_{ss}$
T, °C
mole fraction Di

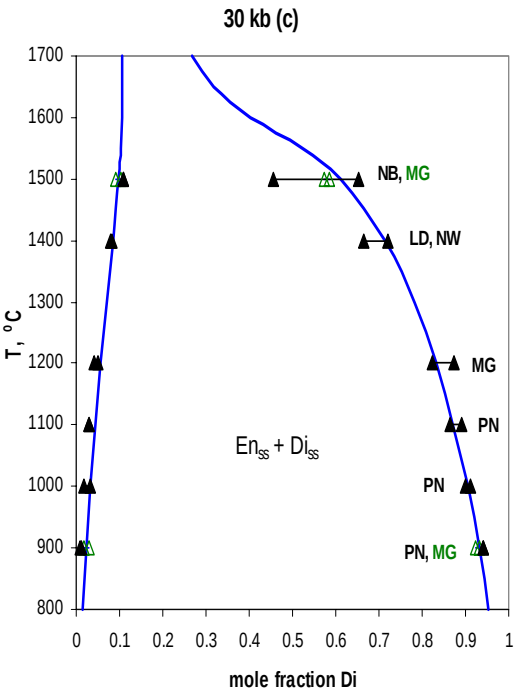
30 kb (c)
NB, MG
LD, NW
MG
PN
PN
PN, MG
En$_{ss}$ + Di$_{ss}$
T, °C
mole fraction Di

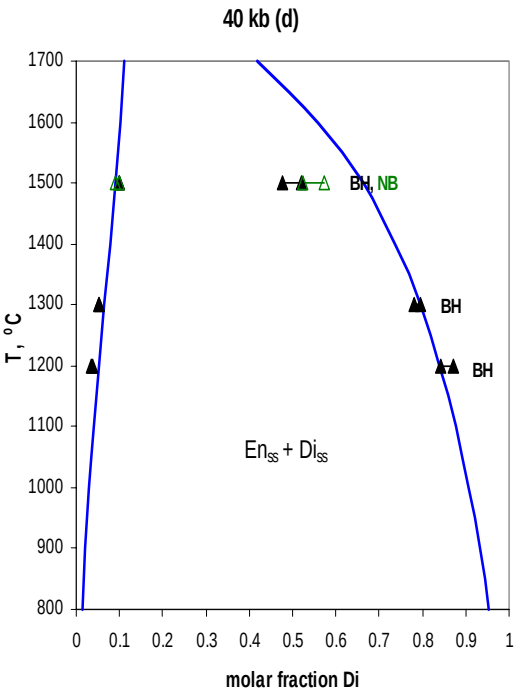
40 kb (d)
BH, NB
BH
BH
En$_{ss}$ + Di$_{ss}$
T, °C
molar fraction Di

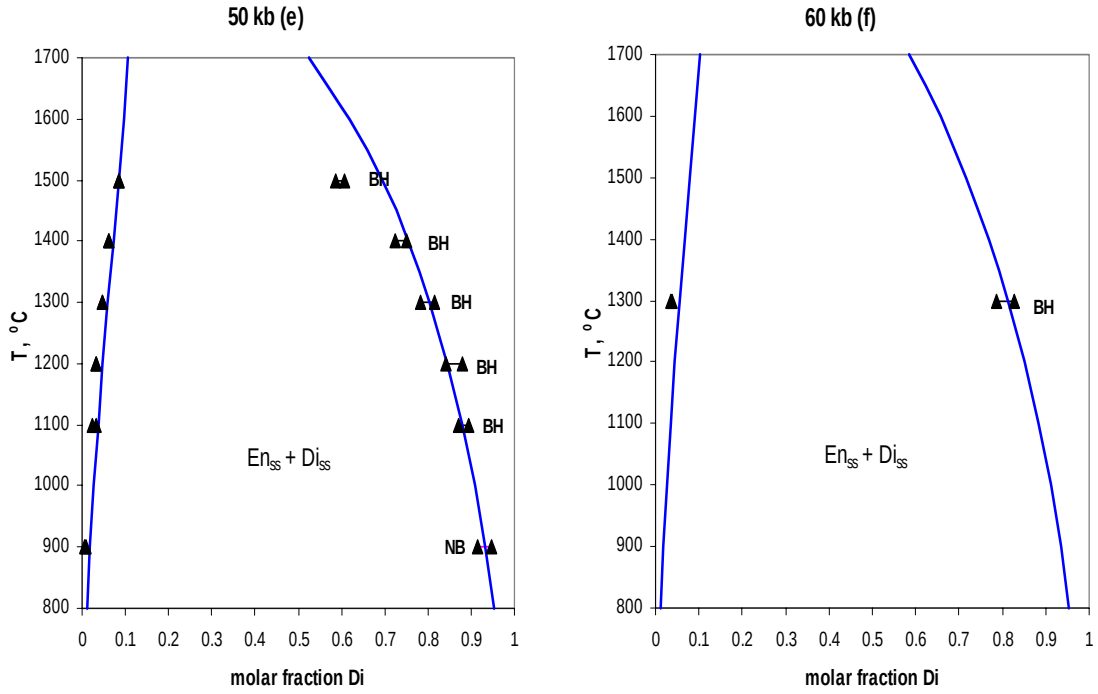

Fig. 5.1 Calculated subsolidus pyroxenes phase equilibria along the enstatite-diopside join for pressures: 15 **(a)**, 20 **(b)**, 30 **(c)**, 40 **(d)**, 50 **(e)**, and 60 **(f)** kbar. Plotted reversal brackets are from experimental studies of Nehru and Wyllie (1974) [NW], Mori and Green (1975) and (1976) [MG], Lindsley and Dixon (1976) [LD], Perkins and Newton (1980) [PN], Schweitzer (1982) [S], Nickel and Brey (1984) [NB], Brey and Huth (1984) [BH].

The model appears to fit in a very satisfactory way available experimental data in the pressure range 15-60 kbar and temperature range 850-1500 ^{o}C. It well reproduces the iron-free pigeonite field at 15 kbar, consistently with Schweitzer's (1982) work, and it would confirm that at 20 kbar pigeonite does not exist as a stable phase. This result is in agreement with all later models (e.g. Lindsley and al., 1981; Nickel and Brey, 1984; Gasparik, 1990) but is in disagreement with earlier works by Kushiro (1968, 1969), who, in his experiments at 20 kbar, obtained, for anhydrous runs, a stability field for iron-free pigeonite.

Some discrepancies can be observed between experimental and calculated clinopyroxene limbs of the En-Di miscibility gap at high *T-P* conditions. However, as pointed out by Gasparik (1990), these discrepancies may simply reflect internal

inconsistencies among the data that cannot be satisfied with any model. Nickel and Brey (1984) showed how experimentally determined compositions of clinopyroxene at high *T-P* conditions are not well constrained and can give very wide reversal brackets, as in their experiments at 1500 ^{o}C and 30 kbar. Problems in the fitting of high *T-P* data could also result from the attempt of reproducing Schweitzer's experimental positioning of the reaction enstatite$_{ss}$ + diopside$_{ss}$ = pigeonite (i.e. $En_{ss} + Di_{ss} = pig$). It has been suggested (Carlson and Lindsley, 1988; Gasparik, 1990; and experimental study of Kushiro and Yoder, 1970) that the reaction at 15 kbar could take place at some 30/40 ^{o}C less than suggested by Schweitzer (1982). Carlson and Lindsley (1988) tried to compromise by lowering the temperature for the three coexisting pyroxenes from 1465 to 1436 ^{o}C, obtaining though only a minor improvement. A further investigation of the $En_{ss} + Di_{ss} = pig$ reaction would be advisable, especially considering how valuable new data on the three coexisting phases could be to constraint clinopyroxene solution properties better.

5.4 CFS system

Similarly to the En-Di join, pyroxene phase relationships in the $Fe_2Si_2O_6$-$CaFeSi_2O_6$ join have also been of particular interest to petrologists for many years, as signified by the number of experimental studies conducted on this system. A main reason for the interest in the Fs-Hd join is that it represents the Mg-free boundary of the pyroxene quadrilateral (see also section 5.5). A correct understanding of phase equilibria relationships on this join and of the way they vary with temperature and pressure is crucial for a precise calibration of a Ca-Fe pyroxene thermodynamic model, which can then be used as a boundary for a model of more complex pyroxenes.

The early work of Bowen et al., (1933) showed that at 1 atm pyroxenes on this join are stable only for compositions close to pure hedenbergite. Pure ferrosilite at low pressure is unstable relative to fayalite and quartz, as proved by Bohlen et al., (1980), who carefully investigated the reaction Fs = Fa + Qtz in the pressure range 10.5-15 kbar and temperature range 700-1050 ^{o}C. The presence of Ca in the system stabilizes pure ferrosilite to slightly lower pressure (Lindsley, 1981), and increasing pressure stabilizes increasingly iron-rich pyroxenes, as showed by Lindsley and Munoz (1969) in their experiments at 20 kbar. Results of Lindsley (1981) and Lindsley and Munoz (1969) demonstrated the presence along the Fs-Hd join of an orthopyroxene-clinopyroxene miscibility gap as well as of a small but definite two-clinopyroxene field, similar to that seen for the En-Di join. At the same time, it has been reported in a number of studies (e.g. Bowen et al., 1933; Turnock, 1962; Lindsley, 1967; Lindsley and Burnham, 1970) that, with increasing temperature, pyroxenes may become unstable and transform to pyroxenoids. In a more recent work, Woodland and O'Neill (1995) have provided further insights on the $Fe_2Si_2O_6$-$CaFeSi_2O_6$ system at high pressure, showing the existence of a two-clinopyroxene miscibility gap that involves a low-Ca clinopyroxene having a high-*P* structure different from the one known for Mg-free pigeonite at lower pressure.

The coexistence of three solutions in a binary join puts very tight constraints on thermodynamic solution models (Lindsley, 1981). At the same time, however, there are large uncertainties associated with the available experimental data (see also Lindsley, 1981

for a discussion of his results and those of Lindsley and Munoz, 1969). In this study, phase relationships along the Fs-Hd join have been calculated at 11.5, 15, 20 and 30 kbar in the temperature range ≈650-1050 ^{o}C. Results of the computation as well as experimental data of Lindsley and Munoz (1969) (20 kbar) and Lindsley (1981) (11.5 and 15 kbar) are plotted on isobaric diagrams in Fig. 5.2.

Examination of the diagrams in Fig. 5.2 shows that there is very good agreement between calculated and existing data. Consistent with Lindsley (1981), the model recognizes the existence of a two-clinopyroxene field at 11.5 and 15 kbar (Fig. 5.2a and 5.2b, respectively), the latter stable at temperatures below ≈885 ^{o}C. Furthermore (Fig. 5.2c), in agreement with Lindsley and Munoz's data, no such two-clinopyroxene field would appear to be stable at 20 kbar. Finally, the calculated Fs-Hd miscibility gap at 30 kbar (Fig. 5.2d) is topologically similar to the En-Di miscibility gap at the same pressure, as already inferred in both Lindsley and Munoz and Lindsley's studies.

Fig. 5.2 Calculated subsolidus pyroxenes phase equilibria along the ferrosilite-hedenbergite join for pressures: 11.5 **(a)**, 15 **(b)**, 20 **(c)**, and 30 **(d)** kbar. Plotted experimental data: 11.5 and 15 kbar, Lindsley (1981); 20 kbar, Lindsley and Munoz (1969). Symbols: black filled triangles, compositions from microprobe analysis; black empty triangles, compositions from X-ray analysis; red filled triangles, compositions of pigeonite in equilibrium with *opx* and/or *cpx*; green circles, compositions of one unmixed *cpx*. Arrows in **(c)** give the direction of compositional changes of coexisting pyroxenes.

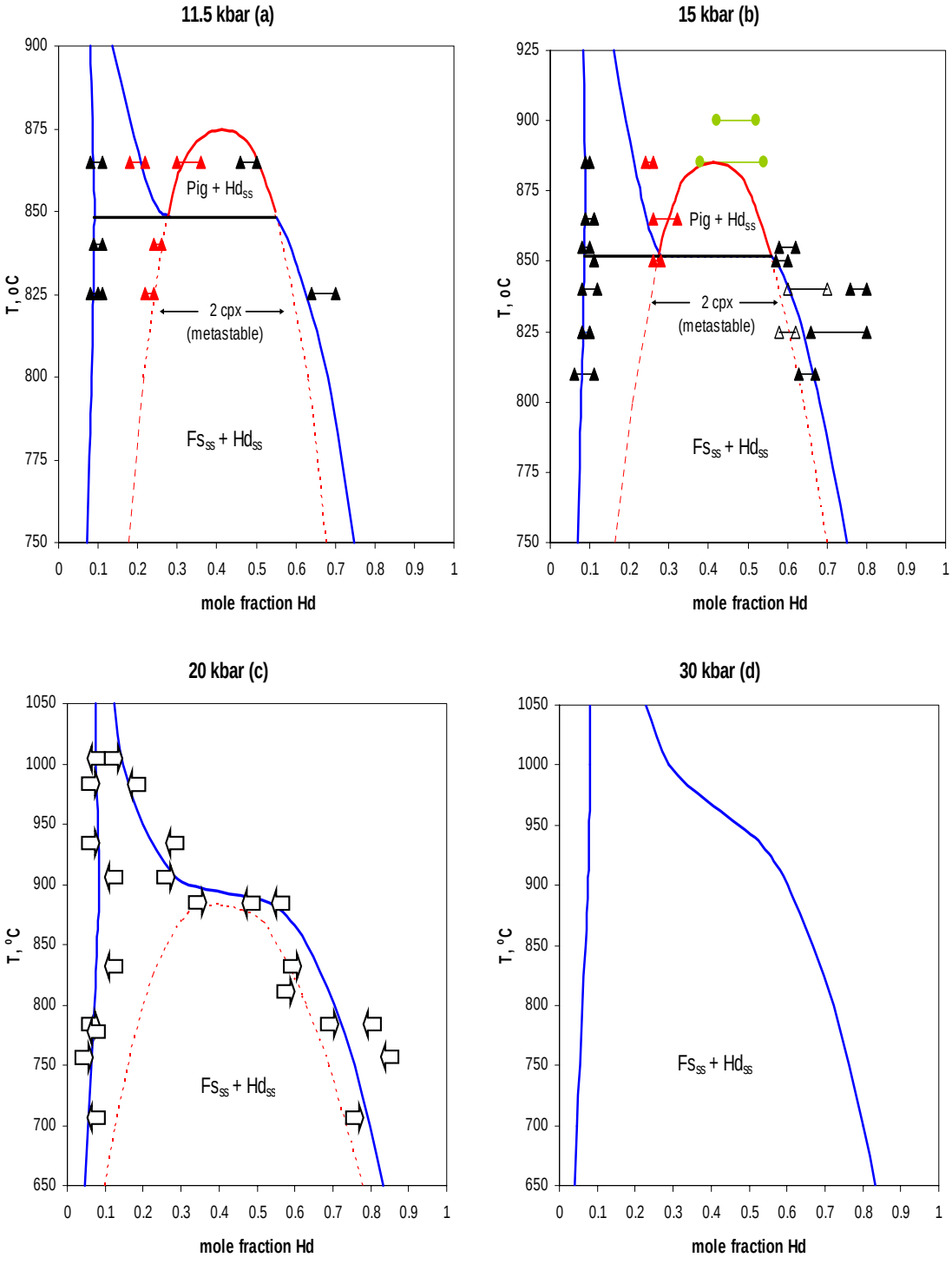
11.5 kbar (a)
15 kbar (b)
20 kbar (c)
30 kbar (d)
T, oC
T, °C
mole fraction Hd
Pig + Hdss
2 cpx
(metastable)
Fss + Hdss

5.5 CMFS system

Most of geothermometry and geobarometry of natural pyroxene-bearing assemblages is based on the analysis of compositions of coexisting quadrilateral pyroxenes and on the modeling of their end-member and solution parameters. Natural pyroxenes, in fact, despite exhibiting a wide compositional variability (see Deer et al., 1992, for a comprehensive review on the subject), fall predominantly within the system $(Ca,Mg,Fe)_2Si_2O_6$ such that their compositions can be described in terms of the four end-members $Mg_2Si_2O_6$, $Fe_2Si_2O_6$, $CaMgSi_2O_6$, $CaFeSi_2O_6$.

Due to the their importance, phase equilibria within quadrilateral pyroxenes have been the focus of many experimental studies (e.g. Mori, 1978; Podpora and Lindsley, 1979; Turnock and Lindsley, 1981; Lindsley and Andersen, 1983; Fonarev and Graphchikov, 1982; Lindsley, 1983; Davidson and Lindsley, 1989) as well as theoretical investigations (e.g. Davidson, 1985; Davidson and Lindsley, 1985 and 1989; Saxena et al., 1985; Shi et al., 1994; Sack and Ghiorso 1994b).

Of specific interest for geothermometric and barometric applications is also the estimation of Mg-Fe partitioning between coexisting pyroxenes and between pyroxenes and other phases in MFS and CMFS systems. Since Ramberg and Devore (1951) and Kretz (1961) proved that Mg-Fe distributions in pyroxenes from igneous and metamorphic rocks are different, many studies have been conducted to quantitatively determine and to thermodynamically model such partitioning, aiming to obtain information on pressure and temperature of pyroxene crystallization (e.g. Nafziger and Muan, 1967; Kitayama and Katsura, 1968; Matsui and Nishizawa, 1974; Bohlen and Boettcher, 1981; Adams and Bishop, 1986; Davidson and Lindsley, 1989; Sack and Ghiorso, 1989; Koch-Müller et al., 1992; von Seckendorff and O'Neill; 1993 Kawasaki and Ito, 1994; Kawasaki, 1999). In addition, the intracrystalline Mg-Fe partitioning between M2 and M1 sites in both ortho- and clinopyroxene solid solutions has also been the subject of numerous investigations. Order-disorder Mg-Fe phenomena depend on the mineral's crystallization temperature, therefore, they represent a useful tool to investigate the thermal history of pyroxene-bearing rocks. Many experimental studies have been conducted to determine the intracrystalline partition coefficient $\left(K_D = (Fe+Mg)^{M1} / (Fe+Mg)^{M2}\right)$ in pyroxene solutions and different

models have been proposed to thermodynamically describe such order-disorder phenomena (see Pasqual et al., 2000; and references therein). In the thermodynamic model derived in this study, as explained in chapter 2, a simplified assumption of random Mg-Fe partitioning between M2 and M1 sites (i.e. $K_D = 1$), for both opx_{ss} and cpx_{ss}, has been made. Moreover, to model Mg-Fe mixing properties in both orthopyroxene and clinopyroxene solid solutions, the symmetric regular Margules formulation has been adopted.

Results of phase equilibria experiments of Turnock and Lindsley (1981), Fonarev and Graphchikov (1982), Lindsley (1983) and Mori (1978) are plotted on isobaric, isothermal diagrams in Fig. 5.3. Plotted in the same figure are the corresponding phase equilibrium compositions as calculated applying the model. The bulk composition of the computed phase equilibria is the same as of the experimental data, so that a direct comparison between the two is meaningful.

Fig. 5.3. Ca-Mg-Fe pyroxene experimental data (red symbols) compared to results of computation (blue symbols), at different *T*-*P* conditions: **(a)** 900 ^{o}C, 1 kbar; **(b)** 750-800 ^{o}C, 2.94 kbar; **(c)** 810-815 ^{o}C, 15 kbar; **(d)** 910-925 ^{o}C, 15 kbar; **(e)** 990 ^{o}C, 15 kbar; **(f)** 1200 ^{o}C, 30 kbar. Plotted experimental data in Figs. 5.3 (a)-(f) are from: (a), Turnock and Lindsley (1981); (b), Fonarev and Graphchikov (1982); (c), (d), (e), Lindsley (1983); (f), Mori (1978). Symbols: filled squares, *opx-cpx* and *opx-pig* assemblages; filled triangles, *cpx-pig* assemblages; empty circles, *opx-cpx-pig* assemblages.

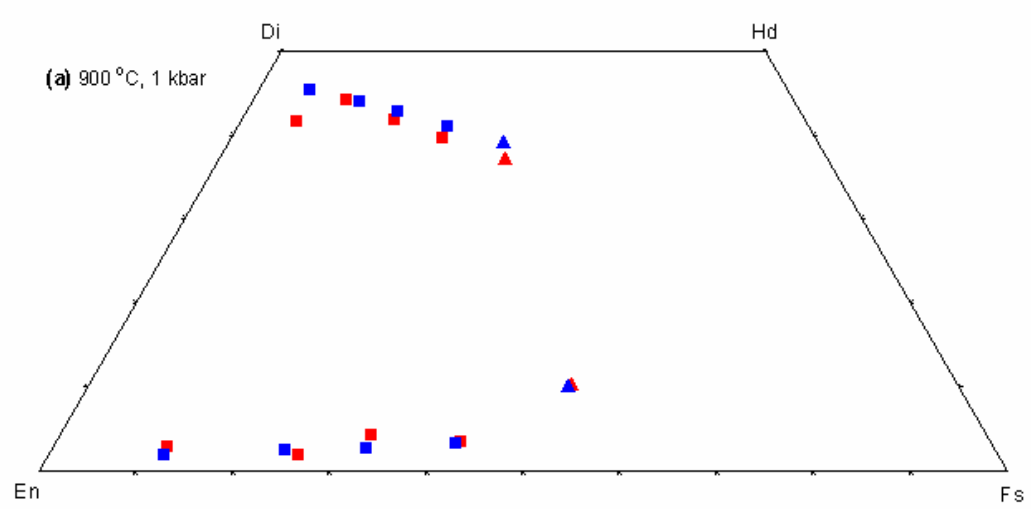
Di
Hd
(a) 900 °C, 1 kbar
En
Fs

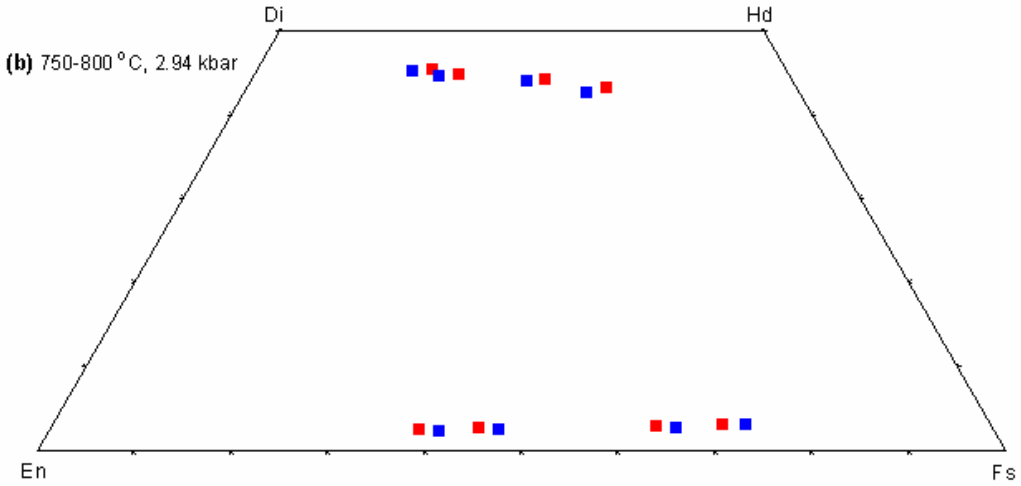
Di
Hd
(b) 750-800 °C, 2.94 kbar
En
Fs

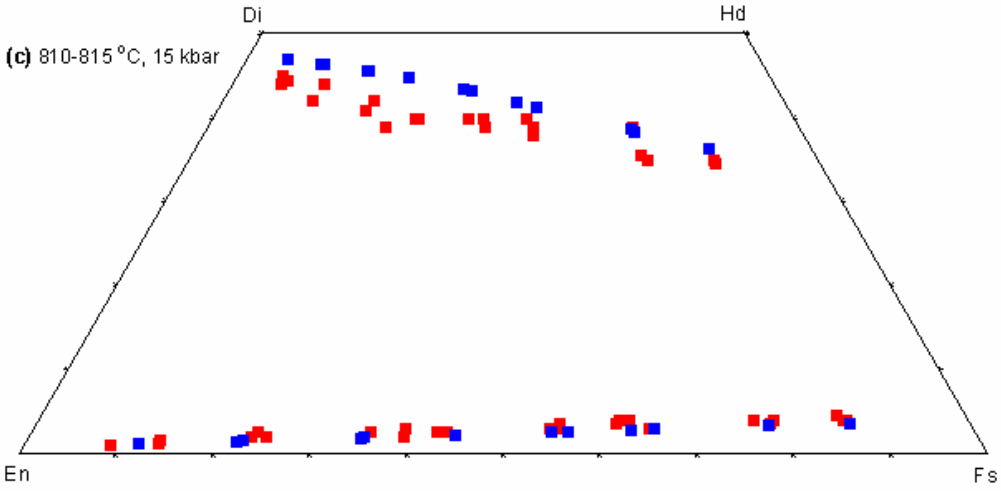
Di
Hd
(c) 810-815 °C, 15 kbar
En
Fs

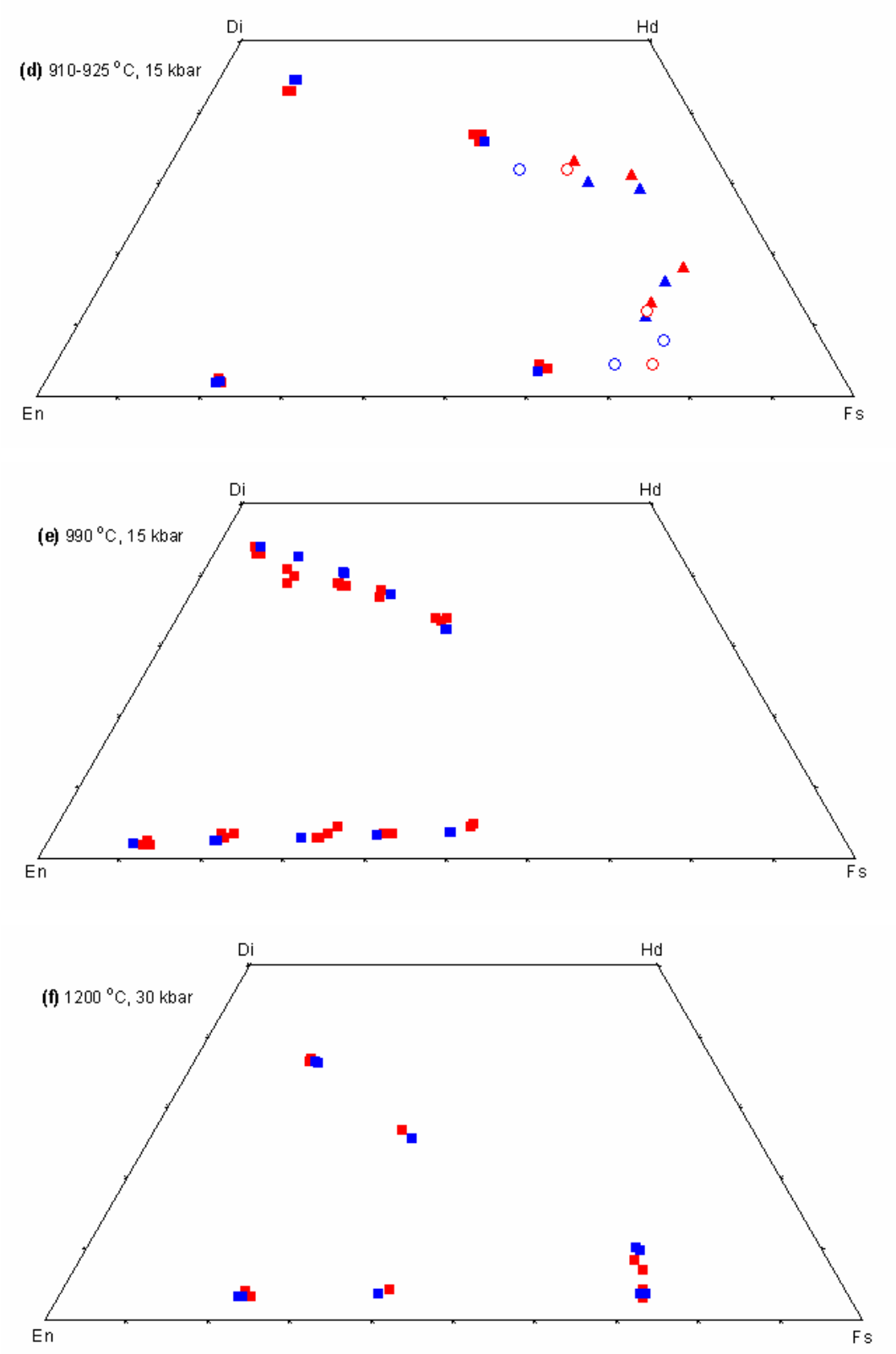
Di
Hd
(d) 910-925 °C, 15 kbar
En
Fs
Di
Hd
(e) 990 °C, 15 kbar
En
Fs
Di
Hd
(f) 1200 °C, 30 kbar
En
Fs

Examination of the diagrams in Fig. 5.3 shows that there is mostly good agreement between computed and experimental data at the various different *T*, *P* and bulk composition conditions. The model, in general, accurately reproduces the position of *opx-cpx, cpx-pig* and *opx-cpx-pig* assemblages within the quadrilateral. However, some differences between calculated and experimental data can be observed. At 810 ^{o}C and 15 kbar, for example, the model, especially for Mg-rich bulk compositions, appears to overestimate (in the *cpx* limb) the width of the *opx-cpx* miscibility gap when compared to Lindsley (1983)'s experiments. It is worth noticing that this discrepancy was not present at the same *T-P* conditions in the CMS system (see Fig. 5.1a), and it occurs only sporadically at other *T-P* conditions in the CMFS system. Moreover, it should be emphasized that also former models (e.g. Lindsley, 1983; Davidson and Lindsley, 1985) show analogous discrepancies respect to experimental data, either at 810 ^{o}C and 15 kbar or at other *T-P* conditions. This seems to suggest that such discrepancies do not reflect systematic inaccuracies in this or in previous models, and they could perhaps be an indication of some inconsistencies among different sets of experimental data.

Some differences also result when comparing calculated widths of *cpx-pig* and *opx-pig* 'solvi' and computed compositions of *opx-cpx-pig* assemblages to the experimentally determined ones. However, it is important to remember that stability fields of *opx-cpx-pig, opx-pig* and *cpx-pig* assemblages in the quadrilateral are quite small and very sensitive to changes in *T-P* conditions. This implies that any potential small inaccuracy in the reported *T-P* values of the experimental data would be enough to account for significant differences in the corresponding computed equilibrium compositions.

5.5.1 Testing the internal consistency between pyroxene and olivine thermodynamic models

Phase equilibria in the CMFS system have then been computed at *T-P* and bulk composition conditions to include also that portion of the quadrilateral where iron-rich orthopyroxenes become unstable relative to the assemblage olivine + quartz. Note that, at this stage, end-member and solution parameters needed for computation of CMFS pyroxenes and olivine have all been derived (this chapter and chapter 4, respectively). As a result, their value had to be considered as fixed. This clearly represents a significant test to

verify the mutual consistency of the pyroxene and olivine solution models, previously independently calibrated.

The accuracy of thermodynamic data for fayalite and ferrosilite end-members (as derived in this study) and for quartz (as found in Holland and Powell, 1990) has first been tested. Relations among fayalite + quartz (α or β) and ferrosilite have been very carefully investigated by Bohlen et al., (1980) over a range of *T-P* conditions. Results of their experiments are plotted in Fig. 5.4. Reactions $Fe_2SiO_4 + SiO_2 = Fe_2Si_2O_6$ and α-Qtz = β-Qtz have then been reproduced using the program, and results of the computations are also plotted (as lines) in Fig.5.4. Comparison between calculated and experimentally determined equilibria shows an excellent accord.

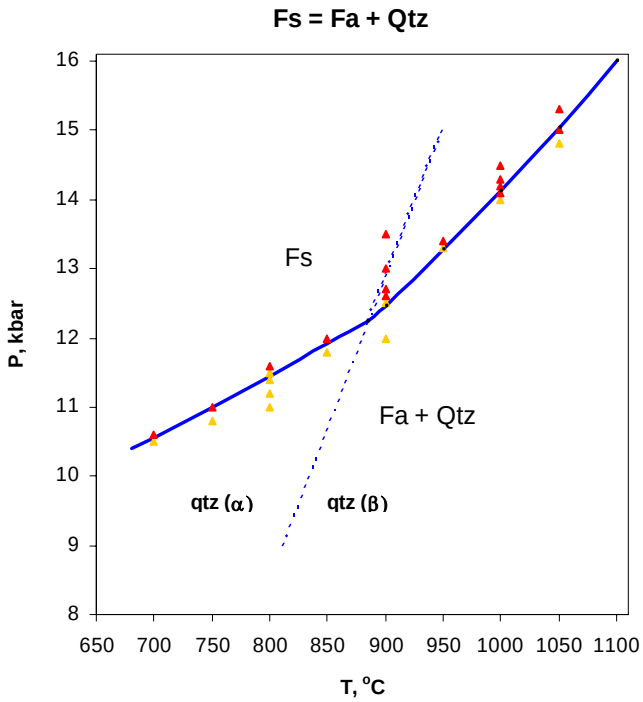

Fig. 5.4. Computed reaction ferrosilite = fayalite + quartz (continuous blue line) compared to experimental data (filled triangles) of Bohlen et al., (1980). Symbols: yellow triangles, Fa+Qtz in; red triangles, Fs in. Dotted blue line represents calculated α-qtz/β-qtz reaction.

The model has then been applied to depict phase equilibria relationships in the CMFS quadrilateral at three different *T-P* conditions (i.e. 800 °C – 1 kbar, 750 °C – 2 kbar, 830 °C – 7 kbar), and for a range of different bulk compositions, to allow a direct

comparison with experimental and model's results of Davidson and Lindsley (1989). Computed phase equilibria from this work are plotted on isothermal, isobaric diagrams in Fig. 5.5 and they display a very satisfactory agreement with the model of Davidson and Lindsley (1989) (see their Fig.4). In particular, diagrams at 830 ^{o}C and 7 kbar, despite their complexity, are remarkably similar. Plotted in Fig. 5.5 are also some experimental results from Davidson and Lindsley that again show an excellent agreement with results of this model.

Fig. 5.5. Calculated phase equilibria in CMFS system for a wide range (from Mg- to Fe-rich) of bulk compositions at three different *T-P* conditions: **(a)** 800 ^{o}C, 1 kbar; **(b)** 750 ^{o}C, 2 kbar; **(c)** 830 ^{o}C, 7 kbar. Symbols: filled blue triangles, *opx-cpx* assemblages; filled green triangles, *cpx-pig* assemblages; filled brown triangles, *opx-pig* assemblages; filled orange diamonds, *cpx-ol-qtz* assemblages; empty blue circles, *opx-cpx-pig* assemblages. Experimental results from Davidson and Lindsley (1989), plotted as red symbols, correspond to: in (a), composition of *opx-cpx* assemblages (filled triangles) and composition of *opx-cpx-pig* assemblage (empty circles); in (b), composition of *opx-cpx-pig* assemblage (empty circles); in (c) composition of *opx-pig-ol+qtz* assemblage (filled circles). NB In (c) some calculated *opx-pig* assemblages have not been plotted to allow a better appearance to experimental data.

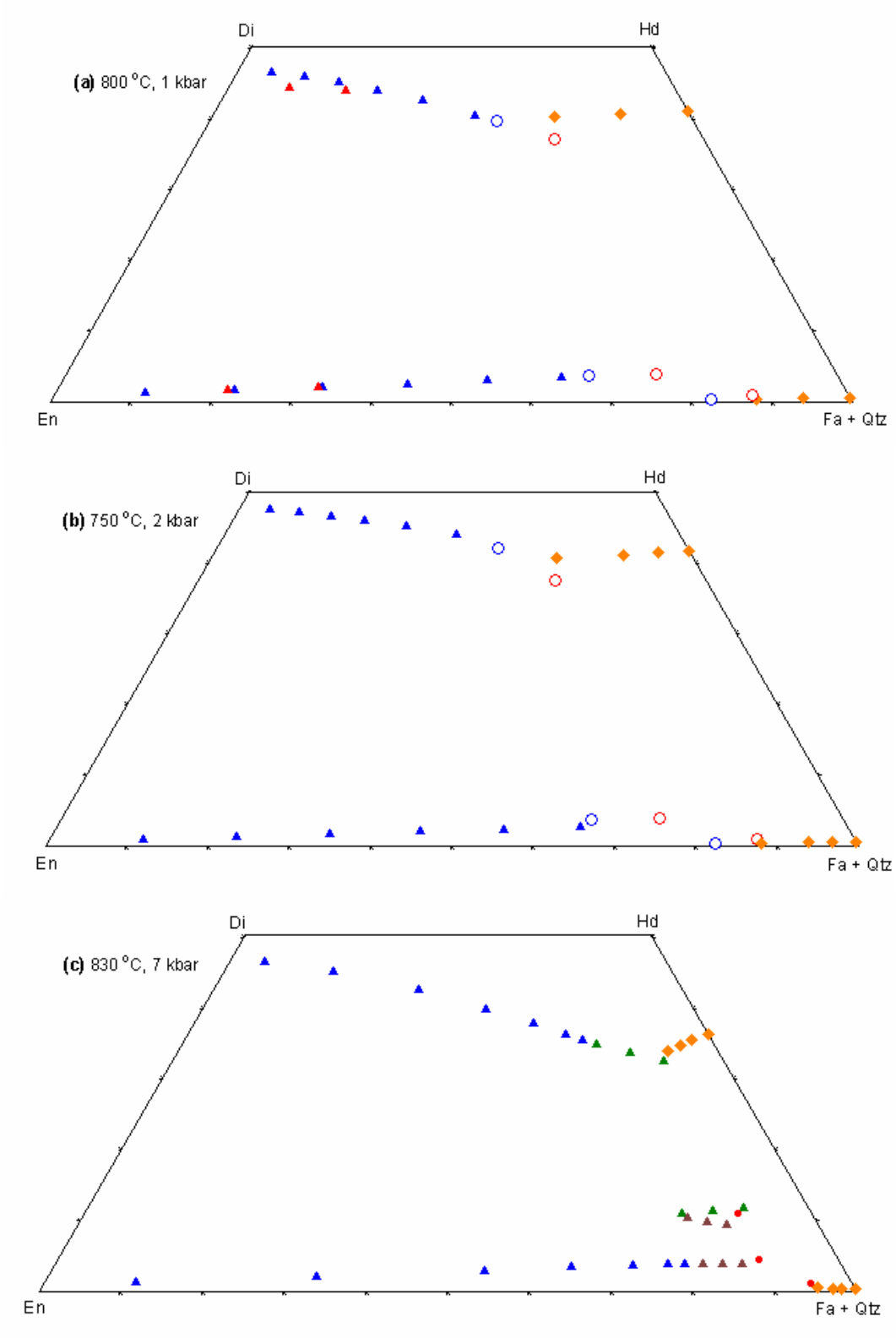
Di
Hd
(a) 800 °C, 1 kbar
En
Fa + Qtz
Di
Hd
(b) 750 °C, 2 kbar
En
Fa + Qtz
Di
Hd
(c) 830 °C, 7 kbar
En
Fa + Qtz

5.6 CMAS system

The relevance for thermobarometric applications of the coexistence in CMAS natural assemblages of ortho- and clinopyroxene has long been recognized. Experimental and thermodynamic investigations have shown that useful thermobarometers can be obtained by measuring the Al content of each pyroxene and analyzing the effect of Al on the Ca-Mg exchange between the two pyroxenes ('En-Di' miscibility gap, see also section 5.3).

A large number of experimental studies have been conducted in the CMAS system, providing many compositional data on coexisting pyroxenes at various *T-P* conditions (e.g. Akella, 1976; Presnall, 1976; Herzberg and Chapman 1976; Fujii, 1977; Mori, 1977; Herzberg, 1978; Perkins and Newton, 1980; Gasparik, 1984; Yamada and Takahashi, 1984; Sen, 1985; Nickel et al., 1985; Carlson, 1989; Klemme, 1998; Xi, 2003), and several different models have been proposed to describe thermodynamically the two-pyroxene phase relationship (e.g. Wood and Banno, 1973; Obata, 1976; Herzberg, 1978; Gasparik, 1984; Wood and Holloway, 1984; Gasparik, 2000).

However, in spite of the great effort devoted to the experimental investigation, many inconsistencies can be found among data in the literature. Such discrepancies most likely reflect experimental difficulties inherent to the CMAS system (Gasparik, 1984). Perkins and Newton (1980) pointed out that is very difficult to perform strict reversals in systems like the CMAS with more than one degree of compositional freedom. Nickel et al. (1985) conducted a scrupulous review of previous works to conclude that only few studies displayed comparable approaches of reversals: Fujii (1977), Perkins and Newton (1980), Yamada and Takahashi, (1984) and their own one. Results from these works, from Sen (1985), Carlson (1989), and from the more recent studies of Klemme (1998) and Xi (2003) have here been used to test the thermodynamic model.

In the cited experiments the Al content in *opx* and *cpx* solid solutions is buffered by either anorthite, or spinel, or garnet, depending on *T-P* and bulk composition conditions. Olivine may also be present. To account for the presence of any of these phases in the computational process, the approach described in chapters 2 and 3 of this thesis has been followed, where values of end-member and solution parameters (apart from olivine, see

chapter 4) have been taken from the literature[21] and have not been further modified. The same approach has also been followed in the fitting of the CMFAS system (section 5.7).

In Fig. 5.6, Ca contents in ortho- and clinopyroxene solid solutions from the experiments of Fujii, Perkins and Newton, Yamada and Takahashi, Nickel et al., Sen and Carlson are plotted on isobaric phase diagrams. In Fig 5.7 and Fig. 5.8, Ca vs. Al contents of opx_{ss} and cpx_{ss} from experimental studies of Klemme and of Xi, respectively, are plotted. The corresponding values of Ca and of Ca vs. Al, as obtained in the computation, are also reported. Considering that the width of brackets in some of the studies cited above has not been clearly reported (see also Nickel at al., 1985), errors bars have not been plotted. On the other hand, plotted values represent the mid-points of experimental reversal brackets.

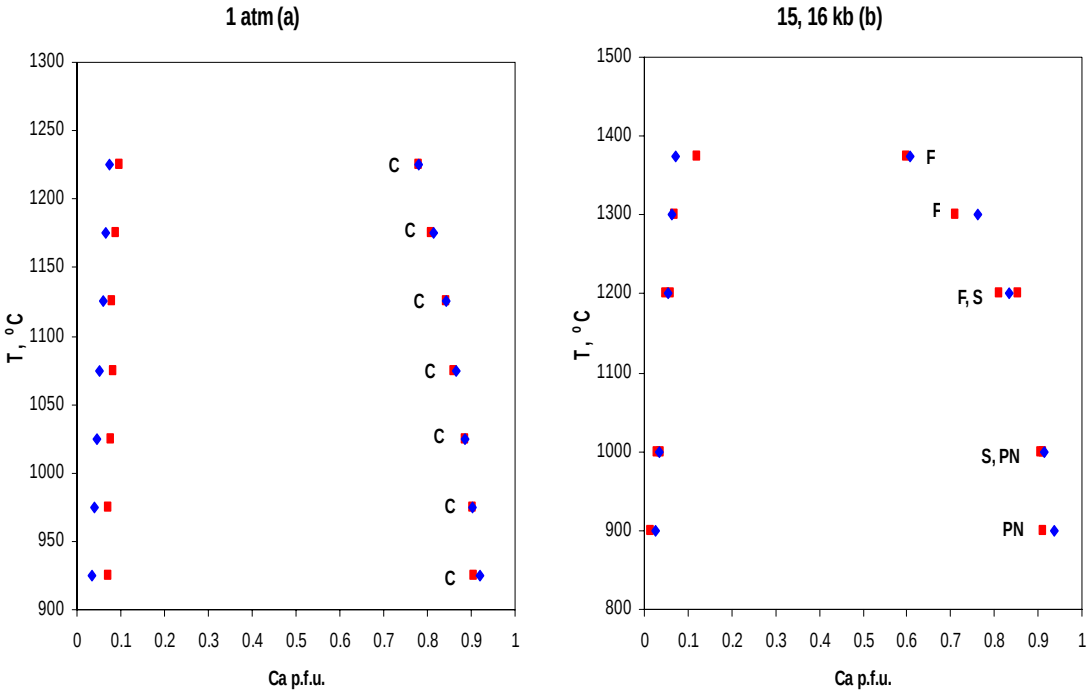

[21] More precisely, values of end-member parameters used in the computation are from Holland and Powell (1990) and (1998), while garnet solution parameters are from Ganguly et al. (1996) and spinel solution parameters from O'Neill and Wall (1987).

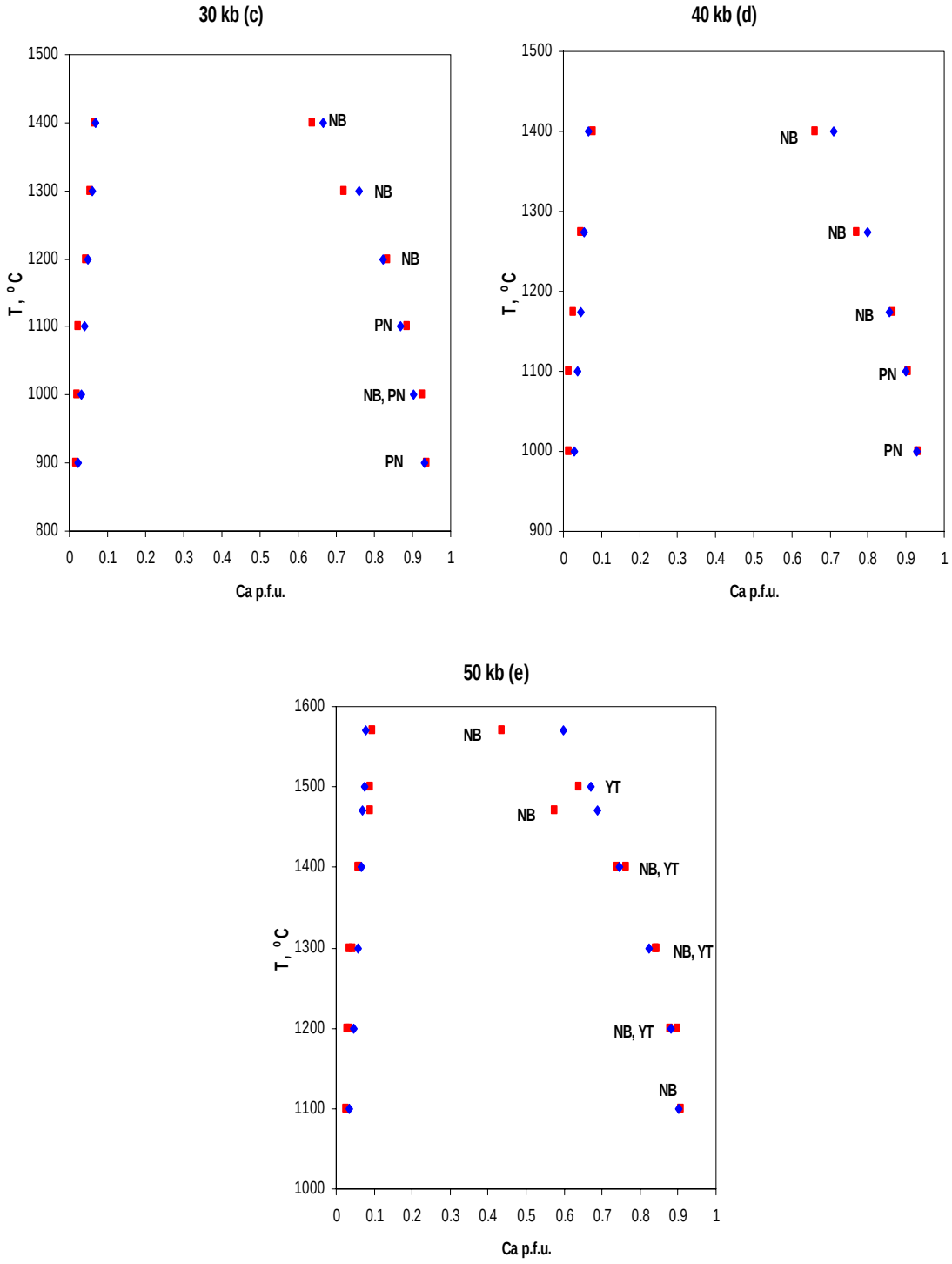

Fig. 5.6. Computed (blue filled diamonds) compared to experimental determined (red filled boxes) Ca contents (expressed in cations per formula unit, i.e. p.f.u.) in *opx* and *cpx*, for pressures: 1 atm **(a)**, 15-16 kbar **(b)**, 30 kbar **(c)**, 40 kbar **(d)**, and 50 kbar **(e)**. Experimental data are from: Perkins and Newton (1980) [PN], Fujii (1976) [F], Nickel et al. (1985) [NB], Yamada and Takahashi (1984) [YT], Sen (1985) [S], Carlson (1989) [C].

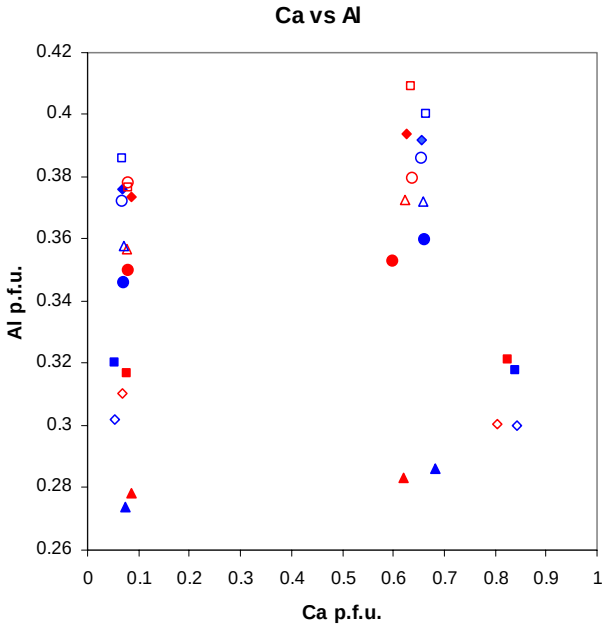

Fig. 5.7. Computed (blue symbols) Ca vs. Al contents in *opx* and *cpx*, compared to experimental data (red symbols) of Klemme (1998). Different symbols indicate different *T-P* conditions: filled diamonds, 23 kbar and 1400 °C; filled triangles, 27 kbar and 1400 °C; filled squares, 18 kbar and 1200 °C; filled circles, 25 kbar and 1400 °C; empty diamonds, 20 kbar and 1200 °C; empty triangles, 23 kbar and 1400 °C; empty squares, 24 kbar and 1400 °C; empty circles, 23 kbar and 1400 °C.

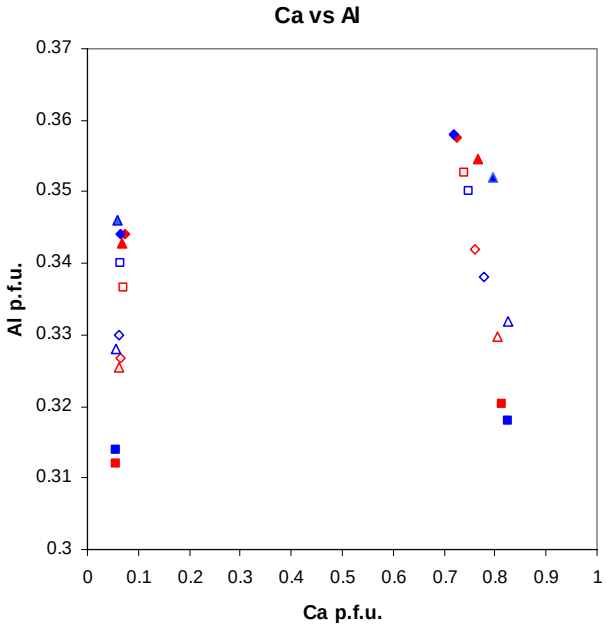

Fig. 5.8. Computed (blue symbols) Ca vs. Al contents in *opx* and *cpx*, compared to experimental data (red symbols) of Xi (2003) at P = 11 kbar. Different symbols indicate different T conditions: filled diamonds, 1310 °C; filled triangles, 1240 °C; filled squares, 1200 °C; empty diamonds, 1260 °C; empty triangles, 1200 °C; empty squares, 1290 °C.

The model appears to fit the experimental data very well at almost all temperature-pressure conditions. At high *T-P* conditions (e.g. Fig. 5.6e), however, the Ca content for the computed *cpx* is usually higher than the corresponding experimental determined value, as already noticed in the CMS system (section 5.3), while the same discrepancy is not found (at least in a systematic way) at lower *T-P* conditions. A possible explanation for this inconsistency between model and experimental data could be a small degree of Ca-Mg disordering between the M1 and M2 sites in the *cpx* phase or, more likely, simply a stronger *T-P* dependence for the *cpx* solvus. In either case a better fit for the high *T-P* data can be obtained by imposing a positive non-ideality in the entropy of mixing and/or a more negative pressure dependence for the solution parameters. On the other hand, this would compromise the excellent model-experiments agreement at lower *T-P* and, in particular, the ability of the model to correctly reproduce the *pig* field on the $Mg_2Si_2O_6$-$CaMgSi_2O_6$ join at 15 kbar. Furthermore, it is worth noting that models that include stronger *T-P* dependence for the solution parameters (e.g. Nickel and Brey, 1984; Carlson and Lindsley, 1988; Gasparik, 1990) do not manage to successfully eliminate all discrepancies.

A clear disagreement can also be noticed between the results of this model and Carlson (1989)'s data at 1 atm (fig. 5.6a). In this case, the model almost exactly reproduces the *cpx* limb of the experimental determined solvus, while the *opx* limb appears to be systematically overestimated in the computation. No satisfactory explanation can be given to justify such discrepancy, especially considering that a similar problem has never been encountered when fitting any of the other systems (CMS, CFS).

In Fig. 5.9 the Al content in *opx* and *cpx* from experimental data is plotted and compared to the corresponding computed values. The agreement between model and experiments is excellent at all *T-P* conditions, with the model's estimation of the amounts of Al in both solid solutions being very close to the experimental determined ones. In addition (Fig. 5.10), the model is able to reproduce some very peculiar features of the experimental data like the fact that $Al^{opx} > Al^{cpx}$ at lower *T*, while at higher *T* the trend is inverted and $Al^{cpx} > Al^{opx}$ (NB Fig. 5.10 should be compared to Fig. 3 and Table 2 of Nickel et. al, 1985).

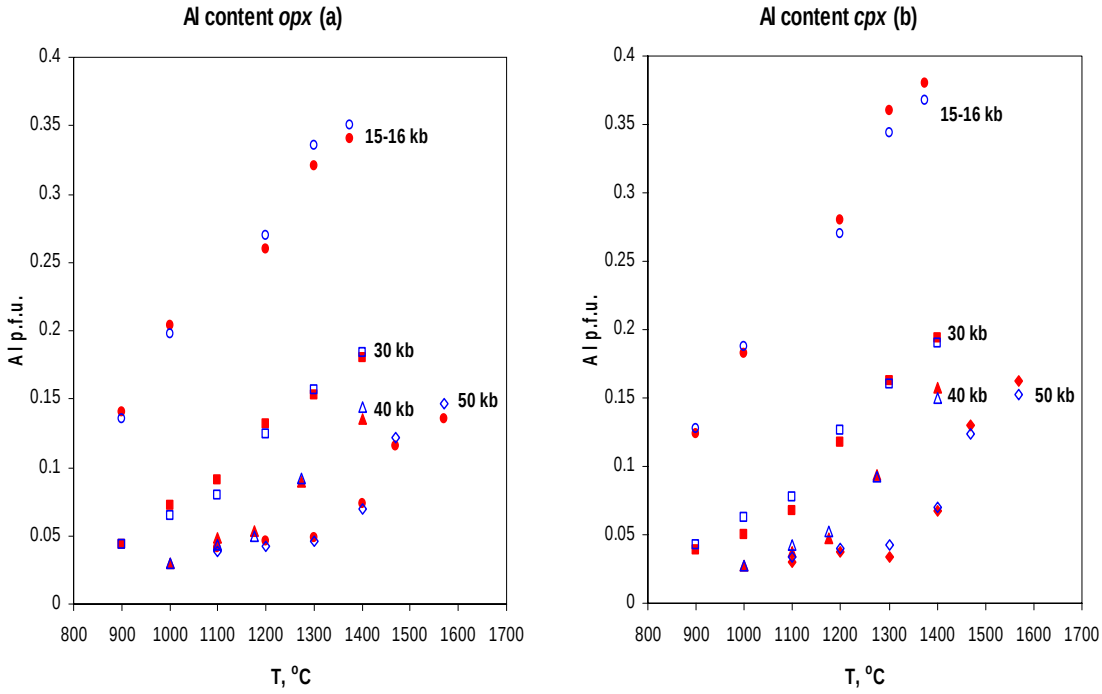

Fig. 5.9. Computed (empty blue symbols) compared to experimental determined (filled red symbols) Al contents in *opx* **(a)** and *cpx* **(b)**. Plotted experimental data are from: 15-16 kbar, [PN] and [F]; 30, 40 and 50 kbar, [NB] and [PN].

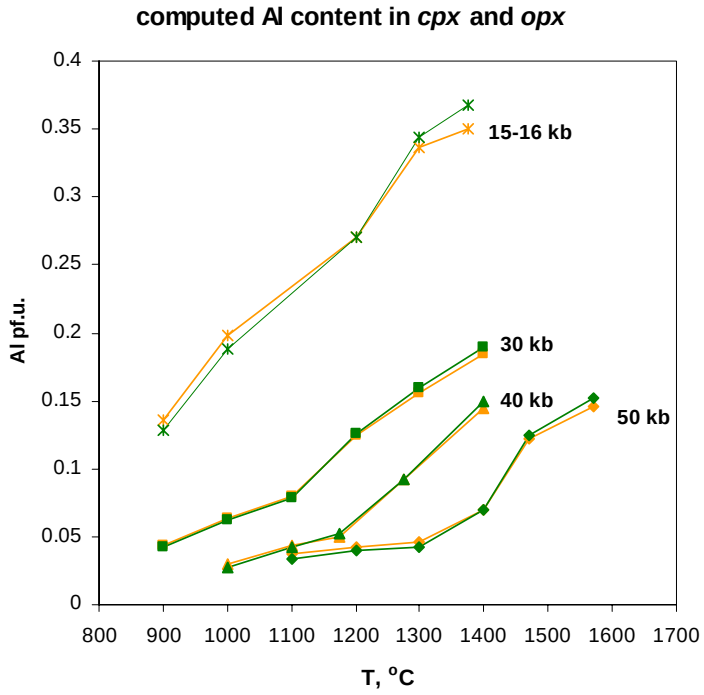

Fig. 5.10. Computed Al contents in *opx* (orange) and *cpx* (green) at different *T*-*P* conditions.

Finally, in Fig. 5.11 'En-Di' miscibility gaps have been calculated using the model and compared to the analogous computed gaps obtained for the CMS system. Given the slight disagreement between experimental and computed data observed at high *T-P* conditions, calculated miscibility gaps have been compared only in the *T-P* range where experimental data are more accurately reproduced by the model. In accord with former studies (e.g. Perkins and Newton, 1980; Sen, 1985), the model recognizes that the presence of Al in the system causes the *opx-cpx* miscibility gap to widen, and that the effect is more pronounced on the *cpx* limb than on the *opx* limb. Moreover, based at least on the results of the computation, the 'Al effect' on the En-Di miscibility gap would appear to be more noticeable at P = 15-16 kbar (Fig. 5.11a) than at higher P conditions (Figs. 5.11b,c,d). This is most likely because the amount of Al in the pyroxenes is much higher at 15 kb than 30 kb.

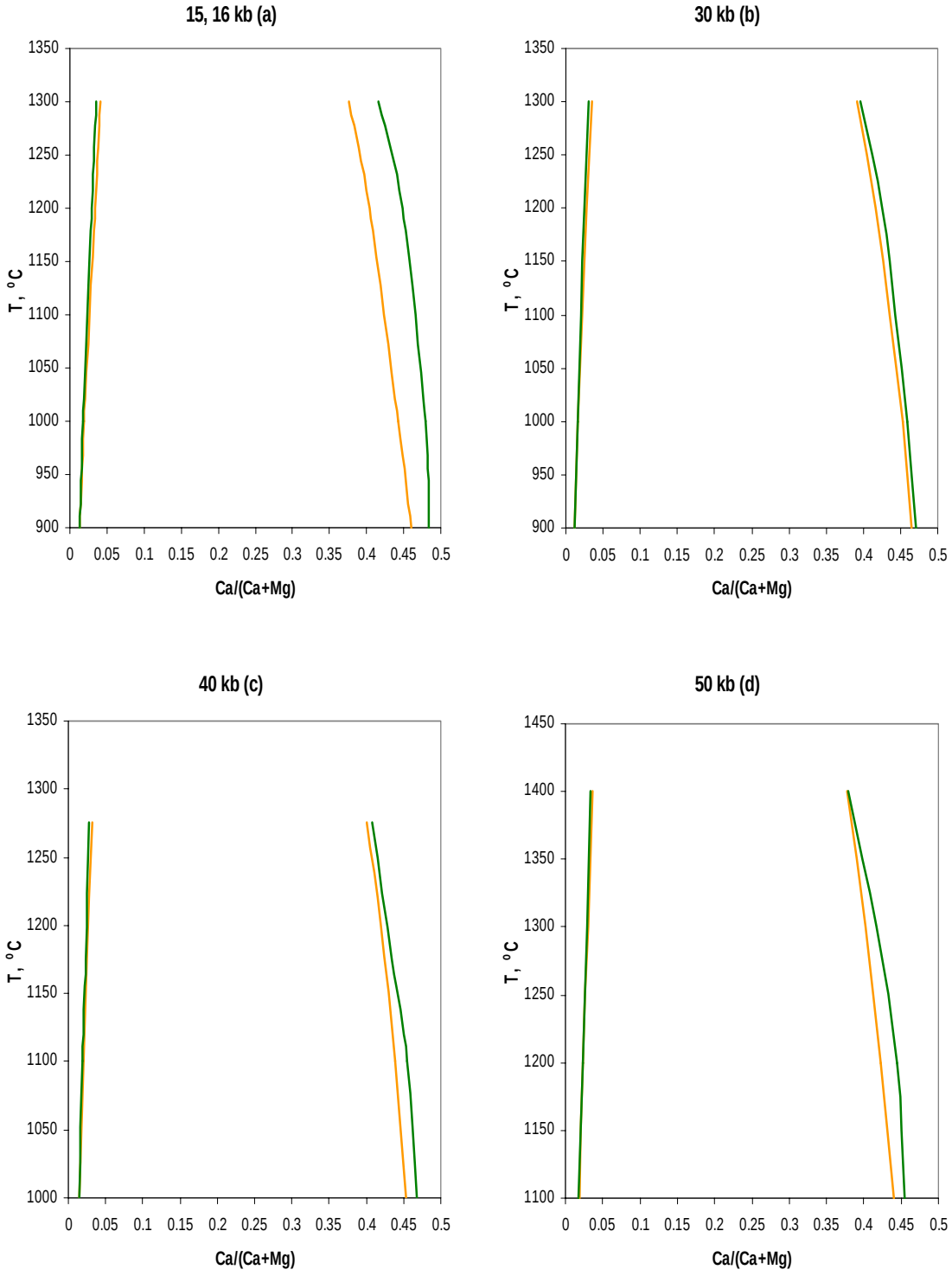

Fig. 5.11. Calculated two-pyroxene miscibility gaps in CMAS (green) and CMS (orange) systems for pressures: 15-16 **(a)**, 30 **(b)**, 40 **(c)** and 50 **(d)** kbar.

5.7 CMFAS system

Assuming that primary mid-ocean ridge basalts are largely generated in the spinel lherzolite stability field by near-fractional fusion and that Na and other incompatible elements will early on become depleted in the source, the melting behaviour of mantle lherzolite should resemble the melting behaviour of simplified lherzolite in the CMFAS system (Gudfinnsson and Presnall, 2000). Furthermore, the CMFAS system is also particularly well suited to explore the Fe-Mg exchange during mantle melting, which represents the most important solid solution involved in partial melting of spinel lherzolite.

However, despite its relevance for investigating upper mantle phase relationships and melting processes, the amount of experimental data available on CMFAS system, and, in particular, the amount of compositional data on coexisting pyroxenes, is considerably less than for any of the other systems investigated in this chapter. Compositions of coexisting CMFAS *opx* and *cpx* can be found in Shi and Libourel (1991), who determined lherzolite phase assemblages at 0.1 MPa pressure, and in Gudfinnsson and Presnall (2000), who studied the melting behaviour of spinel/plagioclase CMFAS lherzolite in the pressure range 0.7-2.8 GPa. Experimental data of Gudfinnsson and Presnall have been used to test the thermodynamic model derived in this study.

In Fig 5.12 and Fig. 5.13, Al and Fe contents from experimental data are plotted and compared to the corresponding computed values for both ortho- and clinopyroxene solid solutions. Model-experiments agreement is excellent at all *T-P* conditions, and the model's estimation of both Al and Fe quantities in the two solid solutions is almost always well within the plotted experimental uncertainties. The only marked exception is the value of Fe content at 17 kbar and ≈1400 ^{o}C, where computed and experimental data clearly differ. In addition, the model very accurately reproduces the variations of Fe contents in the *px* solutions that appear to be directly related to differences in starting materials compositions of Gudfinnsson and Presnall experiments (see their Table I).

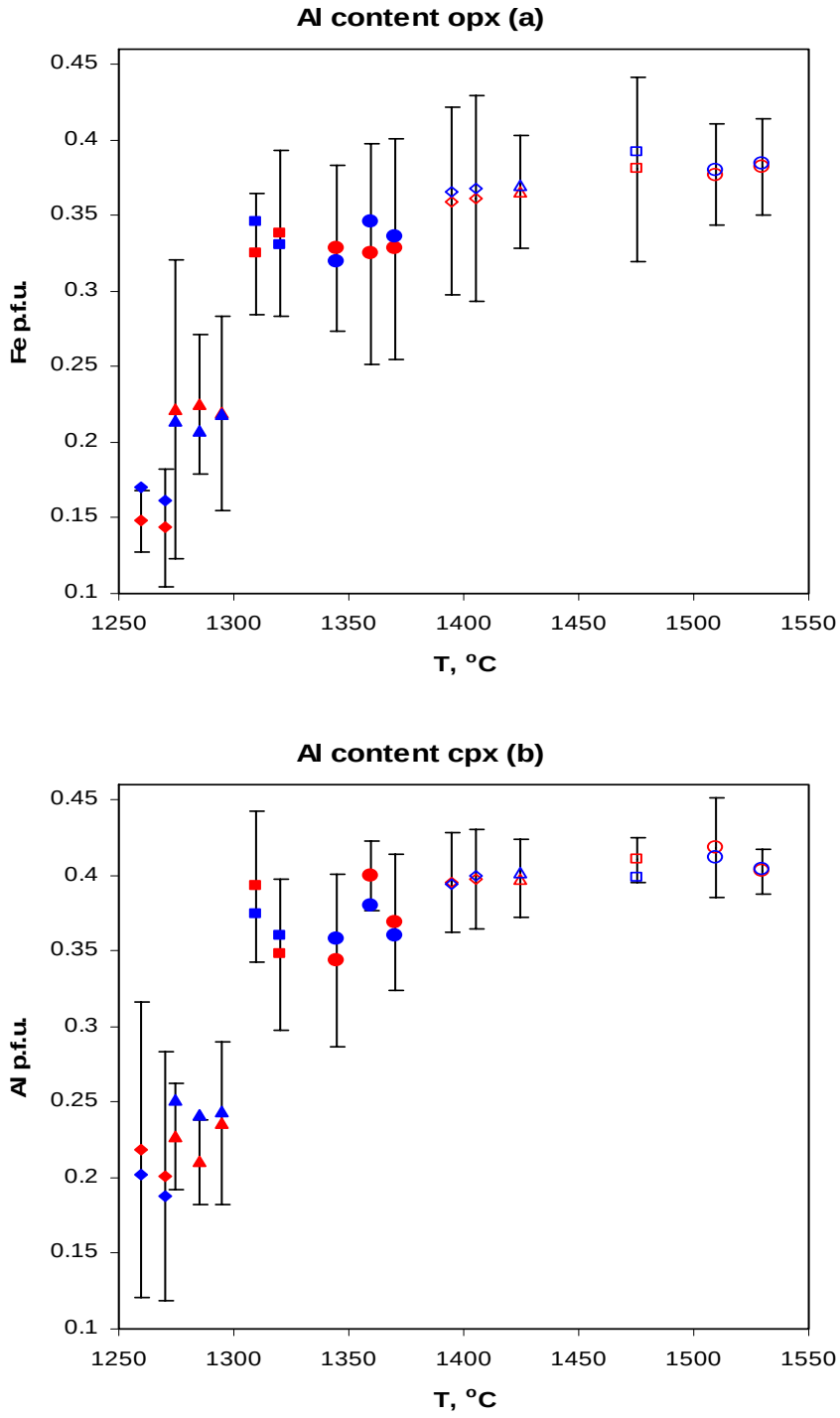

Fig. 5.12. Computed (blue symbols) Al contents (expressed in cations per formula unit, i.e. p.f.u.) in *opx* **(a)** and *cpx* **(b)**, compared to experimental data (red symbols) of Gudfinnsson and Presnall (2000). Different symbols indicate different *T-P* conditions: filled diamonds, 7 kbar and 1260, 1270 ^{o}C; filled triangles, 9 kbar and 1275, 1285, 1295 ^{o}C; filled squares, 11 kbar and 1310, 1320 ^{o}C; filled circles, 14 kbar and 1345, 1360, 1370 ^{o}C; empty diamonds, 17 kbar and 1395, 1405 ^{o}C; empty triangles, 20 kbar and 1425 ^{o}C; empty squares, 23 kbar and 1475 ^{o}C; empty circles, 27 kbar and 1510, 1530 ^{o}C. Error bars of experimental data are also plotted.

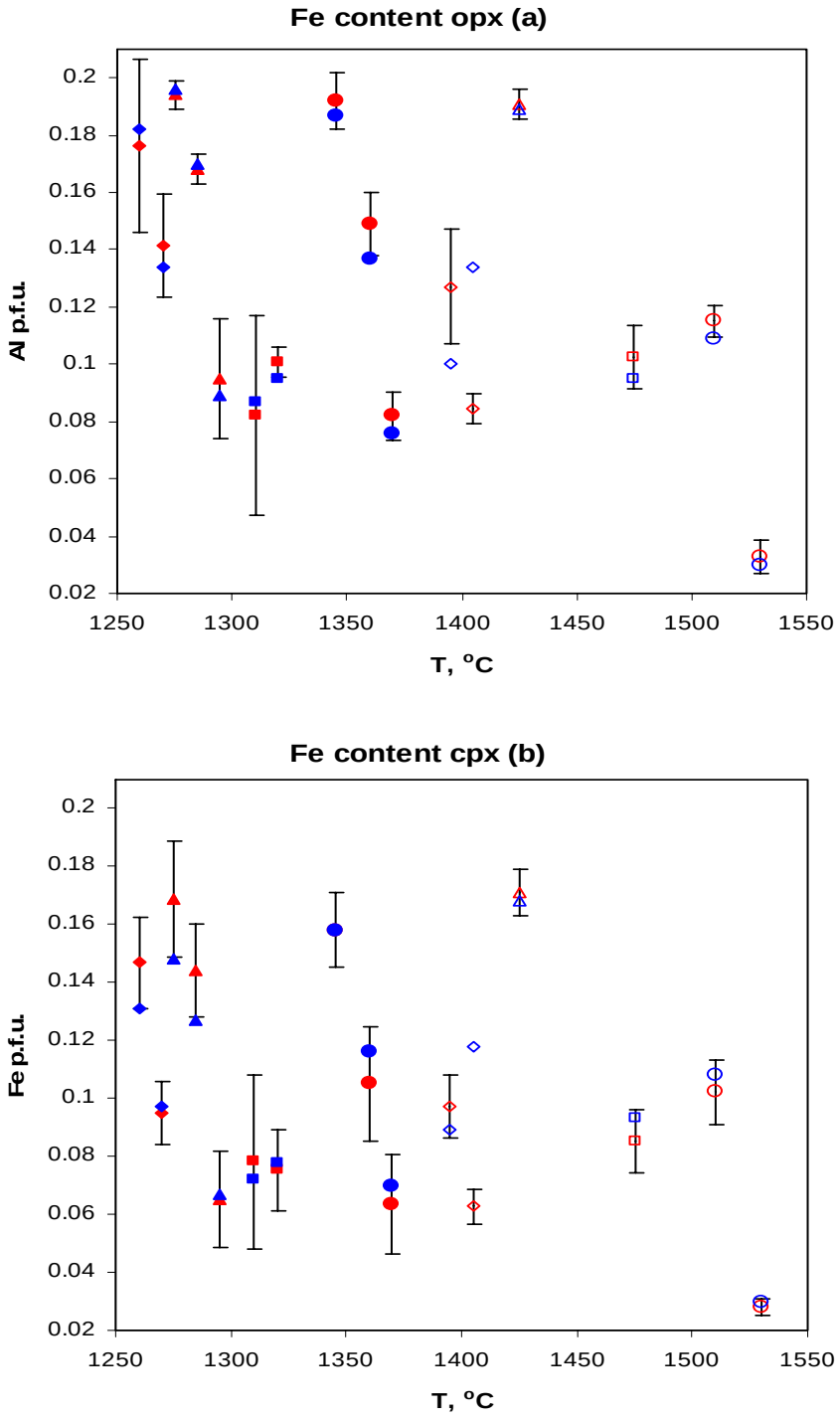

Fig. 5.13. Computed (blue symbols) Fe contents (expressed in cations per formula unit, i.e. p.f.u.) in *opx* **(a)** and *cpx* **(b)**, compared to experimental data (red symbols) of Gudfinnsson and Presnall (2000). Different symbols indicate different *T-P* conditions: filled diamonds, 7 kbar and 1260, 1270 °C; filled triangles, 9 kbar and 1275, 1285, 1295 °C; filled squares, 11 kbar and 1310, 1320 °C; filled circles, 14 kbar and 1345, 1360, 1370 °C; empty diamonds, 17 kbar and 1395, 1405 °C; empty triangles, 20 kbar and 1425 °C; empty squares, 23 kbar and 1475 °C; empty circles, 27 kbar and 1510, 1530 °C. Error bars of experimental data are also plotted.

5.8 Conclusions

In this chapter an internally consistent model for CMFAS pyroxenes has been derived that includes the calibration of end-member and solution parameters for both ortho- and clinopyroxenes. The internal consistency of the derived thermodynamic parameters is guaranteed by the procedure followed in the model's calibration. This represents the first comprehensive model for CMFAS pyroxenes that can simultaneously reproduce in a successfully way phase relationships in the general system as well as in any of its constituent subsystems.

Results presented in this chapter give the opportunity for some considerations on the approach followed in this study to model the ortho- and clinopyroxene solid solutions.

In the past few decades increasingly sophisticated thermodynamic models have been derived to describe pyroxenes phase relationships, especially along binary joins and within the 'quadrilateral'. In some of these models (e.g. Sack and Ghiorso, 1994a and 1994b) order-disorder phenomena are scrupulously taken into account and parameterized. Analogously, numerous experimental studies and theoretical investigations have been carried out to precisely derive solution parameters, aiming to estimate not only the value of excess enthalpy (W_H) but also of excess entropy (W_S) and excess molar volumes (W_V).

On the other hand, the contribution of order-disorder phenomena and excess entropy/molar volumes to the total Gibbs free energy per mole of solution is probably of the order of few dozens Joules, hundreds at the most. At the same time, the total amount of free energy for one mole of solution is of the order of millions of Joules and the end-member part of G (G^{e-m}) represents by far the most important term. Accordingly, in this study priority has been given to research the correct expression of G^{e-m} and to derive internally consistent values for end-member parameters and for the excess enthalpy part of the solution parameters (i.e. no *T-P* dependence has initially been given to the solution parameters). Furthermore, order–disorder phenomena have not been included in the model.

Validity and legitimacy of the approach undertaken in this work are demonstrated by the ability shown by the model in reproducing pyroxene phase relationships in the very wide range of *T-P* and compositions investigated. Here lies the most important conclusion to be drawn. Results presented in this chapter show that once the expression for the end-

member part of G has been properly derived and end-member parameters carefully calibrated, no 'extreme' Margules and/or ordering parameters are needed to accurately reproduce experimental data.

Table 5.1. Pyroxene solution parameters adopted in the computation.

opx_{ss}	W_H (kJ)	W_S (kJ/K)	W_V (kJ/bar)
$W_{Ca-Mg} = W_{Mg-Ca}$	33.5188	0	0
$W_{Ca-Fe} = W_{Fe-Mg}$	19.8529	0	0
$^{(a)}W_{Mg-Fe}$	7.17	0	0
$W^{M1}_{Mg-Al} = W^{M1}_{Al-Mg}$	8.378	0	0
$W^{M1}_{Fe-Al} = W^{M1}_{Fe-Al}$	2.368	0	0
cpx_{ss}	W_H (kJ)	W_S (kJ/K)	W_V (kJ/bar)
W_{Ca-Mg}	30.7954	0	-0.01670E-3
W_{Mg-Ca}	26.8978	0	-0.05843E-3
W_{Ca-Fe}	20.6963	0	0.02710E-3
W_{Fe-Ca}	17.4953	0	-0.08640E-3
$^{(a)}W_{Mg-Fe}$	6.65	0	0
$W^{M1}_{Mg-Al} = W^{M1}_{Al-Mg}$	3.897	0	0
$W^{M1}_{Fe-Al} = W^{M1}_{Fe-Al}$	3.125	0	0

Notes: [a] It is implied that $W^{M2}_{Mg-Fe} = W^{M1}_{Mg-Fe} = W^{M2}_{Fe-Mg} = W^{M1}_{Fe-Mg}$, unless otherwise specified.

Table 5.2. Thermodynamic properties of pyroxene end-members adopted in the computation. $\Delta_f H$ is the molar enthalpy of formation; S^o is the molar entropy of formation; *A, B, C* and *D* are molar heat capacity polynomial coefficients, where the heat capacity is: $C_p = A + BT + CT^{-2} + DT^{-1/2}$; V is the molar volume, αV and βV are the coefficient of thermal expansion and compressibility, respectively, multiplied by molar volume. Units: kJ, K and kbar.

end-member	$\Delta_f H$	S^o	A	B	C	D	V	αV	βV
orhto-En	-3092.9507	0.132413	0.3562	-2.99E-06	-596.9	-3.1853	6.27E-03	1.80E-07	4.60E-09
clino-En	-3088.1666	0.135151	0.3562	-2.99E-06	-596.9	-3.1853	6.33E-03	1.82E-07	4.65E-09
orhto-Fs	-2387.6016	0.192	0.3574	-2.76E-06	-711.1	-2.9926	6.59E-03	2.40E-07	5.80E-09
clino-Fs	-2385.0506	0.194243	0.3574	-2.76E-06	-711.1	-2.9926	6.63E-03	2.41E-07	5.83E-09
orhto-Di	-3200.951	0.144002	0.3145	4.10E-08	-2745.9	-2.0201	6.70E-03	2.23E-07	5.56E-09
clino-Di	-3204.299	0.142717	0.3145	4.10E-08	-2745.9	-2.0201	6.62E-03	2.20E-07	5.50E-09
orhto-Hd	2841.069	0.174753	0.3104	1.26E-05	-1846	-2.04	6.89E-03	2.68E-07	5.68E-09
clino-Hd	-2843.262	0.175	0.3104	1.26E-05	-1846	-2.04	6.79E-03	2.64E-07	5.60E-09
orhto-MgTs	-3297.04	0.13433	0.3476	-6.97E-06	-1781.6	-2.7575	6.41E-03	2.20E-07	5.46E-09
clino-MgTs	-3305.64	0.138	0.3476	-6.97E-06	-1781.6	-2.7575	6.36E-03	1.66E-07	5.30E-09
orhto-CaTs	-3195.261	0.127	0.3714	4.08E-06	-398.4	-3.5471	5.89E-03	1.70E-07	4.30E-09
clino-CaTs	-3187.87	0.132905	0.3714	4.08E-06	-398.4	-3.5471	6.06E-03	1.31E-07	4.47E-09
orhto-Fe^{2+} Ts	-2850	0.1327	0.3311	2.07E-06	-2140	-2.53	6.19E-03	1.79E-07	4.52E-09
clino-Fe^{2+} Ts	-2842	0.1309	0.3311	2.07E-06	-2140	-2.53	6.29E-03	1.82E-07	4.59E-09

5.9 References

Adams, G.E., and Bishop, F.C. (1986) The olivine-clinopyroxene geobarometer: experimental results in the CaO-FeO-MgO-SiO_2 system. *Contributions to Mineralogy and Petrology* **94**, 230-237.

Akella, J. (1976) Garnet pyroxene equilibria in the system $CaSiO_3$-$MgSiO_3$-Al_2O_3 and in a natural mineral mixture. *American Mineralogist* **61**, 589-598.

Atlas, L. (1952) The polymorphism of $MgSiO_3$ and solid-state equilibria in the system $MgSiO_3$-$CaMgSi_2O_6$. *Journal of Geology* **60**, 125-147.

Berman, R.G. (1988) Internally consistent thermodynamic data for minerals in the system Na_2O-K_2O-CaO-MgO-FeO-Fe_2O_3-Al_2O_3-SiO_2-TiO_2H_2O-CO_2. *Journal of Petrology*, **29**, 445-522.

Bohlen, S.R., and Boettcher, A.L. (1981) Experimental investigations and geological applications of orthopyroxene geobarometry. *American Mineralogist* **66**, 951-964.

Bohlen, S.R., Essene, E.J., and Boettcher, A.L. (1980) Reinvestigation and application of olivine-quartz-orthopyroxene barometry. *Earth and Planetary Science Letters* **47**, 1-10.

Bowen, N.L., Schairer, J.F., and Posnjak, E. (1933) The system Ca_2SiO_4-Fe_2SiO_4. *American Journal of Science* **26**, 273-297.

Brey, G., and Huth, J. (1984) The enstatite-*diopside* solvus to 60 kbar. In: Proceedings of the Third International Kimberlite Conference, vol. 2, pp 257-264

Bulatov, V.K., Ryabchikov, I.D., and Brey, G. (2002) Two pyroxene-garnet equilibria in the Na_2O-CaO-MgO-Al_2O_3-SiO_2 system at 2-5 GPa pressure. *Geochemistry International* **40**(10), 929-942.

Carlson, W.D. (1989) Subsolidus phase equilibria near the enstatite-diopside join in CaO-MgO-Al_2O_3-SiO_2 at atmospheric pressure. *American Mineralogist* **74**, 325-332.

Carlson, W.D., and Lindsley, D.H. (1988) Thermochemistry of pyroxenes on the join $Mg_2Si_2O_6$-$CaMgSi_2O_6$. *American Mineralogist* **73**, 242-252.

Chatterjee, N.D., Krüger, R., Haller, G., and Olbricht, W. (1998) The Bayesian approach to an internally consistent thermodynamic database: theory, database, and generation of phase diagrams. *Contributions to Mineralogy and Petrology* **133**, 149-168.

Davidson, P.M. (1985) Thermodynamic analysis of quadrilateral pyroxenes. Part I: Derivation of the ternary non-convergent site-disorder model. *Contributions to Mineralogy and Petrology* **91**, 383-389.

Davidson, P.M., and Lindsley, D.H. (1985) Thermodynamic analysis of quadrilateral pyroxenes. Part II: Model calibration from experiments and applications to geothermometry. *Contributions to Mineralogy and Petrology* **91**, 390-404.

Davidson, P.M., and Lindsley, D.H. (1989) Thermodynamic analysis of pyroxene-olivine-quartz equilibria in the system CaO-MgO-FeO-SiO_2. *American Mineralogist* **74,** 18-30.

Davidson, P.M., Lindsley, D.H., and Carlson, W.D. (1988) Thermochemistry of pyroxenes on the join $Mg_2Si_2O_6$-$CaMgSi_2O_6$: A revision of the model for pressures up to 30 kbar. *American Mineralogist* **73**, 1264-1266.

Davis, B.T.C., and Boyd Jr, F.R. (1966) The join $Mg_2Si_2O_6$-$CaMgSi_2O_6$ and its application to pyroxenes from kimberlites. *Journal of Geophysical Research* **71**, 3567-3576.

Deer, W.A., Howie, R.A., and Zussman, J. (1992) Rock-forming minerals. —Chain Silicates. In, vol. Longman, London and New York, pp Vol. 1A, 143-202

Fei, Y., Saxena, S.K., and Eriksson, G. (1986) Some binary and ternary silicate solution models. *Contributions to Mineralogy and Petrology* **94**, 221-229.

Finnerty, T.A. (1977) Exchange of Mn, Ca, Mg and Al between synthetic garnet, orthopyroxene, clinopyroxene and olivine. *Carnegie Institution of Washington Yearbook* **76**, 572-579.

Fonarev, V.I., and Graphchikov, A.A. (1982) Experimental study of Fe-Mg and Ca-distribution between coexisting ortho- and clino-pyroxenes at P=294 MPa, T=750 and 800°C. *Contributions to Mineralogy and Petrology* **79**, 311-318.

Fujii, T. (1977) Pyroxene equilibria in spinel lherzolite. *Carnegie Institution of Washington Yearbook* **76**, 569-572.

Ganguly, J., Cheng, W., and Tirone M. (1996) Thermodynamics of aluminosilicate garnet solid solution: new experimental data, an optimized model, and thermometric applications. *Contributions to Mineralogy and Petrology* **126**, 137-151.

Gasparik, T. (1984) Two-pyroxene thermobarometry with new experimental data in the system CaO-MgO-Al_2O_3-SiO_2. *Contributions to Mineralogy and Petrology* **87**, 87-97.

Gasparik, T. (1990) A thermodynamic model for the enstatite-diopside join. *American Mineralogist* **75**, 1080-1091.

Gasparik, T. (1996) Melting experiments on the enstatite-diopside join at 70-224 kbar, including the melting of diopside. *Contributions to Mineralogy and Petrology* **124**, 139-153.

Gasparik, T. (2000) An internally consistent thermodynamic model for the system CaO-MgO-Al_2O_3-SiO_2 derived primarily from phase equilibrium data. *Journal of Geology* **108**, 103-119.

Gottschalk, M. (1997) Internally consistent thermodynamic data for rock-forming minerals in the system. *European Journal of Mineralogy* **9**, 175-223.

Gudfinnsson, G.H., and Presnall, D.C. (2000) Melting behaviour of model lherzolite in the system CaO–MgO–Al_2O_3–SiO_2–FeO at 0.7–2.8 GPa. *Journal of Petrology* **41**(8), 1241-1269.

Herzberg, C.T. (1978) Pyroxene geothermometry and geobarometry: experimental and thermodynamic evaluation of some subsolidus phase relations involving pyroxenes in the system CaO-MgO-Al_2O_3-SiO_2. *Geochimica et Cosmochimica Acta* **42**, 945-957.

Herzberg, C.T., and Chapman, N.A. (1976) Clinopyroxene geothermometry of spinel lherzolites. *American Mineralogist* **61**, 626-637.

Holland, T.J.B., Navrotsky, A., and Newton, R.C. (1979) Thermodynamic parameters of $CaMgSi_2O_6$-$Mg_2Si_2O_6$ pyroxenes based on regular solution and cooperative disordering models. *Contributions to Mineralogy and Petrology* **69**, 337-344.

Holland, T.J.B., and Powell, R. (1990) An enlarged and updated internally consistent thermodynamic dataset with uncertainties and correlations: the system K_2O-Na_2O-CaO-MgO-MnO-FeO-Fe_2O_3-Al_2O_3-TiO_2-SiO_2-C-H_2-O_2. *Journal of Metamorphic Geology* **8**, 89-124.

Holland, T.J.B., and Powell, R. (1998) An internally consistent thermodynamic dataset for phases of petrological interest. *Journal of Metamorphic Geology* **16**, 309-403.

Kawasaki, T. (1999) Thermodynamic analysis of partitioning of Ca, Fe and Mg between olivine and clinopyroxene. *Geochemical Journal* **33**, 1-25.

Kawasaki, T., and Ito, E. (1994) An experimental determination of exchange reaction of Fe^{2+} and Mg^{2+} between olivine and Ca-rich clinopyroxene. *American Mineralogist* **79**, 461-477.

Kitayama, K., and Katsura, T. (1968) Activity measurements in orthosilicate and metasilicate solid solutions. I. Mg_2Si_4-Fe_2SiO_4 and $MgSiO_3$-$FeSiO_3$ at 1204°C. *Bulletin of the Chemical Society of Japan* **41**, 1146-1151.

Klemme, S. (1998) Experimental and thermodynamic studies of upper mantle phase relations. *PhD Thesis*, Canberra, Australian National University

Koch-Müller, M., Cemic, L., and Langer, K. (1992) Experimental and thermodynamic study of Fe-Mg exchange between olivine and orthopyroxene in the system MgO-FeO-SiO_2. *European Journal of Mineralogy* **4**, 115-135.

Kretz, R. (1961) Some applications of thermodynamics to coexisting minerals of variable composition. Examples: Orthopyroxene-clinopyroxene and orthopyroxene-garnet. *Journal of Geology* **69**, 361-387.

Kretz, R. (1982) Transfer and exchange equilibria in a portion of the pyroxene quadrilateral as deduced from natural and experimental data. *Geochimica et Cosmochimica Acta* **46**, 411-422.

Kushiro, I. (1968) Synthesis and stability of iron free pigeonite in the system $MgSiO_3$-$CaMgSi_2O_6$ at high pressures. *Carnegie Institution of Washington Yearbook* **67**, 80-83.

Kushiro, I. (1969) The system forsterite-diopside-silica with and without water at high pressures. *American Journal of Science* **267-A**, 269-294.

Kushiro, I., and Yoder Jr, H.S. (1970) Stability field of iron-free pigeonite in the system $MgSiO_3$-$CaMgSi_2O_6$. *Carnegie Institution of Washington Yearbook* **68**, 226-229.

Latypov, R.M., Dubrovskii, M.I., and Alapieti, T.T. (2001) Graphical analysis of the orthopyroxene-pigeonite-augite-plagioclase equilibrium at liquidus temperatures and low pressure. *American Mineralogist* **86**, 547-554.

Lindsley, D.H. (1967) The join hedenbergite-ferrosilite at high pressures and temperatures. *Carnegie Institution of Washington Yearbook* **65**, 230-234.

Lindsley, D.H. (1981) The formation of pigeonite on the join hedenbergite-ferrosilite at 11.5 and 15 kbar: experiments and a solution model. *American Mineralogist* **66**, 1175-1182.

Lindsley, D.H. (1983) Pyroxene thermometry. *American Mineralogist*, 68, 477-493.

Lindsley, D.H., and Anderson, D.J. (1983) A two-pyroxene thermometer. *Journal of Geophysical Research* Suppl. 88, A887-A906.

Lindsley, D.H., and Burnham, C.W. (1970) Pyroxferroite: Stability and X-ray crystallography of synthetic $Ca_{0.15}Fe_{0.85}SiO_3$ pyroxenoid. *Science* **168**, 364-367.

Lindsley, D.H., and Dixon, S.A. (1976) Diopside-enstatite equilibria at 850°-1400°C, 5-35 kb. *American Journal of Science* **276**, 1285-1301.

Lindsley, D.H., Grover, J.E., and Davidson, P.M. (1981) The thermodynamics of the $Mg_2Si_2O_6$-$CaMgSi_2O_6$ join: A review and an improved model. In: Newton, R.C., Navrotsky, A.and Wood, B.J. (eds) Thermodynamics of minerals and melts, vol. Springer Verlag, New York, pp 149-175

Lindsley, D.H., and Munoz, J.L. (1969) Subsolidus relations along the join hedenbergite-ferrosilite. *American Journal of Science* **267A**, 295-324.

Liu, X. (2003) Partial melting of spinel lherzolite. *PhD Thesis*. The Australian National University, Canberra

Matsui, Y., and Nishizawa, O. (1974) Iron(II)-magnesium exchange equilibrium between olivine and calcium-free pyroxene over a temperature range 800°C to 1300°C. *Bull. Bulletin de la Societe Francaise Mineralogie et de cristallographie* **97**, 122-130.

Mori, T. (1977) Geothermometry of spinel lherzolites. *Contributions to Mineralogy and Petrology* **59**, 261-279.

Mori, T. (1978) Experimental study of pyroxene equilibria in the system CaO-MgO-FeO-SiO_2 at high pressures and temperatures. *Journal of Petrology* **19**, 45-65.

Mori, T., and Green, D.H. (1975) Pyroxenes in the system $Mg_2Si_2O_6$-$CaMgSi_2O_6$ at high pressure. *Earth and Planetary Science Letters* **26**, 277-286.

Mori, T., and Green, D.H. (1976) Subsolidus equilibria between pyroxenes in the CaO-MgO-SiO_2 system at high pressures and temperatures. *American Mineralogist* **61**, 616-625.

Nafziger, R.H., and Muan, A. (1967) Equilibrium phase compositions and thermodynamic properties of olivines and pyroxenes in the system MgO-"FeO"-SiO_2. *American Mineralogist* **52**, 1364-1384.

Nehru, C.E., and Wyllie, P.J. (1974) Electron microprobe measurements of pyroxenes coexisting with H_2O-undersaturated liquid in the join $CaMgSi_2O_6$-$Mg_2Si_2O_6$-H_2O at 30 kbars, with applications to geothermometry. *Contributions to Mineralogy and Petrology* **48**, 221-228.

Nickel, K.G., and Brey, G. (1984) Subsolidus orthopyroxene-clinopyroxene systematics in the system CaO-MgO-SiO_2 to 60 kb: a re-evaluation of the regular solution model. *Contributions to Mineralogy and Petrology* **87**, 35-42.

Nickel, K.G., Brey, G., and Kogarko, L.N. (1985) Orthopyroxene-clinopyroxene equilibria in the system CaO-MgO-Al_2O_3-SiO_2 (CMAS) – new experimental results and implications for two-pyroxene thermometry. *Contributions to Mineralogy and Petrology* **91**, 44-53.

O'Neill, H.S.C., and Wall, V.J. (1987) The olivine-orthopyroxene-spinel oxygen geobarometer, the nickel precipitation curve and the oxygen fugacity of the Earth's upper mantle. *Journal of Petrology* **28**, 1169-1191.

Obata, M. (1976) The solubility of Al_2O_3 in orthopyroxenes in spinel and plagioclase peridotites and spinel pyroxenite. *American Mineralogist* **61**, 804-816.

Pasqual, D., Molin, G., and Tribaudino, M. (2000) Single-crystal thermometric calibration of Fe-Mg order-disorder in pigeonites. *American Mineralogist* **85**, 953-962.

Perkins, D., III, and Newton, R.C. (1980) The composition of coexisting pyroxenes and garnet in the system CaO-MgO-Al_2O_3-SiO_2 at 900-1100∞C and high pressures. *Contributions to Mineralogy and Petrology* **75**, 291-300.

Podpora, C., and Lindsley, D.H. (1979) Fe-rich pigeonites: minimum temperatures of stability in the Ca-Mg-Fe quadrilateral (abstr). *EOS* **60**, 420-421.

Presnall, D.C. (1976) Alumina content of enstatite as a geobarometer for plagioclase and spinel lherzolites. *American Mineralogist* **61**, 582-588.

Ramberg, H., and Devore, G. (1951) The distribution of Fe^{++} and Mg^{++} in coexisting olivines and pyroxenes. *Journal of Geology* **59**, 193-210.

Robie, R.A., and Hemingway, B.S. (1995) Thermodynamic properties of minerals and related substances at 298.15 K and 1 bar (10^5 pascals) pressure and at higher temperatures. *United States Geological Survey Bulletin* **2131**, pp. 461.

Robinson, P. (1980) The composition space of terrestrial pyroxenes-internal and external limits. *Review of Mineralogy* **7**, 419-494.

Ross, M., and Huebner, J.S. (1975) A pyroxene thermometer based on temperature-composition relationships of naturally occurring orthopyroxene, pigeonite and augite (extended abstract). In: International Conference on Geothermometry and Geobarometry, vol. Pennsylvania State University,

Sack, R.O., and Ghiorso, M.S. (1989) Importance of considerations of mixing properties in establishing an internally consistent thermodynamic database: thermochemistry of

minerals in the system Mg_2SiO_4-Fe_2SiO_4-SiO_2. *Contributions to Mineralogy and Petrology* **102**, 41-68.

Sack, R.O., and Ghiorso, M.S. (1994a) Thermodynamics of multicomponent pyroxenes: I. Formulation of a general model. *Contributions to Mineralogy and Petrology* **116**, 277-286.

Sack, R.O., and Ghiorso, M.S. (1994b) Thermodynamics of multicomponent pyroxenes: II. Phase relations in the quadrilateral. *Contributions to Mineralogy and Petrology* **116**, 287-300.

Saxena, S.K., and Nehru, C.E. (1975) Enstatite-diopside solvus and geothermometry. *Contributions to Mineralogy and Petrology* **49**, 259-267.

Saxena, S.K., Sykes, J., and Eriksson, G. (1985) Phase equilibria in the pyroxene quadrilateral. *Journal of Petrology* **27**, 843-852.

Schweitzer, E. (1982) The reaction pigeonite = $diopside_{ss}$ + $enstatite_{ss}$ at 15 kbar. *American Mineralogist* **67**, 54-58.

Sen, G. (1985) Experimental determination of pyroxene compositions in the system CaO-MgO-Al_2O_3-SiO_2 at 900°-1200 ^oC and 10-15 kbar using PbO and H_2O fluxes. *American Mineralogist* **70**, 678-695.

Shi, P., and Libourel, G. (1991) The effects of FeO on the system CMAS at low pressure and implications for basalt crystallization processes. *Contributions to Mineralogy and Petrology* **108**, 129-145.

Shi, P.F., Saxena, S.K., Zhang, Z.R., and Sundman, B. (1994) Thermodynamics of the Ca-Mg-Fe-Al-Si-O pyroxenes: I. Theoretical model and assessment of the Ca-Mg-Si-O system. *Calphad* **18**, 47-69.

Tribaudino, M., and Bruno, E. (1993) Effect of Al on enstatite solubility in CMAS clinopyroxenes: 1. Experimental results in the clinopyroxene-orthopyroxene two-phase field at P=18 kbar. *European Journal of Mineralogy* **5**(1), 123-131.

Turnock, A.C. (1962) Preliminary results on melting relations of synthetic pyroxenes on the diopside-hedenbergite join. *Carnegie Institution of Washington Yearbook* **61**, 81-82.

Turnock, A.C., and Lindsley, D.H. (1981) Experimental determination of pyroxene solvi for P ≤ 1 kb, 900 and 1000°C. *Canadian Mineralogist* **19**, 255-267.

von Seckendorff, V., and O'Neill, H.S.C. (1993) An experimental study of Fe-Mg partitioning between olivine and orthopyroxene at 1173, 1273 and 1423 K and 1.6 GPa. *Contributions to Mineralogy and Petrology* **113**, 196-207.

Warner, R.D., and Luth, W.C. (1974) The diopside-orthoenstatite two-phase region in the system $CaMgSi_2O_6$-$Mg_2Si_2O_6$. *American Mineralogist* **59**, 98-109.

Wells, P.R.A. (1977) Pyroxene thermometry in simple and complex systems. *Contributions to Mineralogy and Petrology* **62**, 129-139.

Wood, B.J., and Banno, S. (1973) Garnet-orthopyroxene and orthopyroxene-clinopyroxene relationships in simple and complex systems. *Contributions to Mineralogy and Petrology* **42**, 109-124.

Wood, B.J., and Holloway, J.R. (1984) A thermodynamic model for subsolidus equilibria in the system CaO-MgO-Al_2O_3-SiO_2. *Geochimica et Cosmochimica Acta* **48**, 159-176.

Woodland, A.B., and O'Neill, H.S.C. (1995) Phase relations between $Ca_3Fe_2^{3+}Si_3O_{12} - Fe_3^{2+}Fe_2^{3+}Si_3O_{12}$ garnet and $CaFeSi_2O_6$-$Fe_2Si_2O_6$ pyroxene solid solutions. *Contributions to Mineralogy and Petrology* **121**, 87-98.

Yamada, H., and Takahashi, E. (1984) Subsolidus phase relations between coexisting garnet and two pyroxenes at 50 to100 kbar in the system CaO-MgO-Al_2O_3-SiO_2. In: Kornprobst, J. (ed) Proceedings of the Third International Kimberlite Conference, vol 2. pp 247-255

Chapter 6

Optimizing standard state and mixing properties of solid solution phases: an inverse problem

6.1 Introduction

In the past fifteen years derivation of internally consistent databases (e.g. Berman, 1988; Holland and Powell, 1990 and 1998; Gottschalk, 1997; Chatterjee et al., 1998) and compilations of calorimetric data (e.g. Robie and Hemingway, 1995) have been a major advance in thermodynamic modeling. These studies have led to the creation of datasets that represent a valuable starting point for quantitative petrologic and thermobarometric calculations.

Derivation of the internally consistent datasets is based on simultaneous treatment of a large number of phase equilibrium data as well as on calorimetric studies. However, the technique used may greatly differ between studies. In the case of Holland and Powell (1990, 1998) and of Gottschalk (1997) datasets were calculated using a least square regression technique (REG). Berman (1988) employed a linear mathematical programming algorithm (MAP) with a quadratic objective function, while Chatterjee et al. (1998) derived their database by making use of the Bayesian method. This last approach finds its fundaments in the previous works of Olbricht et al. (1994) and Chatterjee et al. (1994) where it was demonstrated that the Bayesian technique could be used to obtain internally consistent datasets. Furthermore, in these works it was shown that the Bayesian method combines the advantages of MAP (ability to handle inequalities and equalities in energy differences of reactions and elimination of inconsistent experiments) and REG (ability to get a covariance matrix), and it is eminently suited to do the same job done by MAP and REG (Chatterjee et al., 1998).

In deriving the databases, internal consistency is maintained usually by correcting entalphy, $\Delta_f H$, (Holland and Powell, 1990 and 1998) or entalphy and entropy, S^o, (Gottschalk, 1997; Chatterjee et al., 1998) or by adjusting several parameters simultaneously (Berman, 1988). Different approaches reflect some differences in

'philosophy'. In refining only values for $\Delta_f H$ and/or S^o, Holland and Powell (1990, 1998), Gottschalk (1997) and Chatterjee et al. (1998) assumed that all the other parameters and functions are well known and fixed. On the other hand Berman (1988) considered that the parameters and functions for each phase end-member have some experimental error and are therefore targets for optimization (Gottschalk, 1997).

Apart from differences in the technique used and/or in the extent of the parameters refined, the main purpose of all these databases was to derive datasets for rock-forming mineral pure end-members. Contrastingly the goal of this work, as shown in the previous chapters of this theses, is to develop a model for a comprehensive investigation of subsolidus equilibria among solid solution phases at any pressure and temperature condition.

The use of existing databases to investigate subsolidus equilibria among solid solution phases is not without shortcomings. First, these datasets have been largely derived without consideration of the growing body of high quality experimental data on solid solution bearing equilibria, thus omitting very important information that may influence the derived standard state end-member properties (Berman and Aranovich, 1996). Secondly, an arbitrary combination of standard state thermodynamic properties with solid solution models will not in general give results compatible with available experimental data (Berman and Aranovich, 1996). Furthermore, applications of the program '*Gib'* presented in chapters 4 and 5 showed that in order to precisely model phase equilibria involving solid solution an accurate estimation of both thermodynamic data for mineral end-members and solution parameters is needed. This means that an internally consistent set of end-member standard state and mixing properties has to be derived. In order to do this end-member and solution properties must be determined simultaneously from available experimental and thermophysical data.

In their study, Chatterjee et al. (1998) mentioned that the Bayesian method could have been extended to refine also thermodynamic mixing properties. Unfortunately no further publications followed that work. In this study the Bayesian approach is used to derive internally consistent sets of both end-member standard state and solution parameters. In this chapter the procedure to set up a program (called '*GibInv*') is described in detail that allows the simultaneous refinement of any of the end-member and mixing parameters. The

program has been successfully tested in a synthetic case and initially applied to pyroxene in the system CaO-MgO-FeO-Al_2O_3-SiO_2 (i.e. CMFAS). Preliminary results are shown in section 6.10.

6.2 Review of the *forward* approach

Before describing how the thermochemical equilibria problem can be formulated mathematically, it is opportune to briefly summarize how the *forward* problem was outlined and solved (see also chapter 3). Later in this chapter, it will be shown that these two problems are closely related to one another, to the point that they represent two different ways to solve the same problem of optimizing (i.e. minimizing) the Gibbs free energy of the system.

In solving the Gibbs free energy minimization (i.e. GFEM) problem following the *forward* approach the goal was to find the composition and number of moles of phases that at given temperature and pressure condition bring the Gibbs free energy of a closed multi-phase system (i.e. $\mathbf{G}^{\mathbf{system}}$) to its minimum value:

$$\mathbf{G}^{\mathbf{system}} = minimum \;\Rightarrow\; dG = 0, \qquad \text{(i.e. equilibrium condition)} \tag{6.1}$$

Assuming a system consisting of 'p' phases, one has:

$$\mathbf{G}^{\mathbf{system}} = \sum_{\phi=1}^{p} \mathbf{G}^{\phi} = n^1 G^1 + n^2 G^2 + \ldots + n^p G^p = \sum_{\phi=1}^{p} n^{\phi} G^{\phi} \tag{6.2}$$

with:

$\mathbf{G}^{\phi}$ = total Gibbs free energy of phase ϕ,

n^{ϕ} = number of moles of phase ϕ in the system,

G^{ϕ} = molar Gibbs free energy for phase ϕ.

For every phase ϕ in the system the usual expression of the molar Gibbs free energy, G^{ϕ}, is (e.g. Chatterjee, 1991):

$$^{22}\, G^{\phi} = G^{end-members} + G^{ideal} + G^{excess} \qquad (6.3)$$

In chapter 2 it was described how proper expressions for $G^{e\text{-}m}$, G^{id}, and G^{ex} for several different phases (i.e. pyroxene, garnet, olivine, etc…) can be derived and how these expressions, and in particular the formulation of $G^{e\text{-}m}$, can vary depending on the phase(s) considered. At the same time, despite any possible difference in their formulations, $G^{e\text{-}m}$ is always a function of temperature (T), pressure (P), [23]composition $\left(X_{ik}^{\phi}{}'s\right)$ and end-member (E) parameters, i.e. $G^{e-m} = G\left(T, P, X_{ik}^{\phi}, E's\right)$; G^{id} is a function of $X_{ik}^{\phi}{}'s$ and T, i.e. $G^{id} = G\left(T, X_{ik}^{\phi}\right)$; G^{ex} is a function of T, P, $X_{ik}^{\phi}{}'s$ and solution $\left(W^{\phi}\right)$ parameters, i.e. $G^{ex} = G\left(T, P, X_{ik}^{\phi}, W^{\phi,}s\right)$.

Considering a system at fixed T, P conditions equation (6.3) can be re-written as:

$$G^{\phi} = G^{e-m}\left(X_{ik}^{\phi}, E^{\phi,}s\right)_{T,P} + G^{id}\left(X_{ik}^{\phi}\right)_{T} + G^{ex}\left(X_{ik}^{\phi}, W^{\phi,}s\right)_{T,P} \qquad (6.4)$$

In the *forward* problem end-member (E^{ϕ}) and Margules (W^{ϕ}) parameters were assumed to be known, for every phase ϕ in the system. On the other hand, the program *'Gib'* computes the composition and number of moles of phases in the system that satisfy equilibrium condition of equation (6.1).

[22] Throughout the rest of this chapter the abbreviations $G^{e\text{-}m}$ for $G^{end\text{-}member}$, G^{id} for G^{ideal}, G^{ex} for G^{excess} are used.

[23] In chapter 3 it was explained how the compositional dependence of G^{ϕ} is expressed using the 'virtual' site occupancies X_{ik}^{ϕ}'s. Where X_{ik}^{ϕ} indicates the site occupancy of cation *'i'* in sublattice *'k'* for phase ϕ (see also section 3.2).

Schematically, in the *forward* problem at specified *T-P* conditions:

$$\left.\begin{matrix} E^{\phi}s \\ W^{\phi}s \end{matrix}\right\} \; input\ parameters$$

$$\left.\begin{matrix} X_{ik}^{\phi}s \\ n^{\phi}s \end{matrix}\right\} \; unknowns$$

The GFEM problem proved to be *non-linear* because in general for every phase ϕ the molar Gibbs free energy G^{ϕ} depends non-linearly on the site occupancies X_{ik}^{ϕ}'s.

Furthermore, considering the choice of the *unknowns* the minimization has to be carried out under several constraints:

mass balance (*non-linear equality*) constraints for every *cation i* in the system;

$$\mathbf{M_i} = \sum_{\phi=1}^{p} n^{\phi} \sum_{k=1}^{n} X_{ik}^{\phi} \tag{6.5}$$

with:

n = total number of sublattices in phase ϕ,
$\mathbf{M_i}$ = total number of moles of *cation i* in the system,

stoichiometry (*linear equality*) constraints for each phase ϕ, on every sublattice k;

$$S_k^{\phi} = \sum_{i=1}^{c} X_{ik}^{\phi} \tag{6.6}$$

where, the value of S_k^ϕ depends on the type of phase and sublattice considered (e.g. if ϕ = [24]*grt* and *k* = dodecahedral X site, then $S_k^\phi = 3$; or if ϕ = *ol* and *k* = octahedral M2 site, then $S_k^\phi = 1$),

charge balance (*linear equality*) constraints for each phase ϕ;

$$C^\phi = \sum_{i=1}^{c} \beta_i \sum_{k=1}^{n} X_{ik}^\phi \qquad (6.7)$$

with:

c = total number of cations in one mole of phase ϕ,
β_i = individual charge of cation *i*,

where, the value of C^ϕ depends on the type of phase considered (e.g. if ϕ = spinel, then $C^\phi = 8$; or if ϕ = pyroxene, then $C^\phi = 12$);

non-negativity *(linear inequality)* constraints for each phase ϕ;

$$n^\phi \geq 0, \quad X_{ik}^\phi \geq 0 \qquad (6.8)$$

Moreover, in some particular cases (e.g. pyroxene and olivine) additional **ratio** (*non-linear equality*) constraints are imposed on the solution. **Ratio** constraints are needed to handle random distributions of same cations among different sublattices (e.g. Mg and Fe^{2+} among sublattices M2 and M1 in pyroxene solid solution).

[24] Throughout the rest of this chapter the abbreviations *opx* = orthopyroxene, *cpx* = clinopyroxene, *pig* = pigeonite, *grt* = garnet, *ol* = olivine, *sp* = spinel, *pl* = plagioclase, *qtz* = quartz, *ky* = kyanite, *sil* = sillimanite, *cor* = corundum, will normally be used.

In general **ratio** constraints have the form (see also Appendix 3B):

$$C_{\omega}\left(X_{ik}^{\phi}\right)=0 \qquad (\omega=1,\ldots,s) \tag{6.9}$$

with:

s = total number of 'independent' ratio constraints per phase.

To solve the GFEM problem, because of its complexity, the Feasible Iterate Sequential Quadratic programming algorithm (*FSQP*) of Panier and Tits (1993), Zhou, Tits and Lawrence (1998) is used. The *FSQP* solver is a very sophisticated optimization technique that can account for the *non-linear* nature of the problem and can deal with all types of constraints one wants to impose on the solution. Details on the way this solver operates were given in chapter 3.

6.3 Mathematical formulation of the *inverse* problem

The minimization problem given by equation (6.1) could have been solved following a completely different approach (technique) to the one described in chapter 3 and summarized in the previous section.

Once the correct expression of $\mathbf{G}^{\mathbf{system}}$ has been derived and taking into account all the constraints that have to be imposed on the solution, the equilibrium conditions for a closed multi-phase system can be obtained in a straightforward manner using the method of *Lagrange* multipliers (e.g. Arfken, 1985). The expression of $\mathbf{G}^{\mathbf{system}}$ to minimize is the same as in the *forward* problem and it is given by Eq. (6.2), and the constraints that have to be included in the minimization process are those listed in the previous section.

Introducing a *Lagrangian* multiplier for each constraint equation, a *Lagrangian* function L is obtained:

$$L = \sum_{\phi=1}^{p} n^{\phi} G^{\phi} + \sum_{i=1}^{c} \left(\sum_{\phi=1}^{p} n^{\phi} \sum_{k=1}^{n} X_{ik}^{\phi} - M_i \right) \gamma_i + \sum_{\phi=1}^{p} \sum_{k=1}^{n} \left(\sum_{i=1}^{c} X_{ik}^{\phi} - S_k^{\phi} \right) \lambda_k^{\phi} + \sum_{\phi=1}^{p} \left(\sum_{i=1}^{c} \beta_i \sum_{k=1}^{n} X_{ik}^{\phi} - C^{\phi} \right) \rho^{\phi} + \sum_{\phi=1}^{p} \sum_{\omega=1}^{s} \delta_{\omega}^{\phi} C_{\omega}^{\phi} \tag{6.10}$$

In this way, a number of additional, *Lagrangian*, *unknowns* are introduced in the system.

The unconstrained minimum of L will be at the same time the minimum of $\mathbf{G}^{\mathbf{system}}$ under the various constraints, i.e.:

$$L = minimum \equiv \mathbf{G}^{\mathbf{system}} = minimum \Rightarrow \text{equilibrium condition} \tag{6.11}$$

This minimum is obtained by setting to zero the partial derivatives of L with respect to all system's *unknowns* $\left(\gamma_i, \lambda_i^{\phi}, \rho^{\phi}, \delta_{\omega}^{\phi}, n^{\phi}, X_{ik}^{\phi}\right)$:

$$\frac{\partial L}{\partial \gamma_i} = 0 \quad \Rightarrow \mathbf{M_i} = \sum_{\phi=1}^{p} n^{\phi} \sum_{k=1}^{n} X_{ik}^{\phi} \quad \left(k = 1,...,n; \phi = 1,...,p\right) \tag{6.12}$$

gives back mass balance constraint

$$\frac{\partial L}{\partial \lambda_k^{\phi}} = 0 \quad \Rightarrow S_{\mathrm{k}}^{\phi} = \sum_{k=1}^{n} X_{ik}^{\phi} \quad \left(k = 1,...,n\right) \tag{6.13}$$

gives back stoichiometry constraint

$$\frac{\partial L}{\partial \rho^{\phi}} = 0 \quad \Rightarrow C^{\phi} = \sum_{i=1}^{c} \beta_i \sum_{k=1}^{n} X_{ik}^{\phi} \quad \left(k = 1,...,n; i = 1,...,c\right) \tag{6.14}$$

gives back charge balance constraint

$$\frac{\partial L}{\partial \delta^{\phi}} = 0 \quad \Rightarrow \quad \sum_{\omega=1}^{s} C_{\omega} \quad \left(\omega = 1,...,n\right) \tag{6.15}$$

gives back ratio constraint

$$\frac{\partial L}{\partial n^{\phi}} = 0 \quad \Rightarrow G^{\phi} + \sum_{i=1}^{c} \gamma_i \left(\sum_{k=1}^{n} X_{ik}^{\phi} \right) = 0 \quad \left(\phi = 1,..., p \right) \tag{6.16}$$

$$\frac{\partial L}{\partial X_{ik}^{\phi}} = 0 \quad \Rightarrow n^{\phi} \frac{\partial G^{\phi}}{\partial X_{ik}^{\phi}} + \gamma_i n^{\phi} + \lambda_k^{\phi} + \beta_i \rho^{\phi} + \delta_{\omega}^{\phi} \frac{\partial C_{\omega}}{\partial X_{ik}^{\phi}} \quad \left(\phi = 1,...,p; k = 1,...,n; i = 1,...,c \right) \tag{6.17}$$

Had the *forward* problem been formulated using the method of *Lagrange* multipliers extra *unknowns* $\left(i.e.\ \gamma_i, \lambda_i^{\phi}, \rho^{\phi}, \delta_{\omega}^{\phi} \right)$ would have been introduced in the system. From equations (6.16) and (6.17) it is clear that if using this method the *Lagrangian unknowns* would have to be solved simultaneously with $X_{ik}^{\phi}{}'s$ and $n^{\phi}{}'s$, and this would have increased the size of the problem[25]. For this reason also the *FSQP* solver was used to solve the GFEM problem.

At the same time expressions (6.10-6.17) contain valuable information on the nature of the relationship among variables for any closed, multi-phase system at equilibrium condition and could be used to solve a completely different kind of problem.

It is now assumed to be provided with a number of datasets, each referring to different specified *T-P* conditions, that represent the chemical analysis compositions of the phases present in the system at its equilibrium conditions. This means that in the $\mathbf{G}^{\mathbf{system}}$ and G^{ϕ} expressions, together with *T* and *P*, also composition $\left(X_{ik}^{\phi} \right)$ and number of moles $\left(n^{\phi} \right)$ of phases will be considered known[26]. On the other hand, what is now assumed not to be known and what have to be found are the values of the end-member (*E*) and Margules (*W*) parameters such that the system's equilibrium conditions expressed by Eq. (6.12)-(6.17) are satisfied.

The problem can again be seen as one of minimization. It can then be outlined in a very simple way: given a function *f* (i.e. $\mathbf{G}^{\mathbf{system}}$) which depends on some independent

[25] During the course of this study a computer program has been developed to implement the *Lagrange* multiplier method of solving the GFEM problem, but this method was found to be inferior to the *FSQP* both in terms of numerical stability and solution accuracy.

[26] Not always in the chemical analysis compositions the value on n^{ϕ}'s is specified. However, as proved in Appendix 6C, this does not change the nature of the problem to solve. For this reason the remaining part of the argument in this section assumes the n^{ϕ}'s value to be known.

variables (*E's* and *W's*, in this case) one wants to find the value of those variables where *f* takes on a minimum value ($\Rightarrow$ equilibrium conditions). The main difference respect to the problem dealt with in the *forward* approach is that, while in that case one computes data given a model, now the aim is to 'reconstruct' the model (or at least part of it) from a set of measurements. Thus, this represents a typical example of an *inverse* problem.

So recalling again Eq. (6.4):

$$G^{\phi} = G^{e-m}\left(X_{ik}^{\phi}, E^{\phi,}s\right)_{T,P} + G^{id}\left(X_{ik}^{\phi}\right)_{T} + G^{ex}\left(X_{ik}^{\phi}, W^{\phi,}s\right)_{T,P}$$

schematically, for the *inverse* problem at specified *T-P* conditions:

$$\left.\begin{array}{l} X_{ik}^{\phi,}s \\ n^{\phi,}s \end{array}\right\} \; input\ \ parameters$$

$$\left.\begin{array}{l} E^{\phi,}s \\ W^{\phi,}s \end{array}\right\} \; unknowns$$

6.3.1 A linear problem

In order to identify an appropriate technique for solving the *inverse* problem a crucial issue is to find out the nature of the dependence of the equations that specify the system equilibrium conditions (i.e. Eqs. 6.12-6.17) respect to the system's *unknowns* (*E's* and *W's*).

Firstly, it is evident that Eqs. (6.12), (6.13), (6.14) and (6.15) contain only input parameters and do not contain any *unknown*. Since these equations will be always automatically satisfied by the input parameters[27], they are not needed for the *inverse* problem and can be dropped. All the *inverse* problem *unknowns* $\left(E's, W's, \gamma_i, \lambda_i^{\phi}, \rho^{\phi}, \delta_{\omega}^{\phi}\right)$

[27] This is not entirely correct. However, it would be if site occupancies' values were not affected by measurement errors. Unfortunately, since this is not the case, the input parameters, in general, do not exactly satisfy all the constraints. Usually the error is very small and in Appendix 6A it is reported how this issue was treated. The remaining part of the argument in this section assumes site occupancies' measurements are error free.

appear in Eq. (6.16) and in Eq. (6.17). So, it is necessary to verify what kind of dependence there is between the two equations and their *unknown*s.

End-member parameters are all contained in the G^{ϕ} expression. More specifically, recalling once again Eq. (6.4):

$$G^{\phi} = G^{e-m}\left(X_{ik}^{\phi}, E^{\phi,}s\right)_{T,P} + G^{id}\left(X_{ik}^{\phi}\right)_{T} + G^{ex}\left(X_{ik}^{\phi}, W^{\phi,}s\right)_{T,P}$$

it is clear that *E's* are confined in the $G^{e\text{-}m}$ part of G^{ϕ} and *W's* in the G^{ex} part of G^{ϕ}, while G^{id} depends exclusively on input parameters. As a consequence only the G^{e-m} and G^{ex} parts of G^{ϕ} need to be investigated.

As shown in chapter 2 the adopted expression of G^{ex} for any phase ϕ in the system is given by:

$$G^{\phi-ex} = \sum_{k=1}^{n} Q_k \sum_{i=1}^{c}\sum_{y>i}^{c} X'_{ik} X'_{yk} \left\{ \begin{array}{l} W_{ik-yk} \cdot \left[X'_{yk} + \frac{1}{2}\sum_{\substack{j\neq i \\ j\neq y}}^{c} X'_{jk} \right] + \\ W_{yk-ik} \cdot \left[X'_{ik} + \frac{1}{2}\sum_{\substack{j\neq i \\ j\neq y}}^{c} X'_{jk} \right] \end{array} \right\} + \sum_{i=1}^{c}\sum_{y>i}^{c}\sum_{j>y}^{c} X'_{ik} X'_{yk} X'_{jk} W_{ik-yk-jk} \tag{6.18}$$

with:

$$X'_{ik} = \frac{X_{ik}}{Q_k} \tag{6.19}$$

Where, Q_k denotes the number of sites on sublattice *k, n* the total number of sublattices *k*, X_{ik} the site occupancy of the cation *i* on the *k-th* sublattice, and *c* the total number of cations *i*.

Moreover, including the temperature and pressure dependence, the complete expression for every W parameter becomes:

$$W_G = W_H + T \cdot W_S + P \cdot W_V \tag{6.20}$$

Examination of Eq. (6.18) and (6.20) clearly shows that G^{ex} has a linear dependence in the Margules parameters W, i.e.:

$$G^{ex} \Rightarrow \textbf{linear in unknowns (}\boldsymbol{W}\textbf{'s)} \tag{6.21}$$

For the $G^{e\text{-}m}$ part of G^{ϕ} as explained in chapter 2 a general expression like the one for G^{ex} cannot be used. The $G^{e\text{-}m}$ expression has instead to be sorted out case by case, and in general different phases might have different $G^{e\text{-}m}$ expressions. However, regardless how many and what types of phases are included in the system, $G^{e\text{-}m}$ will always have the form:

$$G^{e\text{-}m} = \sum_{i=1}^{m} \Psi^i \times G^{o,i} \quad (i = 1,....,m) \tag{6.22}$$

with:

m = total number of end-members needed to fully derive [28]$G^{e\text{-}m}$,

where, Ψ^i indicates the probability of occurrence of the *i'th* end-member configuration (see also section 2.6).

Some examples of $G^{e\text{-}m}$ for pyroxene, olivine and spinel phases have been presented in other parts of this work (e.g. section 2.8). What is relevant in this context is the fact that Ψ^i is always only a function of input parameters $\left(X_{ik}^{\phi}\right)$and that the *E unknowns* are all contained in G^o.

[28] Note that for 'pure' phases (e.g. quartz), m =1 and $G^{\phi} = G^{e-m} \equiv G^o$.

Unlike Ψ^i, the expression of G^o is invariant for any end-member i in every phase ϕ of the system. The adopted expression of G^o is given by:

$$G^o = \Delta_f H^o_{298K,1bar} - T \cdot S^o_{298K,1bar} + \int_{298K}^{T} C_P dT - T \int_{298K}^{T} \frac{C_P}{T} dT + \int_{1bar}^{P} V dP \tag{6.23}$$

with:

$$C_P = A + B \cdot T + C \cdot T^{-2} + D \cdot T^{-1/2} + E \cdot T^2 + F \cdot T^{-3} \tag{6.24}$$

and

$$V = V_{298K,1bar} + \alpha V_{298K,1bar}(T - 298) - \beta V_{298K,1bar} \cdot P \tag{6.25}$$

The end-member (*E*) *unknown*s, all found among Eq. (6.23), (6.24) and (6.25), are given by:

$$\Delta_f H,\ S^o,\ A,\ B,\ C,\ D,\ E,\ F,\ V,\ \alpha,\ \beta. \tag{6.26}$$

Substituting Eq. (6.24) and (6.25) into Eq. (6.23) one obtains:

$$\begin{aligned} G^o = {} & \Delta_f H^o_{298K,1bar} - T \cdot S^o_{298K,1bar} \\ & + A \cdot \left[(T - 298) - T \ln \frac{T}{298} \right] + B \cdot \left[\frac{1}{2}\left(T^2 - 298^2\right) - T(T - 298) \right] \\ & + C \cdot \left[\left(\frac{1}{298} - \frac{1}{T} \right) - \frac{T}{2}\left(\frac{1}{298^2} - \frac{1}{T^2} \right) \right] + D \cdot \left[2\left(T^{1/2} - 298^{1/2} \right) - 2T\left(\frac{1}{298^{1/2}} - \frac{1}{T^{1/2}} \right) \right] \\ & + E \cdot \left[\frac{1}{3}\left(T^3 - 298^3\right) - \frac{T}{2}\left(T^2 - 298^2\right) \right] + F \cdot \left[\frac{1}{2}\left(\frac{1}{298^2} - \frac{1}{T^2} \right) - \frac{T}{3}\left(\frac{1}{298^3} - \frac{1}{T^3} \right) \right] \\ & + V_{298K,1bar} \cdot P + \alpha V_{298K,1bar}(T - 298) \cdot P - \beta V_{298K,1bar} \cdot \frac{P^2}{2} \end{aligned} \tag{6.27}$$

Note that all terms bracketed, such as $\left[(T - 298) - T \ln \frac{T}{298} \right]$, as well as P and $\frac{P^2}{2}$ are function of input parameters T and/or P.

Now setting:

$$z_1 = 1 \tag{6.28}$$

$$z_2 = T \tag{6.29}$$

$$z_3 = \left[(T - 298) - T\, ln \frac{T}{298} \right] \tag{6.30}$$

$$z_4 = \left[\frac{1}{2}\left(T^2 - 298^2\right) - T(T - 298) \right] \tag{6.31}$$

$$z_5 = \left[\left(\frac{1}{298} - \frac{1}{T} \right) - \frac{T}{2}\left(\frac{1}{298^2} - \frac{1}{T^2} \right) \right] \tag{6.32}$$

$$z_6 = \left[2\left(T^{1/2} - 298^{1/2} \right) - 2T\left(\frac{1}{298^{1/2}} - \frac{1}{T^{1/2}} \right) \right] \tag{6.33}$$

$$z_7 = \left[\frac{1}{3}\left(T^3 - 298^3\right) - \frac{T}{2}\left(T^2 - 298^2\right) \right] \tag{6.34}$$

$$z_8 = \left[\frac{1}{2}\left(\frac{1}{298^2} - \frac{1}{T^2} \right) - \frac{T}{3}\left(\frac{1}{298^3} - \frac{1}{T^3} \right) \right] \tag{6.35}$$

$$z_9 = P \tag{6.36}$$

$$z_{10} = (T - 298) \tag{6.37}$$

$$z_{11} = \frac{P^2}{2} \tag{6.38}$$

And substituting Eq. (6.28-6.38) into Eq (6.27) the simplified expression of G^o is obtained:

$$\begin{aligned} G^o = {} & \Delta_f H^o_{298K,1bar} \cdot z_1 - S^o_{298K,1bar} \cdot z_2 + A \cdot z_3 + B \cdot z_4 + C \cdot z_5 + D \cdot z_6 \\ & + E \cdot z_7 + F \cdot z_8 + V \cdot z_9 + \alpha V \cdot z_{10} + \beta V \cdot z_{11} \end{aligned} \tag{6.39}$$

Similarly to the G^{ex}-*W's* relationship, examination of (6.27) reveals that, for fixed T and P, G^o (and therefore $G^{e\text{-}m}$) has a linear dependence in the end-member (E) *unknown*s, i.e.:

$G^{e\text{-}m} \Rightarrow$ **linear in *unknowns* (*E's*)** (6.40)

The natural consequence of Eq. (6.21) and Eq. (6.40) is that for any phase ϕ in the system there is always a linear dependence of G^{ϕ} with respect to the *inverse* problem *unknowns* (*E's* and *W's*), i.e.:

G^{ϕ} $\Rightarrow$ **linear in inverse *unknowns* (*E's* & *W's*)** (6.41)

Furthermore in Eq. (6.17), since G^{ϕ} is linear on the *E's* and *W's* and n^{ϕ}'s X_{ik}^{ϕ}'s are in this case input parameters, it follows that also the derivative(s) of G^{ϕ} with respect to the X_{ik}^{ϕ}'s, i.e. $\left(\frac{\partial G^{\phi}}{\partial X_{ik}^{\phi}} \right)$, will be linearly dependent on the *E's*, i.e.:

$$n^{\phi} \frac{\partial G^{\phi}}{\partial X_{ik}^{\phi}} \quad \Rightarrow \textbf{linear in inverse unknowns (}\boldsymbol{E\text{'}s}\textbf{ \& }\boldsymbol{W\text{'}s}\textbf{)} \tag{6.42}$$

Finally, it is necessary to establish the nature of dependence of Eq. (6.16) and Eq. (6.17) respect to the *Lagrangian unknown*s.

In Eq. (6.16) *Lagrangian unknown*s appear within the term:

$$\sum_{i=1}^{c} \gamma_i \left(\sum_{k=1}^{n} X_{ik}^{\phi} \right)$$

while in Eq. (6.17) they have the form:

$$\gamma_i n^{\phi}, \lambda_k^{\phi}, \beta_i \rho^{\phi}, \delta_{\omega}^{\phi} \frac{\partial C_{\omega}}{\partial X_{ik}^{\phi}}$$

Since in the *inverse* problem $\sum_{k=1}^{n} X_{ik}^{\phi}, n^{\phi}, \beta_i, \frac{\partial C_{\omega}}{\partial X_{ik}^{\phi}}$ are all known quantities, Eq. (6.16) and Eq. (6.17) are linearly dependent on $\gamma_i, \lambda_k^{\phi}, \rho^{\phi}, \delta_{\omega}^{\phi}$'s, i.e.:

$$\frac{\partial L}{\partial n^{\phi}} \,\&\, \frac{\partial L}{\partial X_{ik}^{\phi}} \quad \Rightarrow \textbf{linear in inverse unknowns } \gamma_i, \lambda_k^{\phi}, \rho^{\phi}, \delta_{\omega}^{\phi} \tag{6.43}$$

It is emphasized that the important conclusion to be drawn from the mathematical formulation of the *inverse* problem is that for a given set of input parameters $\left(X_{ik}^{\phi}, n^{\phi} \right)$ and

fixed *T, P*, the *Lagrangian* function *L* that is minimized is linear in all the system *unknowns* (*E's, W's* and *Lagrangian* multipliers). This means that the problem corresponds to a '*linear inverse problem*' and in this aspect it is a lot simpler than the GFEM problem of chapter 3 (summarized in section 6.2). As a consequence, in order to solve the *inverse* problem there is no need to adopt particularly sophisticated techniques and more traditional numerical techniques can be used (see section 6.6).

6.4 Structure of the Linear System of equations

In the previous section the linear nature of the *inverse* problem was shown. The next step is to see how the series of linear equations can be properly set up to reach a solution.

A difficulty to overcome arises from the fact that to solve the *inverse* problem numerical methods will be employed outside the field in which they were developed. In order to implement them, the problem needs to be formulated in a 'mathematical' way. Therefore, suitable computer codes have to be developed.

In general, a set of linear algebraic equations looks like (Press et al., 1992):

$$\begin{aligned}
&a_{11}x_1 + a_{12}x_2 + a_{13}x_3 + ... + a_{1t}x_t = b_1 \\
&a_{21}x_1 + a_{22}x_2 + a_{23}x_3 + ... + a_{2t}x_t = b_2 \\
&a_{31}x_1 + a_{32}x_2 + a_{33}x_3 + ... + a_{3t}x_t = b_3 \\
&\cdots\cdots \quad \cdots\cdots \quad \cdots\cdots \quad \cdots\cdots \quad \cdots\cdots \quad \cdots\cdots \\
&a_{m1}x_1 + a_{m2}x_2 + a_{m3}x_3 + ... + a_{mt}x_t = b_m
\end{aligned} \tag{6.44}$$

Where the *unknown*s x_j (j =1, 2, …., t) are related by m equations. In these equations the coefficients a_{ij} (i = 1, 2, …., m; j = 1, 2, …., t) have known values as do the right-hand side quantities b_i (i = 1, 2, …., m).

In this study, in a general case, there are a number (*ndata*) of datasets containing the input parameters (*T, P,* X_{ik}^{ϕ} , n^{ϕ}). From each dataset a number *nd* of equations are obtained which directly correspond to Eq. (6.16) and Eq. (6.17). The type of system each dataset refers to determines the number *nd* of equations obtained. Therefore, this number is a direct

function of the system from a compositional point of view (i.e. how many and what type of oxides characterize the system), and depends on the number and type of phases present in the system.

For each dataset, related by the *nd* equations, there are *nv* + *m unknown*s. Where *nv* indicates the end-member (*E*) and Margules (*W*) *unknown*s, while *m* represents the *Lagrangian unknown*s. Notice that although one is only interested in determining the value of the *nv unknown*s, the system has to be solved for all *m*+*nv unknown*s simultaneously[29]. The number and the type of *Lagrangian unknown*s *m* vary depending on the system considered. On the other hand the number and type of *nv* parameters have to be selected by the operator.

As a consequence, for each dataset the linear system of Eq. (6.44) will look like:

$$
\begin{aligned}
&a_{11}x_1 + a_{12}x_2 + ...+ a_{1nv}x_{nv} + a_{1nv+1}x_{nv+1} + a_{1nv+2}x_{nv+2} + ...+ a_{1nv+m}x_{nv+m} = b_1 \\
&a_{21}x_1 + a_{22}x_2 + ...+ a_{2nv}x_{nv} + a_{2nv+1}x_{nv+1} + a_{2nv+2}x_{nv+2} + ...+ a_{2nv+m}x_{nv+m} = b_2 \\
&a_{31}x_1 + a_{32}x_3 + ...+ a_{3nv}x_{nv} + a_{3nv+1}x_{nv+1} + a_{3nv+2}x_{nv+2} + ...+ a_{3nv+m}x_{nv+m} = b_3 \\
&\cdots\cdots\ \cdots\cdots\ \cdots\cdots\ \cdots\cdots\ \cdots\cdots\ \cdots\cdots\ \cdots\cdots\ \cdots\cdots\ \cdots\cdots\ \cdots\cdots\ \cdots\cdots \\
&a_{nd1}x_1 + a_{nd2}x_2 + ...+ a_{ndnv}x_{nv} + a_{ndnv+1}x_{nv+1} + a_{ndnv+2}x_{nv+2} + ...+ a_{ndnv+m}x_{nv+m} = b_{nd}
\end{aligned}
\qquad (6.45)
$$

Schematically, the structure of the *inverse* problem can be outlined as:

ndata = number of datasets that contain the input parameters (T, P, X_{ik}^{ϕ}, n^{ϕ}).

For each dataset:

nd = number of equations in inversion,

m = number of *Lagrangian unknown*s,

nv = number of *E* & *W unknown*s,

nd, m $\Rightarrow$ depend on the case being considered,

nv $\Rightarrow$ operator's choice.

[29] This is not necessarily true as the *Lagrangian unknowns* could be eliminated analytically, reducing the size of the system to solve. In Appendix 6B the procedure is described that has been followed to write the codes needed to do this operation. These codes have been included in the program '*GibInv*' and they could be used at any time. However, in several tests of the program (see also section 6.9), the size of the system did not appear to be so big that it is a problem to keep the *Lagrangian* variables in. In the rest of this argument it is assumed that the system will be solved for all *m*+*nv unknown*s.

6.5 Examples of the linear system structure

At this point it might be useful to clarify with some examples how the *inverse* problem will be set up in some real cases. This is done by examining five cases in detail.

In particular in ***caseI***, ***caseII*** and ***caseIII***, it will be shown how, depending on the system considered (i.e. chemical composition, number and type of phases), the *Lagrangian* function *L* looks like, how many equations *nd* for each dataset need to be solved, and how many and what type of *m unknown*s have to be included. Furthermore in ***caseIV*** (divided into ***caseIV***^{a} and ***caseIV***^{b}) and ***caseV*** it will be assumed that, given the *Lagrangian* function of ***caseI***, respectively one or two *nv unknown*s are selected to be fitted. In these two cases the *nd* equations to solve will be explicitly derived.

To maintain the continuity of the writing only ***caseI*** and ***caseIV***^{a} are here reported, while ***caseII***, ***caseIII***, ***caseIV***^{b}, and ***caseV*** are reported in Appendix 6.

Both ***caseI*** and ***caseIV***^{a} will involve only pyroxene phases. Before examining these specific cases in detail it is opportune to briefly review type and number of constraints that have to be imposed on pyroxene phases in a general case (see also section 3.4).

In chapter 3 it was shown that the site occupancies for both *opx* and *cpx* phases can be, in a general case, represented as in Table 6.1:

Table 6.1. Cation distribution in pyroxene phase

cation	charge	$^{(a)}$site: M2	$^{(a)}$site: M1	$^{(a)}$site: T
Na	1+	X_{11}	#	#
Ca	2+	X_{21}	#	#
Mg	2+	X_{31}	X_{32}	#
Fe^{2+}	2+	X_{41}	X_{42}	#
Al	3+	#	X_{52}	X_{53}
Cr	3+	#	X_{62}	X_{63}
Fe^{3+}	3+	#	X_{72}	X_{73}
Si	4+	#	#	X_{83}
Ti	4+	#	#	X_{93}

Notes: $^{(a)}$ In the pyroxene's structure cations can be found on three energetically different types of sites:
M2 = distorted octahedral site (1 per formula unit)
M1 = octahedral site (1 per formula unit)
T = tetrahedral site (2 per formula unit)
This leads to the pyroxene general formula: $M2_1M1_1T_2O_6$.

In each phase, on a molar scale, the total amount of every cation i, N_i, is given by the horizontal sum across sites. For example total amount of Ca, (i.e. N_{Ca}) in one mole of *opx*:

$$N_{Ca}^{opx} = X_{21}^{opx} \tag{6.46}$$

Total amount of Mg, (i.e. N_{Mg}) in one mole of *cpx*:

$$N_{Mg}^{cpx} = X_{31}^{cpx} + X_{32}^{cpx} \tag{6.47}$$

And so on for all the other cations i.

The vertical sums of the sites in Table 6.1 give instead for both *opx* and *cpx* the **stoichiometry** constraints, i.e.:

$$X_{11}^{px} + X_{21}^{px} + X_{31}^{px} + X_{41}^{px} = S_{M2}^{px} = 1 \tag{6.48}$$
$$X_{32}^{px} + X_{42}^{px} + X_{52}^{px} + X_{62}^{px} + X_{72}^{px} = S_{M1}^{px} = 1 \tag{6.49}$$
$$X_{53}^{px} + X_{63}^{px} + X_{73}^{px} + X_{83}^{px} + X_{93}^{px} = S_{T}^{px} = 2 \tag{6.50}$$

For both *opx* and *cpx* there are **ratio constraints** to account for the random partitioning of the same cation among different sites. For instance, to impose that Mg and Fe^{2+} have an equal distribution between M2 and M1:

$$\frac{X_{31}^{px}}{X_{31}^{px} + X_{41}^{px}} = \frac{X_{32}^{px}}{X_{32}^{px} + X_{42}^{px}} \tag{6.51}$$

And similarly for Al, Cr and Fe^{3+} between M1 and T sites.

Finally, there are **charge balance** constraints. For both *opx* and *cpx* the crystal chemical formula is given by:

$$\left(X_{11}^{px}, X_{21}^{px}, X_{31}^{px}, X_{41}^{px}\right)_1^{M2}\left(X_{32}^{px}, X_{42}^{px}, X_{52}^{px}, X_{62}^{px}, X_{72}^{px}\right)_1^{M1}\left(X_{53}^{px}, X_{63}^{px}, X_{73}^{px}, X_{83}^{px}, X_{93}^{px}\right)_2^{T} O_6 \qquad (6.52)$$

Since there are six oxigens per formula unit, to satisfy the neutrality of the chemical formula it must be:

$$\begin{aligned}
&\left[1^+ \cdot \left(X_{11}^{px}\right)\right]+ \\
&\left[2^+ \cdot \left(X_{21}^{px}\right)\right]+\left[2^+ \cdot \left(X_{31}^{px}+X_{32}^{px}\right)\right]+\left[2^+ \cdot \left(X_{41}^{px}+X_{42}^{px}\right)\right]+ \\
&\left[3^+ \cdot \left(X_{52}^{px}+X_{53}^{px}\right)\right]+\left[3^+ \cdot \left(X_{62}^{px}+X_{63}^{px}\right)\right]+\left[3^+ \cdot \left(X_{72}^{px}+X_{73}^{px}\right)\right]+ \\
&\left[4^+ \cdot \left(X_{83}^{px}\right)\right]+\left[4^+ \cdot \left(X_{93}^{px}\right)\right] \\
&= C^{px} = 12
\end{aligned} \qquad (6.53)$$

The two examples ***caseI*** and ***caseIV^a*** are now reported.

6.5.1 CaseI

CaO-MgO-SiO_2 (i.e. CMS) system

2 phases: *opx* + *cpx*

In ***caseI*** it is assumed that the only cations present in the system are Ca, Mg and Si. This means that the general Table 6.1 will then reduce to Table 6.2:

Table 6.2. Cation distribution in pyroxene phase for ***caseI***

cation	charge	site: M2	site: M1	site: T
Ca	2+	X_{21}	#	#
Mg	2+	X_{31}	X_{32}	#
Si	4+	#	#	X_{83}

Due to the simplicity of the system only some of the constraints listed for the general case need to be included. These are:

mass balance for every cation *i* in the system.

$$\text{Ca} \Rightarrow n^{opx} \cdot X_{21}^{opx} + n^{cpx} \cdot X_{21}^{cpx} = M_{Ca} \tag{6.53}$$

$$\text{Mg} \Rightarrow n^{opx} \cdot \left(X_{31}^{opx} + X_{32}^{opx}\right) + n^{cpx} \cdot \left(X_{31}^{cpx} + X_{32}^{cpx}\right) = M_{Mg} \tag{6.54}$$

$$\text{Si} \Rightarrow n^{opx} \cdot X_{83}^{opx} + n^{cpx} \cdot X_{83}^{cpx} = M_{Si} \tag{6.55}$$

stoichiometry on every sublattice (i.e. M2, M1, T) for both *cpx* and *opx*.

$$X_{11}^{opx} + X_{21}^{opx} + X_{31}^{opx} + X_{41}^{opx} = S_{M2}^{opx} = 1 \tag{6.56}$$

$$X_{32}^{opx} + X_{42}^{opx} + X_{52}^{opx} + X_{62}^{opx} + X_{72}^{opx} = S_{M1}^{opx} = 1 \tag{6.57}$$

$$X_{53}^{opx} + X_{63}^{opx} + X_{73}^{opx} + X_{83}^{opx} + X_{93}^{opx} = S_{T}^{opx} = 2 \tag{6.58}$$

$$X_{11}^{cpx} + X_{21}^{cpx} + X_{31}^{cpx} + X_{41}^{cpx} = S_{M2}^{cpx} = 1 \tag{6.59}$$

$$X_{32}^{cpx} + X_{42}^{cpx} + X_{52}^{cpx} + X_{62}^{cpx} + X_{72}^{cpx} = S_{M1}^{cpx} = 1 \tag{6.60}$$

$$X_{53}^{cpx} + X_{63}^{cpx} + X_{73}^{cpx} + X_{83}^{cpx} + X_{93}^{cpx} = S_{T}^{cpx} = 2 \tag{6.61}$$

At the same time no **ratio constraints** are needed, while **charge balance** constraints are always automatically satisfied by **stoichiometry**.

The number and type of *Lagrangian unknown*s to be included in the *L* function depends on the case considered. Here, given equations (6.53-6.61), there will be nine *m unknown*s: three **mass balance**, 'γ', and six **stoichiometry**, 'λ'.

To fully derive the *Lagrangian* function *L* the complete expression of $\mathbf{G}^{\mathbf{system}}$ is also needed.

In this two-pyroxene CMS system, $\mathbf{G}^{\mathbf{system}}$ is given by:

$$\mathbf{G}^{\mathbf{system}} = n^{opx} G^{\phi - opx} + n^{cpx} G^{\phi - cpx} \tag{6.62}$$

Where, G^{ϕ} is expressed by eq (6.3), i.e.:

$$G^{\phi} = G^{end-members} + G^{ideal} + G^{excess}$$

Expression of $G^{e-m-opx}$, G^{id-opx} and G^{ex-opx} for both *cpx* and *opx* phases can be assumed to have the same form[30], i.e.:

$$G^{e-m-opx} = X_{21}^{opx} \cdot G_{Di}^{o-opx} + \left(1 - X_{21}^{opx}\right) \cdot G_{En}^{o-opx} \tag{6.63}$$

$$^{31}\, G^{id} = \left(X_{21}^{'-opx} ln X_{21}^{'-opx} + X_{31}^{'-opx} ln X_{31}^{'-opx} + X_{32}^{'-opx} ln X_{32}^{'-opx} + 2X_{83}^{'-opx} ln X_{83}^{'-opx}\right) \cdot RT \tag{6.64}$$

$$G^{ex} = X_{21}^{'-opx} X_{31}^{'-opx} \left(X_{21}^{'-opx}\right) \cdot W_{Mg-Ca}^{M2-opx} + X_{31}^{'-opx} X_{21}^{'-opx} \left(X_{31}^{'-opx}\right) \cdot W_{Ca-Mg}^{M2-opx} \tag{6.65}$$

For the *cpx* the equivalent $G^{e-m-cpx}, G^{id-cpx}, G^{ex-cpx}$ equations can be directly obtained from Eqs. (6.63), (6.64) and (6.65), simply changing the superscript from *opx* to *cpx*.

---

[30] Expression of $G^{\phi\text{-}ex}$ for *opx* and *cpx* could actually slightly differ. In most cases for the *opx* solid solution the symmetric model is adopted, while for the *cpx* the asymmetric model is preferred. This would require a difference in the $G^{\phi\text{-}ex}$ formulation. However, the symmetric model can be considered a simplified case of the asymmetric, from which it can easily be derived. In this specific case, for instance, to swap from asymmetric to symmetric one simply needs to impose: $W_{Ca-Mg} = W_{Mg-Ca}$. Accordingly, the more generic asymmetric formulation of $G^{\phi\text{-}ex}$ is adopted here.

[31] In this case $X_{32}^{'-opx} = X_{83}^{'-opx} \equiv 1$ as a consequence $X_{32}^{'-opx}\, ln\, X_{32}^{'-opx} = X_{83}^{'-opx}\, ln\, X_{83}^{'-opx} \equiv 0$. Since the contribution of these terms to the G^{id} part of $G^{\phi\text{-}opx}$ is equal to zero, they could be omitted from the calculation of $G^{\phi\text{-}opx}$. However, when solving the *inverse* problem it is necessary to calculate not only G^{ϕ} but also the derivatives of G^{ϕ}, and of $G^{e\text{-}m}$, G^{id} and G^{ex}, with respect to the site occupancies. It can easily be proved that the derivative of G^{id} respect to a site occupancy can be ≠ 0 even when the contribution of that site to G^{id} is equal to zero. For instance, if $X_{32}^{'} = 1 \Rightarrow X_{32}^{'}\, ln\, X_{32}^{'} = 0$, but also $\frac{\delta\left(X_{32}^{'}\, ln\, X_{32}^{'}\right)}{\delta X_{32}} = \left(1 + ln\, X_{32}^{'}\right) = 1$. Consequently, the $X_{32}^{'}\, ln\, X_{32}^{'}$ and $2X_{83}^{'}\, ln\, X_{83}^{'}$ terms must be included in the $G^{\phi\text{-}id}$ expression.

Recalling Eq. (6.10), the *Lagrangian* function L in this case will then be:

$$\begin{aligned}
L = {} & n^{opx} G^{\phi-opx} + n^{cpx} G^{\phi-cpx} \\
& + \left\{\left[n^{opx} \times \left(X_{21}^{opx}\right) + n^{cpx} \times \left(X_{21}^{cpx}\right)\right] - M_{Ca}\right\} \times \gamma_{Ca} \\
& + \left\{\left[n^{opx} \times \left(X_{31}^{opx} + X_{32}^{opx}\right) + n^{cpx} \times \left(X_{31}^{cpx} + X_{32}^{cpx}\right)\right] - M_{Mg}\right\} \times \gamma_{Mg} \\
& + \left\{\left[n^{opx} \times \left(X_{83}^{opx}\right) + n^{cpx} \times \left(X_{83}^{cpx}\right)\right] - M_{Si}\right\} \times \gamma_{Si} \\
& + \left[\left(X_{21}^{opx} + X_{31}^{opx}\right) - S_{M2}^{opx}\right] \times \lambda_{M2}^{opx} \\
& + \left[\left(X_{21}^{cpx} + X_{31}^{cpx}\right) - S_{M2}^{cpx}\right] \times \lambda_{M2}^{cpx} \\
& + \left[\left(X_{32}^{opx}\right) - S_{M1}^{opx}\right] \times \lambda_{M1}^{opx} \\
& + \left[\left(X_{32}^{cpx}\right) - S_{M1}^{cpx}\right] \times \lambda_{M1}^{cpx} \\
& + \left[\left(X_{83}^{opx}\right) - S_{T}^{opx}\right] \times \lambda_{T}^{opx} \\
& + \left[\left(X_{83}^{cpx}\right) - S_{T}^{cpx}\right] \times \lambda_{T}^{cpx}
\end{aligned} \tag{6.66}$$

Replacing in Eq. (6.66) $G^{\phi\text{-}opx}$ and $G^{\phi\text{-}cpx}$ with the appropriate expressions of G^{e-m}, G^{id} and G^{ex} yields:

$$\begin{aligned}
L = {} & n^{opx} \cdot \begin{bmatrix} X_{21}^{opx} \cdot G_{Di}^{o-opx} + \left(1 - X_{21}^{opx}\right) \cdot G_{En}^{o-opx} \\ + \left(X_{21}^{'-opx} \, ln X_{21}^{'-opx} + X_{31}^{'-opx} \, ln X_{31}^{'-opx} + X_{32}^{'-opx} \, ln X_{32}^{'-opx} + 2X_{83}^{'-opx} \, ln X_{83}^{'-opx}\right) \cdot RT \\ + X_{21}^{'-opx} X_{31}^{'-opx}\left(X_{21}^{'-opx}\right) \cdot W_{Mg-Ca}^{M2-opx} + X_{31}^{'-opx} X_{21}^{'-opx}\left(X_{31}^{'-opx}\right) \cdot W_{Ca-Mg}^{M2-opx} \end{bmatrix} \\
& + n^{cpx} \cdot \begin{bmatrix} X_{21}^{cpx} \cdot G_{Di}^{o-cpx} + \left(1 - X_{21}^{cpx}\right) \cdot G_{En}^{o-cpx} \\ + \left(X_{21}^{'-cpx} \, ln X_{21}^{'-cpx} + X_{31}^{'-cpx} \, ln X_{31}^{'-cpx} + X_{32}^{'-cpx} \, ln X_{32}^{'-cpx} + 2X_{83}^{'-cpx} \, ln X_{83}^{'-cpx}\right) \cdot RT \\ + X_{21}^{'-cpx} X_{31}^{'-cpx}\left(X_{21}^{'-cpx}\right) \cdot W_{Mg-Ca}^{M2-cpx} + X_{31}^{'-cpx} X_{21}^{'-cpx}\left(X_{31}^{'-cpx}\right) \cdot W_{Ca-Mg}^{M2-cpx} \end{bmatrix} \\
& + \left\{\left[n^{opx} \times \left(X_{21}^{opx}\right) + n^{cpx} \times \left(X_{21}^{cpx}\right)\right] - M_{Ca}\right\} \times \gamma_{Ca} \\
& + \left\{\left[n^{opx} \times \left(X_{31}^{opx} + X_{32}^{opx}\right) + n^{cpx} \times \left(X_{31}^{cpx} + X_{32}^{cpx}\right)\right] - M_{Mg}\right\} \times \gamma_{Mg} \\
& + \left\{\left[n^{opx} \times \left(X_{83}^{opx}\right) + n^{cpx} \times \left(X_{83}^{cpx}\right)\right] - M_{Si}\right\} \times \gamma_{Si} \\
& + \left[\left(X_{21}^{opx} + X_{31}^{opx}\right) - S_{M2}^{opx}\right] \times \lambda_{M2}^{opx} \\
& + \left[\left(X_{21}^{cpx} + X_{31}^{cpx}\right) - S_{M2}^{cpx}\right] \times \lambda_{M2}^{cpx} \\
& + \left[\left(X_{32}^{opx}\right) - S_{M1}^{opx}\right] \times \lambda_{M1}^{opx} \\
& + \left[\left(X_{32}^{cpx}\right) - S_{M1}^{cpx}\right] \times \lambda_{M1}^{cpx} \\
& + \left[\left(X_{83}^{opx}\right) - S_{T}^{opx}\right] \times \lambda_{T}^{opx} \\
& + \left[\left(X_{83}^{cpx}\right) - S_{T}^{cpx}\right] \times \lambda_{T}^{cpx}
\end{aligned} \tag{6.67}$$

Once the expression of L has been derived, the next step is to determine how many equations *nd* must be solved. As already seen for the *Lagrangian unknown*s *m*, the number *nd* also depends on the case being considered. Here there are two phases (*opx* and *cpx*) with four site occupancies $\left(X_{21}, X_{31}, X_{32}, X_{83}\right)$ for each phase. As a consequence, recalling Eqs. (6.16) and (6.17) and applying them to this system, there will be a total number of ten equations (i.e. *nd* = 10) to be solved for each dataset. The ten equations will be obtained from the following differentiations:

$$\frac{\delta L}{\delta X_{21}^{opx}}, \frac{\delta L}{\delta X_{21}^{cpx}}, \frac{\delta L}{\delta X_{31}^{opx}}, \frac{\delta L}{\delta X_{31}^{cpx}}, \frac{\delta L}{\delta X_{32}^{opx}}, \frac{\delta L}{\delta X_{32}^{cpx}}, \frac{\delta L}{\delta X_{83}^{opx}}, \frac{\delta L}{\delta X_{83}^{cpx}}, \frac{\delta L}{\delta n^{opx}}, \frac{\delta L}{\delta n^{cpx}} \tag{6.68}$$

Later in ***caseIV*** explicit examples of such equations will be presented.

To summarize in this ***caseI*** for each dataset:

- *Lagrange* function to minimize is given by Eq. (6.67)
- Number of *Lagrangian unknowns* equal to nine (i.e. *m* = 9)
- Number of data equations equal to ten (i.e. *nd* = 10)

Note that in this specific case the ten data equations derived from each input data are not totally independent due to the presence of nine constraints in the system (i.e. three **mass balance** and six **stoichiometry** constraints). This means that there will be only one '*piece*' of independent information left to solve the *inverse* problem. In section 6.8.2 the important consequence of this issue will be discussed.

6.5.4 CaseIV

CMS	system
2 phases:	*opx* + *cpx*

This example is divided in two parts: ***caseIV***^{a} and ***caseIV***^{b}.

In ***caseIV^a*** the explicit derivation of each one of the ten equations that compose the linear system of equations of ***caseI*** is presented.

In ***caseIV^b*** it is assumed that the *inverse* problem has to be solved for one specific *nv* (i.e. either *E* or *W*) *unknown*. It will then be shown what form the linear system of equations would take in this 'real' case.

CaseIV^a

The ten equations that for each dataset have to be solved are those listed in Eq. (6.68):

$$\frac{\delta L}{\delta X_{21}^{opx}},\frac{\delta L}{\delta X_{21}^{cpx}},\frac{\delta L}{\delta X_{31}^{opx}},\frac{\delta L}{\delta X_{31}^{cpx}},\frac{\delta L}{\delta X_{32}^{opx}},\frac{\delta L}{\delta X_{32}^{cpx}},\frac{\delta L}{\delta X_{83}^{opx}},\frac{\delta L}{\delta X_{83}^{cpx}},\frac{\delta L}{\delta n^{opx}},\frac{\delta L}{\delta n^{cpx}}$$

Where, the full expression of *L* is given by Eq. (6.67):

$$\begin{aligned}
L = {} & n^{opx}\cdot\begin{bmatrix} X_{21}^{opx}\cdot G_{Di}^{o-opx}+\left(1-X_{21}^{opx}\right)\cdot G_{En}^{o-opx} \\ +\left(X_{21}^{'-opx}\,ln\,X_{21}^{'-opx}+X_{31}^{'-opx}\,ln\,X_{31}^{'-opx}+X_{32}^{'-opx}\,ln\,X_{32}^{'-opx}+2X_{83}^{'-opx}\,ln\,X_{83}^{'-opx}\right)\cdot RT \\ +X_{21}^{'-opx}X_{31}^{'-opx}\left(X_{21}^{'-opx}\right)\cdot W_{Mg-Ca}^{M2-opx}+X_{31}^{'-opx}X_{21}^{'-opx}\left(X_{31}^{'-opx}\right)\cdot W_{Ca-Mg}^{M2-opx} \end{bmatrix} \\
& +n^{cpx}\cdot\begin{bmatrix} X_{21}^{cpx}\cdot G_{Di}^{o-cpx}+\left(1-X_{21}^{cpx}\right)\cdot G_{En}^{o-cpx} \\ +\left(X_{21}^{'-cpx}\,ln\,X_{21}^{'-cpx}+X_{31}^{'-cpx}\,ln\,X_{31}^{'-cpx}+X_{32}^{'-cpx}\,ln\,X_{32}^{'-cpx}+2X_{83}^{'-cpx}\,ln\,X_{83}^{'-cpx}\right)\cdot RT \\ +X_{21}^{'-cpx}X_{31}^{'-cpx}\left(X_{21}^{'-cpx}\right)\cdot W_{Mg-Ca}^{M2-cpx}+X_{31}^{'-cpx}X_{21}^{'-cpx}\left(X_{31}^{'-cpx}\right)\cdot W_{Ca-Mg}^{M2-cpx} \end{bmatrix} \\
& +\left\{\left[n^{opx}\times\left(X_{21}^{opx}\right)+n^{cpx}\times\left(X_{21}^{cpx}\right)\right]-M_{Ca}\right\}\times\gamma_{Ca} \\
& +\left\{\left[n^{opx}\times\left(X_{31}^{opx}+X_{32}^{opx}\right)+n^{cpx}\times\left(X_{31}^{cpx}+X_{32}^{cpx}\right)\right]-M_{Mg}\right\}\times\gamma_{Mg} \\
& +\left\{\left[n^{opx}\times\left(X_{83}^{opx}\right)+n^{cpx}\times\left(X_{83}^{cpx}\right)\right]-M_{Si}\right\}\times\gamma_{Si} \\
& +\left[\left(X_{21}^{opx}+X_{31}^{opx}\right)-S_{M2}^{opx}\right]\times\lambda_{M2}^{opx} \\
& +\left[\left(X_{21}^{cpx}+X_{31}^{cpx}\right)-S_{M2}^{cpx}\right]\times\lambda_{M2}^{cpx} \\
& +\left[\left(X_{32}^{opx}\right)-S_{M1}^{opx}\right]\times\lambda_{M1}^{opx} \\
& +\left[\left(X_{32}^{cpx}\right)-S_{M1}^{cpx}\right]\times\lambda_{M1}^{cpx} \\
& +\left[\left(X_{83}^{opx}\right)-S_{T}^{opx}\right]\times\lambda_{T}^{opx} \\
& +\left[\left(X_{83}^{cpx}\right)-S_{T}^{cpx}\right]\times\lambda_{T}^{cpx}
\end{aligned} \tag{6.67}$$

Note that in this case (see also Eq. 2.70, Eq. 6.18 and Eq. 6.19) it will be: $X'_{21} = X_{21}$, $X'_{31} = X_{31}$, $X'_{32} = X_{32}$, $X'_{83} = \frac{X_{83}}{2}$, for both *opx* and *cpx*.

The ten equations are now derived, following the order given by Eq. (6.68):

$$\frac{\partial L}{\partial X_{21}^{opx}} = n^{opx} \cdot \left[\begin{array}{l} G_{Di}^{o-opx} - G_{En}^{o-opx} + RT\left(1 + ln\, X_{21}^{'-opx}\right) \\ + 2X_{21}^{'-opx} X_{31}^{'-opx} \cdot W_{Mg-Ca}^{M2-opx} + \left(X_{31}^{'-opx}\right)^2 \cdot W_{Ca-Mg}^{M2-opx} \end{array} \right] \qquad (6.79)$$
$$+ n^{opx} \cdot \gamma_{Ca} + \lambda_{M2}^{opx}$$

Substituting G_{Di}^{o-opx} and G_{En}^{o-opx} into Eq. (6.79) with their full expression as given in Eq. (6.39) yields:

$$\frac{\partial L}{\partial X_{21}^{opx}} = n^{opx} \cdot \left[\begin{array}{l} \left(\begin{array}{l} \Delta_f H_{298K,1bar}^{o} \cdot z_1 - S_{298K,1bar}^{o} \cdot z_2 + A \cdot z_3 + B \cdot z_4 + C \cdot z_5 + D \cdot z_6 \\ + E \cdot z_7 + F \cdot z_8 + V \cdot z_9 + \alpha V \cdot z_{10} + \beta V \cdot z_{11} \end{array} \right)^{Di-opx} \\ - \left(\begin{array}{l} \Delta_f H_{298K,1bar}^{o} \cdot z_1 - S_{298K,1bar}^{o} \cdot z_2 + A \cdot z_3 + B \cdot z_4 + C \cdot z_5 + D \cdot z_6 \\ + E \cdot z_7 + F \cdot z_8 + V \cdot z_9 + \alpha V \cdot z_{10} + \beta V \cdot z_{11} \end{array} \right)^{En-opx} \\ RT\left(1 + ln X_{21}^{'-opx}\right) + 2X_{21}^{'-opx} X_{31}^{'-opx} \cdot W_{Mg-Ca}^{M2-opx} + \left(X_{31}^{'-opx}\right)^2 \cdot W_{Ca-Mg}^{M2-opx} \end{array} \right] \qquad (6.80)$$
$$+ n^{opx} \cdot \gamma_{Ca} + \lambda_{M2}^{opx} n^{opx}$$

Similarly all the other expressions are obtained. Only the final derivations are here reported.

$$\frac{\partial L}{\partial X_{21}^{cpx}} = n^{cpx}\cdot\left[\begin{array}{l}\left(\begin{array}{l}\Delta_f H^o_{298K,1bar}\cdot z_1 - S^o_{298K,1bar}\cdot z_2 + A\cdot z_3 + B\cdot z_4 + C\cdot z_5 + D\cdot z_6\\ \quad + E\cdot z_7 + F\cdot z_8 + V\cdot z_9 + \alpha V\cdot z_{10} + \beta V\cdot z_{11}\end{array}\right)^{Di-cpx}\\ -\left(\begin{array}{l}\Delta_f H^o_{298K,1bar}\cdot z_1 - S^o_{298K,1bar}\cdot z_2 + A\cdot z_3 + B\cdot z_4 + C\cdot z_5 + D\cdot z_6\\ \quad + E\cdot z_7 + F\cdot z_8 + V\cdot z_9 + \alpha V\cdot z_{10} + \beta V\cdot z_{11}\end{array}\right)^{En-cpx}\\ RT\left(1+ln X_{21}^{'-cpx}\right)+2X_{21}^{'-cpx}X_{31}^{'-cpx}\cdot W_{Mg-Ca}^{M2-cpx}+\left(X_{31}^{'-cpx}\right)^2\cdot W_{Ca-Mg}^{M2-cpx}\end{array}\right] + n^{cpx}\cdot\gamma_{Ca}+\lambda_{M2}^{cpx} \tag{6.81}$$

$$\frac{\partial L}{\partial X_{31}^{opx}} = \begin{array}{l} n^{opx}\cdot\left[RT\left(1+ln X_{31}^{'-opx}\right)+2X_{31}^{'-opx}X_{21}^{'-opx}\cdot W_{Ca-Mg}^{M2-opx}+\left(X_{21}^{'-opx}\right)^2\cdot W_{Mg-Ca}^{M2-opx}\right]\\ +n^{opx}\cdot\gamma_{Mg}+\lambda_{M2}^{opx}\end{array} \tag{6.82}$$

$$\frac{\partial L}{\partial X_{31}^{cpx}} = \begin{array}{l} n^{cpx}\cdot\left[RT\left(1+ln X_{31}^{'-cpx}\right)+2X_{31}^{'-cpx}X_{21}^{'-cpx}\cdot W_{Ca-Mg}^{M2-cpx}+\left(X_{21}^{'-cpx}\right)^2\cdot W_{Mg-Ca}^{M2-cpx}\right]\\ +n^{cpx}\cdot\gamma_{Mg}+\lambda_{M2}^{cpx}\end{array} \tag{6.83}$$

$$\frac{\partial L}{\partial X_{32}^{opx}} = n^{opx}\cdot RT\left(1+ln X_{32}^{'-opx}\right)+n^{opx}\cdot\gamma_{Mg}+\lambda_{M1}^{opx} \tag{6.84}$$

$$\frac{\partial L}{\partial X_{32}^{cpx}} = n^{cpx}\cdot RT\left(1+ln X_{32}^{'-cpx}\right)+n^{cpx}\cdot\gamma_{Mg}+\lambda_{M1}^{cpx} \tag{6.85}$$

$$\frac{\partial L}{\partial X_{83}^{opx}} = n^{opx}\cdot RT\left(1+ln X_{83}^{'-opx}\right)+n^{opx}\cdot\gamma_{Si}+\lambda_{T}^{opx} \tag{6.86}$$

$$\frac{\partial L}{\partial X_{83}^{cpx}} = n^{cpx}\cdot RT\left(1+ln X_{83}^{'-cpx}\right)+n^{cpx}\cdot\gamma_{Si}+\lambda_{T}^{cpx} \tag{6.87}$$

$$\frac{\partial L}{\partial n^{opx}} = X_{21}^{opx}\cdot\begin{pmatrix}\Delta_f H^o_{298K,1bar}\cdot z_1 - S^o_{298K,1bar}\cdot z_2 + A\cdot z_3 + B\cdot z_4 + C\cdot z_5\\ + D\cdot z_6 + E\cdot z_7 + F\cdot z_8 + V\cdot z_9 + \alpha V\cdot z_{10} + \beta V\cdot z_{11}\end{pmatrix}^{Di-opx}$$
$$+\left(1-X_{21}^{opx}\right)\cdot\begin{pmatrix}\Delta_f H^o_{298K,1bar}\cdot z_1 - S^o_{298K,1bar}\cdot z_2 + A\cdot z_3 + B\cdot z_4 + C\cdot z_5\\ + D\cdot z_6 + E\cdot z_7 + F\cdot z_8 + V\cdot z_9 + \alpha V\cdot z_{10} + \beta V\cdot z_{11}\end{pmatrix}^{En-opx}$$
$$+\left(X_{21}^{'-opx}\,ln X_{21}^{'-opx} + X_{31}^{'-opx}\,ln X_{31}^{'-opx} + X_{32}^{'-opx}\,ln X_{32}^{'-opx} + 2X_{83}^{'-opx}\,ln X_{83}^{'-opx}\right)\cdot RT \qquad (6.88)$$
$$+X_{21}^{'-opx}X_{31}^{'-opx}\left(X_{21}^{'-opx}\right)\cdot W_{Mg-Ca}^{M2-opx} + X_{31}^{'-opx}X_{21}^{'-opx}\left(X_{31}^{'-opx}\right)\cdot W_{Ca-Mg}^{M2-opx}$$
$$+X_{21}^{opx}\cdot\gamma_{Ca} + \left(X_{31}^{opx} + X_{32}^{opx}\right)\cdot\gamma_{Mg} + X_{83}^{opx}\cdot\gamma_{Si}$$

$$\frac{\partial L}{\partial n^{cpx}} = X_{21}^{cpx}\cdot\begin{pmatrix}\Delta_f H^o_{298K,1bar}\cdot z_1 - S^o_{298K,1bar}\cdot z_2 + A\cdot z_3 + B\cdot z_4 + C\cdot z_5\\ + D\cdot z_6 + E\cdot z_7 + F\cdot z_8 + V\cdot z_9 + \alpha V\cdot z_{10} + \beta V\cdot z_{11}\end{pmatrix}^{Di-cpx}$$
$$+\left(1-X_{21}^{cpx}\right)\cdot\begin{pmatrix}\Delta_f H^o_{298K,1bar}\cdot z_1 - S^o_{298K,1bar}\cdot z_2 + A\cdot z_3 + B\cdot z_4 + C\cdot z_5\\ + D\cdot z_6 + E\cdot z_7 + F\cdot z_8 + V\cdot z_9 + \alpha V\cdot z_{10} + \beta V\cdot z_{11}\end{pmatrix}^{En-cpx}$$
$$+\left(X_{21}^{'-cpx}\,ln X_{21}^{'-cpx} + X_{31}^{'-cpx}\,ln X_{31}^{'-cpx} + X_{32}^{'-cpx}\,ln X_{32}^{'-cpx} + 2X_{83}^{'-cpx}\,ln X_{83}^{'-cpx}\right)\cdot RT \qquad (6.89)$$
$$+X_{21}^{'-cpx}X_{31}^{'-cpx}\left(X_{21}^{'-cpx}\right)\cdot W_{Mg-Ca}^{M2-cpx} + X_{31}^{'-cpx}X_{21}^{'-cpx}\left(X_{31}^{'-cpx}\right)\cdot W_{Ca-Mg}^{M2-cpx}$$
$$+X_{21}^{cpx}\cdot\gamma_{Ca} + \left(X_{31}^{cpx} + X_{32}^{cpx}\right)\cdot\gamma_{Mg} + X_{83}^{cpx}\cdot\gamma_{Si}$$

In the examples presented in ***caseI-V*** it was always assumed the hypothetical datasets would refer to relatively simple systems. Datasets which refer to more complex systems would, of course, have a larger number of equations to solve and within them an increased number of *Lagrangian unknown*s. However, procedure and methodology described in this section, which lead in the examples proposed in ***caseI-V*** to the derivation of *L, n, m,* etc., can be extended and applied in the same way to any other system.

The very important point to emphasize is that the program can deal with any general case (i.e. any type and number of *nv unknowns* and datasets that refer to any type of system), without the need of explicitly writing in formulae for each case. Hence, one does not have to code up expressions for each case. This is because G^{ϕ} and $\left(\partial G^{\phi}\middle/\partial X_{ik}^{\phi}\right)$ can be evaluated for any set of input parameters and, since these two terms are linearly dependent on the *unknowns*, the coefficients a_{ij}'s can be evaluated by simply calculating G^{ϕ} and

$\left(\partial G^{\phi} \middle/ \partial X_{ik}^{\phi} \right)$ with inversion parameters set to either zero or one. In Appendix 6D the procedure followed to perform this operation is described.

6.6 Solving the *inverse* problem

In sections 6.4 and 6.5 the structure of the inverse problem has been defined and the procedure that has to be followed to derive the needed system of equations illustrated. The task is now to identify what is the appropriate numerical technique to solve the *inverse* problem.

6.6.1 Matrix representation of inverse equations

First of all, a simplified expression is used to represent the system of equations to solve, which, in its general formulation, was given in section 6.4 by Eq. (6.45). This proved to be quite straightforward. A linear set of equations such as that of Eq. (6.45) can be seen as the sum of a number *nd* of vector equations, each one having the form:

$$a_1 x_1 + a_2 x_2 + a_3 x_3 + ... + a_n x_n = b \tag{6.131}$$

As a result, the linear set of *nd* equations given by Eq. (6.45) can be re-written in a matrix form as:

$$A \cdot \underline{x} = \underline{b} \tag{6.132}$$

(NB Here the raised dot denotes matrix multiplication)

Where:

A = matrix of dimension $nd \times M$,

$\underline{x}$ = M vector of *unknowns*, (NB $M \equiv nv + m$)

$\underline{b}$ = nd vector of data.

The graphic representation of Eq. (6.45) in its matrix form will then be:

$$\begin{pmatrix} a_{11},\ldots\ldots,a_{1nv};a_{1nv+1},\ldots\ldots\ldots,a_{1nv+m} \\ a_{21},\ldots\ldots,a_{2nv};a_{2nv+1},\ldots\ldots\ldots,a_{2nv+m} \\ \ldots\ldots\ldots\ldots\ldots\ldots\ldots\ldots\ldots\ldots\ldots\ldots \\ \ldots\ldots\ldots\ldots\ldots\ldots\ldots\ldots\ldots\ldots\ldots\ldots \\ \ldots\ldots\ldots\ldots\ldots\ldots\ldots\ldots\ldots\ldots\ldots\ldots \\ \ldots\ldots\ldots\ldots\ldots\ldots\ldots\ldots\ldots\ldots\ldots\ldots \\ a_{nd1},\ldots,a_{ndnv};a_{ndnv+1},\ldots\ldots,a_{ndnv+m} \end{pmatrix} \times \begin{pmatrix} x_1 \\ \vdots \\ x_{nv} \\ --- \\ x_{nv+1} \\ \vdots \\ \vdots \\ x_{nv+m} \end{pmatrix} = \begin{pmatrix} b_1 \\ b_2 \\ \vdots \\ \vdots \\ \vdots \\ \vdots \\ b_{nd} \end{pmatrix} \tag{6.133}$$

$$A \qquad \underline{x} \qquad \underline{b}$$

To better clarify this issue it might be useful to examine a real case and see what form the matrix in Eq. (6.133) will take, for example considering a CMS two-pyroxene system in which it is assumed $\Delta_f H^{En\text{-}opx}$ to be the only *nv unknown*. In section 6.5.4 it was shown that in this specific case the linear system of equations that, for each dataset, has to be solved is given by Eq. (6.90):

$$a_{11}\Delta_f H^{En\text{-}opx}+a_{12}\gamma_{Ca}+a_{13}\gamma_{Mg}+a_{14}\gamma_{Si}+a_{15}\lambda_{M2}^{opx}+a_{16}\lambda_{M2}^{cpx}+a_{17}\lambda_{M1}^{opx}+a_{18}\lambda_{M1}^{cpx}+a_{19}\lambda_{T}^{opx}+a_{110}\lambda_{T}^{cpx}=b_1$$
$$a_{21}\Delta_f H^{En\text{-}opx}+a_{22}\gamma_{Ca}+a_{23}\gamma_{Mg}+a_{24}\gamma_{Si}+a_{25}\lambda_{M2}^{opx}+a_{26}\lambda_{M2}^{cpx}+a_{27}\lambda_{M1}^{opx}+a_{28}\lambda_{M1}^{cpx}+a_{29}\lambda_{T}^{opx}+a_{210}\lambda_{T}^{cpx}=b_2$$
$$a_{31}\Delta_f H^{En\text{-}opx}+a_{32}\gamma_{Ca}+a_{33}\gamma_{Mg}+a_{34}\gamma_{Si}+a_{35}\lambda_{M2}^{opx}+a_{36}\lambda_{M2}^{cpx}+a_{37}\lambda_{M1}^{opx}+a_{38}\lambda_{M1}^{cpx}+a_{39}\lambda_{T}^{opx}+a_{310}\lambda_{T}^{cpx}=b_3$$
$$a_{41}\Delta_f H^{En\text{-}opx}+a_{42}\gamma_{Ca}+a_{43}\gamma_{Mg}+a_{44}\gamma_{Si}+a_{45}\lambda_{M2}^{opx}+a_{46}\lambda_{M2}^{cpx}+a_{47}\lambda_{M1}^{opx}+a_{48}\lambda_{M1}^{cpx}+a_{49}\lambda_{T}^{opx}+a_{410}\lambda_{T}^{cpx}=b_4$$
$$a_{51}\Delta_f H^{En\text{-}opx}+a_{52}\gamma_{Ca}+a_{53}\gamma_{Mg}+a_{54}\gamma_{Si}+a_{55}\lambda_{M2}^{opx}+a_{56}\lambda_{M2}^{cpx}+a_{57}\lambda_{M1}^{opx}+a_{58}\lambda_{M1}^{cpx}+a_{58}\lambda_{T}^{opx}+a_{59}\lambda_{T}^{cpx}=b_5$$
$$a_{61}\Delta_f H^{En\text{-}opx}+a_{62}\gamma_{Ca}+a_{63}\gamma_{Mg}+a_{64}\gamma_{Si}+a_{65}\lambda_{M2}^{opx}+a_{66}\lambda_{M2}^{cpx}+a_{67}\lambda_{M1}^{opx}+a_{68}\lambda_{M1}^{cpx}+a_{69}\lambda_{T}^{opx}+a_{610}\lambda_{T}^{cpx}=b_6$$
$$a_{71}\Delta_f H^{En\text{-}opx}+a_{72}\gamma_{Ca}+a_{73}\gamma_{Mg}+a_{74}\gamma_{Si}+a_{75}\lambda_{M2}^{opx}+a_{76}\lambda_{M2}^{cpx}+a_{77}\lambda_{M1}^{opx}+a_{78}\lambda_{M1}^{cpx}+a_{79}\lambda_{T}^{opx}+a_{710}\lambda_{T}^{cpx}=b_7$$
$$a_{81}\Delta_f H^{En\text{-}opx}+a_{82}\gamma_{Ca}+a_{83}\gamma_{Mg}+a_{84}\gamma_{Si}+a_{85}\lambda_{M2}^{opx}+a_{86}\lambda_{M2}^{cpx}+a_{87}\lambda_{M1}^{opx}+a_{88}\lambda_{M1}^{cpx}+a_{88}\lambda_{T}^{opx}+a_{89}\lambda_{T}^{cpx}=b_8$$
$$a_{91}\Delta_f H^{En\text{-}opx}+a_{92}\gamma_{Ca}+a_{93}\gamma_{Mg}+a_{94}\gamma_{Si}+a_{95}\lambda_{M2}^{opx}+a_{96}\lambda_{M2}^{cpx}+a_{97}\lambda_{M1}^{opx}+a_{98}\lambda_{M1}^{cpx}+a_{99}\lambda_{T}^{opx}+a_{910}\lambda_{T}^{cpx}=b_9$$
$$a_{101}\Delta_f H^{En\text{-}opx}+a_{102}\gamma_{Ca}+a_{103}\gamma_{Mg}+a_{104}\gamma_{Si}+a_{105}\lambda_{M2}^{opx}+a_{106}\lambda_{M2}^{cpx}+a_{107}\lambda_{M1}^{opx}+a_{108}\lambda_{M1}^{cpx}+a_{108}\lambda_{T}^{opx}+a_{109}\lambda_{T}^{cpx}=b_{10}$$

Writing Eq. (6.90) in a matrix form would yield:

$$\begin{pmatrix} a_{11} & a_{12} & a_{13} & a_{14} & a_{15} & a_{16} & a_{17} & a_{18} & a_{19} & a_{110} \\ a_{21} & a_{12} & a_{23} & a_{24} & a_{25} & a_{26} & a_{27} & a_{28} & a_{29} & a_{210} \\ a_{31} & a_{32} & a_{33} & a_{34} & a_{35} & a_{36} & a_{37} & a_{38} & a_{39} & a_{310} \\ a_{41} & a_{42} & a_{43} & a_{44} & a_{45} & a_{46} & a_{47} & a_{48} & a_{49} & a_{410} \\ a_{51} & a_{52} & a_{53} & a_{54} & a_{55} & a_{56} & a_{57} & a_{58} & a_{59} & a_{510} \\ a_{61} & a_{62} & a_{63} & a_{64} & a_{65} & a_{66} & a_{67} & a_{68} & a_{69} & a_{610} \\ a_{71} & a_{72} & a_{73} & a_{74} & a_{75} & a_{76} & a_{77} & a_{78} & a_{79} & a_{710} \\ a_{81} & a_{82} & a_{83} & a_{84} & a_{85} & a_{86} & a_{87} & a_{88} & a_{89} & a_{810} \\ a_{91} & a_{92} & a_{93} & a_{94} & a_{95} & a_{96} & a_{97} & a_{98} & a_{99} & a_{910} \\ a_{101} & a_{102} & a_{103} & a_{104} & a_{105} & a_{106} & a_{107} & a_{108} & a_{109} & a_{1010} \end{pmatrix} \times \begin{pmatrix} \Delta_f H^{En-opx} \\ \gamma_{Ca} \\ \gamma_{Mg} \\ \gamma_{Si} \\ \lambda_{M2}^{opx} \\ \lambda_{M2}^{cpx} \\ \lambda_{M1}^{opx} \\ \lambda_{M1}^{opx} \\ \lambda_{T}^{opx} \\ \lambda_{T}^{cpx} \end{pmatrix} = \begin{pmatrix} b_1 \\ b_2 \\ b_3 \\ b_4 \\ b_5 \\ b_6 \\ b_7 \\ b_8 \\ b_9 \\ b_{10} \end{pmatrix} \tag{6.134}$$

Where, in Eq. (6.134) the a_{ij}*'s* coefficients are known numbers as well as the right-hand side b_i*'s* quantities. In section (6.5.4) it has been shown how both a_{ij}*'s* and b_i*'s* can be explicitly derived (see Eq.6.92-6.125) and how in this specific case many of the a_{ij}*'s* coefficients would be equal to nought. Replacing in Eq. (6.134), any of the a_{ij}*'s* with either their numerical value (when $a_{ij} = 0$) or with their complete expression (when $a_{ij} \neq 0$), would yield:

$$\begin{pmatrix} \left[n^{opx}\cdot(-z_1)\right] & \left[n^{opx}\cdot 1\right] & [\ 0\ ] & [\ 0\ ] & [1] & [0] & [0] & [0] & [0] & [0] \\ [\ 0\ ] & \left[n^{cpx}\cdot 1\right] & [\ 0\ ] & [\ 0\ ] & [0] & [1] & [0] & [0] & [0] & [0] \\ [\ 0\ ] & [\ 0\ ] & \left[n^{opx}\cdot 1\right] & [\ 0\ ] & [1] & [0] & [0] & [0] & [0] & [0] \\ [\ 0\ ] & [\ 0\ ] & \left[n^{cpx}\cdot 1\right] & [\ 0\ ] & [0] & [1] & [0] & [0] & [0] & [0] \\ [\ 0\ ] & [\ 0\ ] & \left[n^{opx}\cdot 1\right] & [\ 0\ ] & [0] & [0] & [1] & [0] & [0] & [0] \\ [\ 0\ ] & [\ 0\ ] & \left[n^{cpx}\cdot 1\right] & [\ 0\ ] & [0] & [0] & [0] & [1] & [0] & [0] \\ [\ 0\ ] & [\ 0\ ] & [\ 0\ ] & \left[n^{opx}\cdot 1\right] & [0] & [0] & [0] & [0] & [1] & [0] \\ [\ 0\ ] & [\ 0\ ] & [\ 0\ ] & \left[n^{cpx}\cdot 1\right] & [0] & [0] & [0] & [0] & [0] & [1] \\ \left[(1-X_{21}^{opx})\cdot 1\right] & \left[X_{21}^{opx}\cdot 1\right] & \left[X_{31}^{opx}\cdot 1\right] & \left[X_{83}^{opx}\cdot 1\right] & [0] & [0] & [0] & [0] & [0] & [0] \\ [\ 0\ ] & \left[X_{21}^{cpx}\cdot 1\right] & \left[X_{31}^{cpx}\cdot 1\right] & \left[X_{83}^{cpx}\cdot 1\right] & [0] & [0] & [0] & [0] & [0] & [0] \end{pmatrix} \times \begin{pmatrix} \Delta_f H^{En-opx} \\ \gamma_{Ca} \\ \gamma_{Mg} \\ \gamma_{Si} \\ \lambda_{M2}^{opx} \\ \lambda_{M2}^{cpx} \\ \lambda_{M1}^{opx} \\ \lambda_{M1}^{cpx} \\ \lambda_{Si}^{opx} \\ \lambda_{Si}^{cpx} \end{pmatrix} = \begin{pmatrix} b_1 \\ b_2 \\ b_3 \\ b_4 \\ b_5 \\ b_6 \\ b_7 \\ b_8 \\ b_9 \\ b_{10} \end{pmatrix} \tag{6.135}$$

Note that in Eq. (6.135) it was chosen not to substitute the b_i*'s* quantities with their complete expressions, as such expressions can be very large and would cause Eq. (6.135) to look quite confused. However, the b_i*'s* full expressions can be directly obtained from the equations derived in section 6.5.4. For instance b_1 = Eq. (6.95), b_2 = Eq (6.98), and so on until b_{10} = Eq. (6.125).

Therefore, Eq. (6.135) is the equivalent in matrix form of the series of linear equations that, given one input dataset, would have to be solved in order to calculate the value of $\Delta_f H^{En\text{-}opx}$ for a CMS two-pyroxene system.

So far only matrixes have been considered (i.e. Eq. 6.133 and Eq. 6.134) that were representations of systems of linear equations derived assuming to have just one set of input parameters. In a more realistic case there will be a number *ndata* of datasets and consequently *ndata* systems of linear equations to solve. Each dataset would introduce extra *Lagrangian unknowns*, whose number and type, as explained in section 6.5, will depend on the nature of the system the input data refers to. On the other hand, the number and type of the *nv unknowns* one wants to calculate, once selected, will not change as they do not depend on the dataset being considered.

An example will help to clarify this point.

The case examined in section 6.5.4 is again considered. In that example it was assumed to have only one set of input data (i.e. *data1*) referring to a CMS two-pyroxene system. It was also assumed to calculate just one *nv* parameter, more precisely $\Delta_f H^{En\text{-}opx}$. It was afterwards proved that in the series of ten linear equations (see Eq. 6.90) derived from that dataset there are ten *unknowns*: the only *nv* parameter selected as *unknown*, i.e. $\Delta_f H^{En-opx}$, and nine *Lagrangian* (i.e. m_1*) unknowns*, consequence of the type of the system. It is now assumed to have two datasets instead of one and it is also assumed that the second dataset (i.e. *data2*) refers to the same type of system as *data1*. This would introduce ten additional linear equations to solve, and within them, again a total of ten *unknowns*: the same *nv* parameter originally selected (i.e. $\Delta_f H^{En\text{-}opx}$), plus nine extra 'new' *Lagrangian* (i.e. m_2) *unknowns*. This means that as a result of having these two sets (i.e.

data1 and *data2*) of input parameters the *inv*erse problem would consist of a total of twenty linear equations to solve with among them one *nv unknown* and eighteen *Lagrangian unknowns* (i.e. m_1+m_2). Furthermore, it is assumed to have a third dataset (i.e. *data3*), but this time *data3* will refer to a different system from *data1* and *data2*. More precisely it is assumed *data3* to refer to a CMAS two-pyroxene system, that is, the same system as the one considered in the example of section 6.5.3. As shown in that example, a dataset of this kind will introduce fourteen additional linear equations and within them a total of twelve *unknowns*: again $\Delta_f H^{En\text{-}opx}$, unchanged respect to *data1* and *data2*, plus eleven extra *Lagrangian* (i.e. m_3) *unknowns*. So, the *inv*erse problem resulting from having *data1*, *data2* and *data3* as input parameters, and $\Delta_f H^{En\text{-}opx}$ as the only selected *nv unknown*, would consist of a system of thirty-four linear equations and among them thirty *unknowns*: one *nv* plus twenty-nine *Lagrangian unknowns* (i.e. $m_1 + m_2 + m_3$). The same procedure would then be followed for any other additional input dataset. At the end, in this particular case where just one *nv* parameter was selected, the structure of the *inv*erse problem could be summarized as given by:

ndata $\Rightarrow$ set of linear equations,

one nv (i.e. $\Delta_f H^{En\text{-}opx}$) $\Rightarrow$ the 'selected' *unknown*,

$$mtot \left(mtot = \sum_{i=1}^{ndata} m_i \right) \Rightarrow Lagrangian\ unknowns.$$

With:

m_i = *Lagrangian unknowns* referring to dataset *i*.

To make the above conclusion valid for a general case it is enough to assume to select a larger, not specified, number of *nv unknowns*, say *NV*. The structure of the problem will then basically be the same as in the above example. The only difference would be having *NV unknowns* instead of just one.

In this way, the representation in matrix form of the *inv*erse problem for a general case (i.e. *ndataset* of input parameters, *NV* selected *unknowns*) will be:

$$\begin{pmatrix} [a_{NV}][a_{m_1}][\#][\#][\#],\ldots\ldots\ldots\ldots\ldots\ldots,[\#] \\ [a_{NV}][\#][a_{m_2}][\#][\#],\ldots\ldots\ldots\ldots\ldots\ldots,[\#] \\ [a_{NV}][\#][\#][a_{m_3}][\#],\ldots\ldots\ldots\ldots\ldots\ldots,[\#] \\ [a_{NV}][\#][\#][\#][a_{m_4}],\ldots\ldots\ldots\ldots\ldots\ldots,[\#] \\ \ldots\ldots\ldots\ldots\ldots\ldots\ldots\ldots\ldots\ldots\ldots\ldots\ldots\ldots \\ \ldots\ldots\ldots\ldots\ldots\ldots\ldots\ldots\ldots\ldots\ldots\ldots\ldots\ldots \\ \ldots\ldots\ldots\ldots\ldots\ldots\ldots\ldots\ldots\ldots\ldots\ldots\ldots\ldots \\ \ldots\ldots\ldots\ldots\ldots\ldots\ldots\ldots\ldots\ldots\ldots\ldots\ldots\ldots \\ \ldots\ldots\ldots\ldots\ldots\ldots\ldots\ldots\ldots\ldots\ldots\ldots\ldots\ldots \\ [a_{NV}][\#][\#][\#][\#],\ldots\ldots\ldots\ldots\ldots\ldots,[a_{m_{ndata}}] \end{pmatrix} \times \begin{pmatrix} NV \\ --- \\ m_1 \\ m_2 \\ m_3 \\ m_4 \\ \vdots \\ \vdots \\ \vdots \\ \vdots \\ \vdots \\ m_{ndata} \end{pmatrix} = \begin{pmatrix} b_{data1} \\ b_{data2} \\ b_{data3} \\ b_{data4} \\ \vdots \\ \vdots \\ \vdots \\ \vdots \\ \vdots \\ b_{ndata} \end{pmatrix} \qquad (6.136)$$

Where, in Eq. (6.136) a_{NV} indicates the coefficients referring to the *NV unknowns* and a_{m_i} (i = 1, …., *ndata*) those referring to the *Lagrangian unknowns*.

6.6.2 Solution by Singular Value Decomposition

For each dataset the linear system of equations to solve, written in a matrix form, is given by Eq. (6.132):

$$A \cdot \underline{x} = \underline{b} \qquad (6.132)$$

with:

A = matrix of dimension $nd \times M$,

$\underline{x}$ = M vector of *unknowns*,

$\underline{b}$ = nd vector of data.

To solve the linear system of equations the *Singular Value Decomposition* technique (i.e. *S.V.D.*) is used (e.g. Press, 1992). In this way, the solution of Eq. (6.132) is given by:

$$\underline{x} = V \cdot \Lambda \cdot U^T \cdot \underline{b} \tag{6.137}$$

with:

V = eigen vectors matrix of dimension $M \times M$
Λ = diagonal matrix of eigen values of dimension $M \times M$
U^T = orthogonal matrix of dimension $nd \times M$,

In practice, the matrix probability $V \cdot \Lambda \cdot U^T$ is constructed out of only the non zero eigen values. This is done by setting a 'cut off' level (typically 10^{-4}-10^{-5}). Eigen values below that level are eliminated, reducing the size of the matrixes. The solution of Eq. (6.132) will then be given by:

$$\underline{x} = V_p \cdot \Lambda_p \cdot U_p^T \cdot \underline{b} \tag{6.138}$$

6.7 Weighting each equation in *inversion*

A very important issue to consider in the data fitting process is that the input data parameters are generally not exact. They are in fact subject to measurement errors or *noise* in the contest of data modeling. These errors are usually caused by small inaccuracies of the equipment and/or technique used to perform the analysis, and can depend also on the conditions under which the analysis took place in the laboratory. Measurement errors are commonly reasonably small and they are in general provided together with the analysis' value. Beside this type of errors there are also what can be called 'experimental' errors. In this case the error could be the result of something that went wrong and was not noticed when doing the experiment or even of a conceptual mistake in planning and/or conducting the experiment. The type of input data that will be used for the fitting process in this work is now considered. In this case a set of data should be considered affected by an

'experimental' error if, for example, the person conducting the experiment had analyzed the composition of the coexisting phases assuming the system had reached the equilibrium conditions while it had not. It is obvious that the input data $\left(P,T,X_{ij}^{\phi},n^{\phi}\right)$ in this case could never satisfy the system equilibrium conditions given by Eq. (6.16) and (6.17), simply because it refers to a system that was not at equilibrium. This second type of error is usually quite difficult to identify and basically impossible to quantify.

As a result of the error, experimental data will never exactly fit the model, even assuming that the model is truly correct, and they may also be inconsistent with each other. For this reason it is important to include in the data fitting process a way to assess whether the model is appropriate, that is, to test the *goodness-of-fit* against some useful statistical standard. In the remaining part of this section the procedure followed in order to get a measure of the *goodness-of-fit* is described.

As shown in section 6.6, the linear system of equations to solve can be written in the matrix form (i.e. Eq. 6.132):

$$A \cdot \underline{x} = \underline{b}$$

Eq (6.132) could also be expressed as:

$$\sum_{j=1}^{Mtot} a_{ij} x_j = b_i \qquad \left(i = 1,...,N\right) \tag{6.139}$$

With:

Mtot = total number of *unknowns* in the system (i.e. *Mtot* = *NV* + *mtot*),
N = total number of linear equations in the system.

Where, the a_{ij}*'s* coefficients and b_i*'s* quantities are known numbers that, since they depend on the input data, are effected by error.

Given Eq. (6.139) a chi-square measure of *goodness-of-fit* in $A \cdot \underline{x} = \underline{b}$ it is obtained from:

$$X^2(\underline{x}) = \sum_{i=1}^{N} \frac{\left(b_i - \sum_{j=1}^{Mtot} a_{ij} x_j \right)^2}{\sigma_i^2} \tag{6.140}$$

Where σ_i^2 is the variance of the numerator given errors in the data and ignoring cross-variances.

Since both a_{ij}*'s* and b_i*'s* are functions of the input data the variance of the numerator, σ_i^2, can be obtained from:

$$\sigma_i^2 = var\left(b_i - \sum_{j=1}^{Mtot} a_{ij} x_j \right) = var(b_i) + \sum_{j=1}^{Mtot} x_j^2 \, var(a_{ij}) \tag{6.141}$$

Where, the variance of the b_i*'s* quantities, $var(b_i)$, and of the a_{ij}*'s* coefficients, $var(a_{ij})$, can be expressed respectively as:

$$var(b_i) = \sigma_{b_i}^2 \tag{6.142}$$

$$var(a_{ij}) = \sigma_{a_{ij}}^2 \tag{6.143}$$

From Eq. (6.141) it is clear that to obtain the numerator variance, σ_i^2, an estimate of $\sigma_{b_i}^2$ and $\sigma_{a_{ij}}^2$ is needed. In the program '*GibInv*' this is achieved in a subroutine, named *Monte*, where a *Monte Carlo* simulation is performed for each dataset. In this way a very precise estimate of the measurement error that affects the input data is obtained.

Substituting Eq. (6.142) and (6.143) in Eq. (6.141), yields:

$$\sigma_i^2 = \sigma_{b_i}^2 + \sum_{j=1}^{Mtot} x_j^2 \sigma_{a_{ij}}^2 \tag{6.144}$$

Once the expression of the numerator variance is obtained it is convenient to consider the *diagonal data covariance matrix*, or C_M^{-1}, which is given by:

$$C_M^{-1} = \frac{1}{\sigma_i^2} \tag{6.145}$$

Finally, substituting Eq. (6.145) into Eq. (6.144) and rewriting Eq. (6.144) in vector form, yields:

$$X^2(\underline{x}) = (\underline{b} - A\underline{x})^T \cdot C_M^{-1}(\underline{b} - A\underline{x}) \tag{6.146}$$

Properly testing the *goodness-of-fit,* X^2, plays an important role in the data fitting process and for this reason it was decided to include it in the program. The mere fitting of parameters should never be considered as the end-all of parameter estimation. To be authentically useful a fitting procedure should always provide a statistical measure of *goodness-of-fit* together with the parameters evaluations and the error estimates on the parameters. Had the value of X^2 suggested that the model was unlikely to match the data, then the parameters' estimation obtained in the fitting process should have probably been considered worthless. In that case doubts could be risen on the quality of the data used or, in the most unwanted case, on the accuracy of the model.

6.8 Prior constraints on *inversion*

An important point to consider when solving the *inv*erse problem is that in some cases it can be assumed to have already an idea of what the value of the *unknowns* could be. It is worth reminding that the final goal is to find values of end-member (*E*) and Margules

(*W*) parameters and some of these values may have already been determined in previous studies. If this is the case they could then be considered as *known* parameters and consequently left out from the fitting process. On the other hand, the operator could still decide to treat them as *unknowns* but at the same time he/she would like to be able to use the information obtainable from previous studies. In this case the way to proceed would be to consider the available existing value of an *unknown* as its *initial guess*, then fitting that parameter to see if its value satisfies the system equilibrium conditions or it needs to be adjusted. As a result, when using an *initial guess*, the goal would become more *refining* existing parameters' values than *deriving* them from scratch. Furthermore, to be genuinely useful the *initial guess* needs to have its reliability quantified. This means that the *initial guess* has to be provided also with a number that denotes a gaussian weight on its value. This is the equivalent of imposing additional constraints on the solution, as the program will prefer solutions within that range of values. The example presented in section 6.8.2 will help to clarify this point.

Using *prior information* on the *unknowns* can also be the only possible way to obtain a meaningful solution in a different situation. Sometimes one might be in the position of trying to recover the value for a certain number of *unknowns* without having enough input data to constraint them. A further complication could arise from the fact the *unknowns* one wants to solve the problem for might have values that differ for one or more orders of magnitude. In this case the program will almost certainly not be able to find a sensible solution, as *trade off* processes will probably occur. To obtain a valid solution the only way is to give the program an additional help, in the form of the *initial guess*. The example presented in section 6.8.2 will help to clarify this point too.

6.8.1 Implementing prior constraints

Currently for each dataset the *inv*erse problem solves the linear system of equations given by Eq. (6.132) or in the equivalent graphic representation by Eq. (6.133).

To add *Gaussian prior information* (or more correctly '*quadratic penalty for departures from prior model*') on all variables a joint (prior) probability density function is introduced (e.g. Menke, 1989):

$$e^{-1/2} = \left(x - \underline{x}_o\right)^T \times C_T^{-1}\left(\underline{x} - \underline{x}_o\right) \tag{6.147}$$

Where, C_T^{-1} is known as the *inverse prior covariance matrix*.

Usually:

$$C_T^{-1} = \begin{pmatrix} e_1^{-2} & 0 & \ldots\ldots\ldots\ldots & 0 \\ 0 & e_2^{-2} & \ldots\ldots\ldots\ldots & 0 \\ 0 & \ldots\ldots & \ddots & \ldots\ldots\ldots & 0 \\ 0 & \ldots\ldots\ldots & \ddots & \ldots\ldots & 0 \\ 0 & \ldots\ldots\ldots\ldots & \ddots & \ldots\ldots & 0 \\ 0 & \ldots\ldots\ldots\ldots & \ldots\ldots & e_T^{-2} \end{pmatrix} \tag{6.148}$$

That is, C_T^{-1} is a diagonal matrix with prior covariances e_i^{-2}.

To impose the *prior information* on the solution of the data an augmented linear system of equations has to be solved:

$$\begin{pmatrix} a_{11},\ldots\ldots,a_{1nv};a_{1nv+1},\ldots\ldots\ldots\ldots,a_{1nv+m} \\ \ldots\ldots\ldots\ldots\ldots\ldots\ldots\ldots\ldots\ldots\ldots\ldots\ldots\ldots \\ \ldots\ldots\ldots\ldots\ldots\ldots\ C_D^{-1/2} \ldots\ldots\ldots\ldots\ldots\ldots \\ \ldots\ldots\ldots\ldots\ldots\ldots\ldots\ldots\ldots\ldots\ldots\ldots\ldots\ldots \\ a_{nd1},\ldots,a_{ndnv};a_{ndnv+1},\ldots\ldots\ldots\ldots,a_{ndnv+m} \\ ---------- \\ a_{nd+1},\ldots\ldots,a_{nd+1nv};a_{nd+1nv+1},\ldots\ldots,a_{nd+1nv+m} \\ \ldots\ldots\ldots\ldots\ldots\ldots\ldots\ldots\ldots\ldots\ldots\ldots\ldots\ldots\ldots \\ \ldots\ldots\ldots\ldots\ldots\ldots\ C_T^{-1/2} \ldots\ldots\ldots\ldots\ldots\ldots \\ \ldots\ldots\ldots\ldots\ldots\ldots\ldots\ldots\ldots\ldots\ldots\ldots\ldots\ldots \\ a_{nd+T},\ldots,a_{nd+Tnv};a_{nd+Tnv+1},\ldots\ldots,a_{nd+Tnv+m} \end{pmatrix} \times \begin{pmatrix} x_1 \\ \vdots \\ x_{nv} \\ --- \\ x_{nv+1} \\ \vdots \\ \vdots \\ x_{nv+m} \end{pmatrix} = \begin{pmatrix} b_1 \\ \vdots \\ \vdots \\ \vdots \\ b_{nd} \\ ---- \\ \vdots \\ \vdots \\ x_o \\ \vdots \\ \vdots \end{pmatrix} \tag{6.149}$$

In this way T extra rows are added to the system:

$$C_T^{-1/2}\underline{x} = \underline{x}_o \tag{6.150}$$

The augmented system of equations given by Eq. (6.149) can be written in matrix form as:

$$F \cdot \underline{x} = \underline{g} \tag{6.151}$$

Then the least square solution of the linear system (Eq. 6.151) is found by minimizing ϕ:

$$\phi(x) = \left(Fx - \underline{g}\right)^T \times \left(F\underline{x} - \underline{g}\right) \tag{6.152}$$

Substituting C_D^{-1}, C_T^{-1}, F and $\underline{g}$ into Eq. (6.152), yields:

$$\phi(x) = \left(b - A\underline{x}\right)^T C_D^{-1}\left(\underline{b} - A\underline{x}\right) + \left(x - x_o\right)^T C_M^{-1}\left(\underline{x} - \underline{x}_o\right) \tag{6.153}$$

So the augmented system (Eq. 6.149) is equivalent to the least squares minimization of $\phi(x)$.

For Eq. (6.150) T extra equations are added:

$$\underline{x} = \underline{x}_o \tag{6.154}$$

With weights:

$$e_i^{-1} \qquad (i = 1,....,T) \tag{6.155}$$

As the e_i^{-1}'s get smaller with respect to elements of C_D^{-1} the prior constraints increase in weight.

The choice of including these additional constraints on the *unknowns* when solving the *inv*erse problem will be always up to the operator. The program has been set up in a way that every time it is run a file named '*inv.options'* is called. In that file there is the option that can be switched '*on*' or '*off*' in order to use or not the *prior information*.

6.8.2 Usefulness of initial guess

The importance and convenience of having implemented in the program the option to add *prior information* on *unknowns* can be demonstrated with some numerical examples.

For these examples a CMS two-pyroxene system will be considered and it will be assumed that the input parameter data will consist of just one dataset. Note that this is the same case as the one examined in section 6.5.1

In section 6.5.1 it was shown that in this case the *inverse* problem will solve a system of ten linear equations with nine *Lagrangian unknowns* among them. At the same time it was also shown that these ten equations are not totally independent due to the presence of nine constraints in the system: three **mass balance** and six **stoichiometry** constraints. As a consequence, despite the fact that ten equations are derived from the input data, only one '*piece*' of independent information will actually be available to solve them.

In a first step the value of $^{32}\Delta_f H^{En\text{-}opx}$ will be calculated. In this way an additional *nv unknown* is introduced in the system. The game is to see if the value of that *unknown* can be recovered with the only one '*piece*' of information available.

[32] In the CMS two-pyroxene system *prior information* is available for all the end-member (*E*) and solution (*W*) parameters, including $\Delta_f H^{En\text{-}opx}$. Having chosen to treat $\Delta_f H^{En\text{-}opx}$ as the only *unknown* implies that existing data for any other *E* and *W* parameter have been used. Therefore, sSuch parameters have in this case to be seen as part of the input data.

Initially the program is run with the option '*prior information*' switched off. The result obtained is[33]:

$$\Delta_f H^{En-opx} = -3091.41\ kJ \tag{6.156}$$

This value can be compared to some of those available from existing databases, for example: $\Delta_f H^{En-opx} = 3091.104\ kJ$ (Berman, 1988), $\Delta_f H^{En-opx} = 3090.26\ kJ$ (Holland and Powell, 1998), $\Delta_f H^{En-opx} = 3089.699\ kJ$ (Chatterjee et al., 1998). It is clear that all these values (the one recovered and those from existing databases) are very close as they differ for less than 0.1 % one from the other. It can then be concluded that the program has found a sensible solution[34].

The second test will consist in calculating simultaneously the value of $\Delta_f H^{En-opx}$ and $S^{o-En-opx}$, where examples of existing values for $S^{o-En-opx}$ are: $S^{o-En-opx} = 132.34\ J$ (Berman, 1988), $S^{o-En-opx} = 132.5\ J$ (Holland and Powell, 1998), $S^{o-En-opx} = 132.531\ J$ (Chatterjee et al., 1998). This means that the game is now trying to solve the system of equations for one more *unknown*, still with just one '*piece*' of information.

[33] The *E unknowns*' values ($\Delta_f H^{En-opx}$ and, later, $S^{o-En-opx}$) here derived have a meaning exclusively on the view of the purpose of this section and they do not have to be considered as the final result of a data fitting process. This means that these are not the values that have been used to compute the pyroxene phase equilibria shown in chapter 5.

[34] Note that one could not expect the program to recover for $\Delta_f H^{En-opx}$ exactly the same value of one found in the existing databases. Among the above mentioned databases, in fact, the values of the *E* and *W* parameters are in general slightly different and they are also different to those adopted here, which have been treated as input parameters. It is obvious that one cannot expect to be able to recover the same value for an *unknown* (i.e. $\Delta_f H^{En-opx}$ in this case) using a different set on input parameters (all the other *E's* and *W's*). On the other hand, the *E*'s and *W*'s values adopted here are close to those found in the cited databases. For this reason it can still be considered as '*good'* or '*sensible'* or '*satisfactory'* a $\Delta_f H^{En-opx}$ solution value that is close to those chosen for comparison.

Initially the program is again run with the option '*prior information*' switched off. The result obtained is:

$$\Delta_f H^{En-opx} = -0.001984\ kJ \quad (6.157)$$

$$S^{o-En-opx} = 2560.85\ J \quad (6.158)$$

It is clear that this time the program did not find a sensible value for either $\Delta_f H^{En\text{-}opx}$ or $S^{o\text{-}En\text{-}opx}$ as *'trade off'* phenomena have occurred.

Finally, the third test is to solve the problem for the same two *unknowns*, but this time adding *prior information*. More in detail the value of $\Delta_f H^{En-opx}$ and $S^{o-En-opx}$ found in Holland and Powell (1998) are chosen as *initial guess*. Furthermore, since it is decided to let the program look for 'preferred solutions' within a very large range of values, the $\Delta_f H^{En-opx}$ and $S^{o-En-opx}$ initial values are left free of varying respectively of $\pm 525\ kJ$ and $\pm 114.0\ J$.

The program is run and the output is:

$$\Delta_f H^{En-opx} = -3091.22\ kJ \quad (6.159)$$

$$S^{o-En-opx} = 132.563\ J \quad (6.160)$$

That is, the program, with the help provided by the *initial guess*, did manage to find a good solution.

It is important here to notice that the *prior information* the program was provided with in this last case were extremely 'weak' ones. In particular, $\pm 525\ kJ$ for $\Delta_f H^{En-opx}$ and $\pm 114.0\ J$ for $S^{o-En-opx}$, while the variance of the correspondent values among all the available databases is respectively less than $\pm 3\ kJ$ and less than $\pm 1\ J$. At the same time, the values recovered are perfectly satisfactory. This therefore represents a very good evidence of the usefulness of the *prior information* option. In particular this example shows

that imposing prior constraints on the solution's value might have the crucial effect of eliminating any instability in the program.

The choice of adding *prior information* on solution will be completely left to the operator. The decision has to be made case by case, based on several criteria that depend mainly on the complexity of the problem to solve. In particular the number of *unknowns*' values to calculate and the number of input datasets (i.e. amount of information) available are expected to play an important role in taking the decision, as shown in the above examples. Sometime doubts on the quality of the *initial guess* might convince the operator not to use it, while in other cases *initial guess* may not be available at all.

6.9 Testing the program

Before the program can be used to [35]refine end-member and/or solution parameters, it needs to be properly tested.

In sections 6.2 and 6.3 the close relationship in the formulation of *forward* and *inverse* approach was shown. It was also described how the expressions of the *Lagrangian* function L and of $\mathbf{G}^{\mathbf{system}}$ are closely related and how the minimum of L, solution of the *inverse* problem, should also represent the minimum of $\mathbf{G}^{\mathbf{system}}$, solution of the *forward* problem. Furthermore it was explained that the solution of the *forward* problem could also be obtained by minimizing L. Mainly for computational reasons, it was instead decided to use the solver *FSQP*. The crucial issue is now to verify whether the consistency between *forward* and *inverse* formulation can be numerically proved.

This can be done in a straightforward manner using a 'synthetic test'. The program '*Gib*' can be used to generate a number of datasets that can then be employed as input data for the program '*GibInv*'. In this way first of all it is known exactly what should be the value of any possible *E* and *W unknown* selected for refinement. These parameters are in fact part of the input data in the *forward* problem and their value is stored in the *gib.dat* file. Secondly, the input data of '*GibInv*', being the output of the program '*Gib*', will be in first

[35] Since now on the term 'refining' an *unknown*'s value will be used in a more broaden sense of 'calculating' such value. This means that unless otherwise specified it will not be distinguished between calculating the value from scratch and refining an existing one.

order error free[36]. As a result, no error propagation issue will need to be considered. To prove that the consistency between *forward* and *inverse* formulation is maintained some of the *E* and/or *W* parameters have to be selected as *unknowns* and their original value (i.e. as found in *gib.dat*) should be recovered.

6.9.1 Preparing the test: synthetic datasets

Datasets from any kind of system could be employed to do the test. It was arbitrary opted to use the program '*Gib*' to generate 24 datasets for a CMFS two-pyroxene system at several different *T-P* and bulk composition conditions. These datasets are given in Table 6.6.

[36] This is not completely correct. The input data of the program *'GibInv'* has to be on the form of weight per cent of oxides, while the output of the program '*Gib'* is on site occupancies. A transformation from site occupancies into oxides' weight per cent is therefore needed and a program, named *'oxide'*, has been written to perform that task. In the process a small error, or '*noise'*, can be introduced and can propagate throughout the program. However, since this error is very small the input data can be regarded as error free even after the transformation.

Table 6.6. Outputs of program '*Gib*' used as input datasets in the synthetic test.

	X_{21}	X_{31}	X_{32}	X_{41}	X_{42}	X_{83}	**n**	T	P
opx	0.03	0.859	0.886	0.11	0.114	2	0.764	1083	15000
cpx	0.953	0.043	0.916	0.004	0.084	2	1.236	1083	15000
opx	0.037	0.755	0.784	0.208	0.216	2	1.199	1083	15000
cpx	0.944	0.048	0.844	0.009	0.156	2	0.801	1083	15000
opx	0.037	0.749	0.778	0.214	0.222	2	0.978	1083	15000
cpx	0.943	0.048	0.84	0.009	0.16	2	1.022	1083	15000
opx	0.046	0.626	0.656	0.328	0.344	2	0.815	1083	15000
cpx	0.931	0.052	0.755	0.017	0.245	2	1.185	1083	15000
opx	0.046	0.622	0.652	0.332	0.348	2	0.747	1083	15000
cpx	0.93	0.053	0.752	0.017	0.248	2	1.253	1083	15000
opx	0.054	0.524	0.554	0.422	0.446	2	0.967	1083	15000
cpx	0.918	0.056	0.678	0.026	0.322	2	1.033	1083	15000
opx	0.057	0.476	0.505	0.466	0.495	2	1.08	1083	15000
cpx	0.91	0.057	0.638	0.032	0.362	2	0.92	1083	15000
opx	0.067	0.36	0.386	0.573	0.614	2	0.821	1083	15000
cpx	0.886	0.06	0.523	0.054	0.477	2	1.179	1083	15000
opx	0.047	0.622	0.653	0.331	0.347	2	0.745	1088	20000
cpx	0.928	0.054	0.751	0.018	0.249	2	1.255	1088	20000
opx	0.065	0.403	0.431	0.532	0.569	2	0.707	1088	20000
cpx	0.893	0.061	0.566	0.046	0.434	2	1.293	1088	20000
opx	0.063	0.42	0.448	0.517	0.552	2	0.952	1088	20000
cpx	0.897	0.06	0.583	0.043	0.417	2	1.048	1088	20000
opx	0.07	0.337	0.362	0.593	0.638	2	1.181	1088	20000
cpx	0.875	0.061	0.493	0.063	0.507	2	0.819	1088	20000
opx	0.073	0.308	0.333	0.619	0.667	2	0.671	1088	20000
cpx	0.866	0.061	0.458	0.073	0.542	2	1.329	1088	20000
opx	0.061	0.443	0.472	0.495	0.528	2	1.075	1088	20000
cpx	0.902	0.06	0.606	0.039	0.394	2	0.925	1088	20000
opx	0.043	0.852	0.891	0.104	0.109	2	0.742	1183	25000
cpx	0.928	0.065	0.91	0.006	0.09	2	1.258	1183	25000
opx	0.052	0.749	0.79	0.199	0.21	2	1.19	1183	25000
cpx	0.911	0.073	0.827	0.015	0.173	2	0.81	1183	25000
opx	0.052	0.744	0.786	0.203	0.214	2	0.956	1183	25000
cpx	0.91	0.074	0.824	0.016	0.176	2	1.044	1183	25000
opx	0.063	0.628	0.671	0.309	0.329	2	0.694	1183	25000
cpx	0.885	0.083	0.727	0.031	0.273	2	1.306	1183	25000
opx	0.063	0.631	0.673	0.306	0.327	2	0.768	1183	25000
cpx	0.886	0.083	0.729	0.031	0.271	2	1.232	1183	25000
opx	0.073	0.531	0.573	0.396	0.427	2	0.909	1183	25000
cpx	0.856	0.092	0.638	0.052	0.362	2	1.091	1183	25000
cpx	0.083	0.423	0.462	0.494	0.538	2	0.561	1183	25000
opx	0.801	0.104	0.524	0.095	0.476	2	1.439	1183	25000
cpx	0.082	0.432	0.471	0.485	0.529	2	0.848	1183	25000
opx	0.808	0.103	0.534	0.09	0.466	2	1.152	1183	25000
cpx	0.049	0.787	0.827	0.165	0.173	2	0.501	1183	25000
opx	0.918	0.007	0.858	0.012	0.142	2	1.499	1183	25000
cpx	0.062	0.644	0.686	0.294	0.314	2	0.699	1183	25000
opx	0.889	0.082	0.741	0.029	0.259	2	1.301	1183	25000

6.9.2 Selecting the unknowns: the inv.dat file

The following step is to select the *nv unknowns* whose value will be recovered. To do that a file named *inv.dat* is opened, the chosen *unknowns* selected, then the file is saved. The program, every time it is run, automatically calls that file.

It is opportune here to explain the way the file *inv.dat* has been set up. Considering that refining *E* and *W* parameters represents the goal of the *inverse* problem it is important to have the option of selecting them with as much freedom and flexibility as possible.

In the *inv.dat* file first all the [37]*W* parameters are listed. For each of them four rows of information are entered:

```
1)  1 1 2 3
2)  23.2188    7.50        0    0
3)  2.5E-3     1.0E-5      0    0
4)  7.0E-7     1.0E-9      0    0
```
(6.161)

In each row four numbers are written that indicate:

Row 1)

First number: phase type ⇒ 1 = [38]*opx*, 2 = *cpx*, 3 = *pig*, 4 = *grt*, 5 = *ol*, 6 = *sp*, 7 = *pl*, 8 = *qtz*, 9 = *ky*, 10 = *sil*, 11 = *cor*

Second number: site type, e.g. ⇒ 1 = [39]site M2, 2 = site M1, 3 = site T

Third and fourth numbers: cation type ⇒ 1 = Na, 2 = Ca, 3 = Mg, 4 = Fe^{2+}, 5 = Al, 6 = Cr, 7 = Fe^{3+}, 8 = Si, 9 = Ti.

Row 2)

First number: initial guess value for W_H

Second number: possible variance in the W_H's initial guess value

Third number: option for parameter refinement selection.

Two possible values 0 ⇒ parameter is not selected to be refined

[37] Note that the complete expression for any *W* parameter is given by (i.e. eq. 6.20): $W_G = W_H - TW_S + PW_V$. Each term of W_G is treated has a possible unknown. Unit is kJ.

[38] Note that some of these phases (e.g. quartz) are never present as solid solutions, but only as pure phase. Therefore no *W* parameters are needed for them. The above numeration, however, is maintained to be consistent with the *E* parameters' numeration (see later in this section) and with the numeration adopted in the *forward* problem.

[39] This is for pyroxene phases (*opx*, *cpx* and *pig*). For other phases numbers 1,2,3 refer to different type of sites depending on the phase structure, e.g. for *grt* it would be 1 = site X, 2 = site Y, 3 = site Z (see also section 6.5.3).

1 ⇒ parameter is selected to be refined

Fourth number: additional constraint to enable the operator to swap between symmetric and asymmetric model (see Eq. 6.162 and 6.163 later in this section).

Rows 3) and 4)

Same as in row 2), for *Ws* and *Wv*, respectively.

To summarize, the four rows of Eq. (6.161) will identify the solution parameter Ca-Mg (i.e.$W_{Ca\text{-}Mg}$) for site M2 of *opx*. The value of the optional initial guess for W_H, W_S and W_V's is 33.2188, 2.5E-3 and 7.0E-7 kJ respectively, and, if used, the possible variance of such value will be ±7.5, ±1.0E-5, ±1.0E-9 kJ respectively. None among W_H, *Ws* and *Wv* have been selected to be refined and the distribution of Ca and Mg in site M2 is assumed to be asymmetric.

It is now assumed that for the *opx* phase a symmetric model to account of the Ca-Mg distribution in site M2 will be adopted (i.e.$W_{Ca\text{-}Mg} = W_{Mg\text{-}Ca}$). It is also assumed that the parameter W_H will be refined, and that W_S and W_V can be considered equal to zero. In the file *inv.dat* this will be equivalent to:

```
1 1 2 3
23.2188      7.50        1      3
  0.0        0.0         0      0
  0.0        0.0         0      0
```
(6.165)

```
1 1 3 2
23.2188      7.50        1      3
 0.0         0.0         0      0
 0.0         0.0         0      0
```
(6.166)

In Eqs. (6.162) and (6.163) the actual numerical value of the last number in the second row (i.e. 3 in this case) is not important. As said before that number is used only to swap from asymmetric to symmetric model. This is done by assigning the same number to

the parameters one wants to impose having an identical solution value (i.e. $W_{Ca\text{-}Mg}$ and $W_{Mg\text{-}Ca}$ in this case).

After the *W*, the *E* parameters for every end-member are entered in the *inv.dat* file. For each of them 12 rows of information are written:

```
1        4
-3090.18        15.0            0       0
0.132           1.1E-03         0       0
0.3562          3.5D-02         0       0
-2.99D-06       2.9D-07         0       0
-596.9          59.69           0       0
-3.1853         0.31853         0       0
0.00            0.00            0       0
0.00            0.00            0       0
6.26D-03        6.26D-04        0       0
1.8D-07         1.2D-08         0       0
4.6D-09         4.6D-10         0       0
```

(6.164)

Two numbers are entered in row 1), they indicate:

First number: phase type (same as for the *W's*, i.e. 1 = *opx*, 2 = *cpx*, etc.)

Second number: end-member type, e.g. ⇒ 1 = [40]jadeite, 2 = ureyite 3 = acmite,
4 = enstatite, 5 = ferrosilite,
6 = diopside, 7 = hedenbergite, etc.

Rows 2)-12) contain information for parameters [41] $\Delta_f H^o$, S^o, *A, B, C, D, E, F, V,* αV, βV, respectively. In each row the first three numbers have the same meaning as already seen for the *W* parameters: first number is the initial guess value, second number is the variance in the initial guess value, third number specifies whether the parameter will be refined. The fourth number of each row indicates whether during the fitting process the *E* parameter is imposed to take the same value of the correspondent parameter of another end-member. An example will help to clarify this point. It can be assumed that one wants to refine the heat capacity coefficients *A* and *B* for clino-diopside and ortho-diopside end-members. A good

[40] Listed here are just seven of the thirty-two possible end-members for a pyroxene phase in a general Na-Ca-Mg-Fe^{2+}-Al-Cr-Fe^{3+}-Si-Ti system. The full list of end-members was given in Appendix 2A.
[41] Units are kJ, bars, K.

initial guess value of A and B is known for clino-diopside, while no *prior information* on the same parameters is available for ortho-diopside. The way to proceed would be to first assign to the ortho-diopside A and B the same initial guess value as in clino-diopside, then to impose that during the fitting $A^{orhto-diopside} \equiv A^{clino-diopside}$ and $B^{orhto-diopside} \equiv B^{clino-diopside}$. In the *inv.dat* file this would yield:

```
1        6
  -3198.18        5.0             0       0
     0.144        1.26D-03        0       0
     0.3145       3.14D-02        1       4
     4.1D-08      4.10D-09        1       5
  -2745.9         2.74            0       0
    -2.02         0.20            0       0
     0.00         0.00            0       0
     0.00         0.00            0       0
     6.69D-03     6.69D-04        0       0
     2.22D-07     2.22D-08        0       0
     5.56D-09     5.56D-10        0       0
```

(6.165)

```
2        6
  -3200.58        5.0             0       0
     0.143        1.25D-03        0       0
     0.3145       3.14D-02        1       4
     4.1D-08      4.10D-09        1       5
  -2745.9         2.74            0       0
    -2.02         0.20            0       0
     0.00         0.00            0       0
     0.00         0.00            0       0
     6.62D-03     6.62D-04        0       0
     2.20D-07     2.20D-08        0       0
     5.50D-09     5.50D-10        0       0
```

(6.166)

6.9.3 Synthetic test results

For the test case it was decided to try to recover the value of the following four E *unknowns*: $\Delta_f H^{ortho-En}$, $\Delta_f H^{ortho-Fs}$, $\Delta_f H^{clino-Di}$, $\Delta_f H^{clino-Hd}$. The program was then run keeping the option *prior information* switched off and making use of the 24 input datasets of section 6.9.1. The output of the program was:

$$\begin{aligned}
\Delta_f H^{ortho-En} &= -3091.11 \\
\Delta_f H^{ortho-Fs} &= -2388.72 \\
\Delta_f H^{clino-Di} &= -3200.60 \\
\Delta_f H^{clino-Hd} &= -2842.24
\end{aligned} \tag{6.167}$$

The correspondent values of the four parameters in the file *gib.dat* were:

$$\begin{aligned}
\Delta_f H^{ortho-En} &= -3091.10 \\
\Delta_f H^{ortho-Fs} &= -2388.75 \\
\Delta_f H^{clino-Di} &= -3200.58 \\
\Delta_f H^{clino-Hd} &= -2842.22
\end{aligned} \tag{6.168}$$

Comparison between Eq. (6.167) and Eq. (6.168) shows that the values of the *unknowns* recovered by '*GibInv*' are extremely close to the corresponding 'true' values in *gib.dat*. This represents a remarkable achievement. It has to be reminded that in the fitting process the program '*GibInv*' did not make use of the initial guess values (i.e. *prior information* was switched off). This means that the program did not have any indication of what the *unknowns*' values should have been and it has calculated them completely from scratch. Clearly, this result represents a strong evidence of the consistency between *forward* and *inverse* formulation.

The relationship between *forward* and *inverse* approach with the techniques chosen to solve both problems and their established mutual consistency can be schematically illustrated as in Fig. 6.1. Notice the central position of the 'Lagrange equations' box. Two arrows converge towards the box indicating that both problems could have been solved using those equations but the arrow from '*FORWARD* problem' is barred to point out that a different path in that case has been followed. In this way it is emphasized that two completely different techniques have been employed for the solution of the two problems. In the figure the demonstrated *forward-inverse* consistency is represented as the completion of a 'circle'.

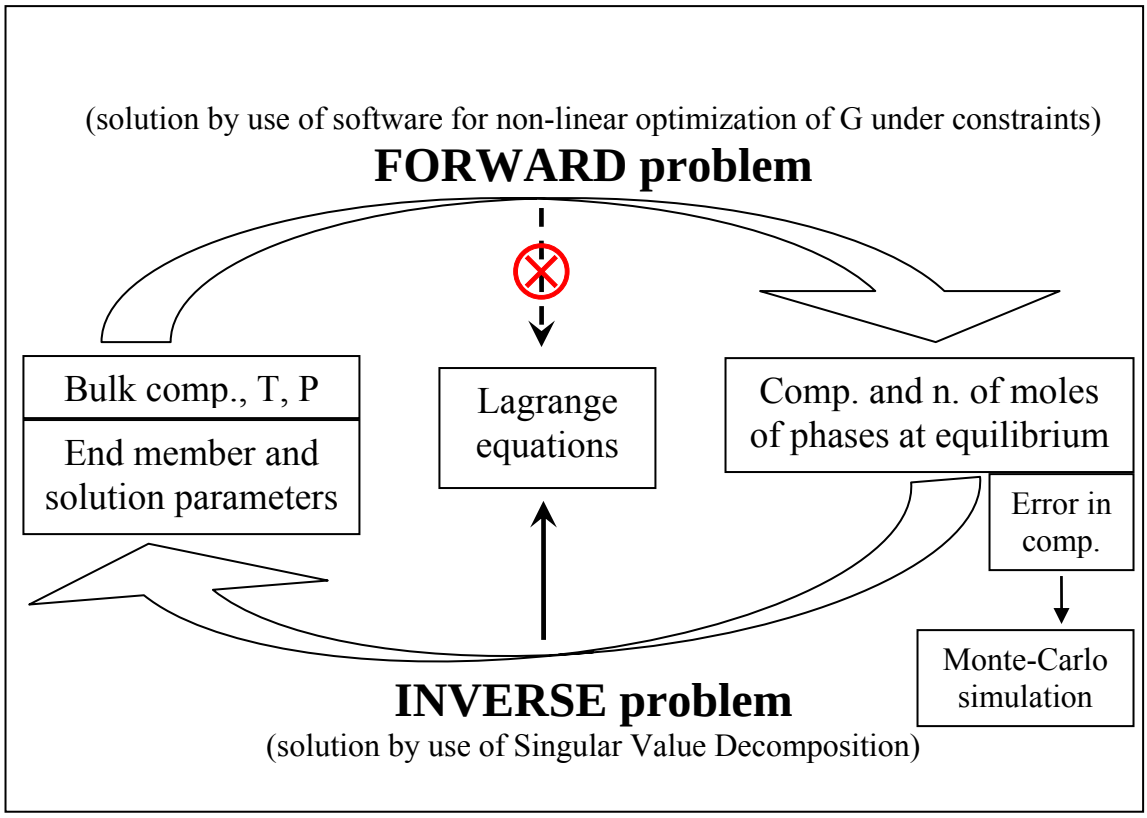

Fig. 6.1. Schematic representation of the relationship between *forward* and *inverse* problems.

Further tests have been carried out to verify the ability of the program to simultaneously refine larger number of *unknowns*, this time making use of the *prior information*. For simplicity the same CMFS two-pyroxene system has been considered and the same 24 input datasets used. Reported here are the results of two tests, named *prior1* and *prior2*.

In *prior1* the efficiency of '*GibInv*' has been checked to recover parameters whose value differs of several orders of magnitude, i.e. $\Delta_f H$, S^o, *W's*. Results of this test are given in Table 6.7.

In *prior2* the test consisted in calculating the value of all possible sixteen W_H's parameters for the specific CMFS two-pyroxene case. Results of *prior2* are reported in Table 6.8.

Outcomes of test *prior1* and *prior2* are very encouraging. The program was provided with quite 'weak' *initial guesses* (see last column on the right in Tables 6.7 and

6.8), and despite this it managed to successfully recover all the unknown values. In these 'error free' experiments '*GibInv'* showed an excellent stability that, reinforced by the use of the *prior information*, allowed the simultaneous refinement of several *unknowns*. The established consistency between *forward* and *inverse* approach and the conclusions drawn from test *prior1* and *prior2* endorse the use of the program to solve the *inverse* problem in real cases, i.e. using experimental data that are not error free.

Table 6.7. Results of test *prior1*.

unknown	**output *GibInv***	**initial guess**	[(b)]**i.g. variance**
$\Delta_f H^{ortho-En}$	-3090.95 kJ	– 3091.10 kJ	± 10.0 kJ
$\Delta_f H^{ortho-Fs}$	-2388.68 kJ	– 2388.75 kJ	± 10.0 kJ
$\Delta_f H^{clino-Di}$	-3201.50 kJ	– 3200.58 kJ	± 10.0 kJ
$\Delta_f H^{clino-Hd}$	-2842.78 kJ	– 2842.22 kJ	± 10.0 kJ
$S^{o-orhto-En}$	132.469 J	132.340 J	± 5.0 J
$S^{o-orhto-Fs}$	191.828 J	191.764 J	± 5.0 J
$S^{o-clino-Di}$	142.310 J	142.500 J	± 5.0 J
$S^{o-clino-Hd}$	174.338 J	174.200 J	± 5.0 J
[(a)] [(c)] $W^{opx}_{Ca-Mg} = W^{opx}_{Mg-Ca}$	32.2512 kJ	33.0 kJ	± 10.0 kJ
[(a)] W^{cpx}_{Ca-Mg}	17.7222 kJ	18.0 kJ	± 10.0 kJ
[(a)] W^{cpx}_{Mg-Ca}	19.7659 kJ	20.0 kJ	± 10.0 kJ

Notes: [(a)] The *W unknowns* are instead W_H*'s unknowns*. The *'H'* has been omitted for simplicity of notation;
[(b)] Abbreviation 'i.g.*'* is for *'*initial guess*'*;
[(c)] $W^{opx}_{Ca-Mg} = W^{opx}_{Mg-Ca}$ imposed during the fitting.

Table 6.8. Results of test *prior2*.

[(a)] ***unknown***	**output *GibInv***	**initial guess**	[(b)]**i.g. variance**
[(c)] $W^{opx}_{Ca-Mg} = W^{opx}_{Mg-Ca}$	32.125	33.0	± 5.0
[(c)] $W^{opx}_{Ca-Fe} = W^{opx}_{Fe-Ca}$	19.429	20.0	± 5.0
[(c)] $W^{opx-M2}_{Mg-Fe} = W^{opx-M2}_{Fe-Mg}$	6.284	6.631	± 5.0
[(c)] $W^{opx-M1}_{Mg-Fe} = W^{opx-M1}_{Fe-Mg}$	8.548	8.368	± 5.0
W^{cpx}_{Ca-Mg}	28.387	28.5000	± 5.0
W^{cpx}_{Mg-Ca}	29.171	28.5000	± 5.0
W^{cpx}_{Ca-Fe}	19.719	19.5000	± 5.0
W^{cpx}_{Fe-Ca}	18.736	19.5000	± 5.0
[(c)] $W^{cpx-M2}_{Mg-Fe} = W^{cpx-M2}_{Fe-Mg}$	5.125	4.545	± 5.0
[(c)] $W^{cpx-M1}_{Mg-Fe} = W^{cpx-M1}_{Fe-Mg}$	8.566	7.332	± 5.0

Notes: [(a)] The *W unknowns* are instead W_H*'s unknowns*. The *'H'* has been omitted for simplicity of notation. Unit is kJ;
[(b)] Abbreviation 'i.g.*'* is for *'*initial guess*'*;
[(c)] Imposed during the fitting.

6.10 Inversion preliminary results: application to pyroxene assemblages

At the time of writing this theses the program '*GibInv*' has been set up and employed on assemblages of coexisting pyroxenes (*opx*, low Ca and high Ca *cpx*; two or three depending on bulk composition and *T-P* conditions). In this section preliminary results are presented that were obtained in the refinement of end-member and solution parameters for pyroxenes in CaO-MgO-FeO-Al_2O_3-SiO_2 (i.e. CMFAS) systems. Before showing the results, the procedure followed in the fitting process will be described.

6.10.1 Setting up input datasets for inversion.

Pyroxene assemblages in CaO-MgO-FeO-SiO_2 (i.e. CMFS), CaO-MgO-Al_2O_3-SiO_2 (i.e. CMAS) and CMFAS systems and in their subsystems have been widely investigated in the past and a quite large number of experimental data is available. The program has been set up in a way that all these data together with the relative error could be simultaneously used in the fitting process. At the same time one might instead prefer to carry out the fitting with just a number of selected experimental data. For this reason several different input data file have been prepared and every time the program is run the operator has to specify the input data that will be employed.

Every input data file is organized in a way that at the beginning a number is read which indicates how many datasets will be read in and used by the program during the fitting process. Every dataset consists of:

- a number that defines the type of system the data refers to, i.e. number and type of phases present in the system, number and type of cations for each phase
- *P*, error in *P*, *T*, error in *T*
- chemical composition of coexisting phases expressed in weight per cent of oxides and related estimated error

As a result, an example of input data file would then be[42]:

```
25
   10
    27000.0     400.0   1773.0    10.0
54.3    9.9     0.0     34.6    0.0     1.8     0.0     0.0     0.0     0.0     0.0     0.0
1.1     1.5     0.0     0.6     0.0     0.3     0.0     0.0     0.0     0.0     0.0     0.0
51.8    9.7     0.0     24.5    0.0     15.0    0.0     0.0     0.0     0.0     0.0     0.0
1.1     0.2     0.0      0.6    0.0      0.8    0.0     0.0     0.0     0.0     0.0     0.0
```

Where:

25 ⇒ total number of datasets read in[43]
10 ⇒ following dataset refers to two coexisting pyroxenes (*opx* + high-Ca *cpx*) in the system CMAS[44].
27000.0, 400.0 ⇒ *P* and error in *P* (in bars)
1773.0, 10.0 ⇒ *T* and error in *T* (in K)
54.3 9.9 etc. ⇒ composition of *opx*[45],
1.1 1.5 etc. ⇒ error in *opx* composition
51.8 9.7 etc. ⇒ composition in *cpx*
1.1 0.2 etc. ⇒ error in *cpx* composition

As explained in section 6.9.1 the program *'GibInv'* expects the phase compositions in the input data file to be expressed in weight per cent of oxides, while sometimes compositional data might be in cations per formula unit. In this case a transformation from cations per formula unit into oxides' weight per cent will be needed. The program *'oxide'* mentioned in section 6.9.1 performs this task too.

Sometimes in the experimental data the error is not reported. When this is the case, given that no experimental data can be considered error free, an error is assumed. For oxides whose weight per cent is more than 50% the error assumed is equal to the 2% of their value (i.e. oxide = 54.3 ⇒ error = 1.086), for oxides whose weight per cent is less than

[42] Experimental data from Klemme (1998).
[43] Here, for simplicity, the information referring to only one dataset out twenty-five has been written. However, the way the remaining twenty-four datasets are entered would be exactly the same.
[44] Inside the program, at the beginning of the subroutine '*invsetup'* all the other possible cases are listed (e.g. 1 = *opx* + high-Ca *cpx* in CMS system, 2 = *opx* + high-Ca *cpx* + low-Ca *cpx* in CMS system, etc.).
[45] The order followed in entering compositions and errors, which is the same for any phase, is: SiO_2, Al_2O_3, Fe_2O_3, MgO, MnO, CaO, FeO, Na_2O, K_2O, NiO, TiO_2, Cr_2O_3.

50% and more than 10% the error assumed is equal to the 3% of their value (i.e. oxide = 24.5 $\Rightarrow$ error = 0.735), for oxides whose weight per cent is less than 10% the error is equal to the 5% of their value (i.e. oxide = 7.8 $\Rightarrow$ error = 0.39).

6.10.2 Fitting strategy.

In section 6.9 it was shown that any of the *E* and *W* parameters could be selected in the *inv.dat* file to be refined. However, during the fitting process it was opted to adjust only *W*'s, $\Delta_f H^o$'s and S^o's parameters, while heat capacity functions (i.e. *A, B, C, D, E* parameters) molar volumes (i.e. *V*'s) and coefficients of thermal expansion (i.e. α's) and compressibility (i.e. β's) were left unchanged.

The program, as said in the previous section, has been set up to allow the simultaneous used of all available experimental data. Using a large number of input datasets means that a large quantity of '*pieces of information*' (see also section 6.8.2) is made available for the program to solve the inversion problem. In this way many *unknowns* could be refined with just one run of the program. The employment of large number of experiment data to perform the simultaneous refinement of several parameters is the usual procedure adopted in the derivation of existing databases (e.g. Holland and Powell, 1990 and 1998; Gottschalk, 1997; Chatterjee, 1998). One important advantage of this procedure being the obtainment of databases that are internally consistent.

The same procedure has been initially adopted in this work, however it did not prove to be the most effective one. In a first attempt *E* and *W* parameters have been refined all together using some 300 experimental data. On one hand, the parameters obtained in this way proved to be accurate enough to reproduce the general trend of pyroxene phase equilibria in the investigated systems[46]. On the other hand, they appeared to be inadequate to allow a precise calculations of miscibility gaps, for instance when trying to reproduce the pigeonite stability field in CMS, CFS and CMFS systems.

As a consequence a different approach was followed. The fitting has been initially performed on simple systems (i.e. CMS and CFS), using only a selection of the available

[46] It is understood that any time parameters have been refined using '*inv*' they were then tested. This means that in the *gib.dat* file existing parameters were substituted with the refined ones. The program '*Gib*' was then run and the test consisted in verifying how well experimental data were reproduced.

experimental data (see following section 6.10.3 for a detailed description of the way the fitting has been carried out in the CMS case). Once the *E* and *W* parameters in these systems have been refined their value has then been considered as known. For instance after the fitting in the CMS system the value of the following parameters had to be considered as fixed: W_{Ca-Mg}^{M2}, W_{Mg-Ca}^{M2}, $\Delta_f H^{En}$, $\Delta_f H^{Di}$, S^{o-En} and S^{o-Di} for both *opx* and *cpx*. Similar conclusion after the fitting in the CFS system for the parameters W_{Ca-Fe}^{M2}, W_{Fe-Ca}^{M2}, $\Delta_f H^{Fs}$, $\Delta_f H^{Hd}$, S^{o-Fs} and S^{o-Hd}. As a result, when doing the fitting in the CMFS system the only other *unknowns* whose value needed to be refined were the *W* parameters that account for the non ideal mixing of Mg-Fe on M1 and M2 sites, i.e.: W_{Mg-Fe}^{M2}, W_{Fe-Mg}^{M2}, W_{Mg-Fe}^{M1} *and* W_{Fe-Mg}^{M1}. Proceeding in this way all the needed *E* and *W* parameters' values for pyroxene in CMFAS system have been derived. Reported in Tables (6.9) and (6.10) is the final result of the fitting.

The refinement of *E* and *W* parameters obtained in this way proved to be of a much better quality than with any other fitting strategy attempted. Moreover, the procedure adopted guarantees that internal consistency is maintained. On the other hand, standard deviations associated with any of the refined *unknowns* are still quite large (see section 6.10.3 and Tables 6.9 and 6.10) and the program seemed unable to further refine them. The main problem appears to be the error in the input data and to the way it propagates throughout the program. Attempts of using only experimental data with small errors did not bring any considerable improvement in the fitting, likely due to inconsistency between the data.

At the end to better reproduce the pyroxene phase equilibria the parameters refined with *'GibInv'* needed to be slightly adjusted on a 'trail and error' basis. Comparison between the *E's* and *W'*s values used for the pyroxene phase equilibria computation given in Tables (5.1) and (5.2) and those of Tables (6.9) and (6.10) gives an indication of the entity of the adjustment required.

The fitting strategy here adopted may be subject to some criticism. First of all, using only some experimental data instead of all implies that valuable information has been left out from the fitting process. Secondly sometimes (i.e. in the fitting of the CFS system) the

only few data available were characterized by a quite large uncertainty that could affect the possibility of properly constraining the *unknowns*'s values. Thirdly, since the fitting was done in several steps (see also section 6.10.3), it proved to be very time consuming. Moreover, the *E's* and *W'*s so obtained needed a further adjustment done on a 'trial and error' basis. For all these reasons it will probably be advisable in the future to modify the fitting strategy. This will be possible when very delicate issues such as the error in experimental data and the related error propagation within the program will be more properly addressed.

6.10.3 Example of fitting procedure in CMS system

Experimental data from Lindsley and Dixon (1976), Perkins and Newton (1980), Mori and Green (1975) and (1976).

Parameters selected to be fitted for both *opx* and *cpx*: enthalpy and entropy of formation of enstatite and diopside end-members (i.e. $\Delta_f H$'s and S^o's), W^{M2}_{Ca-Mg} and W^{M2}_{Mg-Ca}.

The fitting has been carried out in three distinct steps:

1. Refinement of only $\Delta_f H$'s and S^o values.
2. Refinement of only *W'*s values
3. Refinement of $\Delta_f H$'s, S^o's and *W'*s together.

Prior information was available for all the selected parameters. In step 1 existing values were adopted for *W* parameters, while for $\Delta_f H$'s and S^o's a very weak initial guess was used. In step 2 the refined values of $\Delta_f H$'s and S^o's were then considered as known parameters and the refinement of the *W*'s was done with the option '*prior information*' switched off. In step 3 all the selected *unknowns* were refined at the same time using values obtained in step 1 and step 2 as initial guess and adopting the respective standard deviations as variance on initial guess.

Following is reported the progressing of the fitting step by step:

Step1

unknown	**output '*GibInv*'**	[47]**st. dev.**	**initial guess**	[48]**i.g. variance**
$\Delta_f H^{ortho-En}$	-3092.195 kJ	5.23	-3091.104 kJ	± 10.0 kJ
$\Delta_f H^{ortho-Di}$	-3201.410 kJ	5.71	-3198.251 kJ	± 10.0 kJ
$\Delta_f H^{clino-En}$	-3088.711 kJ	5.45	-3086.083 kJ	± 10.0 kJ
$\Delta_f H^{clino-Di}$	-3203.530 kJ	5.06	-3200.583kJ	± 10.0 kJ
$S^{o-orhto-En}$	132.391 J	1.21	132.340 J	± 2.0 J
$S^{o-orhto-Di}$	144.104 J	1.03	143.881 J	± 2.0 J
$S^{o-clino-En}$	132.398 J	1.12	135.164 J	± 2.0 J
$S^{o-clino-Di}$	142.610 J	0.98	142.500 J	± 2.0 J

Chi-square = 4.188

[49]*Step2*

unknown	**output '*GibInv*'**	**st. dev.**
[50] $W_{Ca-Mg}^{M2-opx} = W_{Mg-Ca}^{M2-opx}$	32.3663 kJ	4.92
W_{Ca-Mg}^{M2-cpx}	32.7659 kJ	5.86
W_{Mg-Ca}^{M2-cpx}	24.7222 kJ	6.71

Chi-square = 1.974

[47] Abbreviations used: st. dev. = standard deviation, i.g. = initial guess.
[48] Initial guess' value form Sack and Ghiorso (1994b).
[49] Initially W_S and W_V have also been treated as *unknowns* and included in the fitting process. However this did not seem to improve the quality of the fitting. In addition standard deviations associated to their output values were very high. It was then decided to set $W_S = W_V \equiv 0$ and keep W_H as the only parameter to refine. In the rest of this chapter it will then be assumed that $W_H \equiv W_G$.
[50] For *opx* solid solution adopted symmetric model, for *cpx* solid solution adopted asymmetric model.

Step 3

Here output and st. dev. values from *step1* and *step2* are used as initial guess and i.g. variance values.

unknown	**output '*GibInv*'**	**st. dev.**	**initial guess**	**i.g. variance**
$\Delta_f H^{ortho-En}$	-3092.591 kJ	2.75	-3092.195 kJ	5.23
$\Delta_f H^{ortho-Di}$	-3201.205 kJ	2.80	-3201.400 kJ	5.71
$\Delta_f H^{clino-En}$	-3088.495 kJ	2.98	-3088.711 kJ	5.45
$\Delta_f H^{clino-Di}$	-3203.850 kJ	2.75	-3203.530 kJ	5.06
$S^{o-orhto-En}$	132.413 J	1.03	132.391 J	1.21
$S^{o-orhto-Di}$	144.002 J	0.95	144.104 J	1.03
$S^{o-clino-En}$	135.151 J	0.98	132.398 J	1.12
$S^{o-clino-Di}$	142.717 J	0.93	142.610 J	0.98
$W^{opx}_{Ca-Mg} = W^{opx}_{Mg-Ca}$	32.4512 kJ	1.84	32.3663 kJ	4.92
W^{cpx}_{Ca-Mg}	32.1149 kJ	3.57	32.7659 kJ	5.86
W^{cpx}_{Mg-Ca}	24.9620 kJ	3.72	24.7222 kJ	6.71

Chi-square = 1.831

6.10.4 Inversion results

Analogous procedure has been adopted when fitting the selected *E* and/or *W* parameters in the other systems. Final results are summarized in Tables (6.9) and (6.10). Note that reported in the tables are only the values of the *unknowns* (with related standard deviations) that have been refined. The values of the remaining *E* and *W* parameters can be found in Tables (5.1) and (5.2).

Table 6.9. Refined $\Delta_f H$'s and S^o's thermodynamic data.

end-member	$\Delta_f H$	st. dev.	S^o	st. dev.
ortho-enstatite	-3092.591 kJ	2.75	132.413 J	1.03
ortho-ferrosilite	-2388.152 kJ	3.15	192.000 J	0.98
ortho-diopside	-3201.205 kJ	2.80	144.002 J	0.95
ortho-hedenbergite	-2840.869 kJ	2.64	174.753 J	1.05
ortho-Ca-Ts	-3298.040 kJ	2.46	134.330 J	1.34
ortho-Mg-Ts	-3195.035 kJ	3.25	127.000 J	1.65
ortho-Fe-Ts	-2852.150 kJ	4.23	132.700 J	2.54
clino-enstatite	-3088.495 kJ	2.98	135.151 J	0.98
clino-ferrosilite	-2385.150 kJ	2.23	194.243 J	0.99
clino-diopside	-3203.850 kJ	2.75	142.717 J	0.93
clino-hedenbergite	-2843.458 kJ	2.14	175.000 J	1.04
clino-Ca-Ts	-3305.250 kJ	3.05	138.000 J	1.81
clino-Mg-Ts	-3187.540 kJ	3.62	132.905 J	1.74
clino-Fe-Ts	-2846.050 kJ	4.51	130.900 J	2.04

Table 6.10. Refined solution parameters.

solution parameter	*opx*	st. dev.	*cpx*	st. dev.
W^{M2}_{Ca-Mg}	32.4512 kJ	1.84	32.1149 kJ	3.72
W^{M2}_{Mg-Ca}	32.4512 kJ	1.84	24.9620 kJ	3.57
W^{M2}_{Ca-Fe}	19.1250 kJ	1.72	19.5605 kJ	3.42
W^{M2}_{Fe-Ca}	19.1250 kJ	1.72	18.2648 kJ	3.54
[(a)] W_{Mg-Fe}	7.5560 kJ	0.94	6.8600 kJ	1.63
[(b)] W^{M1}_{Mg-Al}	7.3784 kJ	2.02	4.3973 kJ	2.25
[(b)] W^{M1}_{Fe-Al}	4.1520 kJ	3.4	2.650 kJ	2.24

Notes: [(a)] $W^{M2}_{Mg-Fe} = W^{M2}_{Fe-Mg} = W^{M1}_{Mg-Fe} = W^{M1}_{Fe-Mg} \equiv W_{Mg-Fe}$ imposed on solution for both *opx* and *cpx*;

[(b)] $W^{M1}_{Mg-Al} = W^{M1}_{Al-Mg}$ and $W^{M1}_{Fe-Al} = W^{M1}_{Al-Fe}$ imposed on solution for both *opx* and *cpx*.

6.11 Conclusions and future work

The procedure followed to write a program, '*GibInv*', that allows simultaneous refinement of end-member and mixing parameters has been here described and its major features illustrated in detail. The program has been set up in a way to allow complete freedom in the choice of the *unknowns* (in number and type) to be refined.

From its initial application to a test and a 'real' case (see sections 6.9 and 6.10 respectively) some important conclusions can be drawn. First, the internal consistency between *forward* and *inverse* approaches has been demonstrated as well as the ability of the inversion procedure to accurately recover E and W parameters' values in synthetic problems. This represents an achievement of crucial importance considering that the parameters refined with '*GibInv*' will then be used in '*Gib*' to forward model phase equilibria compositions. Secondly, it has been proved that the Bayesian method is a valid technique to solve the *inverse* problem even when this is extended to the derivation of mixing properties in addition to end-member parameters. Numerical examples reported in section 6.10 showed the ability of '*GibInv*' to successfully derive at the same time several different solution and end-member parameters. However, analysis of the very same results (see Tables 6.9 and 6.10) clearly shows that the program needs to be improved. The quality of the program's outputs, independently to the number and type of *unknowns* refined and to the strategy adopted in the refinement process, has not proved to be completely satisfactory, as standard deviations associated to the values of the *unknowns* (see Tables 6.9 and 6.10) are too big and the program at this stage seems unable to further refine them. Moreover, to reproduce pyroxene phase equilibria data with the desired accuracy (see also chapter 5), the parameters refined with '*GibInv*' needed to be slightly adjusted on a 'trail and error' basis. Inconsistency between the different sets of experimental data used in the fitting process along with the error that affects the data and the way it propagates within the program are probably the major reasons for lowering the output's quality.

To deal with these issues in the program a Monte Carlo (MC) simulation is performed for each dataset. However, results given in Tables 6.9 and 6.10 seem to suggest that this is not enough. The solution of this problem could be the employment of the Markov chain Monte Carlo (MCMC) method instead of the simpler MC, as already

successfully done by Chatterjee et al. (1998). This technique initially was not included in the program because it is very expensive from a computational point of view, but it now appears a viable alternative.

In conclusion, results presented in this chapter have to be seen as the first step of a more extensive study that once completed will yield the compilation of an internally consistent dataset of standard state and mixing properties for end-members and solid solution phases in complex systems. Derivation of these data and their incorporation in the program '*Gib*' will then lead to the creation of a very comprehensive thermodynamic modeling tool for investigating Earth's phase/melting relationships at any pressure and temperature conditions.

6.12 References

Arfken G. (1985) Mathematical methods for physicists. 3rd ed. *Academic Press, San Diego*

Berman R. G. (1988) Internally-consistent thermodynamic data for minerals in the system Na_2-K_2O-CaO-MgO-FeO-Fe_2O_3-Al_2O_3-SiO_2-TiO_2-H_2O-CO_2. *Journal of Petrology* **29**, 445-552.

Berman R. G. and Aranovich L. Y. (1996) Optimized standard state and solution properties of minerals. I. Model calibration for olivine, orthopyroxene, cordierite, garnet, and ilmenite in the system FeO-MgO-CaO-Al_2O_3-TiO_2-SiO_2. *Contributions to Mineralogy and Petrology* **126**, 1-24.

Chatterjee N. D. (1991) Applied Mineralogical Thermodynamics. Selected topics. *Springer Verlag Berlin*.

Chatterjee N. D., Krüger R., Haller G., and Olbricht W. (1998) The Bayesian approach to an internally consistent thermodynamic database: theory, database, and generation of phase diagrams. *Contributions to Mineralogy and Petrology* **133**, 149-168.

Chatterjee N. D., Miller K., and Olbricht W. (1994) Bayes estimation: a novel approach to derivation of internally consistent thermodynamic data for minerals, their uncertainties, and correlations. II. Applications. *Physics and Chemistry of Minerals* **21**, 50-62.

Gottschalk M. (1997) Internally consistent thermodynamic data for rock forming minerals. *European Journal of Mineralogy* **9**, 175-223.

Holland T. J. B. and Powell R. (1990) An enlarged and updated internally consistent thermodynamic dataset with uncertainties and correlations: the system K_2O-Na_2O-CaO-MgO-MnO-FeO-Fe_2O_3-Al_2O_3-TiO_2-SiO_2-C-H-O_2. *Journal of Metamorphic Geology* **8**, 89-124.

Holland T. J. B. and Powell R. (1998) An internally consistent thermodynamic dataset for phases of petrological interest. *Journal of Metamorphic Geology* **16**, 309-403.

Klemme S. (1998) Experimental and thermodynamic studies of upper mantle phase relations. *Ph.D. Thesis*. Australian National University, Canberra.

Lindsley D. H. and Dixon S. A. (1976) Diopside-enstatite equilibria at 850°-1400°C, 5-35 kb. *American Journal of Science* **276**, 1285-1301.

Menke W. (1989) Geophysical Data Analysis: Discrete Inverse Theory. Geophysical Data Analysis. *Academic Press, San Diego.*

Mori T. and Green D. H. (1975) Pyroxenes in the system $Mg_2Si_2O_6$-$CaMgSi_2O_6$ at high pressure. *Earth and Planetary Science Letters* **26**, 277-286.

Mori T. and Green D. H. (1976) Subsolidus equilibria between pyroxene equilibria in the system CaO-MgO-FeO-SiO_2. *American Mineralogist* **61**, 616-625.

Olbricht W., Chatterjee N. D., and Miller K. (1994) Bayes estimation: a novel approach to derivation of internally consistent thermodynamic data for minerals, their uncertainties, and correlations. I. Theory. *Physics and Chemistry of Minerals* **21**, 36-49.

Panier E. R. and Tits A. L. (1993) On combining feasibility, descent and superlinear convergence in inequality constrained optimization. *Mathematical Programming* **59**, 261-276.

Perkins D. I. and Newton R. C. (1980) The composition of coexisting pyroxenes and *grt* in the system CaO-MgO-Al_2O_3-SiO_2 at 900-1100^{o}C and high pressures. *Contributions to Mineralogy and Petrology* **75**, 291-300.

Press W. H., Teukolsky S. A., Vetterling W. T., and Flannery B. P. (1992) Numerical Recipes in Fortran. The Art of Scientific Computing. *Cambridge University Press*.

Robie R. A. and Hemingway B. S. (1995) Thermodynamic properties of minerals and related substances at 298.15 K and 1 bar (10^5 Pascals) pressures and at higher temperatures. *United States Geological Survey Bulletin **2131,*** pp. 461.

Sack R. O. and Ghiorso M. S. (1994b) Thermodynamics of multicomponent pyroxenes: II. Phase relations in the quadrilateral. *Contributions to Mineralogy and Petrology* **116**, 287-300.

Zhou J. L., Tits A. L., and Lawrence C. T. (1998) User's guide for FFSQP: a FORTRAN code for solving constrained nonlinear (Minimax) optimization problems, generating iterates satisfying all inequality and linear constraints. *University of Maryland.*

Appendix 6

6.5.2 CaseII

$CaO\text{-}MgO\text{-}Al_2O_3\text{-}SiO_2$ (i.e. CMAS) system

2 phases: *opx* + *cpx*

This is a very similar system to ***caseI***, the only difference is the addition of one extra cation (Al) in the system. In this example it will be evidenced how the function *L* changes and the number of equations *nd* varies, just adding one cation in the system.

Considering the chemical composition of the system, the general site occupancy distribution given in Table 6.1 in this case reduces to Table 6.3:

Table 6.3. Cation distribution in pyroxene phase for ***caseII***.

cation	charge	site: M2	site: M1	site: T
Ca	2+	X_{21}	#	#
Mg	2+	X_{31}	X_{32}	#
Al	3+	#	X_{52}	X_{53}
Si	4+	#	#	X_{83}

Due to the presence of Al an additional **mass balance** constraint is required:

$$\text{Al} \Rightarrow n^{opx} \cdot \left(X_{52}^{opx} + X_{53}^{opx}\right) + n^{cpx} \cdot \left(X_{52}^{cpx} + X_{53}^{cpx}\right) = M_{Al} \tag{6.69}$$

Furthermore, in this case, having the **stoichiometry** constraints satisfied will not automatically guarantee that the phase is charge balanced. As a consequence two (one per phase) additional **charge balance** constraints are needed:

$$2^+ \cdot X_{21}^{opx} + 2^+ \cdot \left(X_{31}^{opx} + X_{32}^{opx}\right) + 3^+ \cdot \left(X_{52}^{opx} + X_{53}^{opx}\right) + 4 \cdot \left(X_{83}^{opx}\right) = C^{opx} = 12 \tag{6.70}$$

$$2^+ \cdot X_{21}^{cpx} + 2^+ \cdot \left(X_{31}^{cpx} + X_{32}^{cpx}\right) + 3^+ \cdot \left(X_{52}^{cpx} + X_{53}^{cpx}\right) + 4 \cdot \left(X_{83}^{cpx}\right) = C^{cpx} = 12 \tag{6.71}$$

The total number of *Lagrangian unknown*s will then be equal to twelve (i.e. m = 12): four **mass balance**, 'γ', six **stoichiometry**, 'λ', and two **charge balance**, 'ρ').

The *Lagrangian* function L is, therefore, given by:

$$
\begin{aligned}
L = {} & n^{opx} G^{\phi-opx} + n^{cpx} G^{\phi-cpx} \\
& + \left\{\left[n^{opx} \times \left(X_{21}^{opx}\right) + n^{cpx} \times \left(X_{21}^{cpx}\right)\right] - M_{Ca}\right\} \times \gamma_{Ca} \\
& + \left\{\left[n^{opx} \times \left(X_{31}^{opx} + X_{32}^{opx}\right) + n^{cpx} \times \left(X_{31}^{cpx} + X_{32}^{cpx}\right)\right] - M_{Mg}\right\} \times \gamma_{Mg} \\
& + \left\{\left[n^{opx} \times \left(X_{52}^{opx} + X_{53}^{opx}\right) + n^{cpx} \times \left(X_{52}^{cpx} + X_{53}^{cpx}\right)\right] - M_{Al}\right\} \times \gamma_{Al} \\
& + \left\{\left[n^{opx} \times \left(X_{83}^{opx}\right) + n^{cpx} \times \left(X_{83}^{cpx}\right)\right] - M_{Si}\right\} \times \gamma_{Si} \\
& + \left[\left(X_{21}^{opx} + X_{31}^{opx}\right) - S_{M2}^{opx}\right] \times \lambda_{M2}^{opx} \\
& + \left[\left(X_{21}^{cpx} + X_{31}^{cpx}\right) - S_{M2}^{cpx}\right] \times \lambda_{M2}^{cpx} \\
& + \left[\left(X_{32}^{opx} + X_{52}^{opx}\right) - S_{M1}^{opx}\right] \times \lambda_{M1}^{opx} \\
& + \left[\left(X_{32}^{cpx} + X_{52}^{cpx}\right) - S_{M1}^{cpx}\right] \times \lambda_{M1}^{cpx} \\
& + \left[\left(X_{53}^{cpx} + X_{83}^{opx}\right) - S_{T}^{opx}\right] \times \lambda_{T}^{opx} \\
& + \left[\left(X_{53}^{cpx} + X_{83}^{cpx}\right) - S_{T}^{cpx}\right] \times \lambda_{T}^{cpx} \\
& + \left[2^{+} \cdot X_{21}^{opx} + 2^{+} \cdot \left(X_{31}^{opx} + X_{32}^{opx}\right) + 3^{+} \cdot \left(X_{52}^{opx} + X_{53}^{opx}\right) + 4^{+} \cdot \left(X_{83}^{opx}\right) - C^{opx}\right] \times \rho^{opx} \\
& + \left[2^{+} \cdot X_{21}^{cpx} + 2^{+} \cdot \left(X_{31}^{cpx} + X_{32}^{cpx}\right) + 3^{+} \cdot \left(X_{52}^{cpx} + X_{53}^{cpx}\right) + 4^{+} \cdot \left(X_{83}^{cpx}\right) - C^{cpx}\right] \times \rho^{cpx}
\end{aligned}
\tag{6.72}
$$

The complete expression of L (i.e. equivalent to Eq. 6.67 in ***caseI***) could then be obtained in a straightforward manner by substituting into Eq. (6.72) the appropriate expressions for $G^{\phi\text{-}opx}$ and $G^{\phi\text{-}cpx}$.

Similar to ***caseI***, the system of equations to be solved for each dataset is obtained by applying Eq. (6.16) and Eq. (6.17) to Eq. (6.72). Due to the increased number of site occupancies (two more for each phase) the number nd of equations is now fourteen (i.e. nd = 14).

These equations will result from the following differentiations:

$$
\begin{aligned}
& \frac{\delta L}{\delta X_{21}^{opx}}, \frac{\delta L}{\delta X_{21}^{cpx}}, \frac{\delta L}{\delta X_{31}^{opx}}, \frac{\delta L}{\delta X_{31}^{cpx}}, \frac{\delta L}{\delta X_{32}^{opx}}, \frac{\delta L}{\delta X_{32}^{cpx}}, \frac{\delta L}{\delta X_{52}^{opx}}, \\
& \frac{\delta L}{\delta X_{52}^{cpx}}, \frac{\delta L}{\delta X_{53}^{opx}}, \frac{\delta L}{\delta X_{53}^{cpx}}, \frac{\delta L}{\delta X_{83}^{opx}}, \frac{\delta L}{\delta X_{83}^{cpx}}, \frac{\delta L}{\delta n^{opx}}, \frac{\delta L}{\delta n^{cpx}}
\end{aligned}
\tag{6.73}
$$

To summarize in ***caseII*** for each dataset:

- *Lagrange* function to minimize is given by Eq. (6.72)
- Number of *Lagrangian unknowns* equal to twelve (i.e. $m = 12$)
- Number of data equations equal to fourteen (i.e. $nd = 14$)

Therefore, in this case for each dataset there will be two '*pieces*' of information available to solve the *inverse* problem.

6.5.3 CaseIII

CMAS system

3 phases: *opx* + *cpx* + *grt*

This example is presented mainly to show how to handle the derivation of L and nd when the input dataset refers to a system that includes also a phase different from pyroxene.

Everything shown in ***caseII*** about the *opx* and *cpx* phases is valid also for ***caseIII*** and is not here repeated.

For the *grt* phase the general cation distribution scheme is given by Table 6.4:

Table 6.4. Cation distribution in *grt* phase.

cation	charge	[(a)]site: X	[(a)]site: Y	[(a)]site: Z
Na	1+	#	#	#
Ca	2+	X_{21}	#	#
Mg	2+	X_{31}	#	#
Fe^{2+}	2+	X_{41}	#	#
Al	3+	#	X_{52}	#
Cr	3+	#	X_{62}	#
Fe^{3+}	3+	#	X_{72}	#
Si	4+	#	#	X_{83}
Ti	4+	#	#	X_{93}

Notes: [(a)] In the *grt*'s structure cations can be found on three energetically different types of sites:
X = distorted dodecahedral site (3 per formula unit),
Y = octahedral site (2 per formula unit),
Z = tetrahedral site (3 per formula unit).
This leads to the *grt* general formula: $X_3Y_2Z_3O_{12}$.

The *grt* solid solution is simpler to deal with than the pyroxene one. In chapter 3 (section 3.4.3 and Fig. 3.3) it was shown that for a *grt* phase, given the cation distribution of Table 6.4, **charge balance** constraints will be always automatically satisfied by **stoichiometry** constraints and that no **ratio constraints** will be needed, no matter how many and what type of cations are present in the system. At the same time **mass balance** and **stoichiometry** constraints are handled in a similar way to the pyroxene solid solution, treatment given in ***caseI*** and ***caseII***.

Given the chemical composition of this system, Table 6.4 reduces to Table 6.5:

Table 6.5. Cation distribution in *grt* phase for ***caseIII***.

cation	charge	site: X	site: Y	site: Z
Ca	2+	X_{21}	#	#
Mg	2+	X_{31}	#	#
Al	3+	#	X_{52}	#
Si	4+	#	#	X_{83}

Site occupancies $X_{21}^{grt}, X_{31}^{grt}, X_{52}^{grt}$ *and* X_{83}^{grt} will have to be included in the existing **mass balance** expression and three (one per site) additional **stoichiometry** constraints need to be added:

$$X_{21}^{grt} + X_{31}^{grt} = S_X^{grt} = 3 \tag{6.74}$$

$$X_{52}^{grt} = S_Y^{grt} = 2 \tag{6.75}$$

$$X_{83}^{grt} = S_Z^{grt} = 3 \tag{6.76}$$

The *Lagrangian* function L in this case will then be:

$$
\begin{aligned}
L = {} & n^{opx} G^{\phi-opx} + n^{cpx} G^{\phi-cpx} + n^{grt} G^{\phi-grt} \\
& + \left\{\left[n^{opx} \times \left(X_{21}^{opx}\right) + n^{cpx} \times \left(X_{21}^{cpx}\right) + n^{grt} \times \left(X_{21}^{grt}\right)\right] - M_{Ca}\right\} \times \gamma_{Ca} \\
& + \left\{\left[n^{opx} \times \left(X_{31}^{opx} + X_{32}^{opx}\right) + n^{cpx} \times \left(X_{31}^{cpx} + X_{32}^{cpx}\right) + n^{grt} \times \left(X_{31}^{grt}\right)\right] - M_{Mg}\right\} \times \gamma_{Mg} \\
& + \left\{\left[n^{opx} \times \left(X_{52}^{opx} + X_{53}^{opx}\right) + n^{cpx} \times \left(X_{52}^{cpx} + X_{53}^{cpx}\right) + n^{grt} \times \left(X_{52}^{grt}\right)\right] - M_{Al}\right\} \times \gamma_{Al} \\
& + \left\{\left[n^{opx} \times \left(X_{83}^{opx}\right) + n^{cpx} \times \left(X_{83}^{cpx}\right) + n^{grt} \times \left(X_{83}^{grt}\right)\right] - M_{Si}\right\} \times \gamma_{Si} \\
& + \left[\left(X_{21}^{opx} + X_{31}^{opx}\right) - S_{M2}^{opx}\right] \times \lambda_{M2}^{opx} \\
& + \left[\left(X_{21}^{cpx} + X_{31}^{cpx}\right) - S_{M2}^{cpx}\right] \times \lambda_{M2}^{cpx} \\
& + \left[\left(X_{21}^{grt} + X_{31}^{grt}\right) - S_{X}^{grt}\right] \times \lambda_{X}^{grt} \\
& + \left[\left(X_{32}^{opx} + X_{52}^{opx}\right) - S_{M1}^{opx}\right] \times \lambda_{M1}^{opx} \\
& + \left[\left(X_{32}^{cpx} + X_{52}^{cpx}\right) - S_{M1}^{cpx}\right] \times \lambda_{M1}^{cpx} \\
& + \left[\left(X_{52}^{grt}\right) - S_{Y}^{grt}\right] \times \lambda_{Y}^{grt} \\
& + \left[\left(X_{53}^{opx} + X_{83}^{opx}\right) - S_{T}^{opx}\right] \times \lambda_{T}^{opx} \\
& + \left[\left(X_{53}^{opx} + X_{83}^{cpx}\right) - S_{T}^{cpx}\right] \times \lambda_{T}^{cpx} \\
& + \left[\left(X_{83}^{grt}\right) - S_{Z}^{grt}\right] \times \lambda_{Z}^{grt} \\
& + \left[2^{+} \cdot X_{21}^{opx} + 2^{+} \cdot \left(X_{31}^{opx} + X_{32}^{opx}\right) + 3^{+} \cdot \left(X_{52}^{opx} + X_{53}^{opx}\right) + 4^{+} \cdot \left(X_{83}^{opx}\right) - C^{opx}\right] \times \rho^{opx} \\
& + \left[2^{+} \cdot X_{21}^{cpx} + 2^{+} \cdot \left(X_{31}^{cpx} + X_{32}^{cpx}\right) + 3^{+} \cdot \left(X_{52}^{cpx} + X_{53}^{cpx}\right) + 4^{+} \cdot \left(X_{83}^{cpx}\right) - C^{cpx}\right] \times \rho^{cpx}
\end{aligned}
\tag{6.77}
$$

Since with respect to ***caseII*** one phase ($n^{\phi\text{-}grt}$) has been added with four site occupancies $\left(X_{21}^{grt}, X_{31}^{grt}, X_{52}^{grt} \text{ and } X_{83}^{grt}\right)$, the total number of equations *nd* to be solved for each dataset now expands to nineteen (the fourteen equations of ***caseII*** plus five) i.e. *nd* = 19.

These equations will be obtained adding to the 14 derivatives of Eq. (6.73) five more equations:

$$
\frac{\delta L}{\delta X_{21}^{grt}}, \frac{\delta L}{\delta X_{31}^{grt}}, \frac{\delta L}{\delta X_{52}^{grt}}, \frac{\delta L}{\delta X_{83}^{grt}}, \frac{\delta L}{\delta n^{grt}} \tag{6.78}
$$

To summarize in ***caseIII*** for each dataset:

- *Lagrange* function to minimize is given by Eq. (6.77)
- Number of *Lagrangian unknowns* equal to fifteen (i.e. *m* = 15)
- Number of data equations equal to nineteen (i.e. *nd* = 19)

Therefore, in this case for each dataset there will be four '*pieces*' of information available to solve the *inverse* problem.

CaseIV^{b}

In this specific case, considering the expression of L given by Eq. (6.67), there are up to 56 *nv* (44 *E* and 12 *W*) parameters that could be chosen as *unknown*s for the *inverse* problem. Notice that, since the G^{o} term in L always has the same expression (given by Eq. 6.39), for every phase end-member in the system there are eleven *E* parameters (i.e. $\Delta_f H^{o}$, S^{o}, *A, B, C, D, E, F, V,* α, β) that can be treated as *unknown* for the *inverse* problem. In this CMS two-pyroxene system there are four end-members (i.e. En^{opx}, Di^{opx}, En^{cpx} and Di^{cpx}) and this gives $11 \times 4 = 44$ potential *E unknown*s. In addition, contained in the G^{ex} part of $\boldsymbol{G^{system}}$, there are also a number of *W* (Margules) parameters that can be treated as *unknown*. In this case expression of $G^{ex\text{-}opx}$ is given by Eq. (6.65) while for the *cpx* the equivalent G^{ex-cpx} expression can be directly be obtained from Eq. (6.65) by simply changing the superscript from *opx* to *cpx*. In this way, one obtains 12 more (6 per phase) potential *W unknown*[51]. Here, for simplicity, it can be assumed that the only *nv* parameter whose value has to be considered unknown will be $\Delta_f H^{En\text{-}opx}$ (i.e. $nv = 1 \equiv \Delta_f H^{En\text{-}opx}$).

At the beginning of section 6.4 it was shown (i.e. Eq 6.45) that in the *inverse* problem the system of equations that for each data has to be solved would, in its most widespread formulation, look like:

$$
\begin{aligned}
&a_{11}x_1 + a_{12}x_2 + \ldots\ldots + a_{1nv}x_{nv} + a_{1nv+1}x_{nv+1} + a_{1nv+2}x_{nv+2} + \ldots\ldots + a_{1nv+m}x_{nv+m} = b_1\\
&a_{21}x_1 + a_{22}x_2 + \ldots\ldots + a_{2nv}x_{nv} + a_{2nv+1}x_{nv+1} + a_{2nv+2}x_{nv+2} + \ldots\ldots + a_{2nv+m}x_{nv+m} = b_2\\
&a_{31}x_1 + a_{32}x_3 + \ldots\ldots + a_{3nv}x_{nv} + a_{3nv+1}x_{nv+1} + a_{3nv+2}x_{nv+2} + \ldots\ldots + a_{3nv+m}x_{nv+m} = b_3\\
&\ldots\ldots\ \ldots\ldots\ \ldots\ldots\ \ldots\ldots\ \ldots\ldots\ \ldots\ldots\ \ldots\ldots\ \ldots\ldots\ \ldots\ldots\ \ldots\ldots\\
&a_{nd1}x_1 + a_{nd2}x_2 + \ldots. + a_{ndnv}x_{nv} + a_{ndnv+1}x_{nv+1} + a_{ndnv+2}x_{nv+2} + \ldots.. + a_{ndnv+m}x_{nv+m} = b_{nd}
\end{aligned}
$$

[51] Here it is worth recalling that the complete expression for any *W* parameter is given by (i.e. Eq. 6.20): $W_G = W_H - TW_S + PW_V$. Each term of W_G represents a possible unknown.

With:

nd total number of equations,

nv = total number of *E & W unknown*s,

m = total number of *Lagrangian unknown*s.

Where, in this specific example:

$nd = 10$ ($\Rightarrow$ direct consequence of the type of system)

$nv = 1$ ($\equiv \Delta_f H^{En\text{-}opx}$) ($\Rightarrow$ operator's choice)

$m = 9$ (= 3 *'γ'* and 6 *'λ' unknown*s) ($\Rightarrow$ direct consequence of the type of system)

As a consequence, for each dataset, the system of ten equations given by Eq. (6.80-6.89) that have to be solved could in a general way be represented as:

$$
\begin{aligned}
&a_{11}\Delta_f H^{En\text{-}opx}+a_{12}\gamma_{Ca}+a_{13}\gamma_{Mg}+a_{14}\gamma_{Si}+a_{15}\lambda_{M2}^{px}+a_{16}\lambda_{M2}^{px}+a_{17}\lambda_{M1}^{px}+a_{18}\lambda_{M1}^{px}+a_{19}\lambda_{T}^{px}+a_{110}\lambda_{T}^{px}=b_1\\
&a_{21}\Delta_f H^{En\text{-}opx}+a_{22}\gamma_{Ca}+a_{23}\gamma_{Mg}+a_{24}\gamma_{Si}+a_{25}\lambda_{M2}^{px}+a_{26}\lambda_{M2}^{px}+a_{27}\lambda_{M1}^{px}+a_{28}\lambda_{M1}^{px}+a_{29}\lambda_{T}^{px}+a_{210}\lambda_{T}^{px}=b_2\\
&a_{31}\Delta_f H^{En\text{-}opx}+a_{32}\gamma_{Ca}+a_{33}\gamma_{Mg}+a_{34}\gamma_{Si}+a_{35}\lambda_{M2}^{px}+a_{36}\lambda_{M2}^{px}+a_{37}\lambda_{M1}^{px}+a_{38}\lambda_{M1}^{px}+a_{39}\lambda_{T}^{px}+a_{310}\lambda_{T}^{px}=b_3\\
&a_{41}\Delta_f H^{En\text{-}opx}+a_{42}\gamma_{Ca}+a_{43}\gamma_{Mg}+a_{44}\gamma_{Si}+a_{45}\lambda_{M2}^{px}+a_{46}\lambda_{M2}^{px}+a_{47}\lambda_{M1}^{px}+a_{48}\lambda_{M1}^{px}+a_{49}\lambda_{T}^{px}+a_{410}\lambda_{T}^{px}=b_4\\
&a_{51}\Delta_f H^{En\text{-}opx}+a_{52}\gamma_{Ca}+a_{53}\gamma_{Mg}+a_{54}\gamma_{Si}+a_{55}\lambda_{M2}^{px}+a_{56}\lambda_{M2}^{px}+a_{57}\lambda_{M1}^{px}+a_{58}\lambda_{M1}^{px}+a_{58}\lambda_{T}^{px}+a_{59}\lambda_{T}^{px}=b_5\\
&a_{61}\Delta_f H^{En\text{-}opx}+a_{62}\gamma_{Ca}+a_{63}\gamma_{Mg}+a_{64}\gamma_{Si}+a_{65}\lambda_{M2}^{px}+a_{66}\lambda_{M2}^{px}+a_{67}\lambda_{M1}^{px}+a_{68}\lambda_{M1}^{px}+a_{69}\lambda_{T}^{px}+a_{610}\lambda_{T}^{px}=b_6\\
&a_{71}\Delta_f H^{En\text{-}opx}+a_{72}\gamma_{Ca}+a_{73}\gamma_{Mg}+a_{74}\gamma_{Si}+a_{75}\lambda_{M2}^{px}+a_{76}\lambda_{M2}^{px}+a_{77}\lambda_{M1}^{px}+a_{78}\lambda_{M1}^{px}+a_{79}\lambda_{T}^{px}+a_{710}\lambda_{T}^{px}=b_7\\
&a_{81}\Delta_f H^{En\text{-}opx}+a_{82}\gamma_{Ca}+a_{83}\gamma_{Mg}+a_{84}\gamma_{Si}+a_{85}\lambda_{M2}^{px}+a_{86}\lambda_{M2}^{px}+a_{87}\lambda_{M1}^{px}+a_{88}\lambda_{M1}^{px}+a_{88}\lambda_{T}^{px}+a_{89}\lambda_{T}^{px}=b_8\\
&a_{91}\Delta_f H^{En\text{-}opx}+a_{92}\gamma_{Ca}+a_{93}\gamma_{Mg}+a_{94}\gamma_{Si}+a_{95}\lambda_{M2}^{px}+a_{96}\lambda_{M2}^{px}+a_{97}\lambda_{M1}^{px}+a_{98}\lambda_{M1}^{px}+a_{99}\lambda_{T}^{px}+a_{910}\lambda_{T}^{px}=b_9\\
&a_{101}\Delta_f H^{En\text{-}opx}+a_{102}\gamma_{Ca}+a_{103}\gamma_{Mg}+a_{104}\gamma_{Si}+a_{105}\lambda_{M2}^{px}+a_{106}\lambda_{M2}^{px}+a_{107}\lambda_{M1}^{px}+a_{108}\lambda_{M1}^{px}+a_{109}\lambda_{T}^{px}+a_{1010}\lambda_{T}^{px}=b_{10}
\end{aligned}
\qquad (6.90)
$$

Examining Eq. (6.80-6.89) it is clear that the term $\Delta_f H^{En\text{-}opx}$ appears only in Eq. (6.80) and Eq. (6.88), i.e. the first and ninth equation, respectively. This means that in Eq. (6.90) among all the a_{ij} coefficients of the first column only a_{11} and a_{91} are $\neq 0$, while a_{21}, a_{31}, a_{41}, a_{51}, a_{61}, a_{71}, $a_{91} = 0$. Similarly, a comparison between Eq. (6.80) and the first row of Eq. (6.90) reveals that among the *'γ'* coefficients only a_{12} (i.e. γ_{Ca}) will be $\neq 0$, while a_{13}

and a_{14} (i.e. γ_{Mg} and γ_{Si}) are = 0. Proceeding in an analogous way one can easily determine all the other a_{ij} coefficients among the ten rows of Eq. (6.90) whose value is ≠ 0.

So, for the CMS two-pyroxene case, the system of linear equations that in order to calculate the value of $\Delta_f H^{En\text{-}opx}$ requires to be solved reduces to:

$$
\begin{aligned}
&a_{11}\Delta_f H^{0-En-opx}_{298K,1bar} + a_{12}\gamma_{Ca} + a_{15}\lambda^{opx}_{M2} = b_1\\
&a_{22}\gamma_{Ca} + a_{26}\lambda^{cpx}_{M2} = b_2\\
&a_{33}\gamma_{Mg} + a_{35}\lambda^{opx}_{M2} = b_3\\
&a_{43}\gamma_{Mg} + a_{46}\lambda^{cpx}_{M2} = b_4\\
&a_{53}\gamma_{Mg} + a_{57}\lambda^{opx}_{M1} = b_5\\
&a_{63}\gamma_{Mg} + a_{68}\lambda^{cpx}_{M1} = b_6\\
&a_{74}\gamma_{Si} + a_{79}\lambda^{opx}_{T} = b_7\\
&a_{84}\gamma_{Si} + a_{810}\lambda^{cpx}_{T} = b_8\\
&a_{91}\Delta_f H^{0-En-opx}_{298K,1bar} + a_{92}\gamma_{Ca} + a_{93}\gamma_{Mg} + a_{94}\gamma_{Si} = b_9\\
&a_{102}\gamma_{Ca} + a_{103}\gamma_{Mg} + a_{104}\gamma_{Si} = b_{10}
\end{aligned}
\qquad (6.91)
$$

The value of the a_{ij}'s coefficients that are different from zero are known numbers that can be estimated in a straightforward manner from a comparison between Eq. (6.91) and Eq. (6.80-6.89).

The right-hand side b_i's (i = 1, 10) quantities are also known. Their value can again be obtained from Eq. (6.80-6.89) where it is assumed that any other *nv* (either *E* or *W*) parameter apart from $\Delta_f H^{En\text{-}opx}$ will be a known quantity.

For each *row* of Eq (6.91) the value of the a_{ij}'s coefficients that are ≠ 0 and of the b_i's quantities in this case will be:

[52]*row1*

$$a_{11} = n^{opx} \cdot (-) z_1 = -1 \qquad (6.92)$$

[52] For simplicity in this example $n^{opx} = n^{cpx} \equiv 1$

$$a_{12} = n^{opx} \cdot 1 = 1 \tag{6.93}$$

$$a_{15} = 1 \tag{6.94}$$

$$b_1 = n^{opx} \cdot \begin{bmatrix} \left(\begin{array}{l} \Delta_f H^o_{298K,1bar} \cdot z_1 - S^o_{298K,1bar} \cdot z_2 + A \cdot z_3 + B \cdot z_4 + C \cdot z_5 + D \cdot z_6 \\ \quad + E \cdot z_7 + F \cdot z_8 + V \cdot z_9 + \alpha V \cdot z_{10} + \beta V \cdot z_{11} \end{array} \right)^{Di-opx} \\ -\left(\begin{array}{l} -S^o_{298K,1bar} \cdot z_2 + A \cdot z_3 + B \cdot z_4 + C \cdot z_5 + D \cdot z_6 \\ \quad + E \cdot z_7 + F \cdot z_8 + V \cdot z_9 + \alpha V \cdot z_{10} + \beta V \cdot z_{11} \end{array} \right)^{En-opx} \\ RT\left(1 + ln\, X^{'-opx}_{21}\right) + 2X^{'-opx}_{21} X^{'-opx}_{31} \cdot W^{M2-opx}_{Mg-Ca} + \left(X^{'-opx}_{31}\right)^2 \cdot W^{M2-opx}_{Ca-Mg} \end{bmatrix} \tag{6.95}$$

<u>*row2*</u>

$$a_{22} = n^{cpx} \cdot 1 = 1 \tag{6.96}$$

$$a_{26} = 1 \tag{6.97}$$

$$b_2 = n^{cpx} \cdot \begin{bmatrix} \left(\begin{array}{l} \Delta_f H^o_{298K,1bar} \cdot z_1 - S^o_{298K,1bar} \cdot z_2 + A \cdot z_3 + B \cdot z_4 + C \cdot z_5 + D \cdot z_6 \\ \quad + E \cdot z_7 + F \cdot z_8 + V \cdot z_9 + \alpha V \cdot z_{10} + \beta V \cdot z_{11} \end{array} \right)^{Di-cpx} \\ -\left(\begin{array}{l} \Delta_f H^o_{298K,1bar} \cdot z_1 - S^o_{298K,1bar} \cdot z_2 + A \cdot z_3 + B \cdot z_4 + C \cdot z_5 + D \cdot z_6 \\ \quad + E \cdot z_7 + F \cdot z_8 + V \cdot z_9 + \alpha V \cdot z_{10} + \beta V \cdot z_{11} \end{array} \right)^{En-cpx} \\ + RT\left(1 + ln\, X^{'-cpx}_{21}\right) + 2X^{'-cpx}_{21} X^{'-cpx}_{31} \cdot W^{M2-cpx}_{Mg-Ca} + \left(X^{'-cpx}_{31}\right)^2 \cdot W^{M2-cpx}_{Ca-Mg} \end{bmatrix} \tag{6.98}$$

<u>*row3*</u>

$$a_{33} = n^{opx} \cdot 1 = 1 \tag{6.99}$$

$$a_{35} = 1 \tag{6.100}$$

$$b_3 = n^{opx} \cdot \left[RT\left(1 + ln\, X^{'-opx}_{31}\right) + 2X^{'-opx}_{31} X^{'-opx}_{21} \cdot W^{M2-opx}_{Ca-Mg} + \left(X^{'-opx}_{21}\right)^2 \cdot W^{M2-opx}_{Mg-Ca} \right] \tag{6.101}$$

<u>*row4*</u>

$$a_{43} = n^{cpx} \cdot 1 = 1 \tag{6.102}$$

$$a_{46} = 1 \tag{6.103}$$

$$b_4 = n^{cpx} \cdot \left[RT\left(1 + ln\, X^{'-cpx}_{31}\right) + 2X^{'-cpx}_{31} X^{'-cpx}_{21} \cdot W^{M2-cpx}_{Ca-Mg} + \left(X^{'-cpx}_{21}\right)^2 \cdot W^{M2-cpx}_{Mg-Ca} \right] \tag{6.104}$$

row5

$$a_{53} = n^{opx} \cdot 1 = 1 \tag{6.105}$$
$$a_{57} = 1 \tag{6.106}$$
$$b_5 = n^{opx} \cdot RT\left(1 + ln\, X_{32}^{'-opx}\right) \tag{6.107}$$

row6

$$a_{63} = n^{cpx} \cdot 1 = 1 \tag{6.108}$$
$$a_{68} = 1 \tag{6.109}$$
$$b_6 = n^{cpx} \cdot RT\left(1 + ln\, X_{32}^{'-cpx}\right) \tag{6.110}$$

row7

$$a_{74} = n^{opx} \cdot 1 = 1 \tag{6.111}$$
$$a_{79} = 1 \tag{6.112}$$
$$b_7 = n^{opx} \cdot RT\left(1 + ln\, X_{83}^{'-opx}\right) \tag{6.113}$$

row8

$$a_{84} = n^{cpx} \cdot 1 = 1 \tag{6.114}$$
$$a_{810} = 1 \tag{6.115}$$
$$b_8 = n^{cpx} \cdot RT\left(1 + ln\, X_{83}^{'-cpx}\right) \tag{6.116}$$

row9

$$a_{91} = \left(1 - X_{21}^{opx}\right) \cdot 1 \tag{6.117}$$
$$a_{92} = X_{21}^{opx} \cdot 1 \tag{6.118}$$
$$a_{93} = X_{31}^{opx} \cdot 1 \tag{6.119}$$
$$a_{94} = X_{83}^{opx} \cdot 1 \tag{6.120}$$

$$b_9 = X_{21}^{opx} \cdot \begin{pmatrix} \Delta_f H^o_{298K,1bar} \cdot z_1 - S^o_{298K,1bar} \cdot z_2 + A \cdot z_3 + B \cdot z_4 + C \cdot z_5 \\ + D \cdot z_6 + E \cdot z_7 + F \cdot z_8 + V \cdot z_9 + \alpha V \cdot z_{10} + \beta V \cdot z_{11} \end{pmatrix}^{Di-opx}$$
$$+ \left(1 - X_{21}^{opx}\right) \cdot \begin{pmatrix} - S^o_{298K,1bar} \cdot z_2 + A \cdot z_3 + B \cdot z_4 + C \cdot z_5 \\ + D \cdot z_6 + E \cdot z_7 + F \cdot z_8 + V \cdot z_9 + \alpha V \cdot z_{10} + \beta V \cdot z_{11} \end{pmatrix}^{En-opx} \qquad (6.121)$$
$$+ \left(X_{21}^{'-opx} \, ln \, X_{21}^{'-opx} + X_{31}^{'-opx} \, ln \, X_{31}^{'-opx} + X_{32}^{'-opx} \, ln \, X_{32}^{'-opx} + 2 X_{83}^{'-opx} \, ln \, X_{83}^{'-opx}\right) \cdot RT$$
$$+ X_{21}^{'-opx} X_{31}^{'-opx} \left(X_{21}^{'-opx}\right) \cdot W_{Mg-Ca}^{M2-opx} + X_{31}^{'-opx} X_{21}^{'-opx} \left(X_{31}^{'-opx}\right) \cdot W_{Ca-Mg}^{M2-opx}$$

<u>*row10*</u>

$$a_{102} = X_{21}^{cpx} \cdot 1 \qquad (6.122)$$
$$a_{103} = X_{31}^{cpx} \cdot 1 \qquad (6.123)$$
$$a_{104} = X_{83}^{cpx} \cdot 1 \qquad (6.124)$$
$$b_{10} = X_{21}^{cpx} \cdot \begin{pmatrix} \Delta_f H^o_{298K,1bar} \cdot z_1 - S^o_{298K,1bar} \cdot z_2 + A \cdot z_3 + B \cdot z_4 + C \cdot z_5 \\ + D \cdot z_6 + E \cdot z_7 + F \cdot z_8 + V \cdot z_9 + \alpha V \cdot z_{10} + \beta V \cdot z_{11} \end{pmatrix}^{Di-cpx}$$
$$+ \left(1 - X_{21}^{cpx}\right) \cdot \begin{pmatrix} \Delta_f H^o_{298K,1bar} \cdot z_1 - S^o_{298K,1bar} \cdot z_2 + A \cdot z_3 + B \cdot z_4 + C \cdot z_5 \\ + D \cdot z_6 + E \cdot z_7 + F \cdot z_8 + V \cdot z_9 + \alpha V \cdot z_{10} + \beta V \cdot z_{11} \end{pmatrix}^{En-cpx} \qquad (6.125)$$
$$+ \left(X_{21}^{'-cpx} \, ln \, X_{21}^{'-cpx} + X_{31}^{'-cpx} \, ln \, X_{31}^{'-cpx} + X_{32}^{'-cpx} \, ln \, X_{32}^{'-cpx} + 2 X_{83}^{'-cpx} \, ln \, X_{83}^{'-cpx}\right) \cdot RT$$
$$+ X_{21}^{'-cpx} X'-_{31}^{cpx} \left(X_{21}^{'-cpx}\right) \cdot W_{Mg-Ca}^{M2-cpx} + X_{31}^{'-cpx} X_{21}^{'-cpx} \left(X_{31}^{'-cpx}\right) \cdot W_{Ca-Mg}^{M2-cpx}$$

6.5.4 CaseV

CMS	system
2 phases:	*opx* + *cpx*

This example is equivalent to the one in ***caseIV**b* in everything except that here it is assumed that one wants to calculate the value of two *nv* parameters: $\Delta_f H^{En-opx}$ (same as before) and $B^{En\text{-}opx}$.

In this case, following an analogous procedure to the one shown in ***caseIV**b* one would obtain that the system of linear equations to solve in order to calculate the value of $\Delta_f H^{En\text{-}opx}$ and $B^{En\text{-}opx}$ reduces to:

$$
\begin{aligned}
&a_{11}\Delta_f H^{0-En-opx}_{298K,1bar} + a_{12}B^{En-opx} + a_{13}\gamma_{Ca} + a_{16}\lambda^{opx}_{M2} = b_1\\
&a_{23}\gamma_{Ca} + a_{27}\lambda^{cpx}_{M2} = b_2\\
&a_{34}\gamma_{Mg} + a_{36}\lambda^{opx}_{M2} = b_3\\
&a_{44}\gamma_{Mg} + a_{47}\lambda^{cpx}_{M2} = b_4\\
&a_{54}\gamma_{Mg} + a_{58}\lambda^{opx}_{M1} = b_5\\
&a_{64}\gamma_{Mg} + a_{69}\lambda^{cpx}_{M1} = b_6\\
&a_{75}\gamma_{Si} + a_{710}\lambda^{opx}_{T} = b_7\\
&a_{85}\gamma_{Si} + a_{811}\lambda^{cpx}_{T} = b_8\\
&a_{91}\Delta_f H^{0-En-opx}_{298K,1bar} + a_{92}B^{En-opx} + a_{93}\gamma_{Ca} + a_{94}\gamma_{Mg} + a_{95}\gamma_{Si} = b_9\\
&a_{103}\gamma_{Ca} + a_{104}\gamma_{Mg} + a_{105}\gamma_{Si} = b_{10}
\end{aligned}
\qquad (6.126)
$$

Since a new *unknown*, $B^{En\text{-}opx}$, is introduced in the system, now *nv* = 2. At the same time the number and type of equations *nd* to solve and the number and type of *Lagrangian unknowns* remain unchanged. As previously explained *m* and *nd* depend on the nature of the system, which is here unchanged from ***caseIV*^{b}**. The only change on the *m unknown*s will concern the indexes of their coefficients. These have in fact to be incremented by one (e.g. what before was a_{12} now becomes a_{13}) due to the fact that *nv* has also increased by one (i.e. before *nv* =1, now *nv* = 2).

Comparing Eq (6.126) to Eq. (6.91) it is clear that, once the difference in the indexes has been taken into account, *rows2 - 8* and *row10* in Eq. (6.126) and in Eq. (6.91) are identical.

On the other hand, in *row1* and *row9* the introduction of the new *unknown* (i.e. B^{En-opx}) will cause an extra a_{ij} coefficient to be ≠ 0 and the b_i's quantities to have their value modified. Any other parameter in these two rows will also be unchanged respect to Eq. (6.91).

More in detail, the value of the extra a_{ij} coefficient and of the b_i's quantities for *row1* and *row9* in this case will be given by:

row1

$$a_{12} = n^{opx} \cdot z_4 = 1 \cdot \left[\frac{1}{2}\left(T^2 - 298^2\right) - T\left(T - 298\right) \right] \tag{6.127}$$

$$b_1 = n^{opx} \begin{bmatrix} \begin{pmatrix} \Delta_f H^o_{298K,1bar} \cdot z_1 - S^o_{298K,1bar} \cdot z_2 + A \cdot z_3 + B \cdot z_4 + C \cdot z_5 + D \cdot z_6 \\ + E \cdot z_7 + F \cdot z_8 + V \cdot z_9 + \alpha V \cdot z_{10} + \beta V \cdot z_{11} \end{pmatrix}^{Di-opx} \\ - \begin{pmatrix} - S^o_{298K,1bar} \cdot z_2 + A \cdot z_3 + C \cdot z_5 + D \cdot z_6 \\ + E \cdot z_7 + F \cdot z_8 + V \cdot z_9 + \alpha V \cdot z_{10} + \beta V \cdot z_{11} \end{pmatrix}^{En-opx} \\ RT\left(1 + ln\, X^{\prime -opx}_{21}\right) + 2X^{\prime -opx}_{21} X^{\prime -opx}_{31} \cdot W^{M2-opx}_{Mg-Ca} + \left(X^{\prime -opx}_{31}\right)^2 \cdot W^{M2-opx}_{Ca-Mg} \end{bmatrix} \tag{6.128}$$

row9

$$a_{92} = \left(1 - X^{opx}_{21}\right) \cdot z_4 = \left(1 - X^{opx}_{21}\right) \cdot \left[\frac{1}{2}\left(T^2 - 298^2\right) - T\left(T - 298\right) \right] \tag{6.129}$$

$$\begin{aligned} b_9 = {} & X^{opx}_{21} \cdot \begin{pmatrix} \Delta_f H^o_{298K,1bar} \cdot z_1 - S^o_{298K,1bar} \cdot z_2 + A \cdot z_3 + B \cdot z_4 + C \cdot z_5 \\ + D \cdot z_6 + E \cdot z_7 + F \cdot z_8 + V \cdot z_9 + \alpha V \cdot z_{10} + \beta V \cdot z_{11} \end{pmatrix}^{Di-opx} \\ & + \left(1 - X^{opx}_{21}\right) \cdot \begin{pmatrix} - S^o_{298K,1bar} \cdot z_2 + A \cdot z_3 + C \cdot z_5 \\ + D \cdot z_6 + E \cdot z_7 + F \cdot z_8 + V \cdot z_9 + \alpha V \cdot z_{10} + \beta V \cdot z_{11} \end{pmatrix}^{En-opx} \\ & + \left(X^{\prime -opx}_{21}\, ln\, X^{\prime -opx}_{21} + X^{\prime -opx}_{31}\, ln\, X^{\prime -opx}_{31} + X^{\prime -opx}_{32}\, ln\, X^{\prime -opx}_{32} + 2X^{\prime -opx}_{83}\, ln\, X^{\prime -opx}_{83} \right) \cdot RT \\ & + X^{\prime -opx}_{21} X^{\prime -opx}_{31} \left(X^{\prime -opx}_{21} \right) \cdot W^{M2-opx}_{Mg-Ca} + X^{\prime -opx}_{31} X^{\prime -opx}_{21} \left(X^{\prime -opx}_{31} \right) \cdot W^{M2-opx}_{Ca-Mg} \end{aligned} \tag{6.130}$$

Appendix 6A

Allowing for errors in site occupancies measurements

Phase compositions that represent, together with T and P, the input data for the program '*GibInv*' are usually expressed in weight per cent of oxides. From the weight per cent of oxides the program (subroutine *rowcat*) first calculates the equivalent composition expressed in cations per formula unit, and then the site occupancy values. For every phase composition the total amount in weight per cent should be by definition equal to 100%. Similarly, stoichiometry and charge balance constraints should always be satisfied. However, due to calibration errors in the machine used to do the analysis, an electron microprobe most of the times, this sum is often not exactly 100%. More importantly, when the program calculates the equivalent composition expressed, first in cations per formula unit, then in site occupancies, these inaccuracies in the analysis related to the machine's calibration might cause stoichiometry and/or charge balance constraints not to be satisfied anymore. Although inaccuracies in chemical analysis and consequent errors in constraints are very small, it is undesirable to input these into the inversion procedure which assumes that all data constraints are satisfied by the data.

In this Appendix 6A a procedure is described that has been adopted to allow for error in the composition analysis. As an example, the procedure is described for the case of a pyroxene phase. However, an analogous procedure would apply to any other phase.

Ideally, with no inaccuracy in the pyroxene chemical analysis, the N_i's of Table 6A.1 would be error free. This, in a general nine-cation case, would yield:

$$\sum_{i=1}^{9} N_i = 4 \qquad (6A.1)$$

And vertical sums for each site would give:

$$X_{11} + X_{21} + X_{31} + X_{41} = 1 \quad (6A.2)$$

$$X_{32} + X_{42} + X_{52} + X_{62} + X_{72} = 1 \quad (6A.3)$$

$$X_{53} + X_{63} + X_{73} + X_{83} + X_{93} = 2 \quad (6A.4)$$

That is, **stoichiometry** constraints satisfied for each site

Moreover, it would also be:

$$\sum_{i=1}^{9} \beta_i N_i = 12 \quad \text{(NB: } \beta_i \text{ = individual charge of cation } i\text{)} \quad (6A.5)$$

That is, **charge balance** constraint satisfied

In a real case, since N_i's are not error free, one usually has:

$$\sum_{i=1}^{9} N_i = 4 + \varepsilon_s \quad (6A.6)$$

Where, ε_s represents the total error on estimate of cations that can be seen as the sum of stoichiometry errors on each site (see Table 6A.1), i.e.:

$$\varepsilon_s = \varepsilon_1 + \varepsilon_2 + \varepsilon_3 \quad (6A.7)$$

As a consequence, the **charge balance** constraint expression of Eq. (6A.5) becomes:

$$\sum_{i=1}^{9} \beta_i N_i = 12 + \varepsilon_c \quad (6A.8)$$

Where, ε_c is the error in the **charge balance**.

Assuming that the nine row sums (see Table 6A.1) are satisfied exactly, Eq. (6A.8) can be rewritten using the site occupancy expressions:

$$\sum_{i=1}^{9} \beta_i \sum_{j=1}^{3} X_{ij} = 12 + \varepsilon_c \tag{6A.9}$$

The total stoichiometry error, ε_s, has now to be distributed among the sites to give the site stoichiometry error in a way that Eq. (6A.7) would hold. The simplest way is to assume that the amount of stoichiometry error in M2 is equal to the error in M1 and half to the error in T $\left(\Rightarrow \varepsilon_1 = \varepsilon_2 = \frac{1}{2}\varepsilon_3\right)$. In this way it is obtained:

$$\varepsilon_1 = \varepsilon_2 = \frac{\varepsilon_s}{4} \tag{6A.10}$$

$$\varepsilon_3 = \frac{\varepsilon_s}{2} \tag{6A.11}$$

Accounting for the error, the expressions for the site **stoichiometry** constraints become:

$$X_{11} + X_{21} + X_{31} + X_{41} = 1 + \varepsilon_1 = S_1 \tag{6A.12}$$

$$X_{32} + X_{42} + X_{52} + X_{62} + X_{72} = 1 + \varepsilon_2 = S_2 \tag{6A.13}$$

$$X_{53} + X_{63} + X_{73} + X_{83} + X_{93} = 2 + \varepsilon_3 = S_3 \tag{6A.14}$$

Where, only two of the three site **stoichiometry** constraints are independent, as a result, one can be eliminated algebraically.

In conclusion, to allow for the error in the analysis of the pyroxene composition, in a general case, the following system of equations has to be solved:

$$X_{11} = N_{Na} \tag{6A.15}$$

$$X_{21} = N_{Ca} \tag{6A.16}$$

$$X_{31} + X_{32} = N_{Mg} \quad (6A.17)$$

$$X_{41} + X_{42} = N_{Fe^{2+}} \quad (6A.18)$$

$$X_{52} + X_{53} = N_{Al} \quad (6A.20)$$

$$X_{62} + X_{63} = N_{Cr} \quad (6A.21)$$

$$X_{72} + X_{73} = N_{Fe^{3+}} \quad (6A.22)$$

$$X_{83} = N_{Si} \quad (6A.23)$$

$$X_{93} = N_{Ti} \quad (6A.24)$$

$$X_{11} + X_{21} + X_{31} + X_{41} = S_1 \quad (6A.25)$$

$$X_{32} + X_{42} + X_{52} + X_{62} + X_{72} = S_2 \quad (6A.26)$$

$$X_{31}X_{42} = X_{41}X_{32} \quad (6A.27)$$

$$X_{52}\left(X_{63} + X_{73}\right) = X_{53}\left(X_{62} + X_{72}\right) \quad (6A.28)$$

$$X_{62}\left(X_{53} + X_{73}\right) = X_{63}\left(X_{52} + X_{72}\right) \quad (6A.29)$$

Note that as well as for the **stoichiometry** constraints also among the **ratio** constraints (i.e. Eq. 6A.27, 6A.28, 6A.29) only two of the three are independent.

Table 6A.1 Site occupancy distribution for pyroxene in a nine-cation (*Na, Ca, Mg, Fe^{2+}, Al, Cr, Fe^{3+}, Si, Ti*) case. In the *horizontal sum* column the N_i's symbols (i.e. N_{Na}, N_{Ca}, etc.) indicate the total amount of each cation per formula unit, i.e. $N_{Na} = X_{11}$, $N_{Mg} = X_{31} = X_{32}$, etc. In the *vertical sum* row, the quantities $1+\varepsilon_1$, $1+\varepsilon_2$, and $2+\varepsilon_3$ represent the sum of the site occupancy's values for site *M2*, *M1*, and *T* respectively; the quantity $4+\varepsilon_s$ represents the total sum of the cations per formula unit.

cation	**charge**	**site: M2**	**site: M1**	**site:T**	*horizontal sum*
Na	1+	X_{11}	#	#	N_{Na}
Ca	2+	X_{21}	#	#	N_{Ca}
Mg	2+	X_{31}	X_{32}	#	N_{Mg}
Fe^{2+}	2+	X_{41}	X_{42}	#	N_{Fe}^{2+}
Al	3+	#	X_{52}	X_{53}	N_{Al}
Cr	3+	#	X_{62}	X_{63}	N_{Cr}
Fe^{3+}	3+	#	X_{72}	X_{73}	N_{Fe}^{3+}
Si	4+	#	#	X_{83}	N_{Si}
Ti	4+	#	#	X_{93}	N_{Ti}
vertical sum		$1+\varepsilon_1$	$1+\varepsilon_2$	$2+\varepsilon_3$	$4+\varepsilon_s$

Appendix 6B

Elimination of *Lagrange* variables for the linear system of equations

In section 6.4 it was shown that, for each dataset, the *inv*erse problem has to be solved not only for the selected *nv* (i.e. *E* and/or *W*) *unknowns*, but also for a number *m* of *Lagrangian unknowns*. At the same time, in general, one is interested in determining the value of only the *nv unknowns*. In this Appendix 6B the procedure is elucidated that can be followed in order to eliminate all the *Lagrangian* variables from the system of equations to solve.

The set of linear equations written in matrix form is given by Eq. (6B.1):

$$A \cdot \underline{x} = \underline{b} \tag{6B.1}$$

Where:

A = matrix of dimension $nd \times M$

$\underline{x}$ = M vector of *unknowns* (N.B. $M \equiv nv + m$)

$\underline{b}$ = nd vector of data

And the graphic representation of Eq. (6B.1) is then:

$$\underbrace{\begin{pmatrix} a_{11},\ldots\ldots,a_{1nv};a_{1nv+1},\ldots\ldots\ldots,a_{1nv+m} \\ a_{21},\ldots\ldots,a_{2nv};a_{2nv+1},\ldots\ldots\ldots,a_{2nv+m} \\ \ldots\ldots\ldots\ldots\ldots\ldots\ldots\ldots\ldots\ldots\ldots\ldots \\ \ldots\ldots\ldots\ldots\ldots\ldots\ldots\ldots\ldots\ldots\ldots\ldots \\ \ldots\ldots\ldots\ldots\ldots\ldots\ldots\ldots\ldots\ldots\ldots\ldots \\ \ldots\ldots\ldots\ldots\ldots\ldots\ldots\ldots\ldots\ldots\ldots\ldots \\ a_{nd1},\ldots.,a_{ndnv};a_{ndnv+1},\ldots\ldots\ldots,a_{ndnv+m} \end{pmatrix}}_{A} \times \underbrace{\begin{pmatrix} x_1 \\ \vdots \\ x_{nv} \\ --- \\ x_{nv+1} \\ \vdots \\ \vdots \\ x_{nv+m} \end{pmatrix}}_{\underline{x}} = \underbrace{\begin{pmatrix} b_1 \\ b_2 \\ \vdots \\ \vdots \\ \vdots \\ \vdots \\ b_{nd} \end{pmatrix}}_{\underline{b}} \tag{6B.2}$$

The goal is to eliminate all the m, $\left(m = x_{nv+m} - x_{nv}\right)$, *Lagrangian unknowns* from the linear system, so that a $\left(nd - m\right)\times nv$ system of equations is left to be solved rather than a $nd \times \left(nv + m\right)$ system as it is now.

This is obtained by using the technique known as *Gaussian elimination with implicit pivoting* (e.g. Arfken, 1985). At each step one row and one column will be eliminated. It is now assumed row 'i' and column 'j' of the 'x_j' variable are eliminated.

$$\begin{array}{l} \qquad\qquad\quad \textit{'real' unknowns} \qquad\qquad \textit{Lagrangian unknowns} \\ \textit{row } i \rightarrow \begin{pmatrix} A_{11},\ldots\ldots,A_{1nv} \mid a_{1nv+1},\ldots\ldots\ldots,a_{1nv+m} \\ A_{21},\ldots\ldots,A_{2nv} \mid a_{2nv+1},\ldots\ldots\ldots,a_{2nv+m} \\ \ldots\ldots\ldots\ldots\ldots\mid\ldots\ldots\ldots\ldots\ldots\ldots \\ \ldots\ldots\ldots\ldots\ldots\mid\ldots\ldots a_{ij}\ldots\ldots\ldots\ldots \\ \ldots\ldots\ldots\ldots\ldots\mid\ldots\ldots\ldots\ldots\ldots\ldots \\ \ldots\ldots\ldots\ldots\ldots\mid\ldots\ldots\ldots\ldots\ldots\ldots \\ A_{nd1},\ldots\ldots,A_{ndnv} \mid a_{ndnv+1},\ldots\ldots\ldots,a_{ndnv+m} \end{pmatrix} \times \begin{pmatrix} x_1 \\ \vdots \\ x_{nv} \\ - - - \\ x_{nv+1} \\ \vdots \\ x_j \\ \vdots \\ x_{nv+m} \end{pmatrix} = \begin{pmatrix} b_1 \\ \vdots \\ \vdots \\ b_i \\ \vdots \\ \vdots \\ b_{nd} \end{pmatrix} \\ \qquad\qquad\qquad\qquad\quad \uparrow \\ \qquad\qquad\qquad\qquad \textit{column } j \end{array} \tag{6B.3}$$

Where, in Eq. (6B.3) the upper case A is introduced to make clear the difference between the two types of *unknowns*.

The *i-th* equation can be written:

$$a_{ij}x_j + \sum_{k=1}^{nv} A_{ik}x_i + \sum_{\substack{k=1 \\ k\neq j}}^{m} a_{ik}x_k = b_i \tag{6B.4}$$

Rearranging Eq. (6B.4) gives:

$$x_j = \frac{1}{a_{ij}} \left(b_i - \sum_{k=1}^{nv} A_{ik} x_i - \sum_{\substack{k=1 \\ k \neq j}}^{m} a_{ik} x_k \right) \tag{6B.5}$$

Substituting (6B.5) into the system (6B.2) would yield that for any row *p*:

$$a'_{pk} = a_{pk} - \frac{a_{pj} \times a_{ik}}{a_{ij}} \qquad \left(k = 1,..., m_j ; k \neq j\right) \tag{6B.6}$$

$$A'_{pk} = A_{pk} - \frac{a_{pj} \times A_{ik}}{a_{ij}} \qquad \left(k = 1,..., nv\right) \tag{6B.7}$$

$$b'_p = b_p - \frac{a_{pj}}{a_{ij}} \times b_i \qquad \left(p = 1,...., nd_j ; p \neq i\right) \tag{6B.8}$$

Note that every time the *i-th* row and *j-th* column are eliminated the entire matrix is transformed into one of size one row and one column smaller.

The question is which row *i* and which column *j* (*j* = 1, …, *nv*) are eliminated first, which second, which third, etc. In *implicit pivoting* the row *i* is chosen, which produces the largest a_{ij} when all rows are scaled to unity, but this means *j* is fixed first. Basically, there is the liberty to choose both *i* and *j* freely so one can choose the *i* and *j* with maximum a_{ij}.

In this way, after repeating this process *m* times, all the *m unknowns* are eliminated. As a result, the reduced system of equations to solve, written in a matrix form, will be:

$$A' \cdot \underline{x}' = \underline{b}' \tag{6B.9}$$

Where:

A' = matrix of dimension $(nd - m) \times nv$

$\underline{x}'$ = nv vector of *unknowns*

$\underline{b}'$ = $(nv - m)$ vector of data

The program '*GibInv*' includes all the codes needed to eliminate the *Lagrangian unknowns*. These codes have been tested and proved to work very well, that is, it can always be decided to solve Eq. (6B.9) instead of Eq. (6B.1). On the other hand, the elimination of the *Lagrangian unknowns* did not proved to increase the quality of the results obtained, nor the stability of the program from a numerical point of view. For this reason in the data fitting process it has always been opted to solve the complete system of equations given by Eq. (6B.1), instead of the reduced one given by Eq. (6B.9). In the program in any case an option has been left that at any time can be switched '*in*' in order to use the *Gaussian elimination*.

Appendix 6C

System equilibrium conditions assuming that n^{ϕ}'s are unknown

In section 6.3 it was shown that the *inverse* problem for any system consisting of a number 'p' of phases solves a series of equations that are directly derived from:

$$\frac{\partial L}{\partial n^{\phi}} = 0 \quad \Rightarrow G^{\phi} + \sum_{i=1}^{c} \gamma_i \left(\sum_{k=1}^{n} X_{ik}^{\phi} \right) = 0 \qquad (\phi = 1,..., p) \tag{6C.1}$$

$$\frac{\partial L}{\partial X_{ik}^{\phi}} = 0 \quad \Rightarrow n^{\phi} \frac{\partial G^{\phi}}{\partial X_{ik}^{\phi}} + \gamma_i n^{\phi} + \lambda_k^{\phi} + \beta_i \rho^{\phi} + \delta_{\omega}^{\phi} \frac{\partial C_{\omega}}{\partial X_{ik}^{\phi}} = 0 \quad (\phi = 1,...,p; k = 1,...,n; i = 1,...,c) \tag{6C.2}$$

It was also said that in the above equations, which refer to specified *T*-*P* conditions, $\left(X_{ik}^{\phi}\right)$ and $\left(n^{\phi}\right)$ will be considered known. In most cases, however, this might not be entirely correct, as the number of moles per phase, n^{ϕ}, will not usually be part of the input parameters. As a consequence n^{ϕ} will in general have to be considered unknown.

The important point is to see how the equilibrium condition equations (6C.1) and (6C.2) change assuming $n^{\phi} = unknown$.

Eq. (6C.1), being the result of the differentiation of L with respect to n^{ϕ}, will obviously remain unchanged.

In Eq. (6C.2) any term in both right and left side of the equation can be divided by n^{ϕ}. The equivalent equilibrium equation is then obtained:

$$\frac{\partial G^{\phi}}{\partial X_{ik}^{\phi}} + \gamma_i + \frac{\lambda_k^{\phi}}{n^{\phi}} + \beta_i \frac{\rho^{\phi}}{n^{\phi}} + \frac{\delta_{\omega}^{\phi}}{n^{\phi}} \frac{\partial C_{\omega}}{\partial X_{ik}^{\phi}} = 0 \qquad (\phi = 1,...,p; k = 1,...,n; i = 1,...,c) \tag{6C.3}$$

This is a very similar to Eq. (6C.2). The value of n^{ϕ}, although not known, is not a variable and it can be considered fixed. As a consequence in Eq. (6C.3) one can simply replace the *unknowns* $\frac{\lambda_k^{\phi}}{n^{\phi}}$, $\frac{\rho^{\phi}}{n^{\phi}}$ and $\frac{\delta_{\omega}^{\phi}}{n^{\phi}}$ with respectively $\lambda_k^{'\phi}$, $\rho^{'\phi}$ and $\delta_{\omega}^{'\phi}$. Substituting them in Eq. (6C.3) the following system of equilibrium equations is obtained:

$$\frac{\partial L}{\partial n^{\phi}} = 0 \quad \Rightarrow G^{\phi} + \sum_{i=1}^{c} \gamma_i \left(\sum_{k=1}^{n} X_{ik}^{\phi} \right) = 0 \quad \left(k = 1,...,n;\ i = 1,...,c\right) \tag{6C.1}$$

$$\frac{\partial L}{\partial X_{ik}^{\phi}} = 0 \ \Rightarrow \ \frac{\partial G^{\phi}}{\partial X_{ik}^{\phi}} + \gamma_i + \lambda_k^{'\phi} + \beta_i \rho^{'\phi} + \delta_{\omega}^{'\phi} \frac{\partial C_{\omega}}{\partial X_{ik}^{\phi}} = 0 \qquad \left(\phi = 1,...,p; k = 1,...n; i = 1,...c\right) \tag{6C.4}$$

The important conclusion is that, as shown by Eq. (6C.3) and (6C.4), the inversion equations are unmodified by the values of n^{ϕ}. As a result, when solving the *inverse* problem if such values are not known an arbitrary value can be assigned to them. Usually it will be $n^{\phi} = 1$ $\left(\phi = 1,...,\ p\right)$, and, since the equations are unchanged, the solution of the *inverse* problem is unchanged.

Appendix 6D

Structure of the Linear System of equations: from specific to general case

In section 6.3 it was shown that Eq. (6.16) and Eq. (6.17) are linearly dependent in all possible *m+nv unknowns*, where *nv* (i.e. the 'real' *unknowns*, whose values one wants to calculate) have to be selected by the operator, while *m* (i.e. the *Lagrangian unknowns*) are directly function of the system considered. Analogously, *m* coefficients (see also Eq. 6.45 and Eq. 6.133) are automatically determined once *nv* coefficients are known.

Given the linear dependence in the *unknowns* of Eq. (6.16) and Eq. (6.17), and dealing only with the *nv unknowns*, expressions of G^{ϕ} and $\left({\partial G^{\phi}}/{\partial X_{ik}^{\phi}} \right)$ can respectively be written:

$$G^{\phi} = G^{\phi}\left(x_1, x_2, \cdots, x_{nv}\right) = \sum_{j=1}^{nv} \alpha_j x_j \qquad \left(\phi = 1, \ldots, p\right) \tag{6D.1}$$

$$\left(\frac{\partial G^{\phi}}{\partial X_{ik}^{\phi}} \right) = \left(\frac{\partial G^{\phi}}{\partial X_{ik}^{\phi}} \right)\left(x_1, x_2, \cdots, x_{nv}\right) = \sum_{j=1}^{nv} \beta_j x_j \quad \left(\phi = 1, \ldots, p; i = 1, \ldots, c; k = 1, \ldots, n\right) \tag{6D.2}$$

To find the a_{qr}'s (q = 1,…, *nd*; r = 1,…, *nv*) coefficients in any equation q within the linear system, if equation q corresponds to Eq. (6D. 1):

$$a_{qj} = \alpha_j \qquad \left(j = 1, \ldots, nv\right) \tag{6D.3}$$

While, if equation q corresponds to Eq. (6D. 2):

$$a_{qj} = \beta_j \qquad \left(j = 1, \ldots, nv\right) \tag{6D.4}$$

It is now assumed that some of the *nv unknowns* have been selected for the fitting process.

Eq. (6D.2) and Eq. (6D.3) become:

$$G^{\phi}\left(x_1, x_2, \cdots, x_{nv}\right) = \sum_{j=1}^{nv} \alpha_j x_j + \alpha'^{\phi} \qquad \left(\phi = 1, \ldots, p\right) \tag{6D.5}$$

$$\left(\frac{\partial G^{\phi}}{\partial X_{ik}^{\phi}}\right)\left(x_1, x_2, \cdots, x_{nv}\right) = \sum_{j=1}^{nv} \beta_j x_j + \beta_{ik}'^{\phi} \quad \left(\phi = 1, \ldots, p; i = 1, \ldots, c; k = 1, \ldots, n\right) \tag{6D.6}$$

Where, α'^{ϕ} and $\beta_{ik}'^{\phi}$ are two constants (i.e. no *unknowns* are contained within these two terms), and included in the program are the codes to calculate the value of G^{ϕ}, $\left(\frac{\partial G^{\phi}}{\partial X_{ik}^{\phi}}\right)$, α'^{ϕ} and $\beta_{ik}'^{\phi}$ for any of the *nv unknowns* being selected.

Two examples can help to clarify this point.

If no *nv unknowns* have been selected $\left(\text{i.e., } x_1 = x_2 = \cdots = x_{nv} = 0\right)$, then:

$$G^{\phi} = \alpha'^{\phi} \tag{6D.7}$$

$$\left(\frac{\partial G^{\phi}}{\partial X_{ik}^{\phi}}\right) = \beta_{ik}'^{\phi} \tag{6D.8}$$

Note that in this case $a_{qr} = 0$ for any equation *q* and any *nv unknown* x_r, and, as a consequence, $\alpha_j, \beta_j = 0$.

If one *nv unknown* has been selected $\left(\text{e.g. } x_1 = 1; x_2 = \cdots = x_{nv} = 0\right)$, and the *q-th* equation corresponds to Eq. (6D. 1), then:

$$G^{\phi}\left(1, 0, \ldots, 0\right) = \alpha_j + \alpha'^{\phi} \tag{6D.9}$$

As a result:

$$\alpha_j = G^{\phi} - \alpha'^{\phi} \tag{6D.10}$$

Where, α_j represents the numerical value of the a_{qj} coefficient.

In a general case (i.e. any type and number of *nv unknowns* selected for the fitting process), depending if the equation q corresponds to either Eq. (6D.1) or Eq. (6D.2), the value of the a_{qr}'s coefficients, will be given by, respectively:

$$\alpha_j = G^{\phi}(x_r) \Big|_{x_r=\delta_{rj}} - G^{\phi}(x_r) \Big|_{x_r=0} \tag{6D.11}$$

$$\beta_j = \frac{\partial G^{\phi}(x_r)}{\partial X_{ik}^{\phi}} \Big|_{x_r=\delta_{rj}} - \frac{\partial G^{\phi}(x_r)}{\partial X_{ik}^{\phi}} \Big|_{x_r=0} \tag{6D.12}$$

With:

$\delta_{rj} = 1$, if $r = j$;

$\delta_{rj} = 0$, if $r \neq j$.

Chapter 7

Conclusions and future work

In this study, the thermodynamic properties of simple and complex crystalline solid solutions have been investigated. Problems presented by the modeling of complex multisite, multicomponent ionic solutions, which are of crucial importance in order to develop a comprehensive model for subsolidus mantle phase equilibria, have been thoroughly addressed. The various methods used in the past to study the mixing properties of binary systems have been reviewed. Approaches previously undertaken for the thermodynamic modeling of simple binary solid solutions have been considered and the shortcomings of applying in a straightforward way the principles found in simple solutions to model complex solutions have been pointed out. A general formalism has then been presented that provides a direct means to derive the Gibbs free energy expression (G) of any compositionally complex crystalline ionic solid solution. This formalism allows modeling the mixing behaviour of reciprocal solutions with inter-dependent substitutions, a subject not properly treated in previous discussions of solid solution thermodynamics in the geological literature. The formalism has been adopted to derive the Gibbs free energy expression for simple and complex solutions of interest for this study and some representative examples of G for pyroxene, olivine and spinel phases have been presented.

An innovative thermodynamic based algorithm has been developed for computing equilibrium phase assemblages as a function of composition, temperature and pressure (i.e. '*forward*' approach). The algorithm, which has been coded as a highly flexible FORTRAN computer program ('*Gib*'), makes use of modern optimization techniques that allow solving the Gibbs free energy minimization problem (GFEM) even when several different linear and non-linear constraints need to be imposed on solutions. The most significant feature of this new approach is the direct minimization of the Gibbs free energy of the system ($\mathbf{G}^{\mathbf{system}}$). This means that chemical potential expressions for system components, which, as shown in this work, can become quite complicated for multicomponent phases, no longer need to be explicitly calculated. Furthermore, with this algorithm no assumption needs to be made concerning the identity of possible thermodynamic components in the phase, as is

instead the case for existing algorithms, even though the identification of such components is often not straightforward and can actually be quite controversial for 'complex' reciprocal solid solutions.

At the time of writing this thesis the program has been set up and successfully tested to perform equilibrium calculations in NaO-CaO-MgO-FeO-Al_2O_3-Cr_2O_3-Fe_2O_3-SiO_2-TiO_2 systems and complete expressions of G have been coded for the following phases: pyroxene(s), garnet, olivine, spinel, plagioclase, quartz, kyanite, sillimanite and corundum. Future work will focus on adding oxide components (MnO, K_2O, REE_2O_3, etc.) and other phases (amphibole, mica, etc.), in order to extend the *T-P* range of applicability of the program. Due to the high flexibility of the algorithm, additional components/phases can be included in a straightforward manner.

To be genuinely useful the algorithm had to be provided with very precise values of both end-member thermodynamic data (*E's*) and solution parameters (*W's*) for any phase to be included in the computation. The computer program ('*GibInv*'), written in the course of this study, allows the derivation of internally consistent thermodynamic data sets by making use of the Bayesian technique (i.e. '*inverse*' approach). The program has been set up to let complete freedom in the choice of the *unknowns* (in number and type) to be refined. As a result, end-member and mixing parameters can simultaneously be refined. The program has initially been applied to a test case. Results obtained proved the ability of the inversion procedure to accurately recover *E* and *W* parameters' values in synthetic problems. Moreover, internal consistency between the *forward* and *inverse* approaches has been demonstrated. The program has then been applied to 'real' cases. End-members and solution parameters have been derived/refined for pyroxene (both ortho- and clinopyroxene) phases in the system CaO-MgO-FeO-Al_2O_3-SiO_2 (i.e. CMFAS) and in its constituent subsystems.

Although very encouraging, the results obtained in these real cases are not completely satisfactory. Standard deviations associated with the values of the *unknowns*, independently of their number and type, were quite large and the program seemed unable to further refine them. Inconsistency between the different sets of experimental data used in the fitting process together with their errors and the way they propagate within the program were probably the major reasons for lowering the output's quality. At the moment, in the

program these issues are dealt with by performing a Monte Carlo (MC) simulation for each data set. Future work will first focus on more properly addressing the crucial 'error propagation' issue, for instance, by employment of the Markov chain Monte Carlo (MCMC) method instead of the simpler MC. The next step will be the inclusion in the program of additional phases (garnet, olivine, plagioclase, etc.), allowing the derivation/refinement of internally consistent thermodynamic data for any system of interest.

The thermodynamic modeling of Ca-Mg-Fe^{2+} olivine and of Ca-Mg-Fe^{2+}-Al pyroxenes has been successfully carried out. End-member and mixing parameters for these phases have been very accurately refined, partly using '*GibInv*' and in part on a 'trial and error' basis. Using '*Gib*', olivine and pyroxene phase equilibria were then calculated over a wide range of different *T*-*P*-bulk composition conditions. The agreement between computed and experimental data is excellent. The excellent quality of the results demonstrates the validity of the approach undertaken in this work to model multisite, multicomponent ionic solutions. Moreover, these results showed that once the expression for the end-member part of *G* has been properly derived and end-member parameters carefully calibrated, no 'extreme' Margules and/or ordering parameters are needed to accurately reproduce experimental data. In addition, these results also demonstrate the efficiency of '*Gib'* in solving minimization problems in complex systems, where a large number of constraints need to be imposed on solutions. The next step will be the employment of the olivine/pyroxene thermodynamic data presented in this work for the construction of more precise thermobarometers.